TTI: 0-6958

Texas A&M Transportation Institute

Developing Performance Specifications for High-Performance Concrete: Technical Report

Technical Report 0-6958-R1

Cooperative Research Program

TEXAS A&M TRANSPORTATION INSTITUTE
COLLEGE STATION, TEXAS

sponsored by the
Federal Highway Administration and the
Texas Department of Transportation
https://tti.tamu.edu/documents/0-6958-R1.pdf

Technical Report Documentation Page

1. Report No.	2. Government Accession No.	3. Recipient's Catalog No.
FHWA/TX-24/0-6958-R1		

4. Title and Subtitle	5. Report Date
DEVELOPING PERFORMANCE SPECIFICATIONS FOR HIGH-PERFORMANCE CONCRETE: TECHNICAL REPORT	Published: June 2024
	6. Performing Organization Code

7. Author(s)	8. Performing Organization Report No.
Anol Mukhopadhyay and Pravin Saraswatula	Report 0-6958-R1

9. Performing Organization Name and Address	10. Work Unit No. (TRAIS)
Texas A&M Transportation Institute The Texas A&M University System College Station, Texas 77843-3135	11. Contract or Grant No. Project 0-6958

12. Sponsoring Agency Name and Address	13. Type of Report and Period Covered
Texas Department of Transportation Research and Technology Implementation Office 125 E. 11th Street Austin, Texas 78701-2483	Technical Report: September 2017–April 2022
	14. Sponsoring Agency Code

15. Supplementary Notes

The project was sponsored by the Texas Department of Transportation and the Federal Highway Administration.
Project Title: Developing Performance Specifications for High-Performance Concrete
URL: https://tti.tamu.edu/documents/0-6958-R1.pdf

16. Abstract

In the past, achieving high strength was considered by the Texas Department of Transportation (TxDOT) as the main design criteria for formulating high-performance concrete (HPC). TxDOT considers mix design options 1–5 in Item 421 as HPC, and these options were developed for alkali silica reaction (ASR) mitigation and not for other durability aspects. Very little work has been done to determine if these options are adequate to provide long-term durability often needed when HPC is specified. The main objective of this project was to develop performance specifications for HPC bridge deck concrete to ensure high performance in terms of durability. The Texas A&M Transportation Institute (TTI) conducted a combination of field investigation and laboratory evaluation to achieve this objective. TTI used both conventional and innovative new lab testing methods to determine the key durability performance characteristics (i.e., addressing chloride and freeze-thaw durability issues based on formation factor-based transport properties, cracking potential based on both autogenous and drying shrinkage considerations, ASR evaluation using rapid and reliable test methods, etc.) for developing performance specifications. TTI then developed specific prescriptive requirements to formulate a wide variety of prescriptive mixtures that can meet the durability requirements matching different exposure conditions. TTI has developed a practice-ready performance evaluation tool that addresses three critical durability parameters of HPC mixtures: ASR, shrinkage-based cracking potential, and chloride-induced rebar corrosion. The use of the tool serves as a combined approach for both performance- and prescriptive-based concrete specifications for HPC bridge deck concrete. This method could potentially encourage contractors to effectively use these finetuned prescriptive HPC mixtures without the need to conduct additional long-duration testing and ensure making long-lasting durable concrete and save taxpayers' dollars.

17. Key Words	18. Distribution Statement
High-Performance Concrete (HPC), Bridge Deck Concrete, Precast Mixtures, Bridge Girders, ASR-Resistant Concrete Mixture, Concrete Durability	No restrictions. This document is available to the public through NTIS: National Technical Information Service Alexandria, Virginia http://www.ntis.gov

19. Security Classif. (of this report)	20. Security Classif. (of this page)	21. No. of Pages	22. Price
Unclassified	Unclassified	208	

Form DOT F 1700.7 (8-72) Reproduction of completed page authorized

DEVELOPING PERFORMANCE SPECIFICATIONS FOR HIGH-PERFORMANCE CONCRETE: TECHNICAL REPORT

by

Anol Mukhopadhyay
Senior Research Scientist
Texas A&M Transportation Institute

and

Pravin Saraswatula
Assistant Research Scientist
Texas A&M Transportation Institute

Report 0-6958-R1
Project 0-6958
Project Title: Developing Performance Specifications for High-Performance Concrete

Sponsored by the
Texas Department of Transportation
and the
Federal Highway Administration

Published: June 2024

TEXAS A&M TRANSPORTATION INSTITUTE
College Station, Texas 77843-3135

DISCLAIMER

This research was sponsored by the Texas Department of Transportation (TxDOT) and the Federal Highway Administration (FHWA). The contents of this report reflect the views of the authors, who are responsible for the facts and the accuracy of the data presented herein. The contents do not necessarily reflect the official views or policies of FHWA or TxDOT. This report does not constitute a standard, specification, or regulation. The senior research scientist in charge of the project was Dr. Anol K. Mukhopadhyay.

The United States Government and the State of Texas do not endorse products or manufacturers. Trade or manufacturers' names appear herein solely because they are considered essential to the object of this report.

ACKNOWLEDGMENTS

This project was sponsored by TxDOT and FHWA. The authors wish to express their appreciation to TxDOT and FHWA personnel for their support throughout this study. Special thanks are extended to Tom Schwerdt for serving as the project manager. The research team highly appreciates the technical feedback provided by Andy Naranjo (TxDOT Champion) during the course of this project. Special thanks to Stefan Hurlebaus for conducting the NDT evaluation during field evaluation and Kai-Wei (Victor) Liu for providing necessary support in ASR testing. Acknowledgment is also given to the staff at the Texas A&M Transportation Institute.

TABLE OF CONTENTS

LIST OF FIGURES

LIST OF TABLES

CHAPTER 1: RESEARCH OVERVIEW

1.1 Problem Statement and Significance of Work

The Texas Department of Transportation (TxDOT) employs Class S high-performance concrete (HPC) predominantly for bridge deck construction in Texas. In the past, achieving high strength was the basis of the main design criteria used to formulate HPC. However, TxDOT's current HPC mix design options (Options 1–5 and 8, Item 421—Hydraulic Cement Concrete (*1*) were primarily developed for alkali silica reaction (ASR) mitigation and not for addressing other durability aspects. Very little work has been done to determine whether these options provide long-term durability, often needed when HPC is specified. As a result, current specifications are predominantly prescriptive, with minimal performance control addressed through assigning requirements for minimum strength, maximum water-to-cement (w/cm) ratio, and permeability (ASTM C 1202). A review of current HPC specifications demonstrates that these limited performance requirements do not vary according to geographical, climatic, and exposure conditions across different regions of Texas. In addition, the current specifications do not address durability requirements by specifying threshold limits of performance indicators related to drying shrinkage (DS), transport properties, chloride, freeze-thaw (F/T) durability, and others.

Current building codes for construction are predominantly structural and do not directly address concrete durability (*2*). Although codes such as ACI 318 identify and define different exposure classes, their provisions to address concrete durability are through a deemed-to-satisfy approach based on prescriptive limits for minimum/maximum cementitious content, maximum w/cm ratio, and others. Prescriptive controls through deemed-to-satisfy limits that indirectly relate to durability have little correlation with field durability performance, especially under different exposure conditions, and are inadequate for durability design and execution. However, recent revisions of highway and state DOT specifications for HPC usage demonstrate the industry's progressive shift toward a performance-based approach to satisfy field durability requirements. Guide specifications by the Federal Highway Administration (FHWA)(*3*) and Portland Cement Association (PCA) identify several performance characteristics and threshold limits for various durability requirements. The American Association of State Highway Transportation Officials (AASHTO) R 101 details performance criteria for pavement mixtures based on failure mechanisms and testing relevant critical properties, emphasizing a systematic approach to mixture qualification, verification, and quality control. Several highway and state agencies have also successfully adopted performance-based approaches in different forms, such as performance specifications, proprietary mix designs, and end-result specifications (ERSs), and applied them at various project stages to enhance durability, quality, and constructability.

A pivotal rationale for developing durable concrete mixtures hinges on evaluating the material's resistance to all potential deterioration mechanisms, followed by selecting mix designs that withstand these exposures for the desired life span. Essential to this process is considering both micro and macro factors and ensuring the HPC mix is tailored for specific applications, desired service life, and environmental conditions even before selecting materials and finalizing the mix

design. Durability prediction requires establishing links between (a) ingredient composition and mix design, (b) composition of solid-phase assemblage, (c) pore solution (PS) chemistry, (d) concrete microstructure, and (e) quantifiable performance indicators related to DS, transport properties, chloride, F/T durability, and others to evaluate the concrete degradation processes in different environments. A comprehensive durability design framework for HPC mixtures involves integrating the performance-based approach using conventional/emerging test methods to measure critical properties effectively with innovative modeling approaches to predict those performance indicators rapidly.

1.2 Objective

The main objective of this project was to develop performance specifications for HPC to ensure high performance in terms of durability. The specific objectives to achieve the main objective are listed below:

1. Field-evaluate selective in-service HPC bridge decks to identify critical durability indicators that influence field performance of HPC deck concrete (cast in place [CIP], Class S) through a combined approach of (a) field investigation of the selective HPC bridge decks, (b) laboratory study of field cores, and (c) application of the existing service life modeling tools.
2. Identify the areas of deficiency in the existing test methods/approaches and develop new test methods/approaches and innovative models to do durability-based performance evaluations of HPC bridge deck mixes that cover all major durability aspects.
3. Evaluate the durability performance of a wide variety of HPC bridge deck (CIP, Class S) mix designs, covering TxDOT Options 1–5 using the comprehensive evaluation approach developed in Item 2.
4. Develop an Excel-based tool (hereby referred to as TxDOT Tool) for comprehensive durability-based performance evaluation of HPC mixes that connects material composition, mix design, HPC properties, durability indicators, and exposure conditions.
5. Evaluate durability performance of selective HPC mixtures through laboratory testing of field-cast and lab-prepared specimens to compare/validate with TxDOT Tool predictions, focusing on achieving Technology Readiness Level (TRL) 8.
6. Assess the interlab repeatability of electrical resistivity test methods (i.e., surface resistivity [SR] and bulk resistivity [BR]) to evaluate single and multi-operator measurement variability and determine these test methods' within-laboratory and interlaboratory repeatability.

1.3 Organization of the Report

The work that was performed under different tasks (according to the original proposal) is presented in this report as chapters.

Chapter 1 is an introduction addressing the research background and objectives, followed by a description of the report's organization.

Chapter 2 provides a comprehensive literature review that was conducted to provide a succinct background on deficiencies in addressing durability in the current HPC mix design practice in Texas. A comprehensive background and critical review addressing current ASR durability evaluation, concrete PS prediction models, and chloride durability are discussed. Finally, the review critically examines the current approaches for resistivity evaluation, various factors that influence resistivity test measurements, and the formation factor (FF) evaluation of concrete mixes.

Chapter 3 presents the performance evaluation of selected in-service HPC bridge deck mixtures through a comprehensive approach combining field investigations, laboratory tests, and service life prediction models. The three-step evaluation approach assessed the condition and predicted the service life of HPC structures designed with Mix Options 1–5 (as outlined in Item 421), providing insights into their current performance and future durability under specific environmental conditions. The findings helped determine if the existing mix design practices meet the mechanical and durability requirements of the selected HPC structures and if the current specifications adequately address durability concerns. Based on the evaluation, the Texas A&M Transportation Institute (TTI) has provided recommendations to enhance the concrete mixes and addressed any identified deficiencies through additional control measures, whether prescriptive or performance based.

Chapter 4 outlines the formulation, testing, and laboratory-based durability assessment of diverse Class S HPC mixtures covering mix design Options 1–5 (as outlined in Item 421, TxDOT Specifications). Initially, TTI created various HPC mixtures by incorporating prescriptive requirements and performance characteristics gleaned from TxDOT's historical projects. Next, a comprehensive durability evaluation of these mix designs was conducted, covering major conventional and standard ASTM/AASHTO test specifications. The performance of HPC mixes was further assessed using innovative and promising testing methods, as recommended by the project. Conclusively, the chapter discusses the recommendation of additional performance-based requirements derived from the test results to ensure that all tested mixes meet the durability standards required for the anticipated severity of exposure conditions.

Chapter 5 presents an overview of the TxDOT Tool, its features, and guidelines to perform a comprehensive durability-based performance evaluation of HPC mixtures using the TxDOT Tool. In this project, the research team developed a simplified, user-friendly Excel spreadsheet (the TxDOT Tool) to enable DOT practitioners and contractors to perform rapid durability-based performance evaluation of CIP HPC bridge deck mixes that covers four major aspects: (1) ASR mitigation, (2) shrinkage, (3) durability to resist chloride ion ingress, and (4) F/T durability.

Chapter 6 covers the field evaluation of selective HPC mixtures to raise the project's TRL from 6 to 8. The research team selected three field projects in the Euless and Dumas regions of Texas to evaluate project specific HPC mixture performance by comparing the laboratory evaluation of field-cast (i.e., specimens cast using field concrete mix) and lab-cast (i.e., prepared in the laboratory) specimens. The field evaluation was conducted during a two-stage field visit (i.e.,

during concrete pouring and post-construction). The activities during the first visit were observing and documenting concrete placement and curing, casting specimens using the field mix, collecting concrete ingredients, etc., whereas the activities during post-construction site visits were measuring bridge deck SR and monitoring shrinkage-induced cracks. In addition, the TxDOT Tool was used to predict the durability performance of the HPC mixtures and compared with the laboratory-measured performance evaluation.

Chapter 7 presents an in-depth analysis of the repeatability and variability of electrical resistivity test methods. SR and BR measurements were conducted on a single concrete mixture type by two different laboratories and multiple operators to evaluate single-operator and multi-operator measurement variability and assess the within-laboratory and interlaboratory repeatability of the test methods.

Finally, Chapter 8 provides a summary and conclusions based on the research findings from this study and potential recommendations for future research and implementation.

CHAPTER 2: LITERATURE REVIEW

The main objective of this study was to develop performance specifications for HPC to ensure high performance in terms of durability. Recent revisions of standard guide specifications for structural and pavement concrete show the industry's progressive shift toward performance-based specifications to achieve durable concrete mixes. Although major HPC specifications are still prescriptive or use a combination of performance and prescriptive provisions, several state DOTs have successfully implemented performance-based specifications by establishing threshold limits for relevant performance indicators. The goal of this literature review was to summarize recent and ongoing efforts by the industries, agencies, state DOTs, and universities to identify, measure, incorporate, and implement performance requirements to achieve long-term durability of HPC.

2.1 Review Approach

One of the goals of this literature review was to understand and review TxDOT's current options for HPC and attempt to identify areas of deficiencies and improvements to incorporate performance-based specifications to meet the durability requirements achieved through review of the following:

- The current TxDOT Specifications for Class S HPC.
- The standard guide specifications and identify strategies required for the implementation of the performance-based specifications approach for HPC:
  - FHWA.
  - AASHTO, "Performance Engineered Materials (PEM)for Concrete Pavement" (AASHTO R 101).
  - PCA.
  - National Ready-Mixed Concrete Association (NRMCA).
- Specification practices used by state DOTs (e.g., prescriptive, performance, or hybrid) for incorporating HPC into their specifications and determining threshold limits of performance requirements.
  - Eleven states (Washington, Oregon, California, Kansas, Iowa, Illinois, Ohio, Virginia, New Jersey, Florida, and Minnesota) were selected based on criteria such as (a) varied climatic and environmental conditions and (b) strategies for successful implementation of performance specifications of HPC.

2.2 Conducting Literature Review

The literature review was conducted based on the above approach, and the findings are presented next.

2.2.1 Review of Class S HPC Specifications in Texas

TxDOT predominantly employs HPC for bridge construction in Texas. TxDOT's current specifications (*1*) have mix design Options 1–5 and 8 for its HPC concrete class as shown in Table 2-1 comprise maximum w/cm ratio of 0.45 and cementitious content not to exceed 700lb/cy of concrete (unless otherwise specified or approved by an engineer). As shown in Table 2-1, HPC mix design Options 1–5 are prescriptive to increase maximum fly ash (FA) replacement to 35 percent for Options 1 and 3. Blended cement, up to 20 percent maximum, is permitted with listed supplementary cementitious materials (SCMs) for Option 4. Mix design Option 8 requires annual testing for deviations from Options 1–5 or the mix design options listed in section 4.2.6.8, "Item 421 Hydraulic Cement Concrete, TxDOT 2014." The performance requirements for HPC currently include minimum strength requirements of 4000 psi, maximum w/cm ratio of 0.45, and an additional < 1500 coulombs (Rapid Chloride Permeability Test [RCPT], ASTM C1202) requirement for HPC mixes with less than 20 percent cement replacement with SCMs. The RCPT can be conducted either following moist curing of 56 days at 73°F or moist curing for 7 days at 73°F, followed by 21 days at 100°F. HPC specifications were incorporated into the earlier versions of 1993 and 2004 specifications as supplemental provisions with prescriptive provisions and performance requirements for permeability through AASHTO T 277 and AASHTO T 259 test limits.

Table 2-1: TxDOT's Current Specifications for Class S and HPC

OPTION	HPC MIX DETAIL	COMMONLY USED REPLACEMENT LEVELS	EXAMPLE LOCATIONS OF TYPICAL USAGE
1	Replace 20% to 35% of the cement with Class F FA.	25% Class F FA	Galveston, Houston, Atalanta, Corpus Christi, and El Paso
2	Replace 35% to 50% of the cement with slag cement or MFFA.	Not a practice because of nonavailability of slag in Texas	
3	Replace 35% to 50% of the cement with a combination of Class F FA or silica fume (SF); however, no more than 35% may be FA, and no more than 10% may be SF.	Not Used	
4	Use Type IP, Type IS, or Type IT cement as allowed in each class of concrete.	Not Used	
5	Replace 35% to 50% of the cement with a combination of Class C FA and at least 6% of SF. However, no more than 35% may be Class C FA, and no more than 10% may be SF.	29% Class C FA + 6% SF	Amarillo, TX
-	Project-specific provisional mix design options	35% Class C FA & 6% SF	Lubbock, TX & Amarillo, TX

A review of concrete classes and mix design options reveals that the current CIP Class S HPC mix design options are predominantly prescriptive with minimum performance requirements (mentioned above). The current cement replacement levels with SCMs for mix design Options 1–5 and 8 were primarily intended to limit/mitigate ASR issues because previous research (*4*) has noted the presence/prevalence of moderate to highly reactive aggregates in several regions of Texas that can cause severe deterioration and are detrimental to the intended service life of these bridge deck structures. A review of the current specifications also demonstrates that these limited performance requirements do not vary according to geographical, climatic, and exposure conditions across different regions of Texas. In addition, the current specifications do not address durability requirements and threshold limits of performance for DS, transport properties, F/T durability, and other long-term performance properties of the current HPC mix design options and have not been previously studied.

2.2.2 Review of Standard Guide Specifications

A detailed comparison of guide specifications, durability, and testing requirements for HPC mixes is summarized in Tables 2-1 and 2-2. Revised grades of performance characteristics and their recommended threshold limits specified by National Cooperative Highway Research Program (NCHRP) Synthesis 441 (*3*) have also been included for comparison. Table 2-2 describes the requirements and testing methods recommended by FHWA and PCA guidelines (*5*). The revised FHWA guidelines on 11 performance characteristics for the three grades of HPC are presented in Table 2-3. Table 2-4provides an overall description of durability requirements and test methods for acceptance identified in AASHTO PEM specifications for pavement mixes.

AASHTO PEM (R 101) specifications address the critical parameters that determine concrete paving mixture performance and recommend implementing these requirements in the following order:

- Mixture qualification—Material and mixture properties for local conditions.
- Mixture verification—At the project level.
- Mixture quality control and acceptance.

Table 2-2: Description of FHWA and PCA Guidelines for HPC

PERFORMANCE CHARACTERISTIC	STANDARD TEST METHOD PROPOSED BY FHWA	PCA GUIDE SPECIFICATION FOR HPC BRIDGE DECKS	
		Deck	Test Methods Recommended
F/T Durability	AASHTO T 161 (ASTM C666) Procedure A	If exposed to freezing and thawing, specify a minimum durability factor based on AASHTO T 161.	AASHTO T 161 ASTM C666 ASTM C 457
Scaling Resistance (SR)	ASTM C672	If exposed to deicing salts, specify a maximum visual rating based on ASTM C 672.	ASTM C672
Abrasion Resistance (AR)	ASTM C944	If abrasion from snowplows is a concern, specify either AR criterion for concrete or criteria for aggregate.	AASHTO T 96 ASTM C 33 ASTM C 779, ASTM C 944
Chloride Penetration (CP)	AASHTO T 277 (ASTM C1202)	If exposed to deicing salts or salt spray, specify maximum limit based on AASHTO T 277.	AASHTO T 277 ASTM C1202
ASR	ASTM C441	Ensure that aggregates used are not potentially reactive or take appropriate control measures	ASTM C 1293 ASTM C 1260 ASTM C 1567 ASTM C 295
Sulfate Resistance	ASTM C1012	n/a	ASTM C1012 ACI 201
Flowability	AASHTO T 119 (ASTM C143) and proposed slump flow (SF) test	Allow contractor to select consistency to achieve consolidation. Specify variability limits.	AASHTO T 119 ASTM C143
Strength	AASHTO T 22 (ASTM C39)	Specify strength(s) and age(s) if the structural behavior depends on having a certain strength; high early strength could increase risk of cracking.	AASHTO T 22 ASTM C39
Elasticity	ASTM C469	Do not specify. Too high modulus of elasticity (MOE) may contribute to cracking of the deck.	ASTM C469
DS	AASHTO T 160 (ASTM C157)	Do not specify; instead, specify required curing procedures, inspection, and crack repair methods.	AASHTO T 160 ASTM C157

Table 2-3: Revised Grades of Performance Characteristics for HPC Structural Concrete (*3*)

PERFORMANCE CHARACTERISTIC	STANDARD TEST METHOD	FHWA HPC PERFORMANCE GRADE		
		1	2	3
F/T Durability (relative dynamic MOE after 300 cycles)	AASHTO T 161 (ASTM C666) Procedure A	70% ≤ *F/T* <80%	80% ≤ *F/T* < 90%	90% ≤ *F/T*
Scaling Resistance (*SC* = visual rating of the surface after 50 cycles)	ASTM C672	3.0 ≥ *SR* > 2.0	2.0 ≥ *SR* > 1.0	1.0 > *SR* ≥ 0.0
AR (*AR* = average depth of wear in mm)	ASTM C944	2.0 > *AR* ≥ 1.0	1.0 > *AR* ≥ 0.5	0.5 > *AR*
CP (*CP* = coulombs)	AASHTO T 277 (ASTM C1202)	2500 ≥ *CP* > 1500	1500 ≥ *CP* > 500	500 ≥ *CP*
ASR (*ASR* = expansion at 56 d) (%)	ASTM C441	0.20 ≥ *ASR* > 0.15	0.15 ≥ *ASR* > 0.10	0.10 ≥ *ASR*
Sulfate Resistance (*SU* = expansion) (%)	ASTM C1012	*SU* ≤ 0.10 at 6 months	*SU* ≤ 0.10 at 12 months	*SU* ≤ 0.10 at 18 months
Flowability (*SF* = slump flow)	AASHTO T 119 (ASTM C143) and proposed SF test	*slump* > 7.5 inches & *SF* < 20 inches	20 ≤ *SF* ≤ 24 inches	24 inches < *SF*
Strength (*fc* = compressive strength)	AASHTO T 22 (ASTM C39)	*8* ≤ *fc* < 10 ksi	10 ≤ *fc* < 14 ksi	14 ksi ≤ *fc*
Elasticity (*MOE* = modulus of elasticity)	ASTM C469	5 ≤ *MOE*< 6 ksi	6 ≤ *MOE* < 7 ksi	7 ksi ≤ *MOE*
DS (DS = microstrain)	AASHTO T 160 (ASTM C157)	800 > *S* ≥ 600	600 > *S* ≥ 400	400 > S
Creep (C = microstrain/pressure unit)	ASTM C512	0.52 ≥ *C* > 0.38/psi	0.38 ≥ *C* > 0.21/psi	0.21/psi ≥ C

Table 2-4: Testing and Durability Requirements from AASHTO PEM (for Pavement Mixtures)

SECTION	PERFORMANCE SPECIFICATION	PROPERTY	SPECIFIED TEST (SEE GLOSSARY)	SPECIFIED VALUE (MIN. REQ.)
6.3.1	Concrete Strength	Flexural Strength	AASHTO T 97	600 psi
6.3.2		Compressive Strength	AASHTO T22	3500 psi
6.4.1.1	Reducing Unwanted Cracking Due to Shrinkage	Volume of Paste		25%
6.4.1.2		Unrestrained Volume Change	ASTM C157	420 microstrains at 28 days
6.4.2.1		Unrestrained Volume Change	ASTM C157	360, 420, 480 microstrains at 91 days for the probability of cracking less than 5, 20, or 50%, respectively, depending upon application.
6.4.2.2		Restrained Shrinkage (Single-Ring Test)	AASHTO T 334	crack-free at 180 days
6.4.2.4		Probability of Cracking (Dual-Ring Test)	AASHTO T 363	5, 20, 50% depending upon application
6.5.1.1	Hardened Cement Paste F/T Durability	W/C Ratio	AASHTO T 318	0.45 (max.)
6.5.1.2		Fresh Air Content	AASHTO T 152, T196, TP 118	5 to 8%
6.5.1.3		Fresh Air Content/ Super Air Meter (SAM)	AASHTO T 152, T196, TP 118	≥ 4% Air; SAM ≤ 0.2%, psi
6.5.2.1		Time of Critical Saturation	"Bucket Test" Specification	X > 30 years
6.6.1.1	Transport Properties/ Permeability	W/C Ratio	AASHTO T 318	Less than 0.45 if subjected to F/T or deicer application; less than 0.50, if otherwise.
6.6.1.2		RCPT Value	AASHTO T 277	2000
6.6.1.3		FF/Resistivity	AASHTO T 358	500
6.6.2.1		Ionic Penetration, F Factor	AASHTO T 365	25 mm at 30 years
6.7.1	Aggregate Stability	D Cracking	AASHTO T 161 ASTM C 1646	N/A
6.7.2		Alkali Aggregate Reactivity	AASHTO PP 65	N/A
6.8.1	Workability	Box Test	~	<6.25 mm, < 30% Surf. Void
6.8.2		Modified V-Kelly Test	~	15–30 mm per root second

Note: N/A = Not Applicable.

A review of the specifications and the associated literature shows the industry's emphasis on moving toward a more performance-based specification that ensures durability, quality, and ease of constructability. Recent revisions of the standard specifications for HPC demonstrate the industry's progressive shift toward a performance-based approach to achieve and address field durability. Guide specifications for HPC, such as FHWA (*6*) and PCA (*7*) identify several performance characteristics and threshold limits set for various durability requirements. The AASHTO PEM (AASHTO R 101, for pavement mixes [(*8*)]) identifies performance characteristics through failure mechanisms, and performance limits are developed based on testing relevant critical properties. In addition, PEM specification is structured around the critical parameters that determine concrete paving mixture performance. The concept is to implement these requirements in the following order: (a) mixture qualification—material and mixture properties for local conditions, (b) mixture verification—at the project level, and (c) mixture quality control and acceptance.

In addition, several researchers and highway agencies have successfully implemented performance specifications applied to different project stages, such as performance specifications, proprietary or contractor mix design, ERS, etc. A review of the specifications and the associated literature shows the industry's emphasis on a more performance-based specification that ensures durability, quality, and ease of constructability. Some strategies for successful implementation of performance specifications include (1) clear specification for the durability requirements with recommendations on using effective test methods and well defined acceptance criteria to verify and enforce the requirements; (2) providing flexibility to the contractor and/or producer to design mixes through strict enforcement of established performance criteria; and (3) ensuring contractor and/or producer's mix design meets requirements for plastic as well as additional requirements for placing and finishing, such as flow and set time, while ensuring strict adherence to the performance requirements for the hardened concrete.

2.2.3 Review of Selective State DOT Specifications for HPC

The HPC specifications of 12 state DOTs/highway agencies (listed below) were reviewed to assess their approach to incorporation and implementation of performance characteristics (durability requirements). These state highway agencies have been chosen to cover a wide range of specifications from the West Coast to the East Coast, such as varieties of climatic regions (e.g., tropical, coastal, etc.) including Washington (WSDOT), Oregon (ODOT), California (Caltrans), Kansas (KDOT), Iowa (Iowa DOT), Illinois Tollway (IL Tollway), Ohio (ODOT), Virginia (VDOT), New Jersey (NJDOT), Florida (FDOT) and Minnesota (MnDOT). *(Note: The Illinois Tollway specifications were reviewed for successful implementation practice of HPC bridge deck mixes for Illinois.)*

Table 2-5 presents the general type of specification for HPC by various state DOTs or highway agencies. The typical specifications for HPC CIP bridge deck mixtures commonly used by 9 state DOTs/highway agencies are presented in Table 2-6. Table 2-7 summarizes key

performance characteristics and their limits identified in the specifications of those 9 state DOTs/highway agencies.

Table 2-5: State DOT Specification Types for Durability Requirements (Bridge Deck)

STATE	TYPE OF SPECIFICATION: (PRESCRIPTIVE/PERFORMANCE/PART PRESCRIPTIVE–PERFORMANCE)	KEY PERFORMANCE-BASED PARAMETERS
WSDOT	Performance-based specification for bridge decks—Concrete Class 4000D. Prescriptive-based specification—For other class of concrete with minimum cementitious contents and SCM replacement percentages.	Contractor mix design for bridge decks: • No set limits on cementitious content (usually 565–610 lb). • FA optional. • Shrinkage limit (AASHTO T 160)—320 microstrains at 28 days.
Oregon	Three HPC mix design options. Option 1: Total prescriptive mix design. Option 2 and 3: Certain prescriptive maximums (SCM substitution limits) to meet performance requirements.	Performance requirements for permeability and shrinkage.
Caltrans	Prescriptive control of cement and SCM percentages through minimum specified amounts of cementitious material.	Special provisions through specific limits on cementitious material, SCM substitutions, and air entrainment for exposure to corrosive, F/T, and deicing chemicals.
KDOT	Low Cracking (LC)–HPC mix design—Completely prescriptive. (LC–HPC for decks)	The mix method of optimized aggregate gradation Mixes are designed to have a high volume of aggregate and low paste content. No mineral admixtures in air entrained LC–HPC Concrete mix
MnDOT	Current HPC Options: 1. LC (KU)–HPC Deck Mix. 2. Contractor mix design—Part prescriptive with certain mix design requirements for ASR mitigation, crack control, etc. to meet performance requirements. 3. Lightweight deck and internal curing mix.	Contractor mix design to lower bridge deck cracking.
Iowa	HPC mix design options for deck and substructure. Option 1: Complete prescriptive mix design. Option 2: Part prescriptive with absolute volume limits and maximum SCM replacement percentages to meet performance requirements.	The HPC mix design option is also used for overlay concrete. Prescriptive specification for Class HPC-O.
IL Tollway	Performance based. Contractor choice of mix design.	Performance requirements established in accordance with AASHTO PEM specifications.
Ohio	Quality control mix design approach. Part prescriptive with certain mix design limits to meet performance requirements.	Well graded combined gradation (optimized gradation) of aggregates required to meet quality control standard.
VDOT	ERS-based.	Stringent permeability limits for harsher climates.
NJDOT	Performance based. Contractor choice of mix design. Part prescriptive maximums for SCM substitutions only to meet desired CP criteria.	SR (AASHTO T 358) replaces RCPT (AASHTO T 277) in specification.
FDOT	Prescriptive mix design practices but performance specification required for ternary blend mixes.	SR (AASHTO T 358) required for ternary blend HPC mixes.

Table 2-6: Key Mix Design Parameters for HPC Application in Bridge Decks along with Placement and Curing Requirements

PERFORMANCE CHARACTERISTIC	WSDOT	ODOT	CALTRANS	KDOT	MNDOT	IOWA DOT	NJDOT	FDOT	IL TOLLWAY (AASHTO PEM)
Cementitious Content, lb/cy	No set limits (usu. 565–610)	n/a	675–800 Corrosive—675 (min.) F/T—590 (min.)	500–540	500–535	624 (min.)	611–700	611–658 (max.)	Max. 700
W/C	n/a	0.40 (max.)	~0.54	0.44–0.45 (max.)	0.42–0.45	0.42 (min.)–0.45 (max.)	0.443	0.41–0.44	n/a
Slump, inch	3.5	5.5±2.5	n/a	1.5–3	1–4/1.5–3	4 (max.)	3±1 inch	7 inches (max. with chemical admixtures)	3–8
Air Content, %	4.5–7.5	4.5–5.5	6±1.5 (F/T)	8±1	6.5/8±1	6.5+2% or−1%	6±1.5 (MSA ≤1 inch) 7±1.5 (MSA 1.5 inches)	A/E required	Min. 4%
Max. Size Aggregate, inch	1.5	≥ 1 inch	1–1.5 inch	Optimized gradation	Optimized gradation	1 inch	1.5–0.75 inch	1.5	1 inch
Compressive Strength, psi	4000 at 28 days	4000 at 28 days	3600 at 28 days; 42 or 56 days for high SCM	3500–5000 at 28 days	4000 at 28 days	4500 at 28 days	4600 at 28 days or 5400 at 56 days	4000 at 28 days	4000 at 14 days
Deck Placement Temp, ºF	55–75	50–80	≥ 45 (Cold weather protection)	55–70	≥ 40 (Cold weather protection)	≥ 50 (Cold weather protection)	50–90	40–85	50/60(Ternary Blend)–85
Curing Type and Duration	Wet burlap for 14 days	Wet burlap for 14 days	Wet burlap for 7 days	Wet burlap for 14 days followed by 7-day curing membrane	Curing compound and wet burlap for 7 days or wet burlap for 14 days curing until concrete attains 65–70% target strength	Wet burlap for 17 days	Curing compound and wet burlap for 3 days	Curing compound and wet burlap for 7 days	Wet burlap for 7 days. Ternary blend HPC curing—4 days

Note: N/A = Not Applicable; n/a = not available.

Table 2-7: Summary of Key Performance Requirements (and Threshold Limits) Identified in the State Specifications

Performance characteristic	Common test method	WSDOT	ODOT	Caltrans	KDOT	MnDOT	Iowa DOT	NJDOT	FDOT	IL Tollway (AASHTO PEM)
Compressive strength	AASHTO T 22/ASTM C 39	✓	✓	✓[1]	✓	✓	✓	✓	✓	✓
F/T durability (x = relative dynamic modulus after 300 cycles)	AASHTO T 161 ASTM C666 Procedure A	✓ (≥90%)	n/a	✓[1]	N/A	✓ (≥90%)	N/A	✓ (≥80%)	N/A	✓ (≥80%)
SC (x = visual rating of the surface after 50 cycles)	ASTM C672	✓ (≤ 2)	n/a	✓[1]	N/A	✓ (≤ 1)	N/A	✓ (≤ 1)	N/A	✓ (limits on total air content, spacing factor)
AR, mm (x = average depth of wear in mm)	ASTM C944	N/A	N/A	N/A	N/A	N/A	N/A	✓ 0.04 (Sub-structure)	N/A	N/A
Permeability (RCPT = coulombs, max.)	AASHTO T 277 ASTM C1202	✓ 2000 at 56 days	✓ 1000 at 90 days	N/A	N/A	✓ 2500 and 1500 at 56, 28 days	✓ 1500 and 2500 at 28 days	n/a	✓ (limits on chloride ion content)	✓ 1250 at 28 days
DS, microstrain	ASTM C157 AASHTO T 160	✓ ≤0.032% at 28 days	✓ ≤0.045% at 28 days	✓ ≤0.045% at 28 days	n/a	✓ ≤0.040% at 28 days		✓ ≤0.045% at 56 days		✓ ≤0.030% at 28 days
MOE	ASTM C469	✓	N/A	N/A	N/A	N/A	N/A	N/A	N/A	N/A
Surface resistivity SR = kOhm-cm	AASHTO T 358	n/a	n/a	n/a	n/a	✓*	n/a	✓ ≥36 at 56 days	✓ Extreme ≥29 Moderate 17–29 Slight ≤ 17	n/a
Workability (SL), inch	ASTM C 143	✓	✓	✓[1]	✓	✓	✓	✓	✓	✓
Alkali reactivity		n/a	n/a	n/a	n/a	n/a	n/a	n/a	n/a	✓ AASHTO T 303 ≤ 0.10% at 16 days

Note: N/A = Not Applicable; n/a = not available.

[1] California specifications: Limits on minimum cementitious content.

* In experimental stages for implementation.

A review of the HPC specifications of 12 states revealed most states use performance-based HPC mix designs predominantly for bridge decks when the major goal is to reduce deck cracking.

WSDOT, IL Tollway, and NJ DOT have predominantly moved toward performance-based specifications for mix designs on bridge decks through proprietary or contractor-choice mix designs. Recent reports from these state agencies have demonstrated that this move was successful in reducing bridge deck shrinkage cracking. KDOT implements a prescriptive specification of LC–HPC through an optimized aggregate gradation (i.e., Kansas University - KU mix method) mix design for bridge deck mixes. The KU mix method of optimized aggregate gradation has been incorporated with similar success by state DOTs like Washington DOT to mitigate bridge deck cracking. MnDOT has included a wide range of HPC choices, like low cracking (LC)-HPC mix, contractor choice of mix design, internal curing technique, etc. However, the contractor's choice mix design has proved to be most successful in reducing deck cracking. A similar successful approach has been demonstrated at VDOT through end result specifications (ERS).

States that have demonstrated successful implementation of performance-based specification for HPC have achieved it through the contractor's choice mix design, that is, by providing the necessary flexibility to the contractor and producer to provide a mix that meets the performance criteria in the way they choose. Threshold limits for performance characteristics like shrinkage, permeability, F/T durability, and SC have been incorporated into specifications. State DOTs, specifically NJDOT and FDOT, have replaced the traditional RCPTs (AASHTO T 277) for permeability requirements with resistivity testing (AASHTO T 358) in the specifications. Free shrinkage limits (ASTM C 157) have been adopted in 7 state specifications, as identified above, for performance control to limit shrinkage cracking on bridge decks.

CHAPTER 3: PERFORMANCE EVALUATION OF SELECTED HPC BRIDGE DECKS THROUGH FIELD AND LABORATORY INVESTIGATION AND SERVICE LIFE PREDICTIONS

This chapter (representing Task 3 in the project) details the performance evaluation of the selected in-service HPC bridge deck mixtures through a comprehensive approach combining field investigations, laboratory tests, and service life prediction models. The three-step evaluation methodology was proposed to assess the condition and predict the service life of HPC structures designed with Mix Options 1–5 (as outlined in Item 421), providing insights into their current performance and future durability under specific environmental conditions. The aim was to determine if the existing mix design practices meet both the mechanical and durability requirements for the selected HPC bridge decks and if the current specifications adequately address durability concerns. Identifying deficiencies (if any) through this evaluation and providing recommendations for additional control measures (performance-based or prescriptive) to minimize the deficiencies was the main goal of this task.

3.1 Evaluation Methodology

The evaluation process involved three key steps:

- Selection of HPC bridge deck structures for field evaluation
- Performing field and laboratory evaluation
  - Evaluation of selected in-service HPC bridge decks using visual inspections and nondestructive testing (NDT) methods, complemented by core sampling for detailed analysis.
  - Laboratory testing of the collected cores, including physical, chemical, and petrographic analyses, to assess the performance of the HPC deck mixtures.
- Utilizing suitable service life prediction models to forecast the long-term performance of these HPC decks under varying exposure conditions (low, medium, and high severity).

3.1.1 Field Evaluation

The field evaluation involved several steps to identify and select bridge deck structures constructed with the most commonly used HPC mix design options/practices to serve as representative structures. The process unfolded as follows:

- Selection of Representative Districts—Districts from each of the six major geographical regions in Texas were chosen based on various severity parameters, including the number of F/T cycles per year, exposure to deicing chemicals, chloride ingress from sea and lake water or the use of chloride-containing aggregates, average annual precipitation, high relative humidity (RH), and potential evaporation rates determined by temperature, RH, and wind speed, as shown in Table 3-1.

- Coordination with Key Stakeholders—Conference calls were held with the project champion and the Project Monitoring Committee of TxDOT. The discussions aimed to outline the selection criteria for field visits, evaluate the performance of HPC bridge decks across districts, and gather insights from their experiences. This process led to the preliminary identification of nine districts for further evaluation.
- Selection of Districts—The nine selected districts were shortlisted based on the number of factors that met requirements, such as the intensity of parameters affecting concrete durability, levels of distress observed in HPC bridge decks through field inspection reports, the age of the bridges, and the mix design practices. Using historical weather data from the National Oceanic and Atmospheric Administration (NOAA) National Centers for Environmental Information (NCEI) and the ACI 305-R nomograph, the potential rate of evaporation was calculated to inform the selection process.

Table 3-1: Critical Environmental Factors and Factors Influencing Rate of Evaporation

LOCATION	REGION	NO. OF F/T CYCLES/ YEAR	AVG. ANNUAL PRECIPITATION (INCHES)	TEMPERATURE ◦F (ANNUAL) (HIGH/LOW/ AVG.)	AVG. (ANNUAL) SNOWFALL INCHES	AVG. WIND SPEED MPH	AVG. RH	RATE OF EVAPORATION— CRITICAL COMBINATION (REFER TO NOTE 3)
Amarillo	Panhandle Plains	11–13	19.56	70.5/43.3/57.3	17.9	13.5	56	0.187
Lubbock	Panhandle Plains	8–10	18.65	73.5/46.8/60.65	9	12.4	54	0.208
Dallas	Prairies and Lakes	5–7	33.70	76.3/54.6/64.3	2.5	10.7	65	0.157
El Paso	Big Bend	5–7	9.69	77.5/51.8/64.65	3.5	8.8	41	0.182
Atlanta	Piney Woods	2–4	48.79	77.4/53.4/63.75	1	8.3	72	0.124
Corpus Christi	Gulf Coast	1	32.26	81.0/62.1/72.15	-	12	76	0.143
Houston	Gulf Coast	1	50.83	78.7/60.1/69.4	-	7.6	75	0.103
Austin	Hill Country	1–2	34.2	80/59/72	0.6	8.4	67	0.133
Laredo	South Texas Plain	1	20.2	85/63/75	-	12	79	0.150

Note:
- Weather data obtained from NOAA's NCEI and its associate entities' websites.
- Rate of evaporation values have been calculated using TxDOT standard evaporation calculation sheet, ACI 305 R nomograph.
- Rate of evaporation—Critical combination has been calculated using combination of monthly high temperatures (May–August) and corresponding wind speed and average humidity levels at 3 p.m. for these cities. Concrete temperature has been assumed to be without any type cooling agent at 80°F for ambient temperatures usually in range of 83–93°F.

- Final Selection for HPC Bridge Decks for Field Evaluation: After thorough document review and analysis, discussions with TxDOT finalized the selection. Four locations encompassing nine bridges were chosen for the field evaluation, as detailed in Table 3-2.

Table 3-2: Final List of Locations and Bridges Selected for Field Survey

LOCATION	BRIDGE NO.	BRIDGE DESCRIPTION	STRUCTURE ID	DATE OF FIELD VISIT
Amarillo	1	SL 335 at BNSF Overpass (westbound [WB] lanes)	04-191-0-2635-02-087	May 22, 2018
	2	SL 335 at Georgia Overpass (WB lanes)	04-191-0-2635-02-084	
	3	IH 27/IH 40 at IH 27 Ramp Connection	04-188-0-0168-10-169	
	4	IH 27 at FM 2219 Underpass	04-191-0-0168-09-158	May 23, 2018
	5	IH 27 at Buffalo Stadium Rd.	04-191-0-0168-09-168	
Littlefield	6	US 84 WB at US 385	05-140-0-0052-05-017	May 24, 2018
Lubbock	7	LP 289 SB at FM 2255 (4th St.)	05-152-0-0783-02-104	
Galveston	8	SH 87 Ferry S SLP 2 at Galveston Bay	12-085-0-0367-06-033	June 05, 2018
	9	IH 45 (NB) Causeway Bridge	12-085-0-0500-01-373	

3.1.2 Perform Field Surveys

The general approach for performing field surveys is described in the flowchart (Figure 3-1). For each bridge location, structural drawings, HPC mix design, and most recent bridge inspection reports were reviewed to better understand the design, construction, materials, and distress patterns exhibited by these bridge decks.

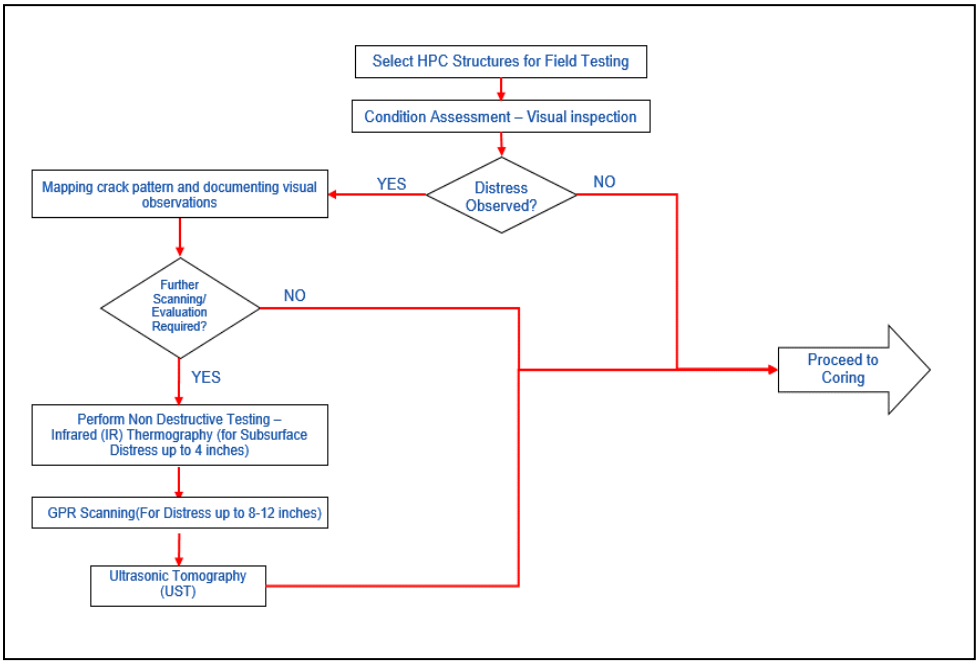

Figure 3-1: General Methodology of Field Survey and Coring

The field survey consisted of visual documentation of different types of distress observed on the bridge decks. Nature, type, and pattern of distress—along with any characteristic features observed—were documented for each type of distress by taking suitable measurements and photographs. Suitable NDT techniques, including ground penetrating radar (GPR) scanning, infrared (IR) thermography, and ultrasonic thermography (UST), were employed at selective locations to evaluate sub surface conditions of these decks. However, no subsurface discontinuities or delaminations were observed at any of the inspected bridge locations.

NDT techniques were also used to identify and obtain the cores from cracked sections for further laboratory visual examination and petrographic evaluation. GPR was also utilized to delineate rebar configurations and to selectively extract cores from areas on the bridge deck that showed no obvious surface distress or subsurface flaws such as delaminations and voids. The cores, typically 3 inches in diameter and 3-4 inches in length, were subject to laboratory testing. Specimen size correction factors were applied to ensure accurate lab results.

3.1.3 Laboratory Testing/Evaluation of Field Cores

The test methods used for laboratory evaluation of field cores are listed in Table 3-3.

Table 3-3: Concrete Property and Tests for Lab Core Evaluation

PROPERTY	PARAMETER
Hardened Properties	• Compressive Strength (ASTM C42) • MOE (ASTM C469)
Transport Properties	• BR (ASTM C1760) • SR (AASHTO T358)
Chloride Ion Analysis	• Water-Soluble Chloride Ion (ASTM C1218/TEX 617-J)
Microstructure	• Petrographic Examinations (ASTM C856)
Depth of carbonation	• International Union of Laboratories and Experts in Construction Materials, Systems and Structures RILEM CPC-18

Water-soluble chloride ion analysis was performed using ASTM 1218—*Standard Test Method for Water-Soluble Chloride in Mortar and Concrete*—by following a more exhaustive hot-water digestion technique per TEX 617-J method, *Determining Chloride in Concrete.* A water-soluble chloride ion test was preferred since the locations selected for the field visit reported using deicing salts on bridge decks to control ice and snow. These salts, which are essentially chloride salts of sodium, magnesium, and calcium, have chloride ions in readily penetrable form (water-soluble) through cracks, etc. High concentrations of chloride ions (above threshold limits) can initiate and/or accelerate corrosion of reinforcing steel, deteriorate concrete, shorten service life, and increase maintenance costs (*9*). Typically, it is estimated that between 50 and 75 percent of the total chloride content in the concrete can be water-soluble and influence the corrosion process (*10*). Of particular importance are chloride concentrations at the rebar depth, typically

2 to 4 inches below the surface. If the corrosion threshold is exceeded, especially at the rebar level, the presence of active corrosion is quite likely; the limits are shown in Table 3-4.

Table 3-4: Limits for Water-Soluble Chloride Ion Testing (ACI 318, 2001)

ITEM NO.	SOURCE	SECTION	TYPE	CHLORIDE LIMITS (MAX.) % BY WEIGHT OF CEMENT
1	*Building Code Requirements for Structural Concrete and Commentary*, ACI 318M-11	Chapter 4—Durability Requirements (Table R 4.3.1)	Reinforced concrete exposed to chloride in service	0.15

Depth of carbonation: The procedure involves the use of a phenolphthalein solution (diluted) as an indicator to measure the depth of carbonation. Phenolphthalein is typically used as a base indicator that, when in contact with or in the presence of a base, will turn fuchsia (above *p*H 9). Although no standard ASTM procedure exists for this test, the methodology is well documented in RILEM CPC-18.

3.1.4 Service Life Evaluation Using ConcreteWorks (Thermal Modeling)

ConcreteWorks software was used to perform concrete thermal analysis and study the service life of concrete. An attempt was made to study the early-age behavior and performance of HPC mix designs for each bridge deck by simulating maximum deck temperature profiles for 7 days after the placement:

- Inputs on member dimensions, shape, mixture proportions, mixture properties, and construction inputs were obtained from plan drawings, mix designs, and petrographic evaluations. Material properties and construction inputs were additionally obtained from TxDOT standard manuals.
- General inputs on placement time and date of construction were obtained from batch tickets (wherever available).
- Environmental inputs on air temperature, wind speed, and ambient RH for 7 days after placement were obtained from the National Climatic Data Center (NCDC) database at the closest airport location (*11*).
- Analysis was run generally for three standard times of day at 6-hour intervals (6 am., 12 pm & 6 pm) and at placement time (if the batch tickets were available).

3.2 Evaluation of HPC Mixtures—Amarillo, Texas

Five bridge decks were selected for field survey in Amarillo, Texas. Table 3-5 summarizes general information for each of the five bridge decks. All five bridges are new construction, with three of them built in 2016, one in 2014, and one in 2009.

The bridge deck system for Bridges #2, #3, and #4 consists of partial-depth, precast concrete panels that span between the top flanges of adjacent steel or concrete beams. The CIP deck placed over the beams and panels forms a composite system and is 8.5 inches at full thickness. Bridge #1 is designed as a 3-span continuous plate girder bridge consisting of stay-in-place metal deck forms (PMDF) at tension flange sections and precast panels at remaining sections. Bridge Deck #5 is a concrete box beam bridge consisting of precast, prestressed concrete beams that are placed next to each other, and the adjacent units generally are connected by longitudinal grouted shear keys. The concrete mix design used for each bridge deck was Class S HPC (TxDOT, 2014 specification) per Item 421. Table 3-6 summarizes the mix design used for each bridge location. Mix design Option 5 (i.e., 29 percent Class C ash + 6 percent SF) was used comprising 516–541 lb/cy cementitious content, design 0.42 w/cm and 4000 psi compressive strength at 28 days. Based on the available truck tickets, the actual w/cm was found to be 0.35–0.38. The use of corrosion inhibitor, fibers, air-entraining admixtures (AEAs), and either Grade 60 dual-coated (epoxy and zinc) or epoxy-coated reinforcing steel was reported.

Table 3-5: Location, Deck Thickness, and Reinforcement Details of Five Selected Bridge Decks, Amarillo, TX

NO	STRUCTURE ID AND LOCATION	YEAR OF CONST.	TYPE OF STRUCTURE AND SUPERSTRUCTURE	REINFORCEMENT TYPE AND DETAILS	DECK THICKNESS DESIGN COVER FOR REINFORCEMENT	BRIDGE INSPECTION RATING (MOST RECENT, YEAR)
1	04-191-2635-02-087 Route: SLP 335 WB Feature Crossed: BNSF RR/Frontage Rd.	2016	3-span continuous weathering steel plate girder Panel type: Galvanized stay-in-place PMDF forms (tension flange area) and 4-inch PCP precast bridge deck panels	Dual-coated (zinc and epoxy) reinforcing steel (Grade 60)	8.5 inches Top: 2.5 inches Bottom: 1.25inches	Bridge not open to traffic at time of inspection (2017)
2	04-191-2635-02-084 Route: SLP 335 (WB) Feature Crossed: Georgia St.	2016	3-simple-span prestressed concrete girder bridge on concrete supports Panel type: Typ., 4-inch PCP precast bridge deck panels	Epoxy-coated reinforcing steel (Grade 60)	8.5 inches Top: 2.5 inches Bottom: 1.25 inches	Bridge not open to traffic at time of inspection (2017)
3	04-191-2635-02-087 Route: IH 27/IH 40 Ramp Connection; IH 27 Potter County	2016	Simple-span prestress concrete Tx54 I-Girder Panel Type: N/A	Epoxy-coated reinforcing steel (Grade 60)	8.5 inches N/A	Bridge not open to traffic at time of inspection (2017)
4	04-191-0168-09-158 Route: FM 2219 Feature Crossed: IH 27	2009	4-simple-span prestress concrete beam unit (Type C) on concrete bent columns panel type: Typ., 4-inch PCP precast bridge deck panels	Epoxy-coated reinforcing steel (Grade 60)	8.5 inches Top: 2.5 inches Bottom: 1.25 inches	2016 Report Deck—7 Superstructure—7
5	04-191-0168-09-168 Route: CR214 (Buff Stadium) Feature Crossed: US 60/87	2014	2-span prestressed concrete box beam bridge on concrete bents. No panels	Epoxy-coated reinforcing steel (Grade 60)	5 inches (min.) Top: 2.5 inches	2016 Report Deck—6 Superstructure—8

Note: N/A = Not Applicable; n/a = not available.

Table 3-6: Concrete Mix Design, Class S HPC (for Cast-in-Place Bridge Deck)

PARAMETER	BRIDGE 1	BRIDGE 2	BRIDGE 3	BRIDGE 4	BRIDGE 5
Project Details/ Project ID	2635-02-028	2635-02-022	0275-01-166	0168-09-107	SP 0421-035
Design compressive strength (psi)	4000	4000	4000	4000	4000
Mix design spec year	2014	2004	2014	2004	2004
Cement content, lb/cy	352	352	352	333	480
FA, Class (F/ C), lb/cy	157 (Class C)	157 (Class C)	157 (Class C)	165 (Class C)	N/A
SF/Ultrafine Fly Ash (UFFA), lb/cy	32 (SF)	33 (UFFA)	32 (SF)	32 (SF)	36 (SF)
W/(C+M) (design max.)	0.42	0.44	0.45	0.43	0.44
Sand, lb/cy	1175	1172	1222	1431	1363
Gravel, lb/cy	1952	1952	1952	1850	1827
AEA (yes/no)	✓	✓	✓	✓	✓
Water reducer (Type A) fl. oz./cwt	5	5	5	4	10
High-range water reducer (Type F) fl. oz/cwt	7	8	7	-	-
Corrosion inhibitor	✓	✓	✓	✓	✓
Fibers	✓	✓	✓	-	✓
W/CM from truck tickets and other information	0.36–0.38 Retarding admixture was added during placement	0.38–0.41	0.36–0.40	0.35–0.37	Truck tickets were not available

Note: N/A = Not Applicable; n/a = not available.

3.2.1 Visual Observations

The summary of visual observations on crack pattern and nature of crack propagation is presented is presented in Figure 3-2. Full-depth transverse cracks were the most predominant and main type of cracking observed at all five bridge decks. The crack spacing varied from 3 ft–10 ft, with most commonly around ~6–8 ft. Transverse cracks typically were noted to be ~0.3 to 0.4 mm wide at the surface and extended across the full width of the deck. Cores obtained at transverse crack locations and on top of rebar showed crack penetration to the level of steel. However, no evidence of corrosion was noted on any of the epoxy-coated reinforcing steel. Prominent longitudinal cracks with ~0.4–0.5 mm width were observed throughout the length and along the centerline of Bridge Deck #5. Minor longitudinal cracks were also noted intermittently along certain spans in the driving lane spaced 4–6 ft apart at Bridge Deck #5. The isolated occurrence of longitudinal cracking was also noted along certain shoulder and driving lane sections at Bridge Decks #1, #3, and #4.

Transverse cracks were the predominant type observed among all bridge decks. Contributing factors like possible high rate of evaporation, low w/cm ratio of these mixtures at placement, and susceptibility to early-age shrinkage cracking was discussed in previous sections. Plastic shrinkage cracks were noted on all bridge decks, with varying degrees of severity. Cores obtained at transverse crack locations and on top of rebar showed crack propagation to the level of rebar but no signs of rebar corrosion at any bridge location. Bridge deck systems with partial depth precast concrete panels and CIP topping demonstrated longitudinal cracks along certain sections which appeared to coincide with girder locations (Bridge Deck #1 and #3), and at Bridge Deck #5, longitudinal cracks were observed at intervals that appeared to match with the supporting box beam girder spacing. At Bridge Deck #4, transverse crack spacing was noted to be similar to panel precast panel lengths. Reduction in deck stiffness over the girders, insufficient support of panels on beams, and shrinkage of the CIP concrete being restrained by the precast concrete panels or differential settlements typically contributes to the nature of longitudinal and transverse cracks observed at these locations, as discussed previously in the literature overview.

According to a study by (*12*) a zigzag (jump) crack pattern can arise from transverse shrinkage cracks propagating with time (due to temperature cycles and DS) that meet between adjacent girders through a jump crack (fine longitudinal crack) from one reinforcing bar to the other, thereby connecting the two adjacent transverse cracks, which was similar in nature to the jump crack observed on Bridge Deck #1.

Transverse crack noted at Bridge Deck #1

Full depth transverse crack propagation on core from Bridge Deck #3

Typ. longitudinal crack propagation on Bridge Deck #4

Longitudinal crack propagation for full length along centerline of the Bridge Deck #5

Jump zigzag-type crack propagation on Bridge Deck #1

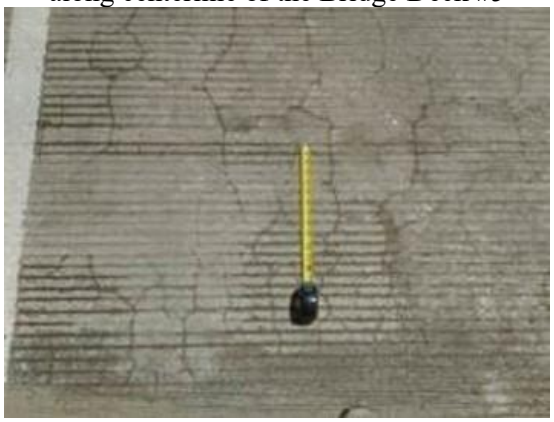

Typical location of map crack pattern on Bridge Deck #2

Figure 3-2: Field Observations from HPC Bridge Decks—Amarillo, Texas

3.2.2 Laboratory Testing of Field Cores

Results from laboratory testing of field cores are shown in Table 3-7 and Figure 3-3. Compressive strength test results generally ranged between 6000–10,000 psi for a design strength of 4000 psi. Static MOE as measured in accordance with ASTM C 469. The mix design for Deck #5 consisted only of cement and SF. Cores tested from this bridge showed relatively low resistivity values compared to cores from the other bridge decks. A relatively higher depth of carbonation was observed at this bridge deck.

Table 3-7: Results from Laboratory Evaluation of Field Cores, Amarillo, Texas

BRIDGE ID	AVG. COMPRESSIVE STRENGTH (PSI)	AVG. STATIC MOE (X 10^6 PSI, MEASURED)	AVG. BULK ELECTRICAL RESISTIVITY (KOHM-CM)	DEPTH OF CARBONATION (MM)
	ASTM C42	ASTM C469	ASTM C1760	Rilem CPC-18, Mod ASTM D698
#1	10042	5.91	167.32	3
#3	9544	5.16	159.50	2
#4	6062	3.87	316.80	3
#5	6101	4.36	55.33	7

Figure 3-4 shows the measured water-soluble chloride ions up to a depth of 1 inch exceeded the threshold value of 0.15 but fell below the threshold value thereafter (i.e., satisfied below threshold at steel depth).

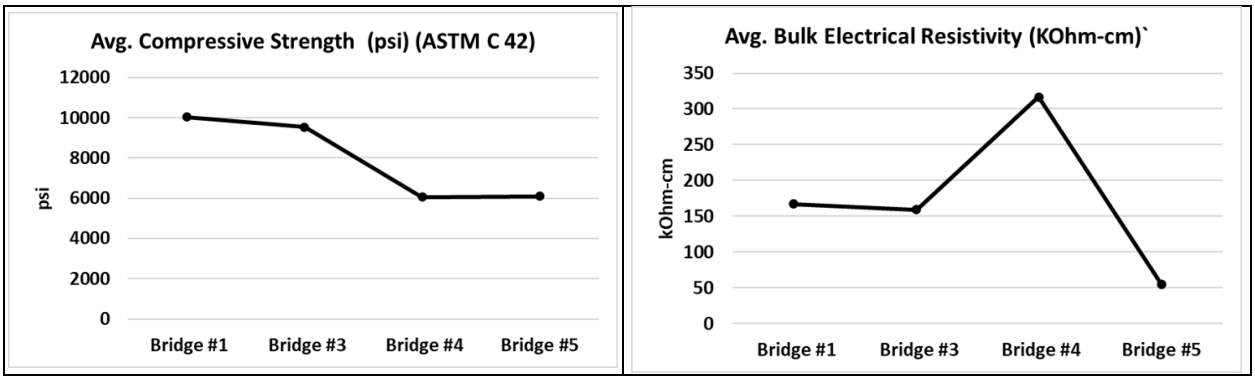

Compression Test Results | Resistivity Test Results

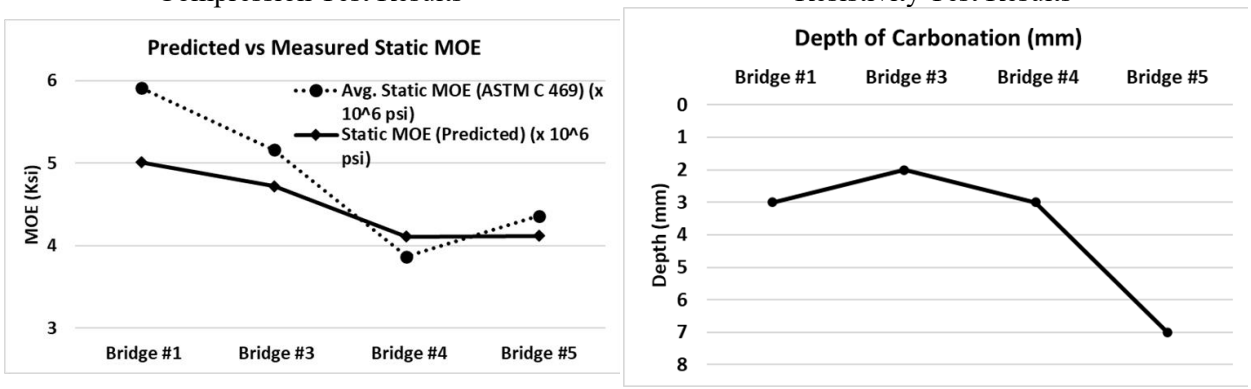

MOE Test Results | Depth of Carbonation Results

Figure 3-3: Laboratory Test Results of Field Cores—Amarillo, Texas

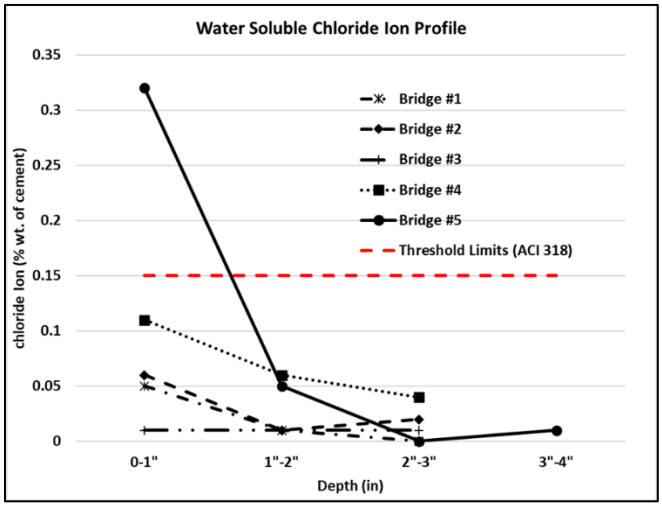

Figure 3-4: Water-Soluble Chloride Ion Concentration from Cores—Amarillo, Texas

Results from a petrographic analysis for bridge deck cores are shown in Figure 3-5. The presence of typical shrinkage cracks, that is, cracks passing through the aggregate–paste (a–p) interfaces and cement paste matrix (CPM) was clearly observed in the samples from Bridge Decks #1, 2, and 4. The relatively porous nature of the interfacial transition zones and sometimes localized fine air void concentration along the aggregate-paste interfaces (Deck #4) were found to be the reason for easy shrinkage crack propagation. These observations support the early-age crack

formation when concrete has yet to gain sufficient strength. The concrete core from Bridge Deck #5 showed porous microstructure and the presence of a large number of interconnected pores consistent with low measured resistivity values. The presence of ASR siliceous components was observed.

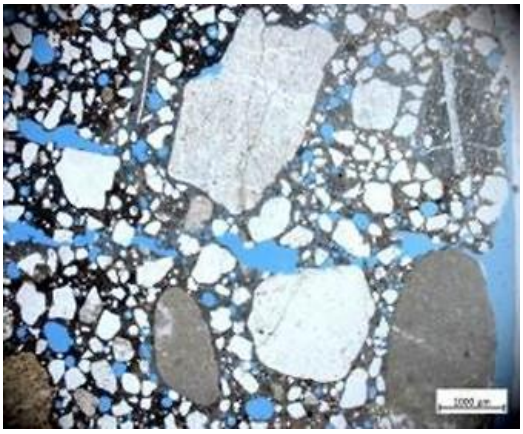

High porosity, large number of interconnected pores noted in cores from Deck #5, Plane Polarized Light (PPL).

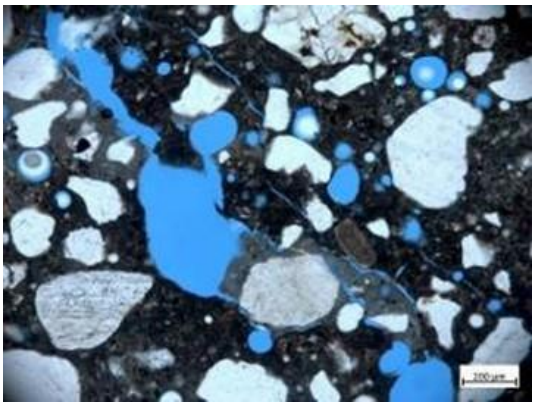

Typ. shrinkage crack propagation noted in cores from Deck #4, PPL.

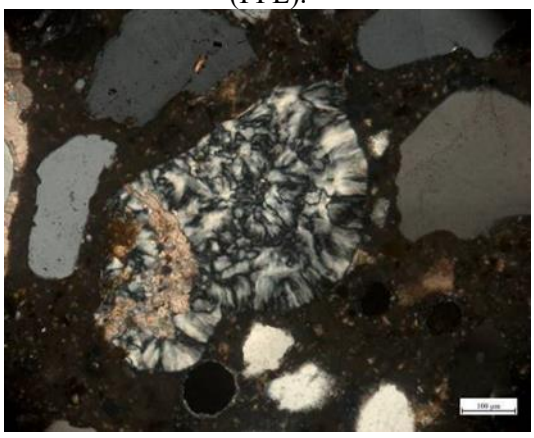

Highly reactive siliceous impurity in coarse aggregate from Bridge #3, Cross Polarized Light (CPL).

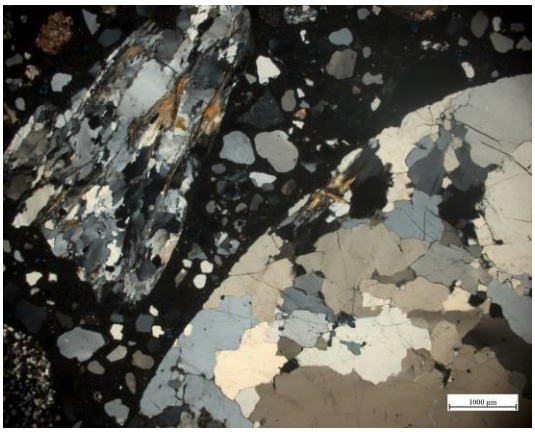

Reactive coarse aggregate (strained quartz) in Bridge Deck #4, CPL

Figure 3-5: Petrographic Analysis—Cores from Amarillo, Texas

3.2.3 ConcreteWorks Modeling

ConcreteWorks' thermal model was used to predict the early-age cracking probability for Bridge Decks #1–4 using the date and time (mostly 3–7 am) of placement from the truck tickets, as shown in Table 3-8. The truck tickets were not available for Bridge Deck #5. Historical weather data were obtained for the specified period from the NCDC database. Additionally, a simulation was also performed for 6 am, 12 pm, and 6 pm placement to detect the lowest temperature differential profile suitable for concrete placement. Although the design w/cm was 0.42–0.44, the actual w/cm was found to be 0.36–0.40 based on truck tickets. Measured slump and air often varied but were within tolerance limits.

Table 3-8: Comparison of Results from ConcreteWorks, Amarillo, TX

BRIDGE ID#	4 AM (TIMING ON TRUCK TICKET)	6 AM	12 PM	6 PM
	Max. Temp Difference (°F)			
Bridge 1 (Nov 23, 2016)	32	18	32	11
Bridge 2 (September 08, 2016)	16	11	20	4
Bridge 3 (October 18, 2016)	11 (Pour at 10 am)	11	25	11
Bridge 4 (Aug 10, 2009)	18	14	15	9

The thermal simulation predicted a medium to very high risk of cracking within the first few weeks after concrete placement, particularly for pours conducted from early morning to noon (4 am to 12 pm). This heightened risk is due to the hydration process heating the concrete around the same time as the day's peak ambient temperatures, thereby exacerbating the temperature increase within the deck. The simulation highlighted that the peak hydration temperature, occurring roughly 18 hours post-placement, aligns with cooler evening or night air temperatures, resulting in the largest temperature differential. Conversely, pours done in the evening or night exhibit a smaller temperature difference and a slower heat development rate, as confirmed by the simulation outcomes.

3.3 Evaluation of HPC Mixtures—Lubbock, Texas

Two bridge decks were selected for the field survey. Table 3-9 summarizes general information for each of the two bridge decks. Bridge #6 was originally built in 1966, but a recent deck replacement (addition) project was undertaken in 2008, while Bridge #7 was built in 2010.

Bridge #6 is a 4-span continuous variable depth slab bridge with a CIP deck measuring 18 inches at the thickest cross section. Reinforcing steel is not epoxy-coated. Bridge #7 is a simple-span prestressed concrete beam bridge with prestressed concrete I Girder units. Reinforcement is epoxy-coated at this location. The concrete mix design used for each bridge deck was Class S HPC (TxDOT 2004 spec), Table 3-10Table 3-10 summarizes the mix design used at each of the bridge locations. A notable difference between the two mix designs is that Bridge Deck #6 used Class F fly ash, while Bridge #7 had Class C fly ash in mix design with UFFA.

Table 3-9: Location and Bridge Deck Details, Lubbock, Texas

NO #	STRUCTURE ID AND LOCATION	YEAR OF CONST.	TYPE OF STRUCTURE AND SUPERSTRUCTURE	REINFORCEMENT TYPE AND DETAILS	DECK THICKNESS DESIGN COVER FOR REINFORCE-MENT	BRIDGE INSPECTION RATING (MOST RECENT, YEAR)
6	05-140-0052-05-017 Route: US 84 WB Feature Crossed: US 385 Littlefield, TX	1966; Recent deck replacement/addition in 2008	4-span continuous variable depth slab bridge. No panels	Reinforcing steel is not epoxy coated.	Cast-in-place deck is 18 inches at the thickest cross section N/A	2017 Deck–7 and Superstructure –7.
7	05-152-0783-02-104 Route: Loop 289 SB Feature Crossed: FM 2255 (4th St.) Lubbock, TX.	2010	3-simple-span prestressed concrete girder bridge on concrete supports Superstructure: Type TX46 Girder	Epoxy-coated reinforcing steel (Grade 60)	8.5 inches Top: 2.5 inches Bottom: 1.25 inches	2015 Deck–7 and Superstructure –8

Table 3-10: Concrete Mix Design, Class S HPC, Lubbock, Texas

PARAMETER	BRIDGE 6	BRIDGE 7
Controlling CSJ	0052-05-037	0783-02-064
Design compressive strength (psi)	4000	4000
Mix design spec year (mix design option)	2004 (1)	2004
Cement content, pcy	348	364
F/C, pcy	188 (Class F)	164(Class C)
SF/UFFA, pcy	-	34 (UFFA)
W/(C+M) (Design max.)	0.45	0.44
Gravel, pcy	1863	1844
Sand, pcy	1292	1274
AEA (Yes/No)	✓	✓
Water reducer (Type A) fl. oz./cwt	6	6
Water reducing reducer (Type B) fl. oz./cwt	1	-
Corrosion inhibitor	-	-
Fibers	✓	✓

3.3.1 Visual Observations

A summary of visual observations on crack pattern and propagation is presented below.

Figure 3-6 shows transverse cracking was the most common and main type of cracking observed at Bridge Deck #6 in the middle third section of each span, with close spacing (2–4 ft). Most of the transverse cracks measured ~0.3 to 0.5 mm wide at the surface and extended full depth. On Bridge #6, cores obtained at transverse crack locations and on top of rebar showed a very fine crack penetration till the level of steel; no corrosion product was noted on rebar at this location. Minor transverse cracking was observed at Bridge Deck #7, spaced 6–8 ft in Span 2. Fine transverse cracks, as noted, also extended parallel to skew joint locations.

A prominent longitudinal crack ran along the centerline (and wheel path of the drive lane) of Bridge Deck #6. Cracks typically extended throughout the length of the bridge deck. Fine and minor longitudinal cracks were also noted along the shoulder at this location.

Diagonal cracks were a common distress type observed on both the bridges' decks. On Bridge Deck #6, these cracks were observed to start along joint locations and propagate along an oblique angle toward the rail end of the deck. A core obtained along this crack showed crack penetration to the full depth of the core. At Bridge Deck #7, which was noted to be a skew bridge, diagonal cracks were started at a right angle to the direction of the armor joint and proceeded toward acute corners at abutment location. These cracks were uniformly spaced at 4–6 ft at one end and 8–10 ft at the opposite end. A core obtained on an oblique crack showed crack penetration to almost full depth.

Transverse Cracks on Bridge Deck #6

Transverse Crack Propagation on Bridge Deck #7

Longitudinal Crack on Bridge Deck #6

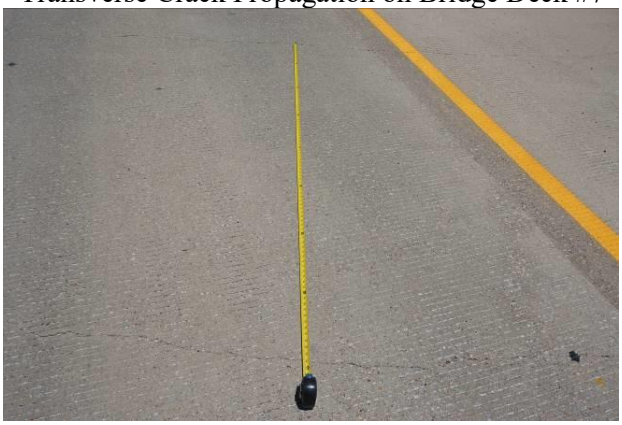

Diagonal Crack Propagation Bridge Deck #7

Map Crack Pattern on Bridge Deck #7

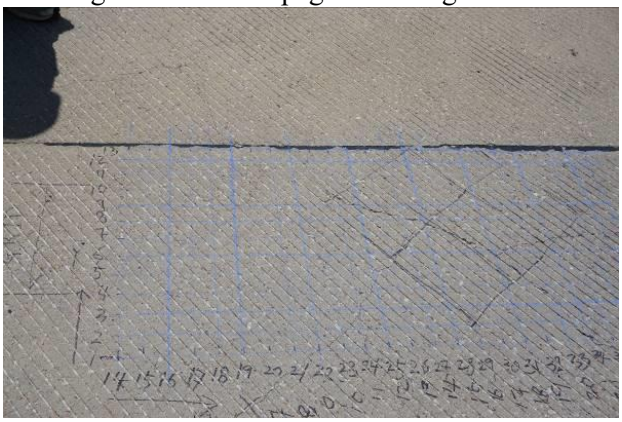

Diagonal Crack at Skew Location Bridge Deck #7

Figure 3-6: Field Observations from Bridge Decks—Lubbock, Texas

Visual observation shows the main type of cracking to be transverse, with varying degrees of severity. The width and type of crack propagation points toward a possible early-age shrinking phenomenon; for instance, on Bridge Deck #7, cracks typically aligned along transverse reinforcing bars. Usually, in bridge decks with a skew, diagonal cracking occurs more in the corner areas because of restraint (torsional forces in acute corners) provided by the abutments and piers. This phenomenon could lead to the type of diagonal cracking noted on Bridge Deck #7. In straight bridges, these cracks could be related to the restraints for concrete shrinkage or to

external loads, as discussed previously. Cores obtained at the oblique crack revealed a crack passing through the aggregate, indicative of the nonshrinking nature of these cracks. Evidence of plastic shrinkage cracking was observed on both the bridge decks with varying degrees of severity; a high intensity of very fine random (or map) meandering patterns of cracks was particularly noted on Bridge Deck #6.

3.3.2 Laboratory Testing of Field Cores

Results from laboratory evaluation of field cores are shown in Table 3-11, Figure 3-7, and Figure 3-8. Compressive strength test results generally ranged between 6000–7000 psi for a 28-day design strength of 4000 psi. The static MOE as measured using ASTM C 469 was closer to values predicted using the ACI equations, and the overall trend differs with compressive strength. Limitations on taking cores with the required dimensions for testing may have caused some variation in results.

Table 3-11: Laboratory Evaluation of Cores, Lubbock, Texas

BRIDGE ID	AVG. COMPRESSIVE STRENGTH (PSI)	AVG. STATIC MOE (X 10^6 PSI, MEASURED)	STATIC MOE (X 10^6 PSI)	AVG. BULK ELECTRICAL RESISTIVITY (KOHM-CM)	DEPTH OF CARBONATION (MM)
	ASTM C42	ASTM C469	Calculated	ASTM C1760	Rilem CPC-18, Mod ASTM D698
#6	10042	5.71	4.21	390.3	5
#7	-	5.24	4.47	143.9	15

A relatively higher distribution of fibers was noted in cores obtained from Bridge Deck #7, which is consistent with lower BR values and large depth of carbonated sections when tested with phenolphthalein. Testing for water-soluble chloride ions indicated higher chloride concentrations up to a depth of around 1 inch but lower concentrations at the rebar level than the threshold value.

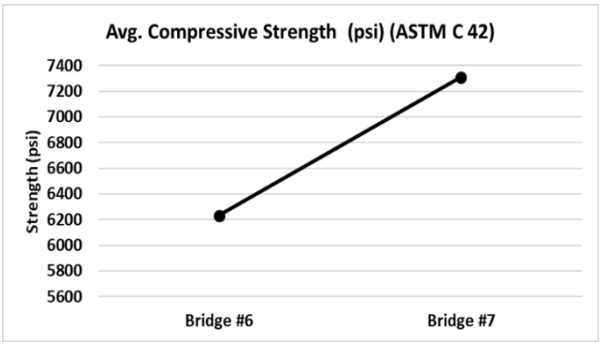

Compression Test Results

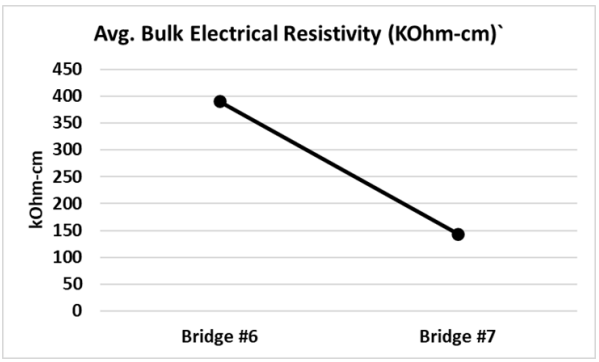

Resistivity Test Results

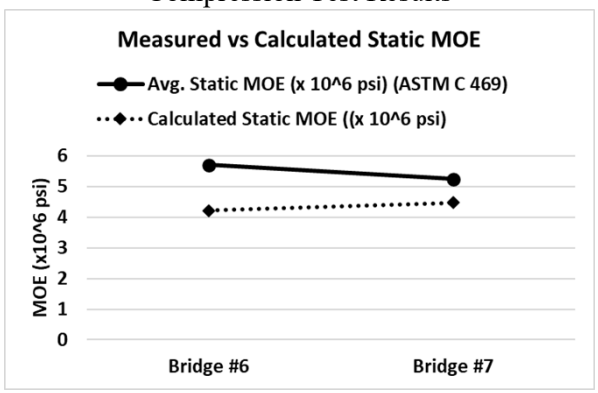

MOE Test Results

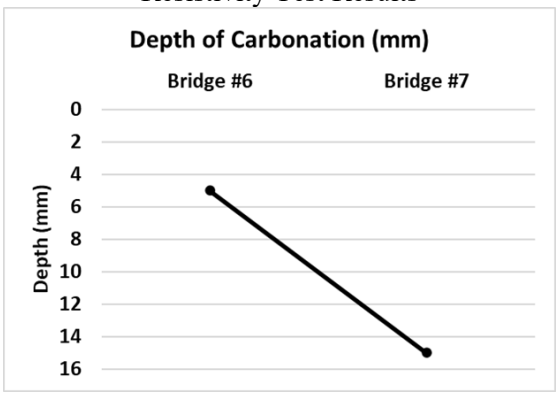

Depth of Carbonation Results

Figure 3-7: Laboratory Evaluation of Field Cores—Lubbock, Texas

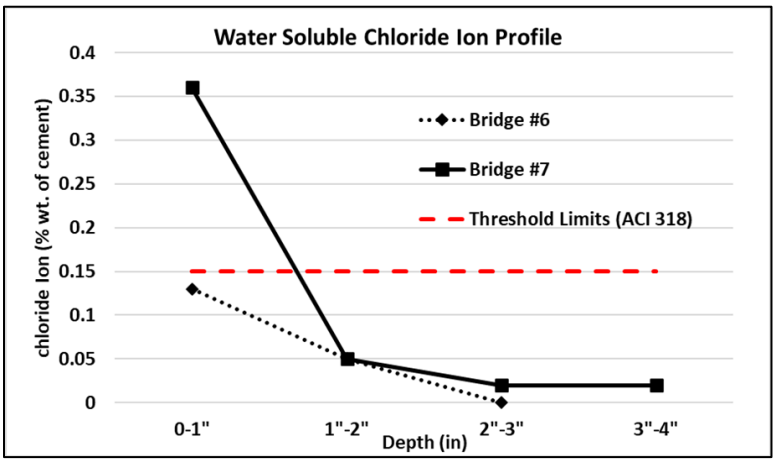

Figure 3-8: Water-Soluble Chloride Concentration—Cores (Lubbock, Texas)

Results from petrographic analysis for cores from bridge decks are selectively presented in Figure 3-9. The presence of intense carbonation along the depth of the entire thin section was observed in the concrete from Bridge Deck #7. This finding is consistent with results noted from phenolphthalein testing for depth of carbonation. The porous nature of the paste (high blue dye impregnation) was commonly observed, which possibly suggests the use of a relatively higher w/cm ratio (higher than the designed w/cm) in the deck mixes. The presence of ASR siliceous components was observed within the aggregates used for making deck concrete. For example,

the prominent presence of siliceous (amorphous) impurities was included with the limestone coarse aggregate particles. In Bridge Deck #6, the presence of cracks passing through a hard quartzite aggregate filled with some ASR gel-like deposits was observed. Further testing is required to confirm the presence of ASR.

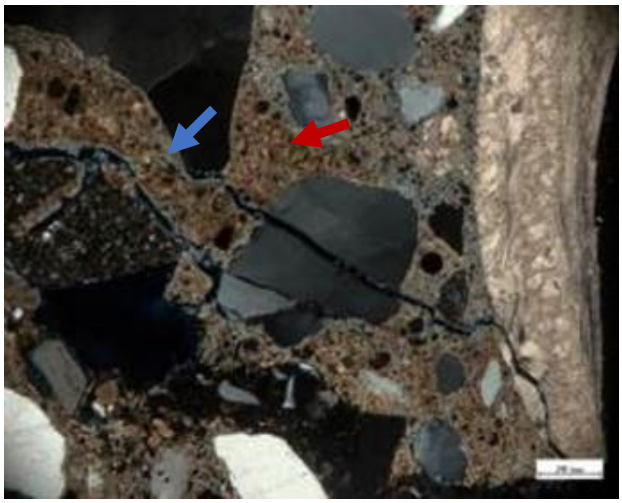

Intense carbonation (red arrows) and crack propagation (blue arrows), Bridge Deck #6, CPL.

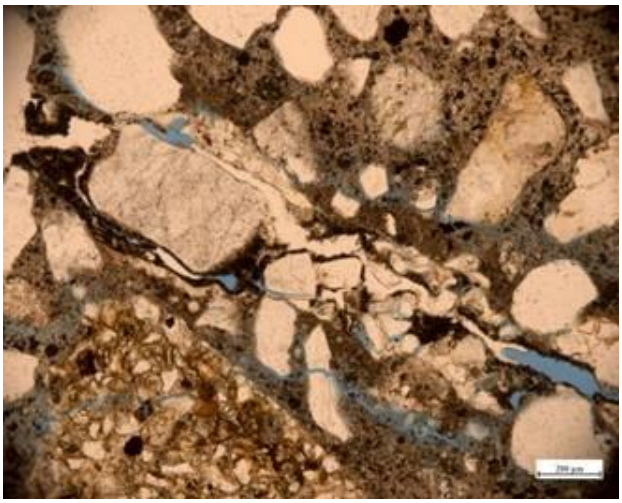

Cracks passing through the aggregate, CPM, and along the a–p interfaces with presence of ASR gel like products, PPL.

Figure 3-9: Petrographic Observations of Cores from Lubbock, Texas

3.3.3 ConcreteWorks Modeling

Accurate records of date (or month) and time of concrete placement, such as truck tickets or batch plant tickets, were not available for both Bridges #6 and #7. Thus, an accurate study of early-age behavior could not be performed.

A generic thermal simulation was performed for Bridge Deck #7 using climatic data from 2010 for March, June, and September to assess the relative temperature differentials that could develop in a bridge deck (Table 3-12). For each month, historical weather data were obtained for the specified period from the NCDC database, and peak values were used for analysis. Overall, the lowest temperature difference was noted for March in comparison to September and June; June recorded the highest. The probability of cracking was also noted to be lower in March than in September and June. Evening–night placement was seen to be generally favorable over daytime placement (6 am to 12 pm) except in September.

Table 3-12: Results from ConcreteWorks, Lubbock, Texas

LUBBOCK	6 AM	12 PM	6 PM
	Max. temp Difference (°F)		
March	9	20	8
June	26	15	7
September	14	8	15

3.4 Evaluation of HPC Mixtures—Galveston, Texas

Two bridge decks were selected for field survey, both constructed in 2006. Table 3-13 summarizes general information for each of the two bridge decks.

Bridge Deck #8 is a concrete box beam bridge consisting of precast, prestressed concrete beams spaced 5 ft apart. Bridge Deck #9 consists of both a post-tensioned concrete box and girder type superstructure, but our limits of field survey covered 3 spans with superstructure type PS concrete girder Type VI. Bridge #9 was reported to be a full-depth precast concrete deck system, with panels spanning transversely across several bridge beams. The panels generally are pre-tensioned in the transverse direction and may be post-tensioned in the longitudinal direction.

Table 3-13: Location and Bridge Deck Details, Galveston, Texas

BRIDGE NO.	STRUCTURE ID AND LOCATION	YEAR OF CONST.	TYPE OF STRUCTURE AND SUPERSTRUCTURE	REINFORCEMENT TYPE AND DETAILS	BRIDGE INSPECTION RATING (MOST RECENT YEAR)
8	12-085-0367-06-033 Route: Galveston Ferry Landing Feature Crossed: Galveston Bay	2006	5-simple-span prestress concrete slab beam bridge with 1 lift span	No epoxy-coated reinforcing steel (site observation)	2016 Deck–7 and Superstructure–7.
9	12-085-0500-01-373 Route: IH 45 NB Feature Crossed: Galveston Bay	2006	One 3-span continuous post-tensioned concrete box girder with 59 simple prestress concrete beam approach spans	No epoxy-coated reinforcing steel (site observation)	2016 Deck–6 and Superstructure–8.

The concrete mix design used for each bridge deck was Class S HPC (TxDOT 2004 specification) summarizes the mix design used at each of the bridge locations. Mix design Option #1 was seen to be the most common mix design practice, with typically ~25 percent–33 percent Class F FA. The coarse aggregate type was noted to be limestone. Visual observation at the core location showed rebar was not epoxy coated at Bridge Deck #8.

Table 3-14: Concrete Mix Design, Class S HPC, Galveston, Texas

PARAMETER	BRIDGE 8	BRIDGE 9
Controlling CSJ	0367-06-054	0050-01-117
Design Compressive Strength (psi)	4000	4000
Mix Design Spec Year	1993	1993
Cement Content, lb/cy	458	409
F/C, lb/cy	119.78 (Class F, ~ 25%)	160 (Class F, ~33%)
W/(C+M) (Design max.)	0.42	0.46
Gravel, pcy	1971	1870
Sand, pcy	1366	1067
AEA (Yes/No)	-	✓
Set Retarder (Type B) fl. oz./cwt	2	6
High-Range Water Reducing Reducer (Type F) fl. oz./cwt	8	1
Corrosion Inhibitor	✓	-
Water Reducer (Type A) fl. oz./cwt	-	4

3.4.1 Visual Observations

Visual observation shows the main type of cracking to be transverse in nature, spaced at varying intervals with varying degrees of severity, as shown in Figure 3-10.

With varying intensities, transverse cracking was the most common and main type of cracking observed at all bridge decks. On Bridge #8, a pair of transverse cracks was also noted on either side of joint locations (on top of bent) spaced ~ 27 inches apart. Transverse cracks spaced 1–4 ft apart were noted at other spans of this bridge deck. Very fine transverse cracks (~0.2 mm wide) were noted uniformly across the width of deck and regularly spaced at 8 ft intervals throughout the length of bridge deck inspected. Cores obtained at transverse crack locations and on top of rebar showed crack penetration till the level of steel. Evidence of moderate–severe corrosion was noted at steel rebar location on Bridge Deck #8. A similar core obtained on top of transverse prestressed cable also showed very fine crack penetration to the level of the prestressing tendon, and minor corrosion product was noted at the location of the tendon. A set of notably wider transverse cracks on Bridge Deck #8 appeared to coincide with edges of bent cap underneath indicative structural nature, possibly arising from differential movements or shrinkage. According to (*13*), longitudinal cracking in spread box beam bridges likely occurred because of a concentration of longitudinal shear forces at the edges of the beams, as evidenced by spacing of cracks matching the beam spacing.

Longitudinal cracks were noted along the wheel path in drive lanes at both bridge decks, but was most predominant at Bridge Deck #9, occurring throughout the length of the bridge surveyed. Minor longitudinal cracks were observed on Bridge Deck #8 at a single-span location and spaced at 8 ft intervals. Core obtained on a longitudinal crack at both bridge decks showed crack propagation to the level of steel. Isolated occurrences of map (Pattern) cracking and delamination

was noted only on Bridge Deck #8, with the crack extending just a few inches beneath the surface at the map crack area.

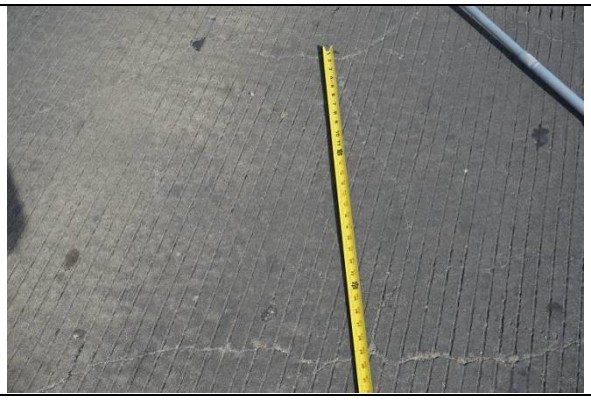

Transverse cracks on Bridge Deck #8

Core on top of rebar (shows corrosion) at transverse crack location on Bridge Deck #8

Longitudinal crack on Bridge Deck #9

Map crack pattern on Bridge Deck #9

Figure 3-10: Field Evaluation, Galveston, Texas

3.4.2 Laboratory Testing of Field Cores

Results from laboratory evaluation of field cores are presented in Table 3-15, Figure 3-11, and Figure 3-12. Compressive strength test results generally ranged between 6000–7000 psi for a 28-day design strength of 4000 psi. Static MOE, as measured in accordance with ASTM C 469, was closer to values predicted using the ACI equations, but the overall trend differs in relation to compressive strength.

Table 3-15: Laboratory Evaluation of Cores, Galveston, Texas

BRIDGE ID	AVG. COMPRESSIVE STRENGTH (PSI)	AVG. STATIC MOE (X 10^6 PSI, MEASURED)	STATIC MOE (X 10^6 PSI)	AVG. BULK ELECTRICAL RESISTIVITY (KOHM-CM)	DEPTH OF CARBONATION (MM)
	ASTM C42	ASTM C469	Calculated	ASTM C1760	Rilem CPC-18, Mod ASTM D698
#8	7631	5.25	4.49	363.54	3
#9	8085	4.74	4.59	283.81	5

Testing for water-soluble chloride ions indicated higher chloride concentrations than the threshold value up to a depth of around 2 inches for Bridge Deck #8 (located in the splash zone). Interestingly, corrosion of the steel rebars (black steel without any protection measures) on the core locations was clearly observed. However, chloride concentrations remained below the threshold value at all the depths for Bridge #9.

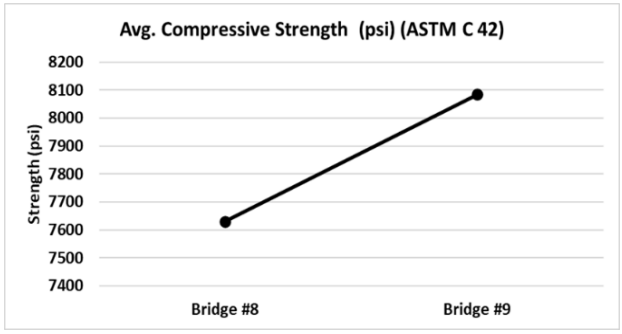

Compression Test Results

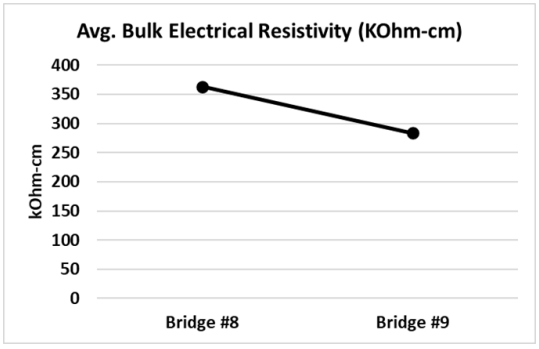

Resistivity Test Results

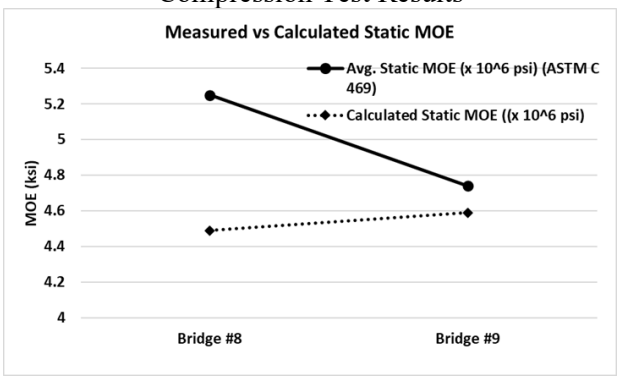

MOE Test Results

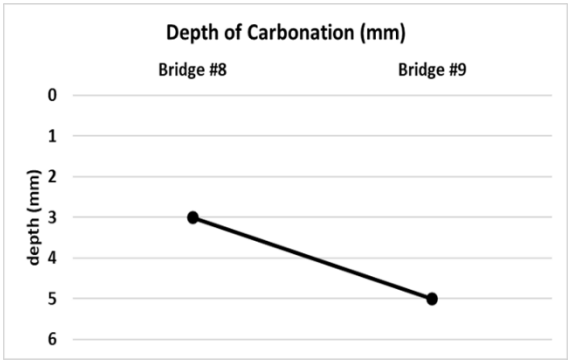

Depth of Carbonation Results

Figure 3-11: Laboratory Test results of Cores from Bridge Decks in Galveston, Texas

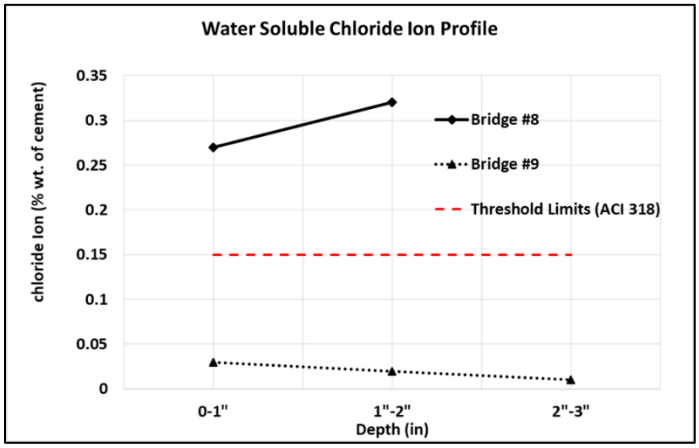

Figure 3-12: Water-Soluble Chloride Core Samples, Galveston, Texas

3.4.3 ConcreteWorks Modeling

Accurate records on the date (or month) and time of concrete placement, such as truck tickets or batch plant tickets, were not available for both Bridges #8 and #9. Thus, an accurate study of

early-age behavior could not be performed. A generic thermal simulation for the region was performed for the year 2006 in March, June, and September to assess the relative temperature differentials that could develop in a bridge deck. For each month, historical weather data were obtained for the specified period from the NCDC database, and peak values were used for analysis.

Analysis showed daily wind speeds and RH levels, in addition to peak temperatures of the day, play a key role in simulation. In 2006, an abstract consideration of seven peak (max., min.) temperatures of the selected months, peak wind speeds, and lowest RH levels showed concrete placement in September was noted to be favorable over March and June. High variation was noted in results and further timewise analysis was not performed. Given the lack of accurate placement time and date, no conclusions could be drawn about this location.

3.5 Recommendations—HPC Mix Evaluation

This chapter primarily focused on understanding material, environmental, and construction factors that contribute to various cracks observed during field surveys through NDT techniques, laboratory testing, and service life prediction models. Efforts were made to simulate and understand early-age cracking behavior involved with concrete placement at different locations, different exposure conditions, and varying seasons. In subsequent tasks, evaluation of trial mixtures using materials sourced from the districts, through innovative and newer techniques such as ring tests for shrinkage, SR, etc., to identify and establish limits for the identified performance characteristics. A combined approach of lab-based durability test results (ASR, sulfate, corrosion) and service life model prediction has been used to highlight the effectiveness and deficiencies of the current HPC options to ensure durability requirements in aggressive environments. Efforts have also been made to predict long-term durability performance (service life) for corrosion, F/T durability, and other key performance indicators. The focus was on understanding the performance of mix design's efficiency to reduce cracking tendency in concrete through identified characteristics in NCHRP Report 380 as well as NCHRP Synthesis 441.

CHAPTER 4: EVALUATE CONCRETE MIX DESIGNS DEVELOPED TO PROVIDE LONG-TERM PERFORMANCE OF BRIDGE DECK HPC

4.1 Objective

The main objective of this study was to develop performance specifications for HPC to ensure high performance in terms of durability. This chapter focuses on the formulation, testing, and durability evaluation of a wide variety of HPC mixtures. The specific objectives of this task were as follows:

- Formulate a wide variety of HPC mixtures after incorporating the suggested prescriptive requirements and performance characteristics identified and obtained from TxDOT's past project records.
- Evaluate durability of these HPC mix designs under the applicable exposure conditions, as identified in this project.
- Evaluate HPC mix performance using innovative and promising test methods, as recommended in this project.
- Recommend additional performance-based requirements based on the test results of the selected performance tests for all the tested mixtures to meet the durability demands (performance-based criteria) that match with the severity of exposure conditions.

4.2 Materials and Mix Designs

4.2.1 Materials and Characterization

4.2.1.1 Cementitious Materials

Type 1 Ordinary Portland Cement (OPC) (ASTM C 150), Class C and Class C FA (ASTM C 618), and silica fume (ASTM C 697) were used to prepare binary and ternary HPC mixtures evaluated in this study. Table 4-1 and Table 4-2 summarize the bulk oxide composition of cementitious materials used in this project, measured using X-ray fluorescence (XRF) and Quantitative X-ray diffraction (QXRD) methods.

Table 4-1: XRF Composition of Cementitious Materials

OXIDE COMPOSITION	TYPE I/II CEMENT		CLASS C FA		CLASS FFA		SF	
	Plant Reported	TTI Lab	Plant Reported	TTI Lab	Plant Reported	TTI Lab	Plant Reported	TTI Lab
CaO	64	63.41	27.28	26.33	13.28	13.98	0.42	0.02
SiO2	21.1	20.43	37.57	37.51	54.44	55.27	97.9	98.2
Al2O3	5.6	6.78	19.45	19.8	19.71	20.35	0.18	0.18
Fe2O3	1.9	2.05	5.7	5.13	4.65	4.70	0.07	0.07
SO3	3.8	3.72	1.8	2.12	0.62	0.69	0.17	0.23
MgO	1.1	1.13	5.5	5.45	2.67	2.82	0.12	0.15
Na2O	0.13	0.15	1.62	1.71	0.35	0.52	0.12	0.16
K2O	0.41	0.43	0.49	0.49	1	0.85	0.54	0.52
LOI %	1.8	1.9	0.53	0.57	0.37	0.37	0.48	0.27
Total	99.84	100	***99.94***	***99.11***	***97.09***	***99.55***	**100**	**99.8**
Na2Oeq	0.43	0.43	1.94	2.03	1.01	1.08	0.48	0.50
C3S	58	54.8	N/A					
C2S	12	20.18						
C3A	14	9.78						
C4AF	6	4.51						

Note: N/A = Not Applicable; n/a = not available.

The crystalline composition of cement was analyzed using the QXRD method coupled with Rietveld refinement. The diffraction patterns were collected using a tabletop X-ray diffractometer at 0.008 2θ step size, 10 seconds per step, and CuKα radiation. QXRD measurements were also performed to identify and quantify crystalline phases and determine the total amorphous content for the FA. Specimens for QXRD were prepared using the backloading technique to minimize preferred orientation. Scans were run from 7 to 70 degrees 2θ, at 0.02 degrees step size and at a counting time of 0.4 seconds per step, resulting in a total measurement time of about 36 minutes per scan. Rietveld-based quantitative phase analysis was performed using TOPAS 5.0 software. The amorphous content of each FA was determined using the partial or no known crystal structure (PONKCS) method.

Table 4-2: QXRD of Cementitious Materials

CEMENT (TYPE I/II)		CLASS C FA		CLASS F FA	
Phase	Mass %	Phase	Mass %	Phase	Mass %
Arcanite	0.27	Amorphous	43.23	Amorphous	65.74
Bassanite	2.06	Anhydrite	1.44	Akermanite	1.36
C3S M1	9.11	Bassanite	1.16	Anhydrite	0.28
C3S M3	45.69	C3A	10.12	Bassanite	1.58
C2S alpha HT	0.89	C3S	2.57	Calcite	0.85
C2S_beta	19.32	Ca-Langbeinite	3.84	Gehlenite	1.39
C3A_cubic	9.59	Calcite	3.09	Hematite	1.5
C3A_orthorhombic	0.19	Lime	0.69	Magnetite	1.64
C4AF	4.51	Gehlenite	3.77	Merwinite	3.22
Calcite	0.97	Hematite	2.41	Mullite	6.59
Dolomite	0.48	Merwinite	10.89	Quartz	13.49
Gypsum	2.88	Mullite	3.64	Thenardite	0.37
Lime	0.23	Periclase	2.11	Arcanite	0.69
Periclase	0.47	Quartz	6.59	Syngenite	0.49
Portlandite	1.96	Thenardite	1.98		
Quartz	0.29	Arcanite	0.6		
Syngenite	0.49				
Thenardite	0.61				

4.2.1.2 Aggregates

In the current research, HPC mixtures were prepared using siliceous river sand as fine aggregates and #57 (1-inch MSA) siliceous river gravel as coarse aggerate; both conformed to ASTM C 33. Both aggregates were also procured from the TexCrete Ready-Mix Concrete Plant in Bryan, Texas. Table 4-3 shows the specific gravity and absorption of course and fine aggregates, measured following ASTM C 127 and ASTM C 128, respectively. In addition, the particle size distribution (gradation) was measured according to ASTM C136 and is shown in Table 4.4.

Table 4-3: Coarse and Fine Aggregate Specific Gravity and Absorption

PROPERTY	COARSE AGGREGATE	FINE AGGREGATES
Specific Gravity Saturated Surface Dry (SSD)	2.72	2.6
Dry Rodded Unit Wt (lb/ft3)	100	N/A
Fineness Modulus	N/A	2.6
Absorption	0.78%	0.44%

Note: N/A = Not Applicable; n/a = not available.

Table 4-4: Coarse and Fine Aggregate Particle Size Distribution

SIEVE SIZE	COARSE AGGREGATE		FINE AGGREGATE	
	% Passing	Specification	% Passing	Specification
1.5 inches	100	100		
1 inch	99.8	95–100		
0.75 inch	92.7	N/A		
0.5 inch	45.6	25-60		
0.375 inch	19.1	N/A		
No. 4	5.3	0-10	99.9	95–100
No. 8	4.7	0-5	98.8	85–100
No. 16			89.9	65–97
No. 30			66.8	25–70
No. 50			32.3	5–35
No. 100			6.0	0–7
No. 200			0.1	Max. 4

Note: N/A = Not Applicable; n/a = not available.

4.2.2 Mix Designs

Eight binary and ternary HPC mixtures, including the control mix ([CEM]; 100 percent OPC), were designed (Table 4-6) for this experimental program, with a design w/cm ratio of 0.42, coarse aggregate factor (CAF) of 0.67, and 520–580 lb/cy of cementitious material. These HPC mixtures were designed following TxDOT's standard mix design practice for bridge deck concrete and matched with field practices in Texas (Item 421, TxDOT 2014), as shown in Table 4-5.

Table 4-5: Final Selected Mix Designs

OPTION	MIX	#A	#B
1	Replace 20% to 35% of the cement with Class F FA.	25% Class F FA	35% Class F FA
3	Replace 35% to 50% of the cement with a combination of Class F FA or SF; however, no more than 35% may be FA, and no more than 10% may be SF.	20% Class F FA + 5% SF	N/A
5	Replace 35% to 50% of the cement with a combination of Class C FA and at least 6% of SF. However, no more than 35% may be Class C FA, and no more than 10% may be SF.	29% Class C FA + 6 % SF	35% Class C FA + 10% SF
X	Binary Low Alkali Loading Mix (New Mix Design Options)	6% SF	35% Class C FA

Note: N/A = Not Applicable; n/a = not available. Under new Option X, mix designs were proportioned replicating HPC mix design practices at two bridge decks from Amarillo and Lubbock districts of Texas, respectively. Although these binary mixtures are not a part of the current HPC specifications, their usage was reported under special provisions. The field performance of these HPC bridge deck mixtures was investigated in Chapter 3. Field investigation and the details are reported under Bridge #5 (ID-04-191-0-0168-09-168) and Bridge #7 (ID-05-152-0-0783-02-104).

In addition to the abovementioned ingredients, all HPC mixtures contained polypropylene fibers, AEA (ASTM C 260), and a Type F High-Range Water Reducer (HRWR, ASTM C 494). The AEA and HRWR dosages were adjusted following the manufacturer's recommendation to meet the specification's target air content (4–6 percent) and workability requirements (3–5 inches) for the HPC mixtures. Table 4-6 lists the HPC mixture proportions evaluated in this study.

Table 4-6: HPC Mix Proportions

MIX DESIGNATION #	CEM	6SF	25F	20F5SF	35F	35C	29C6SF	35C10SF
Cementitious Content (lb/cy)	580	520	584	584	584	520	541	541
Cement, (lb/cy)	580	489	438	438	380	338	352	298
Class F FA, (lb/cy)	N/A	N/A	146	117	204	N/A	N/A	N/A
Class C FA, (lb/cy)	N/A	N/A	N/A	N/A	N/A	182	157	189
SF, (lb/cy)	N/A	31	N/A	29	N/A	N/A	32	54
Coarse Aggregate (1-inch MSA), (lb/cy)	1815	1800	1815	1817	1815	1887	2032	2031
Fine Aggregate, (lb/cy)	1236	1296	1236	1230	1275	1192	1056	1043
Mixing Water, (lb/cy)	232	234	236	239	242	216	220	218
AEA, (fl. oz/100 lb cem)	0.5	0.5	0.5	0.5	0.5	0.5	0.5	0.5
Type F-HRWR, (fl. oz/100 lb cem)	7	7	7	7	7	7	7	7
Fibers (lb/cy)	0.5	0.5	0.5	0.5	0.5	0.5	0.5	0.5
w/cm (design)	0.42	0.42	0.42	0.42	0.42	0.42	0.42	0.42
w/cm (effective)	0.41	0.40	0.40	0.40	0.40	0.40	0.40	0.40

Note: N/A = Not Applicable; n/a = not available.

4.3 Laboratory Evaluation—Test Matrix

Table 4-7 shows the concrete (performance) properties and associated parameters evaluated for all 8 HPC mixtures under Task 6. The standard test method and ASTM/ AASHTO test references discussing specific concrete properties are identified at the start of each section.

Table 4-7: Concrete Property and Parameters Evaluated for HPC Mixtures

SECTION	CONCRETE PROPERTY	PARAMETER
1	Fresh Properties	• Temperature • SL • Unit Weight • Volumetric Air Content • Setting Time • Paste Volume (Based on Mix Design)
2	Hardened Properties	• Compressive Strength • Tensile Strength • MOE
3	Shrinkage	• Autogenous Shrinkage ([AS];23°C and 40 °C) • Free DS • Restrained Shrinkage • Cracking Potential • Creep Potential (Modeling)
4	Pore Solution	• TTI Model-1 • TTI Model-2 o Extraction (selective validation) o GEMS Thermodynamic Modeling
5	Transport Properties	• RCPT
6	Transport Properties Resistivity Tests: Normal Conditioning Regimen	• BR & SR o Sealed Curing (SC) o Saturated Limewater (LW) Curing o Standardized Simulated Pore Solution (SPS) Curing o Matching Pore Solution (MPS) curing
7	Transport Properties Resistivity Tests: Factors of Influence	• Degree of Saturation (DOS) • Ionic Leaching of Pore Solution Alkalis • Drying (Moisture Loss) • Sample Homogeneity (Surface-to-Bulk Resistivity [SR/BR] Ratio)
8	Transport Properties Resistivity Tests: Accelerated Conditioning	• BR & SR o LW Curing o SPS Curing o MPS Curing
9	Transport Properties/ Microstructure	• Formation Factor o Sealed FF o Apparent FF o (Saturated) FF (FF)
10	Chloride Diffusion	• Apparent Chloride Diffusion • Chloride Binding • Effective Chloride Diffusion • Service Life Evaluation–Time to Corrosion Initiation
11	F/T Resistance	• Freeze Thaw Tests
12	Sorptivity	• Rate of Fluid Absorption
13	ASR	• Rapid Evaluation of FA Dosage by the Recently Developed Chemical Screening Tool (CST) Followed by Dosage Comparison between CST and ASTM C1567 and Sorting Out the Ashes That Need Further Validation by a Suitable Concrete ASR Testing (i.e., Accelerate Concrete Cylinder Test [ACCT] Method)

4.4 Laboratory Testing

4.4.1 Fresh Properties

The concrete mixing and determination of fresh concrete properties for HPC mixtures were performed at the TTI laboratory under standard laboratory temperatures of 73.5 ± 3.5 °F (23 ±

2 °C). HPC mixtures in the plastic state were evaluated for the following fresh properties listed in Table 4-8, and the results are tabulated in Table 4-9.

Table 4-8: Test Matrix for Fresh Properties Evaluation

PARAMETER	TEST METHOD	AGE OF TEST	CURING PRACTICE
Temperature	ASTM C 1064	Fresh/ Plastic State	N/A
SL	ASTM C 143		
Unit Weight	ASTM C 138		
Volumetric Air Content	ASTM C 231		
Setting Time	ASTM C 403		
Paste Volume	N/A		

The paste volume for concrete mixtures was calculated based on the volume of cementitious materials, water, and air in the concrete. Determination of paste content is essential to evaluate shrinkage and cracking.

Table 4-9: Results from Fresh Properties Testing of HPC Mixtures

MIX #ID	TEMPERATURE, °F	SL (IN)	UNIT WEIGHT LB/FT^3	AIR CONTENT (%)	SETTING TIME		PASTE VOLUME
					Initial (min)	Final (min)	
CEM	74.3	5.5	145	6.5%	258	463	26.3%
6SF	72.5	4.5	142	6.0%	214	422	25.8%
25F	72.1	5	143	5.5%	334	572	26.1%
20F5SF	73.4	4.5	143	5.0%	369	499	26.2%
35F	72.7	5	143	5.5%	424	642	26.3%
35C	73.6	5	141	5.3%	394	592	25.3%
29C6SF	73.9	4.5	141	5.0%	354	569	25.6%
35C10SF	74.9	4	140	4.5%	266	492	25.8%

4.4.2 Hardened Properties

For testing mechanical properties, 4 × 8-inch (4 ± 0.08 inch diameter and 8 ± 0.16 inch height) concrete cylinders were cast for each HPC mix design and tested following Table 4-10. Cylinders were demolded at the age of 24±2 hours and placed in a controlled environmental chamber maintained at 23 ± 2 °C and 98 ± 2 percent RH, following ASTM C 511 specifications for moist curing regimen.

Table 4-10: Test Matrix for Hardened Properties' Evaluation

PARAMETER	TEST METHOD	AGE OF TESTING	CURING REGIMEN
Compressive Strength	ASTM C 42	7, 14, and 28 days	Moist Curing
Tensile Strength	ASTM C 496		
MOE	ASTM C 469		

Concrete compressive strength (ASTM C 39), static MOE (ASTM C 469), and splitting tensile strength (ASTM C 496) were measured in replicate on three cylinders for each HPC mix, and the results are tabulated in Table 4-11.

Table 4-11: Results from Mechanical Properties Testing of HPC Mixtures

MIX #ID	COMPRESSIVE STRENGTH (F'C, PSI)				SPLIT TENSILE STRENGTH (F'T, PSI)			STATIC MOE (× 10^6 PSI)		
	7d	*14d*	*28d*	*F'c Ratio (28d/7d)*	*7d*	*14d*	*28d*	*7d*	*14d*	*28d*
CEM	3916	4552	4895	1.25	394	431	450	3.03	3.35	3.80
6SF	4476	5644	5819	1.3	427	491	500	3.20	3.65	4.05
25F	3839	4290	5720	1.49	389	416	495	3.01	3.27	4.03
20F5SF	3987	5117	6020	1.51	398	463	510	3.05	3.51	4.10
35F	3586	3658	5379	1.5	373	378	477	2.92	3.07	3.93
35C	4071	3990	5700	1.4	403	398	494	3.08	3.17	4.02
29C6SF	4653	4676	6235	1.34	437	438	521	3.26	3.38	4.16
35C10SF	5153	5664	6750	1.31	465	492	547	3.40	3.66	4.29

The rate of strength development for HPC mixtures was analyzed based on the *F'c* ratio, which is the ratio of 28-day to 7-day compressive strength. According to Mindess and Young (*14*), *F'c* ratios between 1.25 and 1.67 indicate uniformity in strength gain.

As shown in Figure 4-1, at 28 days the compressive strength of all HPC mixtures was noted to be above the threshold limit of 4000 psi (min). The *F'c* ratios (concrete compressive strength [ASTM C 39], static MOE [ASTM C 469], and splitting tensile strength [ASTM C 496]) were measured in replicate on three cylinders for each HPC mix, and the results are tabulated in Table 4-11. All HPC mixtures ranged between 1.25 and 1.5, and the 7-day strengths of HPC mixtures ranged between 65–80 percent of 28-day compressive strengths.

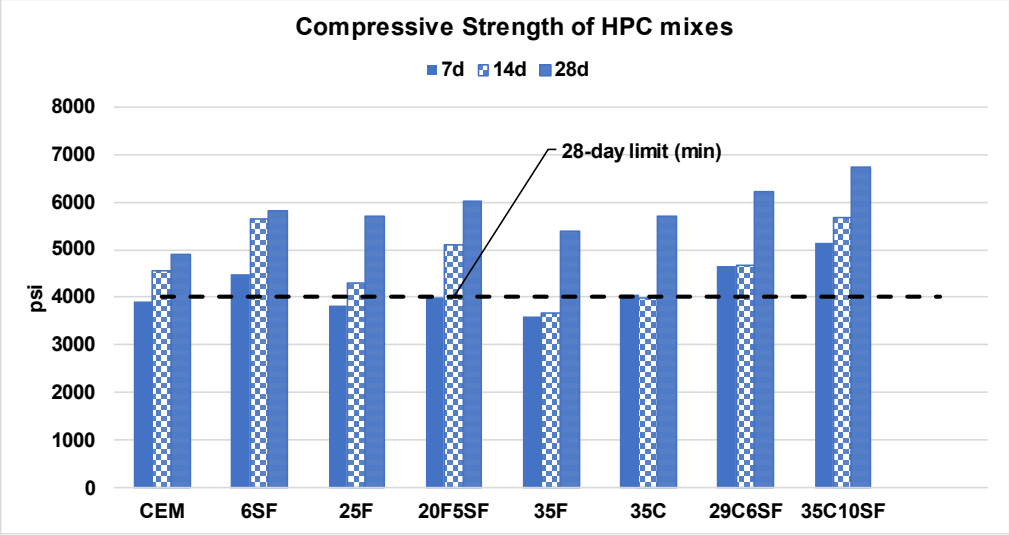

Figure 4-1: Compressive Strength of HPC Mixtures at 7, 14, and 28 Days

4.4.3 Shrinkage

4.4.3.1 Test Matrix

The test matrix to evaluate shrinkage performance of HPC mixtures is shown in Table 4-12 and discussed in the following sections.

Table 4-12: Evaluation Matrix of Shrinkage Performance of HPC Mixtures

PARAMETER	TEST METHOD	AGE OF TESTING	CURING REGIMEN
AS *at 23C and 40C*	Length Change Comparator	Up to 91 Days	Sealed
	Embedded Strain Gauges	Up to 91 Days	Sealed
Free Shrinkage (Mod.)	ASTM C 157	Up to 180 Days	7-Day—Moist Curing
Restrained Shrinkage (Single-Ring test)	ASTM C 1581	28 Days	Moist Curing
Cracking Potential	Based on Restrained Shrinkage	28 Days	N/A
	Based on Free Shrinkage		
Creep Modeling	RILEM B3 Model	28 Days	

4.4.3.2 Test Methods

4.4.3.2.1 AS

A replicate of three concrete prisms (4 × 4 × 12 inches) were cast for each HPC mix design to evaluate the development of AS strain in HPC mixtures. Test samples (prisms) were demolded between 10–12 hours based on the final setting time of the HPC mixtures, which were measured according to ASTM C 403 (Table 4-9). As explained below, AS in HPC test samples was measured using two different approaches.

4.4.3.2.1.1 AS Measurement on Sealed Concrete Prisms Using Embedded Strain Gauges

HPC mixtures were evaluated for AS strain development using embedded strain gauge sensors in sealed concrete prisms. A commercially available strain gauge, KM-120 series, manufactured by Tokyo Sokki, was used to measure the strains during the transition of concrete from a plastic to a hardened state. The KM series of strain gauge was noted to have a significantly low modulus and coefficient of thermal expansion compared to concrete, and therefore was used for internal strain measurement during the early ages of curing. Before casting, three strain gauges were installed in the empty concrete prism molds at the midsection using a procedure recommended by the manufacturer. The molds were oiled and lined with a medium-duty plastic sheet (6 mil/0.15 mm thick) to minimize any interference in strain gauges/data acquisition during sample demolding. After mold preparation, three replicate concrete prisms (4 × 4 × 12 inches) samples were cast for each HPC mix design. Test samples were demolded in a controlled environmental chamber (23 ± 2 °C and 98 ± 2 percent RH) and immediately double-wrapped with a self-sealing polythene film and adhesive aluminum tape to avoid any moisture loss. Subsequently, samples were stored in a thermally insulated Styrofoam box, and the sealed box was placed in the controlled

environmental chamber for the test duration, as per the recommendations of a previous study (*15*). Strain gauges inside concrete were connected to a data acquisition system, and the strain development in sealed specimens was monitored from 1 hour after casting till 28 days.

4.4.3.2.1.2 AS Measurement on Sealed Concrete Prisms Using Length Change Comparator

Based on the modified ASTM C 1698 specifications, a second experiment was performed to monitor the AS strain development in HPC mixtures. A replicate of three concrete prisms (4 × 4 × 12 inches) were cast for each HPC mix design. Test samples (prisms) were demolded in a controlled environmental chamber (23 ± 2 °C and 98 ± 2 percent RH) and immediately double-wrapped with a self-sealing polythene film and adhesive aluminum tape to avoid any moisture loss. Brooks et al. (*16*) noted that sealing concrete prisms with four layers of adhesive aluminum tape effectively prevented moisture loss. Subsequent research studies noted that a combined polythene film and aluminum tape sealing resulted in minimal weight loss from concrete samples (*17*, *18*). Subsequently, test samples were measured for initial length and mass. A length-change comparator conforming to ASTM C490 was used in this current study and was placed in the same ambient environment as samples to avoid any variations due to temperature and moisture change, as per ASTM C 157 guidelines. After initial readings, samples were stored in the same controlled environmental chamber (23 ± 2 °C and 98 ± 2 percent RH), wherein subsequent length and mass readings were taken every day from 1–7 days, followed by at 14, 28, 56, and 91 days. Mass readings were used to monitor the moisture loss from the test specimens throughout the testing period. In current research, the average mass loss was noted in the range of 0.2 percent ± 0.05 percent after 91 days across all test samples, which validates the effectiveness of the sealing technique.

4.4.3.2.2 Free DS

HPC mixtures were evaluated for unrestrained (free) DS according to ASTM C 157, with a modification of initial curing duration of the specimens (i.e., 7 days instead of 28 days) to match the field curing practices (i.e., 7 days wet mat curing). A replicate of three concrete prisms (4 × 4 × 12 inches) were cast for each HPC mix design. Test samples (prisms) were demolded at the age of 24±2 hours and moist-cured in a controlled environmental chamber (23 ± 2 °C and 98 ± 2 percent RH) for 7 days. Subsequently, test samples were measured for initial length using a length change comparator conforming to ASTM C490. After initial readings, samples were placed in a drying chamber maintained at 23 ± 2 °C and 50 percent RH, and subsequent length and mass measurements were recorded up to 180 days. Mass measurement of the test samples at a periodic interval was used to check for any moisture loss and verify the effectiveness of sealing.

4.4.3.2.3 Restrained Single-Ring Shrinkage Test

The cracking potential (CP) /tendency of the selected HPC mixtures was evaluated using a restrained single-ring test, as per ASTM C 1581. A nonabsorptive and nonreactive base made of epoxy-coated plywood was used in this experiment. Before casting, the rings were oiled, and while the inner ring was screwed to the base, the outer ring was held in place using four C clamps placed 90 degrees apart. Next, fresh mixtures were poured and compacted in three layers

on a vibrating table. Finally, concrete specimens (1.5 inches thick and 6 inches tall) were cured by placing in a prewetted burlap sack and covered with plastic. The outer rings were detached from the board at the age of 24 ± 2 hr, and the specimens were moved to the conditioning room and maintained at a temperature of 73.5 ± 3.5 °F (23 ± 2 °C) and 50 ± 5 percent RH; the top surface was coated with a layer of epoxy (curing compound) to prevent moisture loss from the top.

Four strain gauges were wired to the interior surface of the inner ring in a quarter-bridge configuration to monitor the strain development for up to 28 days. The mounting of gauges to the steel ring and connecting strain gauge modules to lead wires was performed following the manufacturer's specifications. A commercially available data acquisition system manufactured by Campbell Scientific was used to continuously record data from each strain gauge at every 30-minute interval up to 28 days. The cracking in concrete rings was monitored through (a) strain development in the steel rings, wherein a decrease in compressive strain (30 με or more) from one or more strain gages would indicate the cracking of the concrete ring and (b) visual inspection for cracks on the outer surface of concrete rings. Furthermore, the room's ambient temperature and RH were continuously monitored by placing sensors next to the test specimen. The strain in the steel rings was recorded over time up to 28 days, and stress rate development in concrete specimens was calculated as per ASTM C 1581.

4.4.3.3 Results and Discussion

4.4.3.3.1 AS Measurements in HPC Mixtures at 23C

4.4.3.3.1.1 AS Measurements Using Embedded Strain Gauges

Following the previous section's procedure, AS strain development for 8 HPC mixtures was monitored up to 91 days, and the results are plotted in Figure 4-2.

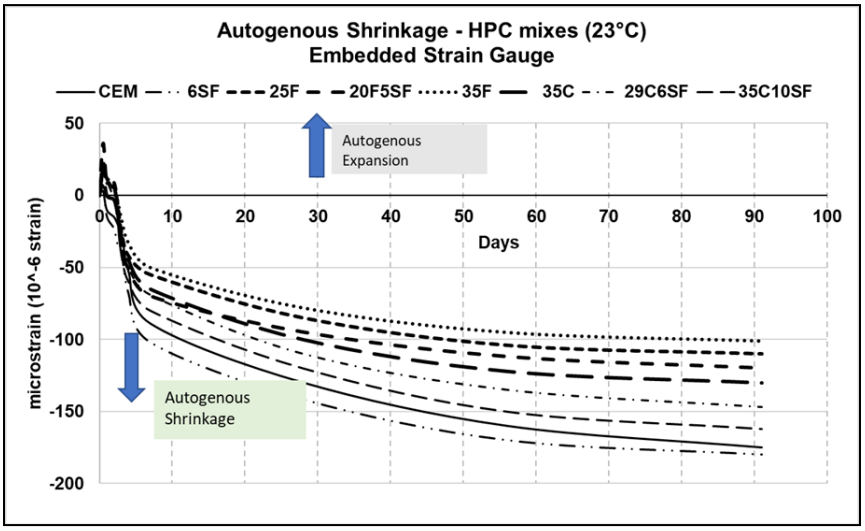

Figure 4-2: AS Strain for HPC Mixtures' Embedded Strain Gauge Measurements

Results from Figure 4-2 demonstrate that the SCM's type, composition, and replacement level primarily influence the AS of the studied HPC mixtures since the w/cm ratio for all the mixtures remained constant. Notably, the presence of SF (Figure 4-3) was seen to increase the overall AS as well as the strain rate (i.e., strain development at early ages, i.e., from 0.5 to 7 days) for binary and ternary HPC mixtures. The mix with 6 percent cement replacement with SF (6SF) showed the highest AS and strain rate compared to all the studied mixtures. Interestingly, the overall AS and strain rates for all HPC mixtures except 6SF are lower than the CEM.

HPC mixtures with 25 percent (25F) and 35 percent (35F) F ash replacements show approximately 40 percent and 55 percent reduction in AS and ~ 20 percent and 30 percent reduction of AS strain rate at early ages, respectively, compared to the CEM. However, 5 percent SF in the ternary mix 20F5SF caused a 10–20 percent increase in AS and an approx. 20–30 percent increase in early-age strain rate when compared to the 25F and 35F binary mixtures (Figure 4-2 and Figure 4-3).

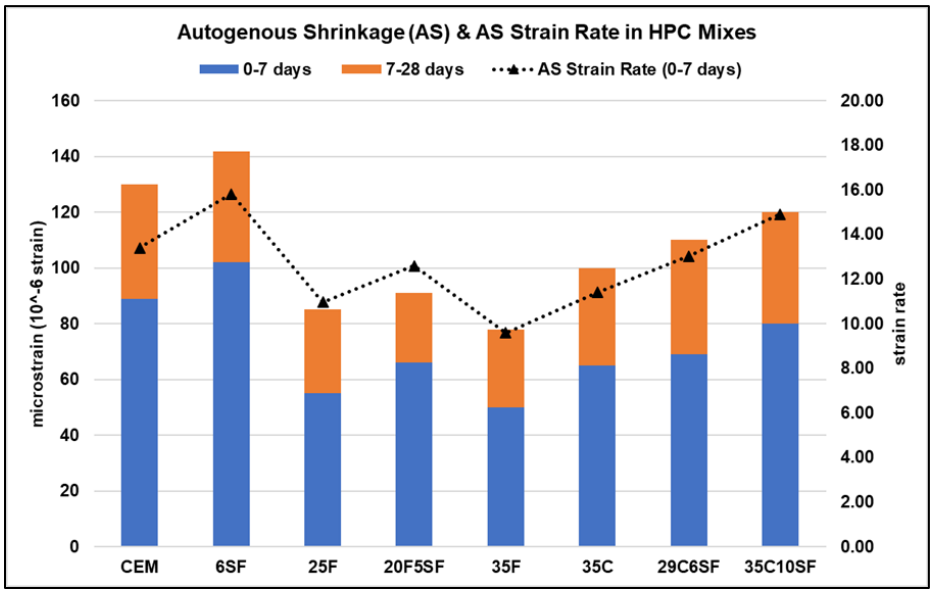

Figure 4-3: AS and Early-Age Strain Rate Development in HPC Mixtures

Cement replacement with 35 percent Class C FA (35C) caused an overall 35 percent reduction in AS and 20 percent reduction in early-age strain rate compared to the CEM. In an investigation of the influence of FA type on both AS and strain rate, the HPC 35F mix demonstrates a 35 percent lower strain rate and an overall 25 percent lower AS than the 35C mix.

Ternary Class C FA mixtures (i.e., 29C6SF and 35C10SF) show higher AS and strain rates than the binary 35C mix and the highest AS measurements compared to all HPC mixtures containing fly ashes. Therefore, the benefit of reduction in AS is not significant for these ternary Class C mixtures with SF compared to the CEM. Among all the ternary mixtures with SF, HPC mixtures 29C6SF and 35C10SF, with a comparatively lower binder content (540 lb/cy), demonstrated a higher AS strain than that at 20F5SF mix, with a relatively higher binder content of 580 lb/cy.

4.4.3.3.1.2 AS Measurements Using Length Comparator

Figure 4-4 shows the AS strain development over time based on length change measurements performed on sealed HPC concrete prisms. Overall, AS shrinkage determined using length comparator measurements show a similar trend with the measurements using embedded strain gauges for all the tested HPC mixtures. However, the absolute values are slightly different. A comparative assessment of AS determined using two methods (Figure 4-5) demonstrates AS strains determined using a length comparator to be approximately within ±10–15 percent of the strain gauge data. In general, AS measurements by the length comparator method are slightly higher when the stain values remain >100 microstrain but are slightly lower when the strain values remain <100 microstrain than those measured by the strain gauge method.

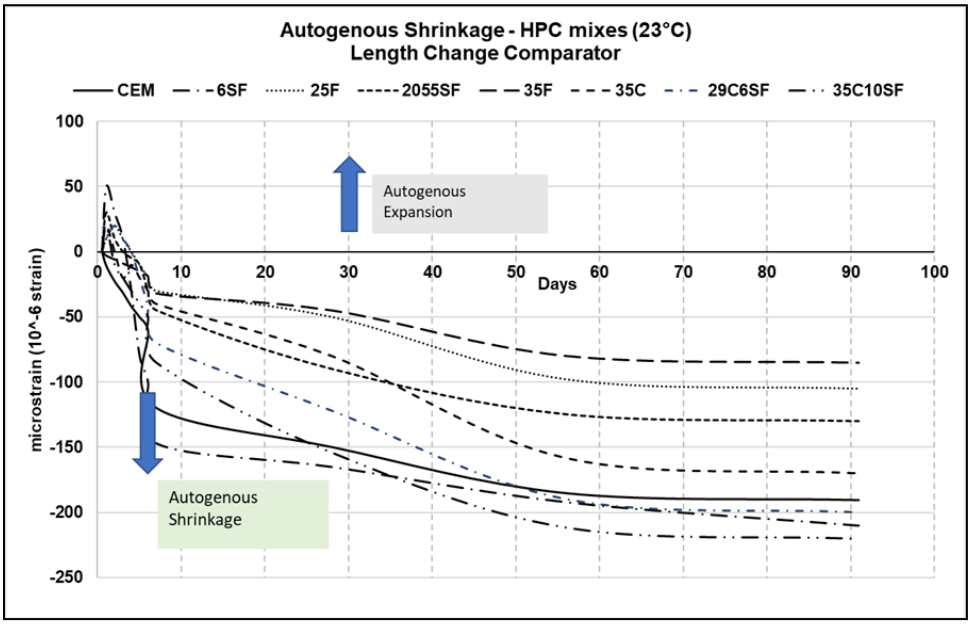

Figure 4-4: AS Strain for HPC Mixtures Measured at 23C—Length Change Comparator Measurements

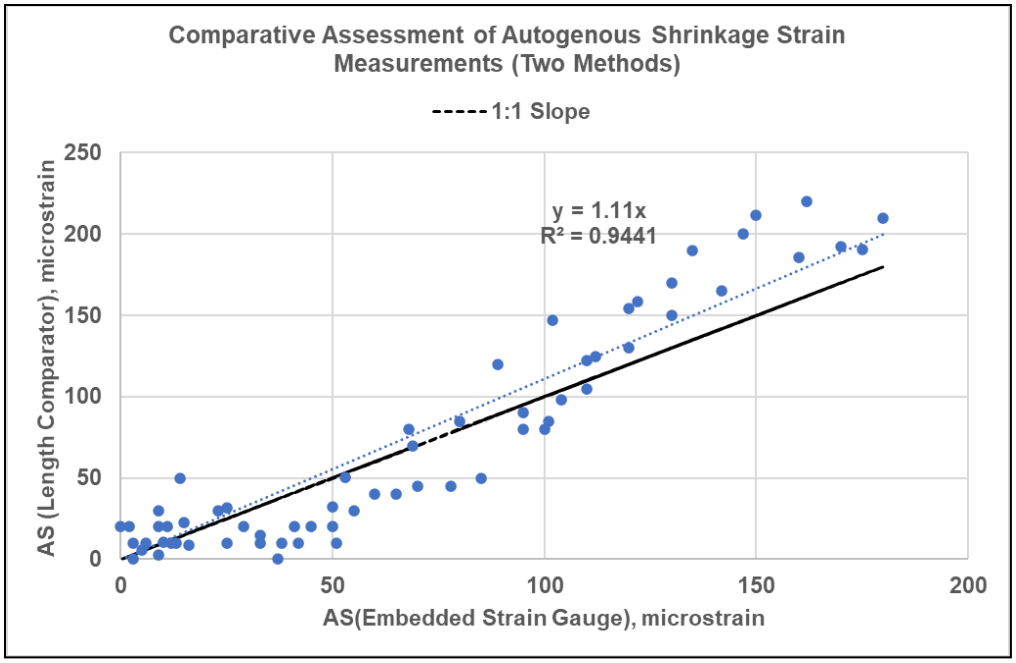

Figure 4-5: AS of HPC Mixtures—Length Comparator vs. Embedded Strain Gauge

Although AS measurement using the embedded strain gauge method provides higher accuracy and reliability, the measurement procedure is complex and cost intensive. The purpose of using the more accurate strain gauge method was to validate the applicability of the simplified method using a length comparator. Overall, AS measurement using a conventional length comparator for the studied HPC mixtures provides acceptable accuracy. Moreover, this simplified procedure of AS determination can be performed at any standard laboratory with minimal cost.

4.4.3.3.1.3 AS Measurements in HPC Mixtures at 40 °C

The influence of higher curing temperatures on AS strain development of HPC mixtures was studied in current research. HPC test samples (prisms) were demolded based on final setting time in a controlled environmental chamber (23 ± 2 °C and 98 ± 2 percent RH) and immediately double-wrapped with a self-sealing polythene film and adhesive aluminum tape to avoid any moisture loss. Next, test samples were measured for initial length and mass. Subsequently, test samples were placed in a controlled environmental chamber (40 ± 2 °C) and measured for AS at 1, 4, 7, 14, and 28 days. At each testing age, test samples were cooled to room temperatures (23 ± 2 °C) for 4–6 hours before length change and mass measurements. Figure 4-6 shows the AS strain of HPC mixtures cured at 40°C of demolding till 28 days.

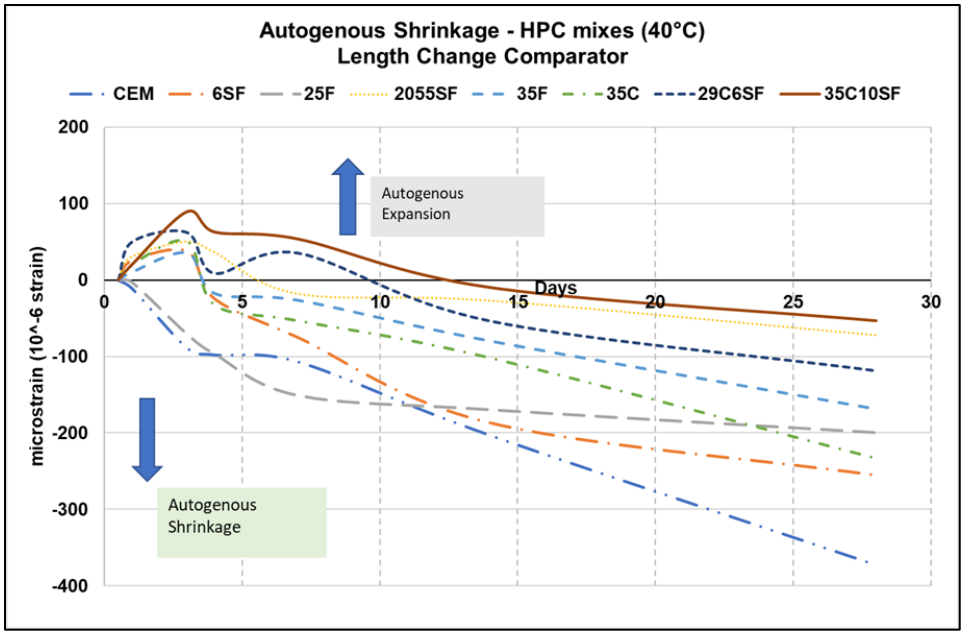

Figure 4-6: AS of HPC Mixtures Measured at 40°C

Results from Figure 4-6 demonstrate that the higher ambient temperatures drastically change the AS behavior of HPC mixtures, and the effect appears to be contingent upon the SCM's type, composition, and replacement level. Of particular significance is the development of early-age AS between 1–3 days due to high ambient (curing) temperatures, and a comparative assessment with AS at 23°C is shown in Figure 4-7.

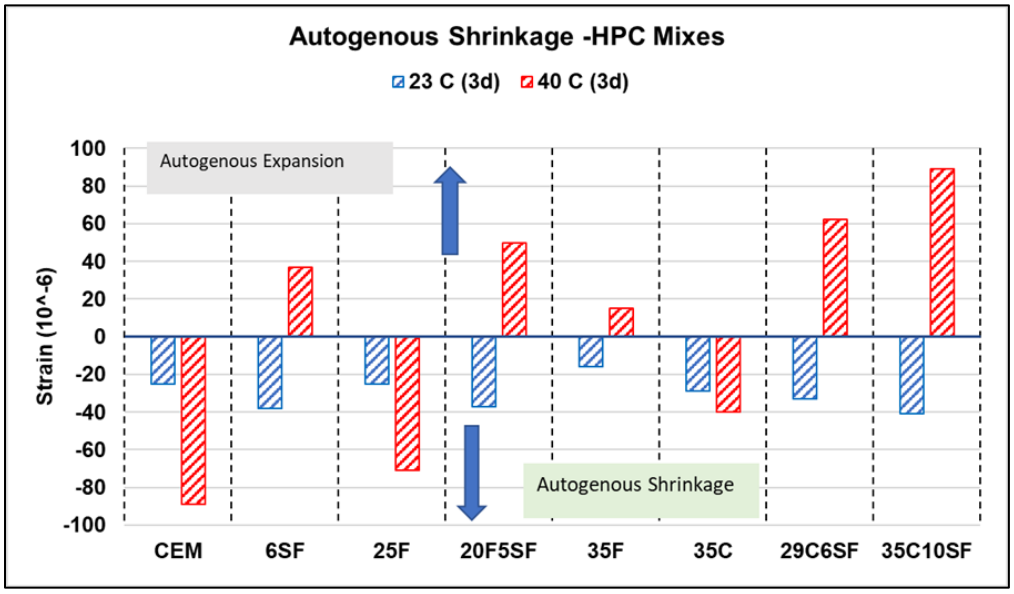

Figure 4-7: AS (Strain Gauge, 23°C vs. 40°C) of HPC Mixtures at 3 Days

Notably, ternary HPC mixtures with SF show an expansion at early ages, with shrinkage strains in the 50–100 microstrain range between 1–3 days. Furthermore, curing at higher ambient temperatures (40°C) is seen to increase the AS by approx. 130–200 percent in these ternary HPC

mixtures when compared to mixtures cured at 23°C. In contrast, the binary HPC mixtures (25°F, 35°F, and 35°C) showed an average increase of 100–120 percent in AS at 40°C as compared to 23°C.

4.4.3.3.1.4 Conclusions

HPC mixtures are typically designed with a low w/cm ratio, which in combination with fine mineral admixtures such as SF and chemical admixtures like HRWR typically result in high AS of these mixtures. The evidence of early-age crack formation was observed during field evaluation (presented in Chapter 3) for the ternary HPC mixture design (29 percent Class C Ash + 6 percent SF) used for bridge decks in Amarillo. Furthermore, experimental work demonstrated that ambient temperatures significantly influenced autogenous strain development in HPC mixtures. Experimental measurements showed that AS strains as high as 100 microstrains could develop in this ternary SF mixture at 3–5 days when ambient temperatures increased from 23°C to 40°C. This feature in conjunction with the contribution from DS and thermal strain (due to early morning placement) was found to be the reason for creating high total strain at early ages and causing crack formation when total strains exceeded the tensile strength in one of the Amarillo bridges (mentioned in Chapter 3).

4.4.3.3.1.5 Recommendations

Autogenous strains can be mitigated through proper selection of materials and effective mixture design techniques, such as internal curing through lightweight aggregates (among other approaches). Several research studies and DOT specifications have demonstrated the use of lightweight aggregates to effectively mitigate early-age AS in HPC mixtures, which was verified through field investigation studies. Additionally, incorporating saturated lightweight aggregates creates secondary effects and influences microstructure properties due to greater hydration and a higher saturation of pores. Thus, internally cured HPC mixtures typically demonstrate a different laboratory performance compared to conventional HPC mixtures. Therefore, since lightweight aggregates are increasingly used in bridge deck mix practices, research efforts are needed to investigate this practice of internal curing toward inclusion in performance-based specifications for HPC.

4.4.3.3.2 Free DS Strain Measurement in HPC Mixtures (ASTM C 157)

Following ASTM C 157, the length change and the mass loss measurements for all the studied HPC mixtures were recorded up to 180 days. The DS strain values over time for each HPC mix are presented in Table 4-13 and are also plotted in Figure 4-8. Although *negative values represent* DS *strains, all the tables and plots in the following sections used the absolute positive values (i.e., removed the negative signs) for convenience.*

Table 4-13: DS Measurements (microstrain) from 7–180 Days of Drying

DAYS	CEM	6SF	25F	2055SF	35F	35C	29C6SF	35C10SF
7	0	0	0	0	0	0	0	0
10	125	185	90	85	70	160	150	175
14	276	284	190	190	150	240	250	270
28	400	436	250	280	230	300	350	382
56	460	470	360	320	300	380	385	400
91	520	500	400	380	360	430	410	425
180	560	524	450	425	410	450	430	453
%COV (3 prisms)	*7.3%*	*6.2%*	*7.7%*	*5.3%*	*6.1%*	*5.9%*	*5.2%*	*6.3%*

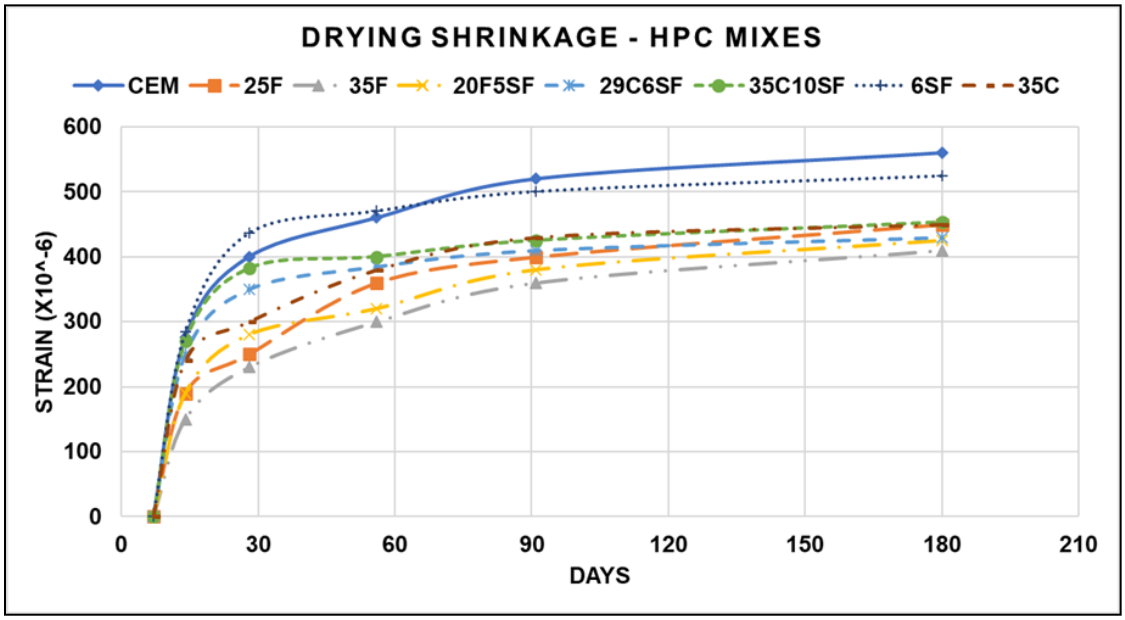

Figure 4-8: Free DS Strains (7–180 days) for HPC Mixtures

Currently, TxDOT specifications do not specify an acceptable limit for DS strain measured by the ASTM C 157. Thus, the DS strains measured for HPC mixtures (Table 4-13) were compared with the DS acceptability limits specified by eight state DOTs for the HPC mixtures as well as limits recommended by national (FHWA and AASHTO) specifications (Table 4-14).

Table 4-14: Comparison of DS Measurements for HPC Mixtures vs. Specification Limits

AGENCY	DS LIMIT (MICROSTRAIN)	AGE (D)	CEM	6SF	25F	20F5SF	35F	35C	29C6SF	35C10SF
FHWA	500	56	✓*	✓*	✓	✓	✓	✓	✓	✓
AASHTO PEM	420	28	✓*	×	✓	✓	✓	✓	✓	✓
Iowa State	500	28	✓	✓	✓	✓	✓	✓	✓	✓
Oregon DOT	450	28	✓*	✓*	✓	✓	✓	✓	✓	✓
Mn DOT	400	28	×	×	✓	✓	✓	✓	✓	✓*
Washington DOT	320	28	×	✓*	×	✓	✓	×	×	×
Illinois tollway	300	28	×	×	✓	✓*	✓	×	×	×
New Jersey DOT	450	56	×	×	✓	✓	✓	✓	✓	✓*

Note: ✓ → lower and higher than threshold DS limits at a given age; × higher than the specified thresh DS limits; ✓*→ shrinkage strains within ± 30 με tolerance limit of threshold DS value.

Based on the comparative assessment of DS data in Table 4-14, a limit of 400 microstrains at 28 days or 450 at 56 days allows all the studied mixtures except the CEM and 6 percent SF mix (6SF). A limit of ≤ 320 disallows 25F, 35C, 29C6SF, and 35C10SF mixtures other than CEM and 6SF mixtures. Moreover, these mixtures did not show any crack formation within 28 days of testing duration in the ring-test (described later). Therefore, a conservative limit of ≤ 320 may not be needed for TxDOT HPC mixtures. Therefore, it seems a limit of 400 microstrains at 28 days or 450 at 56 days can be considered as a DS limit for TxDOT HPC mixtures. However, further work to validate this proposed limit is highly warranted.

4.4.3.3.2.1 Discussion on Free DS Strains

The current study investigated the influence of the SCM type, composition, and replacement level on DS performance as well as on the DS strain development with time (*hereby referred to as strain rate*) at early (7–28 days) and later ages (28–180 days) as shown in Figure 4-9. Binary and ternary HPC mixtures in this study were prepared with binder contents ranging from 520–580 lb/cy based on field mix design practices.

When abiding by ASTM C 157, the 100 percent OPC reference CEM mix with a binder content of 580 lb/cy demonstrated a DS of 400 με at 28 days with an ultimate value of 560 με at 180 days. Cement replacement with 6 percent SF reduced the overall DS strains at 180 days, but the strain rate increased by 10 percent at early ages (7–28 days). However, the DS of both the CEM and 6SF mixtures exceeded 500 με at 91 days. In contrast, cement replacement with fly ashes reduced the DS strains in HPC mixtures; however, the percent reduction depends on the type of FA, replacement level, and presence of other SCMs in the mix.

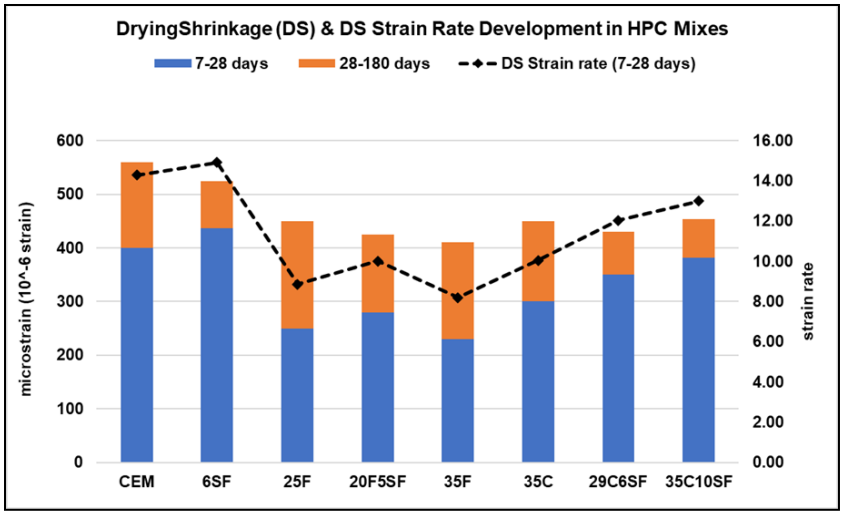

Figure 4-9: Free DS and Rate of Increase in DS Strain between 7–28 Days of Drying

All HPC mixtures containing Class C and Class F fly ashes measured DS strains less than 500 με at 180 days. Compared to CEM, the binary Class F FA mixtures (25F and 35F) demonstrated an overall 20 percent and 30 percent reduction in DS, and the strain rate decreased when Class F FA content increased in the mix (Figure 4-8 and Figure 4-9). Similarly, a 20 percent reduction in DS and a lower strain rate is seen in the binary Class C FA mix (35C) when compared with CEM. However, when the influence of FA type on both DS and strain rate was investigated, the HPC 35C mix demonstrated an overall 30 percent higher DS (28 days) and 20 percent higher DS strain rate (7–28 days) than Mix 35F. Results indicate that Class F ash's use is more effective in reducing DS and strain rate development in the HPC mixtures than is Class C FA.

The presence of SF in the mix had a varying influence on the DS performance of binary (6SF) versus ternary HPC mixtures. For ternary HPC mixtures and at 25 percent and 35 percent cement replacement levels, HPC mixtures 20F5SF and 29C6SF measured a lower ultimate DS strain than binary counterparts 25F and 35C; however, the DS strain rate increased at a faster rate between 7–28 days of drying. Furthermore, at 45 percent cement replacement, the DS strain in 35C10SF mix increased at a rate of 12.99 με/day between 7–28 days of drying (Figure 4-8 and Figure 4-9), which is comparable to the strain rate of 14.29 με/day and 14.91 με/day measured for CEM and 6SF mixtures, respectively.

4.4.3.3.2.2 Influence of AS on DS measurements

AS in concrete is an early-age shrinkage phenomenon caused due to water loss from capillary pores imbibed by hydrating cementitious materials without water loss into the surrounding environment. In contrast, the DS can be defined as the volumetric change due to the drying of hardened concrete—that is, the diffusion of water from hardened concrete into the surrounding environment. However, typically, in concrete structures, AS and DS occur in tandem, and AS needs to be separated from the total shrinkage to determine the DS strains, as shown in Figure 4-10.

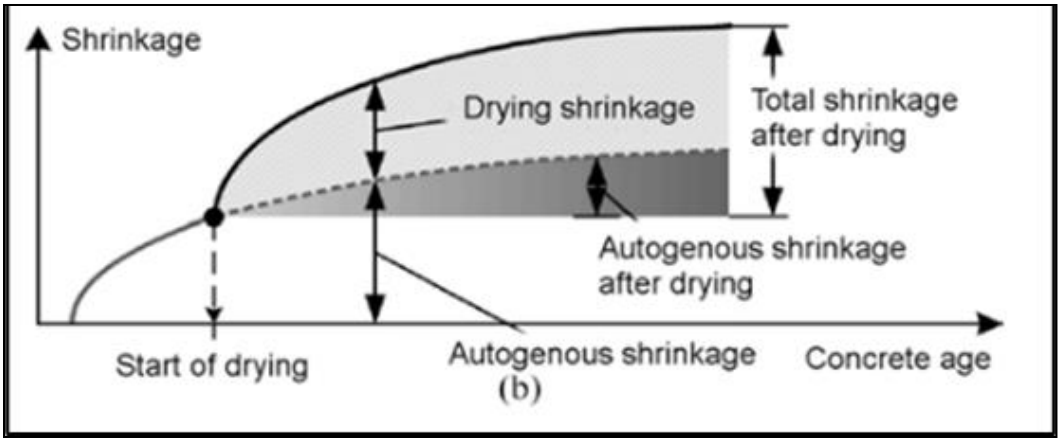

Figure 4-10: Shrinkage Strain Components in High-Strength Concrete Mixtures (*19*)

The DS and AS at 28 days and strain rate increase for AS and DS up to 28 days was compared for HPC mixtures, as shown in Table 4-15. Results demonstrate that high AS at 28 days and higher AS strain rates (0–28 days) in binary and ternary SF–HPC mixtures correlate well with high 28-day DS and rate of DS strain development (7–28 days) for these mixtures.

Table 4-15: Comparison of AS (and Strain Rate) vs. DS (and Strain Rate) for HPC Mixtures

PARAM	CEM	6SF	25F	20F5SF	35F	35C	29C6SF	35C10SF
AS (28 days)	150	165	50	90	45	80	122	154
DS (28 days)	400	436	250	280	230	300	350	382
AS Strain Rate (0–28 days)	5.11	6.88	2.21	3.79	1.54	3.07	4.98	5.74
DS Strain rate (7–28 days)	17.39	18.11	10.60	12.23	10.06	11.73	14.44	15.57

HPC mixtures 6SF, 29C6SF, and 35C10SF demonstrated relatively high DS (≥ 350 με) at 28 days. Additionally, the DS strains increased at a significantly higher rate—14.9 με/day, 12.04 με/day, and 12.99 με/day, respectively—between 7–28 days of drying. As seen in Table 4-15, the 28-day AS of these mixtures is approximately 35–50 percent of 28-day DS, which is comparable to the CEM (38 percent). Thus, for HPC mixtures designed at a low w/cm ratio, the presence of SF appears to influence both AS and DS behavior of the mixtures.

4.4.3.3.2.3 Mass Loss versus Free DS

Based on mass measurements recorded from the ASTM C 157 test, the cumulative mass loss for the test prisms from 7–180 days for each HPC mix is shown in Figure 4-11.

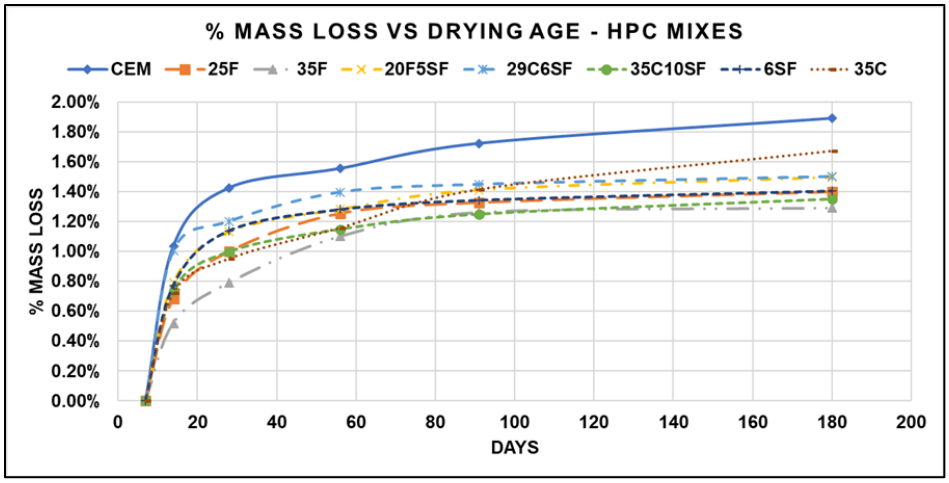

Figure 4-11: Mass Loss for HPC Mixtures (ASTM C 157)

In addition, the cumulative mass loss for each HPC mix was compared with DS measurements at 7, 14, 28, 56, 91, and 180 days of drying from 7–180 days for each HPC mix, and the results are plotted in Figure 4-12. A linear relationship between the DS of HPC test specimens and the cumulative mass loss is seen at all test ages, and the trend for mass loss appears to be consistent with the DS for all HPC mixtures. Notably, in Figure 4-12, the binary and ternary SF mixtures demonstrate a higher slope of DS versus mass loss than binary FA counterparts. Observations support the assessment that a high AS resulting from SF addition also contributes toward an overall DS of these mixtures because the DS strain (Figure 4-11 and Figure 4-12) for SF mixtures increases at a higher rate than moisture loss rate from these samples. Therefore, Figure 4-12 indicates that DS versus mass loss plots are a good indicator to assess the secondary influence from AS and AS strain rate on overall free DS performance of HPC mixtures.

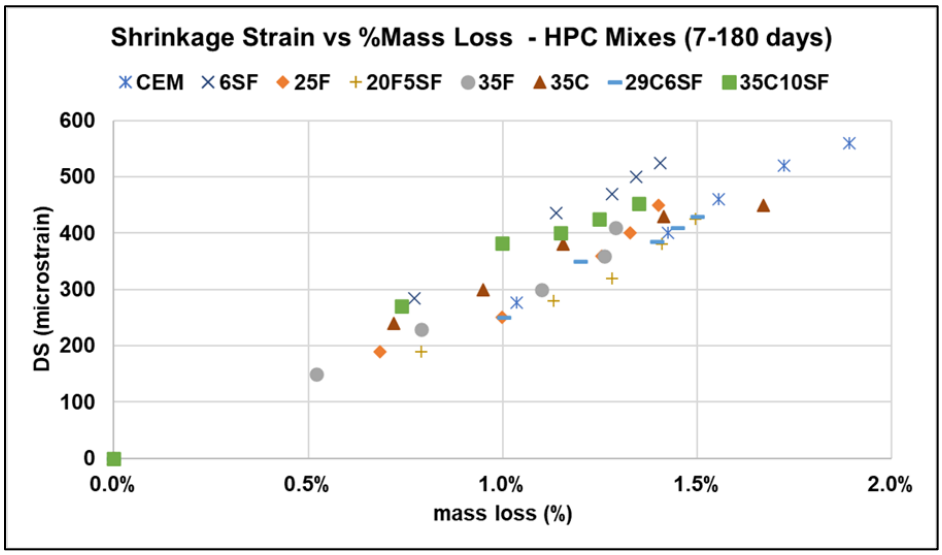

Figure 4-12: Influence of Mass Loss on DS Measurements for HPC Mixtures (7, 14, 28, 91, and 180 Days)

4.4.3.3.3 Restrained Single-Ring Test

HPC mixtures were evaluated for their restrained shrinkage behavior and cracking tendency based on AASHTO T 334's single-ring restrained shrinkage test. A single-ring test was performed on five out of eight HPC mixtures, and rings were monitored for strain development (and cracking) up to 28 days, and the results are plotted in Figure 4-13.

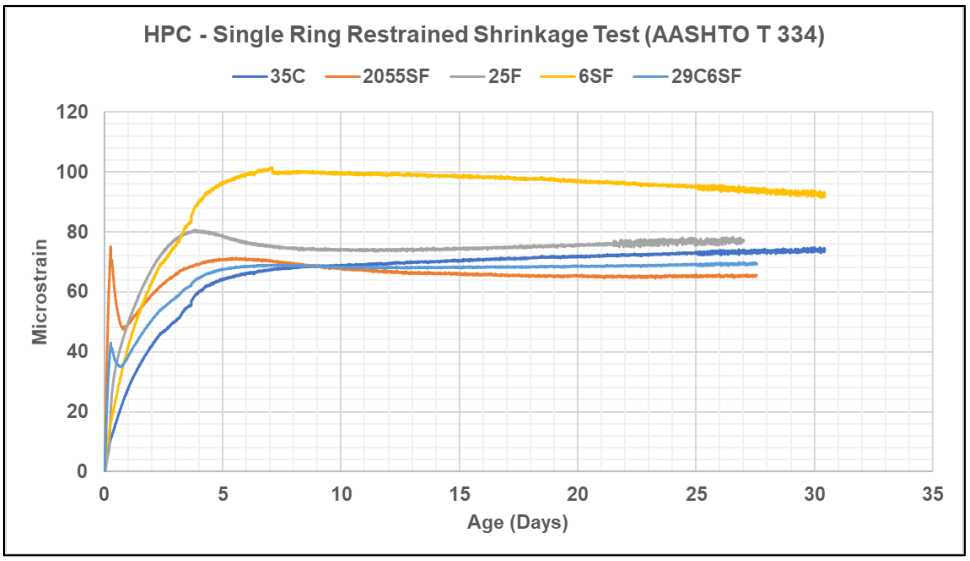

Figure 4-13: Strain Development in HPC Mixtures for Restrained Shrinkage Test

At 28 days, no crack was noted on any ring specimen (five mixtures), and the tests were terminated. The strain rate development and peak stress measured from the ring tests for HPC mixtures was used to calculate the strain factors and thereby evaluate the CP, as discussed in the following section.

4.4.3.3.4 Evaluation of CP of HPC Mixtures

4.4.3.3.4.1 CP Based on Restrained Shrinkage Test

The strain rate factor for each tested ring specimen was determined based on ASTM C 1581 by following Equation 4-1

Equation 4-1 $$\epsilon_{net} = \alpha\sqrt{t} + k$$

Where ϵ_{net} is the net strain (in/in), α is the strain rate factor for each strain gauge on the ring, t is the time elapsed in days, and k is the regression constant. The stress rate factor (q) of test specimens was determined using):

Equation 4-2, where t_r (the time to cracking) was taken as 28–30 days (~ age (days) at test termination for each mix):

Equation 4-2 $$q = G\frac{|\alpha_{avg}|}{2\cdot\sqrt{t_r}}$$

HPC mixtures were ranked for CP using the performance classification (Table 4-16) identified in ASTM C 1581.

Table 4-16: CP of Ring Specimens and Classification (ASTM C 1581)

NET TIME TO CRACKING (DAYS)	AVERAGE STRESS RATE (PSI/DAY)	CP (ΣRING/F'T)	POTENTIAL FOR CRACKING CLASSIFICATION
$0 < t_r \leq 7$	$S \geq 50$	>2.75	High
$7 < t_r \leq 14$	$25 \leq S < 50$	2.15–2.75	Moderate–High
$14 < t_r \leq 28$	$15 \leq S < 25$		Moderate–Low
$t_r > 28$	$S < 15$	<2.15	Low

Furthermore, the tensile strength of concrete (f'_t) and static MOE (E_c) measured for HPC mixtures at 28 days, and the CP of the mix was determined based on the stress to strength ratio, namely, the peak stress in the ring to the tensile strength of the mix, as shown in Equation 4-3:

Equation 4-3 $$CP = \frac{\sigma_{max,ring}}{f't} = \frac{\mu\epsilon_{max,ring} \cdot E_c}{f't}$$

Results from the ring test (strain rate development and peak stress), the CP of test specimens, and their performance classification is tabulated in Table 4-17. Since none of the rings demonstrated any cracks, HPC mixtures were classified for CP based on the average stress rate determined for these mixtures.

Table 4-17: Results from Ring Test and CP for HPC Mixtures

MIX #ID	STRAIN RATE FACTOR, A	STRESS RATE, Q	PEAK STRAIN IN RING	28-DAY—MOE	PEAK STRESS IN RING (Σ'MAX.)	28-DAY SPLIT TENSILE ST (F'T)	CP OF RING (Σ'MAX./F'T)	*POTENTIAL FOR CRACKING—CLASSIFICATION*
	με/day	*psi/day*	*με*	*psi*	*psi*	*psi*		
6SF	18.4	18.20	162	4.1E+06	658	513	1.28	*Moderate–Low*
25F	14.47	14.32	135	4.0E+06	545	509	1.07	*Moderate–Low*
20F5SF	13.41	13.27	133	4.1E+06	546	522	1.05	*Low*
35C	13.45	13.31	109	4.0E+06	438	508	0.86	*Low*
29C6SF	12.53	12.40	115	4.2E+06	479	531	0.90	*Low*

4.4.3.3.5 Cracking Potential Indicator (CPI) Evaluation of HPC Mixtures based on Free Shrinkage

Cracking in concrete mixtures is a function of three primary parameters: (1) free shrinkage strains, (2) concrete's MOE that governs the stress development, and (3) tensile strength of concrete that governs concrete's resistance to cracking under tensile stresses. Accordingly, Fu et al. (*20*) proposed a parameter—CPI—to assess the potential for cracking of concrete mixtures based on ASTM C 157 free shrinkage strains (ϵ_{free}), and mechanical properties' tensile strength of concrete (f'_t), and static MOE (E_c) of concrete, as shown in Equation 4-4.

Equation 4-4 $$CPI = \frac{\epsilon_{free} * E_c}{f'_t}$$

However, CPI's methodology—based on ASTM C 157—of evaluating cracking tendency overestimates the tensile stress because the effect of creep relaxation on free shrinkage strains are ignored (Figure 4-14). Therefore, the parameter CP—can be determined for concrete mixtures by incorporating the effects of creep relaxation through a creep coefficient (ϕ) in combination with ASTM C 157 free shrinkage strains (ϵ_{free}), the tensile strength of concrete (f'_t), and static MOE (E_c), as shown in Equation 4-5:

Equation 4-5

$$CP = \frac{\frac{\epsilon_{free} \cdot E_c}{1+\phi}}{f't}$$

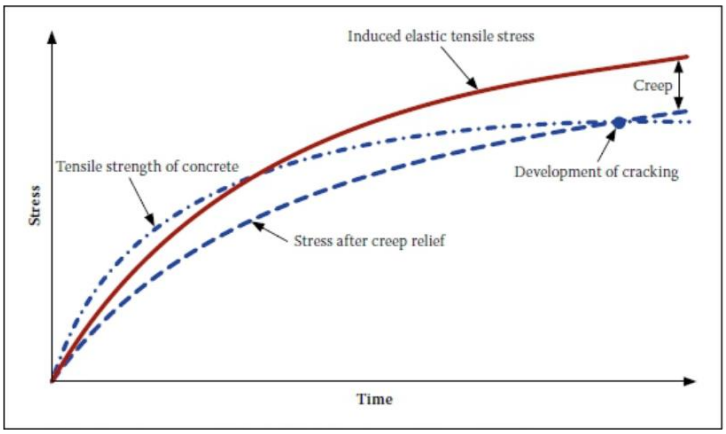

Figure 4-14: Schematic Representation of Crack Development (*21*)

The current research assessed the CP of HPC mixtures by determining both cracking parameters—CPI and CP—at 28 days. In addition, the creep coefficient of HPC mixtures was estimated based on RILEM's B3 predictive model proposed by Baweja and Bazant (*22*). Based on the HPC mix's CPI and CP at 28 days, its potential cracking performance was classified based on the threshold limits proposed in Table 4-18.

Table 4-18: CP Classification Based on 28-Day CPI and CP

CPI	CP	POTENTIAL FOR CRACKING
CPI ≥ 4.0	CP > 1.5	*High*
3.0 ≤ CPI < 4.0	1 < CP ≤ 1.5	*Moderate–High*
2.5 ≤ CPI < 3.0		*Moderate–Low*
CPI < 2.5	CP ≤ 1	Low

Results from the 28-day CPI, CP, and potential cracking performance for HPC mixtures is tabulated in Table 4-19.

Table 4-19: Results from Concrete CP Estimation for HPC Mixtures

MIX #ID	28 DAYS		28 DAYS DRYING SHRINKAGE	CPI (NO CREEP)		CREEP COEFFICIENT	CP (INCLUDING CREEP)	
	f't (psi)	MOE (10^6 psi)	DS (μs)	CPI	Classification	B3 Model	CP	Classification
CEM	447	3.8	400	3.40	Moderate–High	1.79	1.22	Moderate
6SF	467	4.1	436	3.78	Moderate–High	1.60	1.46	Moderate
25F	438	4.0	250	2.30	Low	1.67	0.86	Low
20F5SF	527	4.1	280	2.18	Low	1.63	0.83	Low
35F	506	3.9	230	1.79	Low	1.71	0.66	Low
35C	546	4.0	300	2.21	Low	1.62	0.84	Low
29C6SF	527	4.2	350	2.76	Moderate–Low	1.52	1.10	Moderate
35C10SF	517	4.4	382	3.24	Moderate–High	1.47	1.31	Moderate

4.4.3.4 Conclusions

HPC mixtures containing SF, especially ternary Class C FA and SF mixtures (29C6SF and 35C10SF), demonstrate high tensile strength at early ages. However, a combination of high MOE and low creep coefficient can result in high levels of stress development, which, especially at early ages, could vastly exceed the tensile strength and thus result in cracking.

Results from this section demonstrate that a simple calculation of free shrinkage stress-to-splitting tensile strength provides a simplified assessment of the HPC mix's CP. Especially, the CP of mixtures 29C6SF (moderate–low) and 6SF and 35C10SF (moderate–high) agree well with the observations of high AS and DS and strain rate development at early ages (up to 28 days) in these mixtures. Furthermore, creep relaxation in HPC mixtures appears to play a minimal influence in lowering stress development because all HPC mixtures show a similar 28-day CPI and CP classification for CP.

A single-ring restrained shrinkage test, as per ASTM C 1585 (or AASHTO T 334), presents several difficulties in the proper test setup, casting, and handling test specimens, all of which affect the concrete mix's strain evaluation. During the casting of ring specimens, fresh concrete's compaction and consolidation process often displaces the clamps used in the test setup, thus affecting the concrete ring's geometrical configuration. Moreover, the concrete ring specimens are much larger, heavier, and difficult to handle, making it challenging to conduct rapid and repeatable trials. Furthermore, strain gauges mounted to the ring's surface are susceptible to the environment (temperature and vibration), resulting in inaccurate results.

Therefore, the proposed approach of using free shrinkage strain (ASTM C 157 tests) and consideration of creep coefficient present an effective and practical assessment of stress evaluation in HPC mixtures. Moreover, the free shrinkage stress-to-splitting tensile strength approach also eliminates the dependency on ring tests to estimate and determine the concrete CP of the mixtures. However, in current research, the creep behavior of HPC mixtures was estimated based on the existing B3 models. Therefore, future work is needed to investigate the creep behavior of HPC mixtures experimentally.

4.4.4 Pore Solution Composition and Conductivity of HPC Mixtures

4.4.4.1 Background

4.4.4.1.1 TTI Model-1

Soluble alkali from FA is known to directly modify concrete PS alkalinity (PSA), thereby influencing the ASR durability of concrete mixtures (*23*, *24*). However, several studies on ASR also noted that a high soluble alkali contribution from fly ashes, especially at early ages and from certain Class C fly ashes, could significantly increase PSA, thereby affecting the ASR durability of concrete mixtures (*25–28*). A high PSA in concrete generally presents a highly conducive environment for ASR initiation, especially (a) when fast reactive or highly reactive aggregates are present in the mix, and (b) when insufficient time is available for the pozzolanic reaction to initiate, manifest, and reduce the alkalinity of the PS (*27*). Typically, the alkali fixation in the reaction products (alkali binding) starts simultaneously with the pozzolanic reaction (after approximately 28–90 days), resulting in a gradual reduction of PS conductivity (PSC)/PSA with age (*29*, *30*). However, the effect of alkali binding is contingent on the quantity and stochiometric composition of CSH, which depends upon the type, composition, and reactivity of SCMs as well as the concrete mix proportions. Thus, for the determination of PSA, consideration of water-soluble alkali's (WSA's) contribution from FA in addition to total soluble alkali contribution from cement presents a scientific and suitable approach to evaluate the ASR mitigating potential of fly ashes. Therefore, in the current research, a prediction model TTI Model-1 was developed to estimate concrete mixtures' PSA based on the combined effect of soluble alkali contribution from cement and WSA from fly ashes into concrete PS. Therefore, determining PSA using TTI Model-1 and comparing it with the aggregate's threshold alkalinity (THA) (i.e., PSA ≤ THA) presents an effective approach to tackling the initiation of possible ASR, especially for concrete mixtures with reactive and highly reactive aggregates. The development and results from TTI Model-1 are discussed later as part of the TxDOT Tool.

4.4.4.1.2 TTI Model-2

Previous studies have demonstrated that the concrete PS is directly affected by the soluble alkali contribution from FA rather than the bulk alkali content prescribed by ASTM C618 (2, 17, 22, 23). While cement contributes around 75 percent of total bulk alkalis into the PS at early ages (within 28 days) (*31*), the total soluble alkali from fly ashes is much lower and typically 30–40 percent for Class F ash and 50–55 percent for Class C ashes (*27*, *32–34*). Therefore, the NIST +

ASTM C 311 combined approach presents a robust approach to account for soluble alkali from fly ashes to aid in determining the PS concentration of blended concrete mixtures. However, since the combined approach follows the NIST model, the effect of alkali binding in PSC reduction account only for the incorporation of SF and not from other high siliceous SCMs, such as Class F FA. In contrast, Lothenbach et al. (*35*) noted that while FA hydration releases more alkali into the PS, the pozzolanic reaction results in lower Ca/Si CSH formation—thus, lowering PSA with time due to alkali binding. However, the effect of alkali binding is contingent on the quantity and stochiometric composition of CSH, which depends upon the type, composition, and reactivity of SCMs, as well as the concrete mix proportions. In the current research, a prediction model, TTI Model-2, was developed to estimate the PSC of binary and ternary concrete mixtures containing Class C FA, Class F FA, and SF at long-term hydration ages.

4.4.4.2 Methods

The alkali (Na and K) concentrations in the PS of eight HPC mixtures were determined from 7 to 180 days following the two approaches discussed below. Because the Na and K ions are the primary charge carrier in the PS of concrete mixtures, the electrical conductivity of the PS was calculated based on the alkali (Na, K) and hydroxide (OH) concentrations of each mix using well-established mathematical expressions (1).

4.4.4.2.1 TTI Model-2

In the current research, TTI Model-2 was used to estimate alkali (Na and K) concentrations in the PS concentration of eight HPC mixtures based on the methodology outlined above. Concrete PS composition (i.e., ionic concentrations) is primarily controlled by its ingredients' chemical and mineralogical composition. Therefore, the relevant parameters representing bulk chemical composition, mineralogical composition determined by the QXRD, and available alkali measurements for fly ashes used in the current research are summarized in Table 4-20.

Table 4-20: Bulk Alkali, Mineralogical Composition, and Available Alkali for Fly Ashes

OXIDE COMPOSITION %		CEMENT	CLASS C FA	CLASS F FA	SF
Na_2O_{eq} (Bulk)		*0.43*	*2.02*	*1.08*	*0.51*
QXRD	Crystalline vs. Amorphous (%)	*N/A*	54%/46%	32%/68%	3%/97%
	Theradnite (Na-SO4)	0.23%	1.98%	0.37%	*N/A*
	Arcanite+Syngenite (K-SO4)	0.64%	0.60%	0.69%	*N/A*
Available Alkali (AA, ASTM C 311) [Na_2O_{eq} and (AA/Bulk)]		*N/A*	1.36 (67%)	0.42 (39%)	*N/A*

Note: N/A = Not Applicable; n/a = not available.

4.4.4.2.2 Thermodynamic Modeling

Thermodynamic modeling (GEMS Selektor v 3.5 software) was used to calculate the influence of SCM type, composition, replacement level, and effect of hydration time on the ionic composition of the PS for eight HPC mixtures. Built-in GEMS thermodynamic database PSI-GEMS and Cemdata18 were used to model the cementitious systems' equilibrium reactions and

hydration products consisting of different combinations of cement, tested fly ashes, and SF (*36–38*). Hydration of the binary OPC-FA mixtures was performed by combining an empirical model describing the dissolution of the clinker phases and the FA reaction as a function of time, using an approach described below. When OPC is partially replaced by SiO_2-rich SCMs such as SF/FA, the pozzolanic reaction consumes calcium hydroxide and results in low Ca/Si CSH formation. Prior experimental work has shown that a low (≤1.5) calcium-to-silica (C/S) CSH characteristic of OPC-SCM mixtures binds alkali better than the higher C/S CSH typically found in the OPC system (*39*). The effect of alkali binding was incorporated through the CSH Quaternary (i.e., CSHQ) model proposed by Kulik (*40*). GEMS3K's thermodynamic database recognizes four types of CSH variants based on the C/S ratio: Jennite D (C/S = 2.27), Jennite H (C/S = 1.33), Tobermorite D (C/S = 0.45), and Tobermorite H (C/S = 0.667) (33).

4.4.4.3 Results and Discussion

Since the ionic concentration of Na and K in PS directly correlates with the solution's conductivity, the influence of SCM type, composition and replacement level is presented as changes in PSC of HPC mixtures from 7–180 days, as discussed below. In addition, the discussions on PSC of HPC mixtures from this section will be used to interpret results from electrical RCPT methods (Section 5) and resistivity (Section 6) in this tech memo.

4.4.4.3.1 TTI Model-2

The PSC values of HPC mixtures at 7, 28, 91, and 180 days are shown in Figure 4-15.

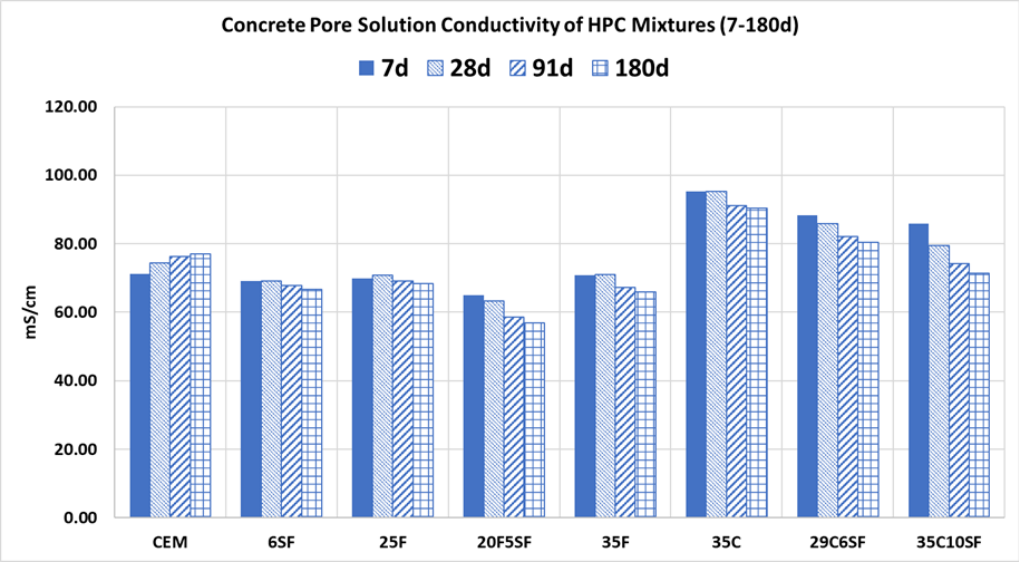

Figure 4-15: PSC of HPC Mixtures (7–180 days)

4.4.4.3.1.1 Plain OPC mix

HPC mixtures were prepared using a Type I/II cement with a bulk alkali content (Na_2O_{eq}) of 0.43 percent. Cement hydration releases a substantial amount of its bulk alkalis into the PS at a very early age (within 7–28 days). A high PSC in CEM mix is a combination of (1) high WSA (~ 69 percent) fraction, available in the PS within 1 day, especially from the soluble alkali sulfate

phases; and (2) a high degree of cem hydration (~75 percent at 28 days), which releases bound alkalis from clinker phases. Because most of the soluble alkalis are released at an early age, the increase in PSC from 7–180 days is negligible (~ 10 percent). In addition, the primary hydration products of cement reaction—CSH with a high Ca/Si—has no or negligible capacity to bind alkalis from the PS, and thus there is a gradual increase in PSC of the plain OPC mix with time.

4.4.4.3.1.2 SF Mix

SF incorporation significantly increases the reaction rate due to its high surface area (nucleation effect) and high pozzolanic activity. At 7 days, the PSC is slightly lower than the CEM because of cement dilution, with some effect from pozzolanic reaction (i.e., formation of low Ca/Si CSH through pozzolanic reaction alkali binding by these low Ca/Si CSH products from the PS). However, the reduction of PSC from 28 to 180 days is primarily due to pozzolanic reaction and alkali binding effects.

4.4.4.3.1.3 Class F FA Mixtures

Class F FA used in this study contained a higher bulk alkali content (1.08 percent Na_2O_{eq}) than cement. However, a significantly lower fraction of the bulk alkali (6 percent WSA and 39 percent AA) combined with a lower soluble alkali and slower degree of reaction of FA reduces the alkali contribution, and therefore the PSC of FA mixtures 25F, 20F5SF, and 35F at early ages (~ 7 days) compared to cement.

For binary FA mixtures 25F and 35F, a decrease in PSC (8 percent and 11 percent, respectively) from 28–180 days can be attributed to the alkali binding by low Ca/Si-CSH formed from FA pozzolanic reactions. Moreover, the dissolution of Al_2O_3-rich Class F FA enhanced the alkali binding capacity of the hydrated phase to further lower the PSC due to the formation of the calcium alumino-silicate hydrate (CASH) phase in these mixtures.

For the ternary 29F6SF mix, a synergistic combination of SF and Class F FA pozzolanic reactions increased the quantity of low Ca/Si CSH and CASH formation. Therefore, from an enhanced alkali binding capacity, the ternary 20F5SF mix demonstrated a more significant PSC reduction (i.e., 12 percent) from 28–180 days than binary F FA mixtures.

4.4.4.3.1.4 Class C FA Mixtures

Class C fly ashes used in current research contained bulk alkali content of 2.02 percent (Na_2O_{eq}), and the alkali tests measured as 14 percent water-soluble and 67 percent available alkali fraction for this FA. Consequently, a high soluble alkali fraction explains a 20–35 percent increase in PSC of 35C, 29C6SF and 35C10SF mixtures compared to CEM at early ages (7 days). Additionally, a lower alkali binding potential of higher Ca/Si-CSH phase formed from Class C FA hydration explains a meager reduction (4–5 percent) in PSC from 28–180 days for 35C mix. In contrast, the ternary combination of Class C FA with SF reduces the PSC by 9 percent and 12 percent in 29C6SF and 35C10SF from 28–180 days. Dilution of cement and Class C FA alkalis and increased potential for alkali uptake by low Ca/Si CSH from SF pozzolanic reaction explains a steeper decrease in PSC compared to binary C FA mix.

4.4.4.3.2 Thermodynamic Modeling

Thermodynamic-based GEMS modeling was used to determine the ionic composition and concentrations in the PS of HPC mixtures in sealed conditions from 7 to 180 days. The ionic concentration of Na, K, and OH determined from GEMS modeling were used to calculate the PSC of HPC mixtures by following the approach outlined by Snyder et al. (*41*). For eight HPC mixtures, PSC estimated based on ionic composition predictions from GEMS thermodynamic modeling were compared with TTI Model-2, and the results are shown in Figure 4-16.

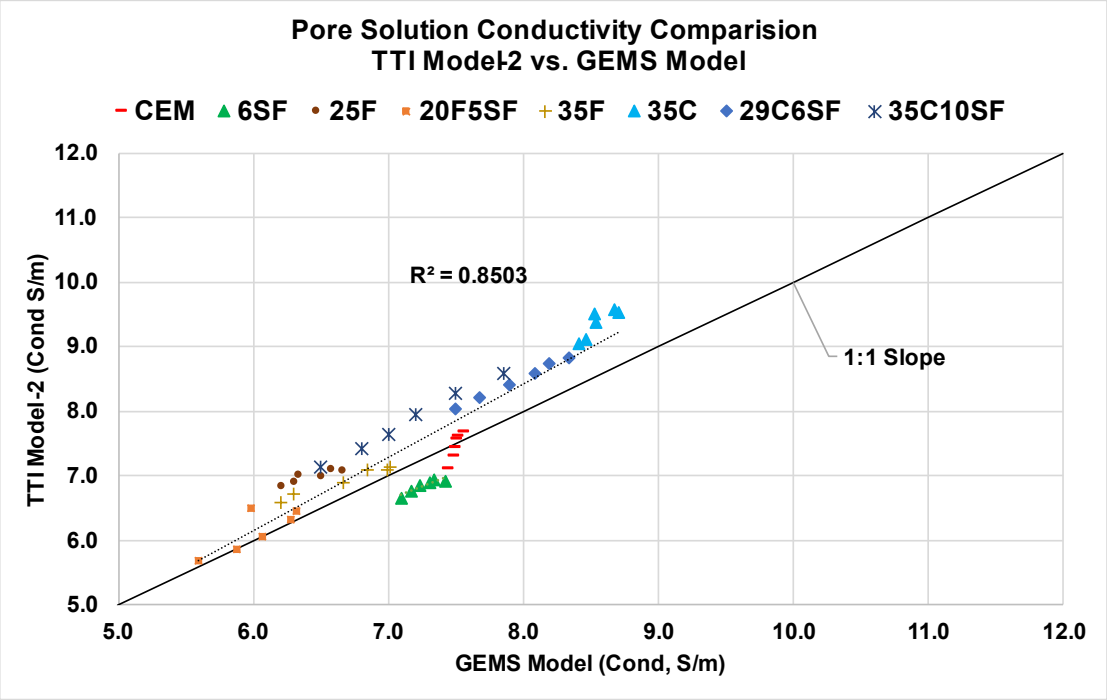

Figure 4-16: Comparison of PSC Based on GEMS Modeling and TTI Model-2

Comparison of results from Figure 4-16 provides a favorable validation of TTI Model-2 predictions of PS composition; that is, the ionic concentration is a close match, as observed between the PSC determined using two approaches. Furthermore, for all binary and ternary HPC mix combinations with SF, Class C and Class F fly ashes, TTI Model-2 estimations of PSC are noted to be within ± 5–7 percent of the GEMS model predictions.

However, TTI Model-2 predictions of PS ionic concentrations (and therefore, the conductivity) are marginally higher for all FA mixtures than GEMS and all ages. A primary reason can be attributed to the methodology, wherein the GEMS model estimates the PS composition of concrete mixtures based on thermodynamic phase equilibria between solid hydration and PSs. Furthermore, the GEMS model incorporates a Gibbs' free energy minimization theory to determine the solid-phase assemblage based on several parameters such as dissolution, precipitation, reaction enthalpies, and solubility products of different phases, temperature, and others. In contrast, TTI Model-2 uses available alkalis and stoichiometric predictions of CSH (alkali binding) to predict PSC of concrete mixtures.

4.4.4.4 Conclusions

While the thermodynamic model can predict PSC with higher accuracy, it does not present a convenient approach for industry practitioners. It is imperative to note that the accuracy of thermodynamic modeling predictions of PSC is contingent upon the accuracy and reliability of inputs used for modeling. For high reliability of outputs, GEMS modeling requires the mineralogical composition of ingredients (crystalline versus amorphous phases) determined based on QXRD measurements, in addition to the bulk oxides' (XRF) composition. Similarly, modeling hydration reactions for SCMs such as FA, SF, and others in GEMS requires the knowledge of the kinetics of SCM's dissolution, namely, a determination of SCM's dissolution with time. For high reliability of outputs, SCM dissolution in the system is measured through QXRD or scanning electron microscopy (SEM) or thermogravimetric analysis (TGA) techniques and fitted to a rate equation to that specific system (*30*, *42*, *43*). However, as an alternative to complex dissolution measurements, simplified assumptions such as assuming a constant reactivity of ingredient over time (*44*) are often employed in the modeling, resulting in lower reliability of outputs.

Therefore, the TTI Model-2 developed in current research presents a simplified approach to predict PSC of binary and ternary mixtures of concrete mixtures containing SF, Class C, and Class F Fly ashes for both research practice and industry implementation.

4.4.5 Rapid Chloride Permeability Tests

4.4.5.1 Test Description

HPC mixtures were evaluated for resistance to chloride ion penetration (i.e., permeability) as per ASTM C 1202 test procedures. For RCPTs, a replicate of nine 4 × 8-inch (4 ± 0.08 inch diameter and 8 ± 0.16 inch height) concrete cylinders were cast for each HPC mix design. Cylinders were demolded at the age of 24 ± 2 hours and placed in a controlled environmental chamber maintained at 23 ± 2 °C and 98 ± 2 percent RH, based on ASTM C 511 recommendations on a moist curing regimen. RCPTs were performed at 28, 56, and 91 days of moist curing with three replicate specimens at each age for each HPC mix design.

Two days before the testing, 4 × 8-inch samples were removed from the moist room and cut using a wet saw to obtain 2-inch (50 mm) thick specimens from its midsection. Next, Sikadur 32 Hi-Mod epoxy was used to seal the sides, and the specimens were left to dry for 5 hours. After drying, test specimens were placed in a vacuum desiccator, sealed, and connected to the vacuum pump. The vacuum pressure was maintained for 3 hours in the desiccator. After that, de-aired/ deionized (DI) water was introduced into the desiccator until the samples were fully submerged, after which vacuum pressure was applied for an additional hour. At the end of the 4 hours, the vacuum pump was shut down, and specimens were left submerged in the desiccator for an additional 18 ± 2 hours. At the end of sample conditioning, specimens were blotted off to SSD condition and placed in an RCPT cell for the experiment. The positive side (anode) of the test

cell was filled with a 0.3N (normality) sodium hydroxide solution (NaOH), and the negative side (cathode) was filled with a 3 percent by mass sodium chloride (NaCl) solution. After checking for leaks, an external voltage of 60 V was applied across the 2-inch specimen for a test duration of 6 hours. The permeability classification with defined RCPT ranges is provided in Table 4-21.

Table 4-21: RCPT Performance Classification as per ASTM C 1202

PERMEABILITY CLASSIFICATION	RCPT
High	>4000
Moderate	4000–2000
Low	2000–1000
Very Low	100–1000
Negligible	<100

4.4.5.2 Results and Discussion

Results (i.e., RCPT values as total charges passed in coulombs) from the RCPT and chloride ion penetrability classification (i.e., permeability classification) at 28, 56, and 91 days for all the tested HPC mixtures are presented in Table 4-22 and plotted in Figure 4-17.

Table 4-22: RCPT Results of HPC Mixtures at 28, 56, and 91 Days and Permeability Classification

% RL	MIX #ID	RCPT (COULOMBS)			PERMEABILITY CLASSIFICATION *(FOLLOWING ASTM C 1202)*		
		28d	56d	91d	28d	56d	91d
0–10%	CEM	2870	2020	1414	Moderate	Moderate	Low
	6SF	2030	1535	1196	Moderate	Low	Low
25%	25F	1675	1224	878	Low	Low	Very Low
	20F5SF	1275	798	721	Low	Very Low	Very Low
35%	35F	1517	1163	800	Low	Low	Very Low
	35C	2050	1445	1148	Moderate	Low	Low
	29C6SF	1997	1760	1081	Low	Low	Low
45%	35C10SF	1895	1630	970	Low	Low	Very Low

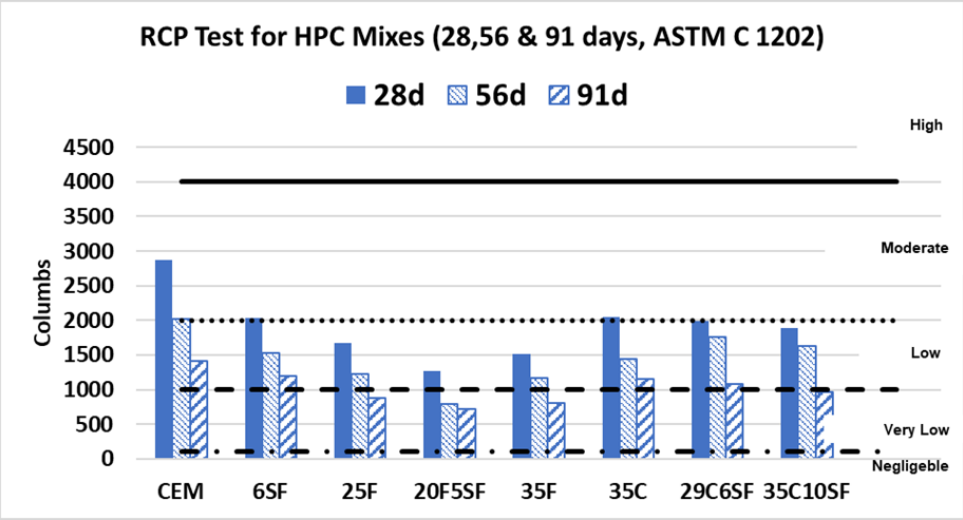

Figure 4-17: RCPT Results for HPC Mixtures at 28, 56, and 91 Days of Moist Curing

Figure 4-17 demonstrates that the SCM type and replacement level are the primary factors influencing the RCPT values. In general, a decreasing trend of the RCPT values from 28 to 91 days was the common characteristic for all the tested HPC mixtures and the CEM. HPC mixtures containing SCM (both binary and ternary mixtures) demonstrated lower RCPT values than the CEM at all ages, which indicates improvement in permeability (densification in microstructure) through SCM pozzolanic reaction and some filler effects. However, the lack of sensitivity of the RCPT is evident from the following two observations.

4.4.5.2.1 At 56 days (recommended testing time)

The CEM was identified as moderate, which was expected. In other words, only one mix (20F5SF) was classified as very low, which was also intended. However, 6SF, 25F, 35F, 35C, 29C6SF, and 35C10SF all were classified as low. In addition, a considerable difference was observed for these mixtures based on the resistivity/FF criteria (discussed later). Therefore, based on the RCPT, all these mixtures should perform the same way—that is, give an indication of less sensitivity of the RCPT.

4.4.5.2.2 At 91 days

The test duration was extended up to 91 days to see if increasing the test duration facilitated a better classification of the mixtures. However, the following observations disproved this expectation:

- The CEM, along with 6SF, 35C, and 29C6SF, were classified as low, meaning that these mixtures should perform the same way, which may not be the case.
- HPC Mixtures CEM and 6SF demonstrated a similar permeability classification at 91 days. However, only the ternary mix 35C10SF demonstrated a very low permeability classification among the Class C FA mixtures at 91 days.
- Class F FA mixtures demonstrated the largest reduction in RCPT values for all ages other than CEM and other SCM mixtures. Although the ternary mix (20F5SF) typically

performed better than binary mixtures (25Fand 35F) at all ages, all three mixtures were classified as *very low* permeability. RCPT failed to identify the 20F5SF mix as a better performing mix than the 25F or 35F.

Therefore, RCPT leads to an inconsistent classification of the studied HPC mixtures and shows no clear trend.

4.4.5.2.2.1 Assessment of Concrete Permeability Reduction based on the RCPT

RCPT uses the total charge passing through the concrete specimen during the 6-hour test duration to assess concrete's permeability based on its resistance to chloride ion penetration.

Concrete's permeability depends on the pore structure of concrete; however, the total charge passed in the RCPT is a function of PSC and pore structure characteristics, namely, their distribution and connectivity. Although SCM incorporation in concrete reduces pore connectivity and refines pore size distribution through filler effect or pozzolanic reaction, it also modifies concrete PS chemistry. SCMs such as SF, fly ashes, etc., significantly influence ionic (Na and K) composition and concentration of the PS through (a) alkali dilution (less soluble alkali contribution from cement into PS); (b) soluble alkali contribution (e.g., some class C ashes contain substantial soluble alkali sulfate phases and contribute soluble alkalis in PS increasing Na, K concentrations); (c) alkali contribution from the amorphous phase through the pozzolanic reaction; and (d) alkali binding (e.g., pozzolanic CASH phases with lower Ca/Si bind alkalis from PS and reduced PSA). Change in PS chemistry directly influences the PS's electrical conductivity and thus directly affects RCPT results. However, SCM composition, type, and replacement level can significantly affect PSC, which may have little to do with chloride permeability. Thus, to fully interpret concrete permeability reduction based on RCPT measurements, the effects of SCM on PSC was investigated and is discussed in the next section.

4.4.5.2.2.2 Influence of PSC on RCPT Measurements

The previous section discussed the effect of SCM type and replacement level on PS chemistry and conductivity. As discussed previously, the change in PS chemistry from SCM incorporation directly affects the PS's electrical conductivity and thus directly influences the RCPT measurements. Therefore, to understand the influence of PS electrical conductivity on RCPT results, RCPT values of the tested HPC mixtures at 28, 56, and 91 days were correlated with their PSC at the same ages, and the results are plotted in Figure 4-18.

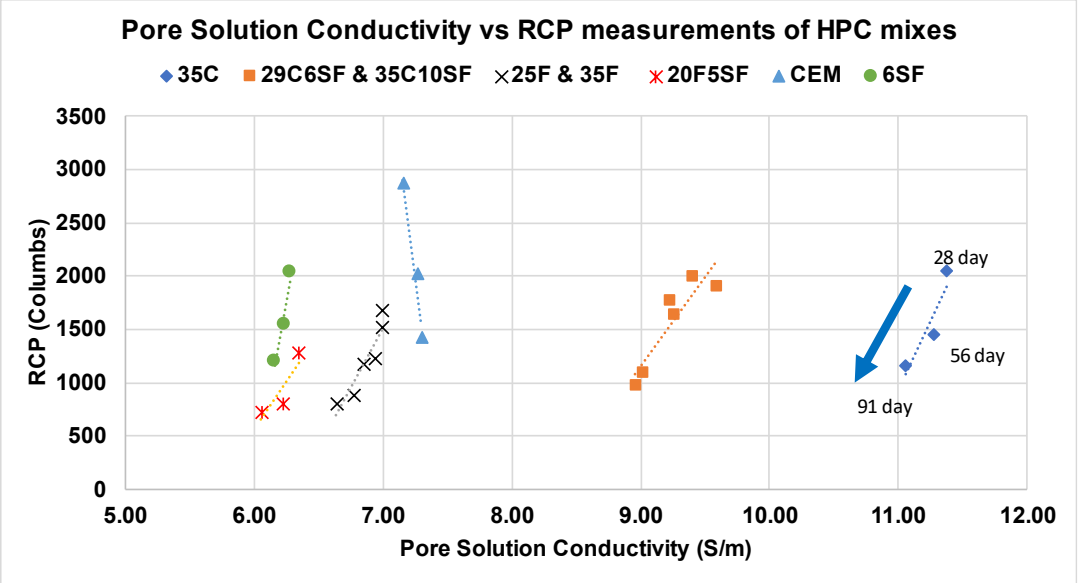

Figure 4-18: Correlation of RCPT Measurements with PSC (Sealed) of HPC Mixtures

RCPT measurements demonstrate a linear relationship with PSC for all HPC mixtures with SCMs—that is, a decrease of PSC with increasing ages correlates with the decrease of RCPT values. This process indicates that the RCPT results were influenced by the change in PSC over time. Therefore, RCPT results detect the combined effects of change in pore structure and connectivity and PSC over time and may not be considered a true representation of pore connectivity (a direct measure of permeability). Results also explain the inconsistent RCPT-based classification of the studied HPC mixtures, therefore revealing no clear trend. Thus, it is clear that the reduction in total charge passed cannot be directly used to assess SCM's influence on permeability reduction in HPC mixtures. Furthermore, several shortcomings of this test pertinent to the *Joule effect*, reproducibility and repeatability of test results, compound ionic migration, effects from conductance of hydroxyl ions, etc., have been widely discussed and comprehensively documented (*45*, *46*). Therefore, it can be postulated that RCPT measurements, especially for mixtures containing SCMs, cannot be used effectively to assess and rank different HPC mixtures for their chloride ion permeability.

4.4.5.3 Conclusion

As in ASTM C 1202, the RCPT uses the total charge passing through the concrete specimen during the 6-hour test duration as a measure of chloride ingress and transport through the concrete pore network. State agencies widely use the RCPT to assess concrete's permeability based on its resistance to chloride ion penetration. More frequently, the reduction in total charge passed between different mixtures or for a single mix at different ages is directly used to assess SCM's influence on permeability reduction through microstructure refinement. Furthermore, the RCPT's applicability and validity of this test to evaluate and rank permeability of concrete with SCMs based on chloride ion penetrability resistance has also been questioned(*46*).

Electrical measurements in concrete such as the RCPT are primarily a function of PSC and pore structure properties; however, the permeability of concrete only depends upon pore structure properties. In a true sense, the RCPT measures the diffusivity of chloride ions in saturated concrete under the application of an external electric field.

4.4.6 Resistivity Tests: Part I—Normal Temperature Conditioning

4.4.6.1 Introduction

Electrical measurements are gaining interest in the concrete industry as a rapid method of characterizing the microstructure and assessing concrete transport properties. The electrical resistivity of concrete is related to the resistivity of the PS, fluid-filled pore volume (porosity) and pore connectivity, as shown in Equation 4-6.

Equation 4-6 $$\rho_b = \frac{\rho_{ps}}{\phi * \beta}$$

Where, ρ_b represents concrete resistivity, ρ_{ps} represents pore solution resistivity of concrete, β represents pore connectivity and ϕ represents porosity of concrete.

Electrical measurements in concrete are primarily a function of three primary parameters: (a) *PS composition*—ionic conductivity, (b) pore structure characteristics—pore volume and pore connectivity, and (c) saturation state—moisture connectivity (*47*). Therefore, interpretations of concrete's microstructure development based on resistivity measurements require proper accountability of PS chemistry/conductivity other than the effects of pore structure characteristics and moisture connectivity. In addition, secondary parameters such as specimen geometry, temperature, curing regimen, leaching, and drying (moisture loss) additionally influence test results.

Curing regimen for concrete samples influences resistivity measurements primarily through leaching of ionic species (typically Na and K) from concrete specimens and saturation levels (DOS i.e., moisture connectivity). Currently, standard specifications for SR tests on concrete (AASHTO T 358) recommend a moist room curing regimen (23 ± 1 °C, RH 98 ± 2 percent) or immersing samples in saturated LW solution, as per ASTM C 511. With LW curing, alkali (Na and K) leaching from the tested concrete specimen into storage LW solution without any Na and K ions is a common phenomenon due to the existence of a concentration gradient (i.e., high alkali concentration in concrete PS versus no alkalis in LW soak solution). The conductivity of LW (~13.01 mS/cm at 21 °C) is several times lower than the conductivity of the concrete PS (~120–130 mS/cm), which supports the existence of this concentration gradient. Experimental studies by Tanesi et. al. (*48*) measured approx. 400 ppm, 300 ppm, and 125 ppm of potassium ion leached from OPC, 25 percent Class F FA, and 50 percent slag specimens, respectively, into LW at 56 days of LW curing. This alkali leaching caused a decrease of their concentration in PS, thereby changing PS resistivity (PSR). For example, Spragg et al. (*49*) demonstrated three times an increase of PSR due to leaching from concrete samples in LW curing. Furthermore, Bu et al. (*50*) demonstrated that alkali leaching could directly affect microstructure formation in some

instances. While a moist room curing regimen could reduce the leaching, previous research suggested that leaching can still occur due to the water that condenses on the surface of a specimen in a moist room (*49*, *51*). In addition, experimental work by Presuel-Moreno et al. (*52*, *53*) demonstrated that sample storage in LW curing versus moist curing (humidity chamber with 100 percent RH) could lead to differences in electrical measurements. In contrast with moist room and LW curing, a SC regimen for concrete has been shown to eliminate leaching (*54*). However, compared to submerged curing regimens such as LW curing, a significantly lower DOS in the SC affects the degree of hydration of concrete samples. In addition, Weiss et al. (*55*) noted that lower moisture content in SC samples could affect their microstructure development, thus additionally influencing the resistivity measurements.

Recently revised specifications for concrete BR tests (ASTM C 1876 and AASHTO TP 119) recommend a submerged SPS curing regimen (curing solution conductivity = 78.74 mS/cm) for sample curing. The concentrations of Na, K, and Ca in SPS represent an average concentration of these ions in a representative common concrete PS. As SPS contains alkali ions, this curing regimen minimizes alkali leaching from the tested concrete specimen into the surrounding soak solution to a greater extent, which leads to avoiding the effects of leaching on resistivity measurements. A reduction in alkali leaching was effective in minimizing variability in BR and SR measurements on concrete (*56*). However, in a recent resistivity study (*57*), researchers extracted PS from 38 paste samples of different concrete mixtures to prepare an individual and mix specific simulated PS for curing concrete samples. Although curing with mix-specific simulated solutions effectively eliminates leaching effects, preparing individual PSs is often a tedious and laborious task and not readily suitable for implementation by field practitioners. Thus, in the current research, a MPS curing regimen was developed as an intermediate solution between mix-specific and SPS curing practices. The Na, K, Ca, and OH ions concentrations in PSC of all the studied HPC mixtures were estimated using TTI Model-2 (presented earlier). For MPS curing, HPC mixtures were grouped based on the type of FA used in the studied HPC mix and then assigned an average PSR for each group, as shown in Table 4-24 and discussed later in detail.

4.4.6.2 Test Matrix

The overall test matrix for evaluating the BR and SR performance of HPC mixtures is shown in Table 4-23 and discussed in the following sections.

Table 4-23: Test Matrix for Evaluating Resistivity Performance of HPC Mixtures

PARAMETER	TEST METHOD	AGE OF TESTING	CURING REGIMEN
BR	ASTM C 1876	7–180 days *Curing Temperature: 23 ± 2 °C*	1. SC 2. LW Curing 3. SPS Curing (ASTM C 1876) 4. MPS curing
SR	AASHTO T 358		

4.4.6.3 Test Methods

For resistivity testing, 4×8-inch (4 ± 0.08 inch diameter and 8 ± 0.16 inch height) concrete cylinders were cast for each HPC mix design. Concrete cylinders were demolded at the age of 24 ± 2 hours and subjected to different curing regimens (Table 4-23), as described in the next section. For each HPC mix design, resistivity measurements were performed on five replicate specimens at 7, 14, 28, 56, 91, and 180 days of the curing period. Test samples (4 × 8-inch concrete cylinders) subjected to SC were unwrapped and rolled in a moist towel to minimize the effects of surface drying (moisture loss) on resistivity measurements at each testing age. For the submerged curing regimen, test samples (4 × 8-inch concrete cylinders) were removed from the storage buckets, washed with tap water to remove curing solution from surfaces, and blotted off to an SSD state with a clean damp cloth prior to resistivity measurements.

4.4.6.3.1 Uniaxial BR Test

BR measurements were performed on 4 × 8-inch (4 ± 0.08 inch diameter and 8 ± 0.16 inch height) concrete cylinders following ASTM C 1876 /AASHTO TP 119 specifications. BR measurements were performed using a commercially available resistivity meter RCON, manufactured by Giatech Scientific, at a frequency of ~1kHz at 23 ± 2°C. During the test, the end sponges of the device were saturated with conductive gel and placed between the specimens to ensure good electrical contact with the end electrodes. Based on test samples' cylindrical geometry and dimensions (4 × 8 inches), a geometric correction factor (GCF) of 1.57 inches (3.98 cm) was used in BR determination.

4.4.6.3.2 SR Tests

SR measurements were performed on 4 × 8-inch (4 ± 0.08 inch diameter and 8 ± 0.16 inch height) concrete cylinders following AASHTO T 358 specifications. A commercially available 4-point Wenner probe SR meter, manufactured by Proceq, was used for the testing. Prior to testing, all test samples (4 × 8-inch concrete cylinders) were marked with lines (parallel to the long axis of the cylinder) at 0, 90, 180, and 270 degrees along the cylinder's circumference. SR was measured along these lines in duplicate, which created eight readings per specimen. The average of these eight readings was reported as a representative SR value for the tested specimen. Based on test samples' cylindrical geometry and dimensions (4 × 8 inches) and 2 inches (50 mm) probe spacing of the test device, a GCF of 1.97 was used in SR determination. In addition, for samples subjected to submerged LW curing regimen, a multiplier of 1.1 was applied to SR measurements, as per AASHTO T 358 recommendations.

4.4.6.4 Specimen Curing and Conditioning Procedures

A comprehensive study covering seven curing/conditioning regimens was undertaken in the current research to evaluate the effect of sample curing and conditioning procedures on concrete resistivity measurements as described below:

Normal Temperature Conditioning Procedure (NC): Under *NC*, concrete cylinders were cured under standard laboratory temperatures of 23 +/- 2°C, from the time of demolding (24 ± 2 hrs.) to

the entire test duration. Concrete cylinders were tested under four different curing regimens: SC, LW curing, SPS curing, and MPS curing regimens, as described below.

4.4.6.4.1 SC Curing

Five 4 × 8-inch concrete cylinders for each HPC mix design were sealed from moisture loss using double-wrap plastic bags and stored in a controlled environmental chamber (23 ± 2 °C, RH 98 ± 2 percent) to minimize evaporation losses. At each testing age, test samples (4 × 8-inch concrete cylinders) were unwrapped, rolled in a moist towel to eliminate any effects of surface drying due to moisture loss (if any) prior to resistivity tests. The test specimen's mass was recorded before and after each resistivity test. After the necessary measurements, samples were resealed with double-wrap plastic bags and placed back in the controlled environmental chamber. Although the effectiveness of the double-wrap technique is often questioned (*58*), a previous study that implemented a similar sealing technique demonstrated a very low coefficient of variation (COV) in resistivity measurements, with an SR/BR ratio close to 1.0 at all testing ages (*47*). Furthermore, in current research, the average mass loss was noted in the range of 0.2 percent ± 0.05 percent after 180 days across all test samples, which is lower than the threshold mass loss of 0.4 percent at 28 days recommended for effective sealing practice (*59*).

4.4.6.4.2 LW Curing

Based on ASTM C 511 curing specifications, test samples (4 × 8-inch concrete cylinders) were immersed in saturated LW baths and stored in a controlled environmental chamber (23 ± 2 °C, RH 98 ± 2 percent). The lime content in baths was periodically monitored (2g/L), and a storage solution to sample volume ratio of 2:1 was maintained throughout the testing period (*47*). At each testing age, samples were removed from the buckets, washed with tap water to remove simulated PS from the surface, and blotted to an SSD state with a clean damp cloth prior to resistivity tests.

4.4.6.4.3 SPS Curing

Following ASTM C 1876 specifications for curing solution (Table 4-24), 102.6 g of dry NaOH, 143.9 g of dry KOH, and 27 g of dry Ca(OH)2 were added to a 5-gallon (18.9 L) bucket to prepare a 3.6 gal (13.5 L) SPS of conductivity of 78.74 mS/cm. Test samples (4 × 8-inch concrete cylinders) were submerged in an SPS bucket solution, and the sealed buckets were placed in a controlled environmental chamber (23 ± 2 °C, RH 98 ± 2 percent) throughout the 180-day testing period. The storage solution to sample volume of each SPS bucket to maintained at 4:1. At each testing age, samples were removed from the buckets, gently washed with tap water to remove the adhered soak solution from the surface and blotted off to SSD condition with a clean damp cloth prior to resistivity tests.

4.4.6.4.4 MPS Curing

The eight HPC mix designs evaluated in the current study were divided into three groups: (1) mixtures with no FA, (2) mixtures with Class F FA, and (3) mixtures with Class C FA, as shown in Table 4-24. First, the concentrations of Na, K, Ca, and OH ions in PSC of all the studied HPC mixtures were estimated using TTI Model-2 (presented earlier). Then, the average

PSC of mixtures in each group was used to determine the composition of the representative PS for that group, followed by an estimation of the NaOH and KOH dosage to prepare that representative soak solution as MPS, as shown in Table 4-24. Finally, the curing solution was saturated with 2 g/L calcium hydroxide (i.e., $Ca(OH)_2$ or CH) to mimic the PSC since concrete PS remain saturated with CH. This kind of MPS greatly minimizes leaching of Na, K, and Ca ions from test specimens into surrounding solution(*49*). Test samples (4 × 8-inch concrete cylinders) were submerged in their respective MPS buckets, and the sealed buckets were placed in a controlled environmental chamber (23 ± 2 °C, RH 98 ± 2 percent) throughout the 180-day testing period. The storage solution to sample the volume of each MPS bucket was maintained at 8:1. At each testing age, samples were removed from the buckets, gently washed with tap water to remove simulated PS from the surface, and blotted off to SSD condition with a clean damp cloth prior to resistivity tests.

Table 4-24: HPC Mixtures' PSC and Simulated PS for Curing

#MIX	PSC (MS/CM)	CURING REGIMEN	GROUP ID	COMPOSITION OF CURING SOLUTION			
				NaOH (g/L)	KOH (g/L)	$Ca(OH)_2$ (g/L)	Conductivity (mS/cm)
CEM	88.10	MPS curing	Group 1: *No FA*	4.8	12.32	2	85.1
6SF	81.10						
25F	75.80		Group 2: *Class F FA mixtures*	4.8	13.44	2	73.5
20F5SF	66.30						
35F	68.40						
35C	116.30		Group 3: *Class C FA mixtures*	14.8	10.08	2	114.5
29C6SF	108.80						
35C10SF	98.90						
All	*Range: 66.30 mS/cm–116.30 mS/cm*	SPS Curing	All	7.6	10.64	2	78.74

4.4.6.5 Results and Discussion—NC Regimen

Five replicate test samples of each HPC mix design were tested for BR and SR measurements at 7, 28, 56, 91, and 180 days for different curing regimens. For brevity, only the results from BR tests for HPC mixtures and their chloride permeability classification for 28, 91, and 180 days pertinent to appropriate performance classification limits are discussed in the following sections. However, SR test measurements after necessary correction factors also demonstrated the same performance classification as BR and were verified for all curing regimens.

4.4.6.5.1 Resistivity Measurements in SC

In addition, sealed BR measurements at 28, 91, and 180 days were evaluated/ranked for chloride ion permeability in accordance with the AASHTO PEM'S performance limits for saturated resistivity, and the results are shown in Figure 4-19. Although these limits are not directly applicable for evaluating sealed resistivity measurements, the purpose of classification is only to enable a relative comparative assessment between the mixtures.

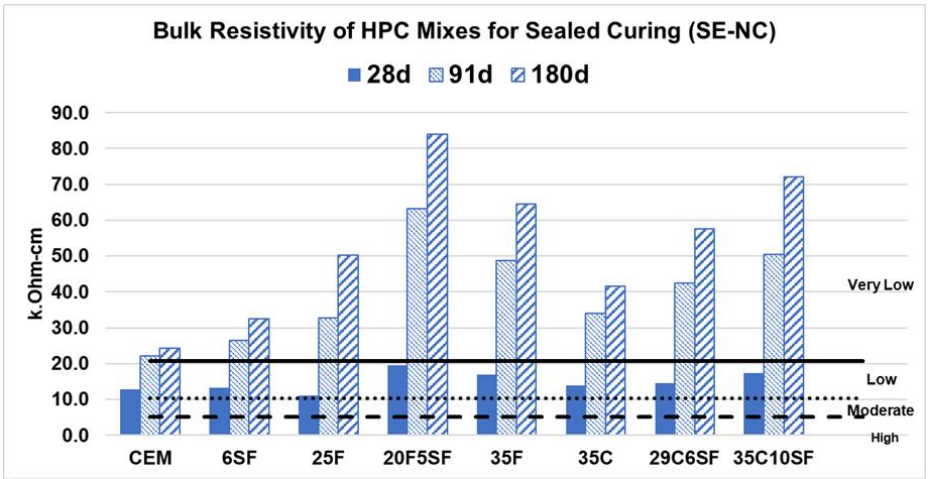

Figure 4-19: Performance Classification of HPC Mixtures in SC Regimen

For a relative assessment of HPC mix performance established on BR measurements, a sealed BR index (BRI) represents the BR value of an HPC mix expressed as a percentage of the 100 percent OPC mix at the same curing age. Results from BRI evaluation for HPC mixtures are shown in Figure 4-20.

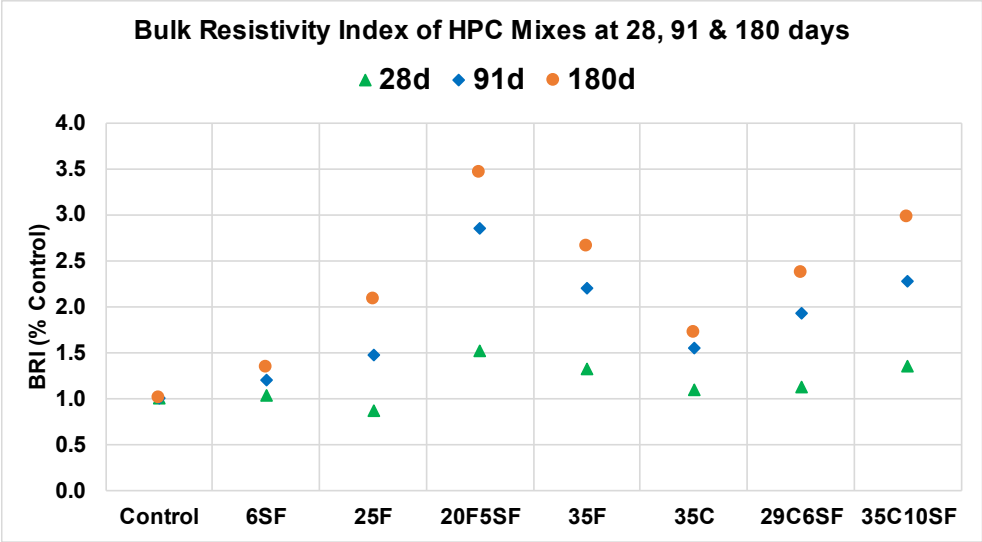

Figure 4-20: BRI for HPC Mixtures at 28, 91, and 180 Days

Cement replacement with 6 percent SF only marginally increased the BR measurements by 20–30 percent when compared to the OPC mix at all ages. However, Class F FA mixtures demonstrate a 200–300 percent increase in BR when compared to OPC, and a significant fraction of this increase is mainly observed at later ages (i.e., 91–180 days) of curing. Compared to the control and two binary Class F FA mixtures, the ternary combination of SF and Class F FA increased BR measurements at both early ages (28 days) as well as at later ages (91–180 days). Similarly, for Class C FA mixtures, the ternary combination of Class C FA with SF had the most significant effect on BR increase in HPC mixtures when compared to the binary 35C HPC mix.

4.4.6.5.2 Influence of PSC on Concrete Resistivity Measurements

Concrete resistivity measurements are a function of its PSC and microstructure parameters—pore volume and pore connectivity—as shown in Equation 4-7, with parameters as defined earlier.

Equation 4-7

$$\rho_b = \frac{1}{\sigma_{ps} \cdot (\phi\beta)}$$

SCM incorporation in concrete refines microstructure and reduces permeability through pozzolanic reactions, which improves the resistivity performance of concrete mixtures. However, incorporation of SCMs such as SF, fly ashes, etc., directly modify the ionic (Na and K) concentration and conductivity of the PS, which directly influences resistivity test measurements, as shown in Figure 4-21.

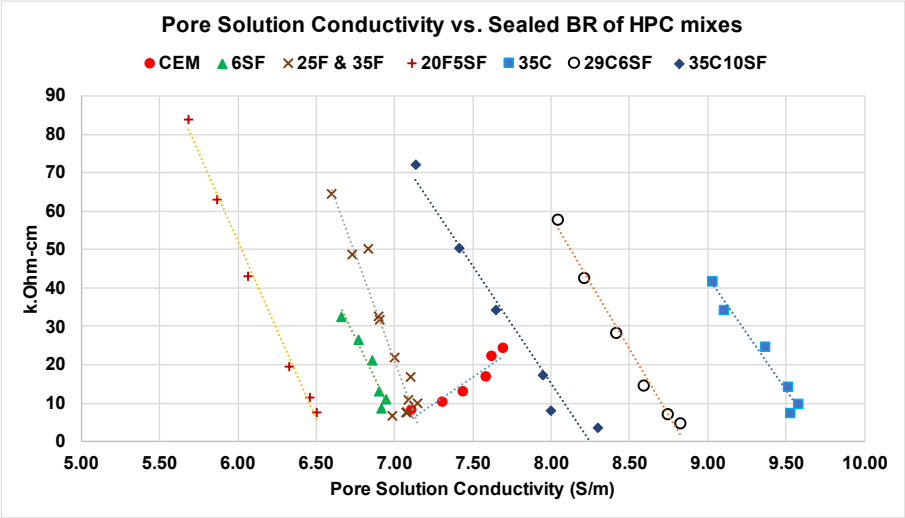

Figure 4-21: Correlation of PSC on Sealed Resistivity Measurements

Resistivity test measurements demonstrate a linear relationship with PSC for all HPC mixtures with SCMs. For all HPC mixtures with SCMs, as PSC decreases with age, the BR measurements proportionally increase. However, for the CEM, resistivity increases with increasing PSC over time. Since the type, composition, replacement level, soluble alkali contribution from the SCM used, and alkali binding by the CASH phase determine the PS composition/conductivity, different HPC mixtures show their characteristic PSC changes over time. The influence of PSC on BR measurement for all the concrete mixtures is clearly manifested.

4.4.6.5.3 Discussion

Supplementary cementing materials, such as FA and SF, improve pore structure and reduce the permeability of hardened concrete. However, results and discussions from this section indicate that they can also significantly affect the PS chemistry of hardened concrete. Concrete permeability indicates the transport of the liquid phase with ions through the pore structure of the concrete. In contrast, the electrical conductivity of concrete is influenced by both the pore structure characteristics and the electrical conductivity of the PS, which varies as a function of

ingredient composition and mix characteristics. Thus, using concrete resistivity measurements to assess permeability reduction directly can result in an incorrect assessment of SCM's performance. Results also agree with previous studies(*60*) that noted that it is not correct to use electrical conductivity of concrete to rank the permeability performance of concrete mixtures containing supplementary cementing materials.

4.4.6.5.4 Saturated LW Curing

BR and SR tests were performed on five replicate specimens for each HPC mix and at 7, 14, 28, 56, 91, and 180 days of LW curing. For brevity, the average BR and SR measurements at 28, 91, and 180 days of SPS curing are summarized in Table 4-25. Following AASHTO T 358 specifications, a curing correction factor of 1.1 was applied to SR measurements for the LW curing regimen.

Table 4-25: BR and SR of HPC Mixtures at 28, 91, and 180 Days of LW Curing Regimen

MIX #ID	BR (KOHM-CM)			SR (KOHM-CM)		
	28d	91d	180d	28d	91d	180d
CEM	10.6	15.3	17.6	8.6	14.6	16.3
6SF	11.7	16.4	20.7	9.0	19.5	22.4
25F	10.3	26.4	46.9	7.8	26.8	53.6
20F5SF	16.9	34.3	51.2	14.2	39.0	52.3
35F	11.3	30.0	49.1	8.7	29.2	48.7
35C	12.1	21.4	27.4	8.7	23.7	28.0
29C6SF	8.8	21.6	38.8	7.2	24.8	39.1
35C10SF	10.2	23.5	41.4	8.2	21.4	40.9

Concrete resistivity measurements are a function of PSC and pore structure characteristics. In the resistivity performance of different HPC mixtures, the composition of the HPC mix—that is, the SCM type, composition, and replacement level—are the primary factors influencing resistivity performance of HPC mixtures. Based on Table 4-25, cement replacement with 6 percent SF increased the resistivity of HPC mixtures by 10–15 percent above the CEM at all ages. In contrast to cement and SF, Class F fly ashes are known to react much more slowly. Accordingly, binary FA HPC mixtures (25F and 35F) demonstrated a lower resistivity at early ages (up to 28 days) than the CEM. However, when curing time was extended from 28 to 180 days, the resistivity of 25F and 35F mixtures increased by 250 percent and 300 percent in comparison to CEM. In contrast, a synergistic combination of Class F FA and SF improved resistivity performance at both early ages (7–28 days) and later ages (28–180 days) in ternary mix 20F5SF in comparison to CEM and binary 25F and 35F mixtures.

Similarly, Class C FA's presence improved resistivity compared to CEMs. Especially compared to Class F FA, the faster hydration kinetics of Class C FA were seen to improve the resistivity performance of 35C mix at early ages (7–28 days) compared to 35F. At early curing ages (7–28 days), both ternary Class C + SF mixtures demonstrated slightly lower resistivity than binary 35C and CEM mixtures. Up to 91 days, the resistivity improvement in these ternary mixtures is

not much compared to the 35C mix. However, at 180 days, a significant improvement in resistivity is manifested in these ternary mixtures in comparison to the 35C mix.

4.4.6.5.5 Relationship between Resistivity and RCPTs

BR and SR under LW curing values for all the HPC mixtures were correlated with RCPT measurements at 28, 56, and 91 days, and the results are shown in Figure 4-22. Note that a GCF of 1.92 and curing correction factor of 1.1 (AASHTO T 358) were applied to SR measurements.

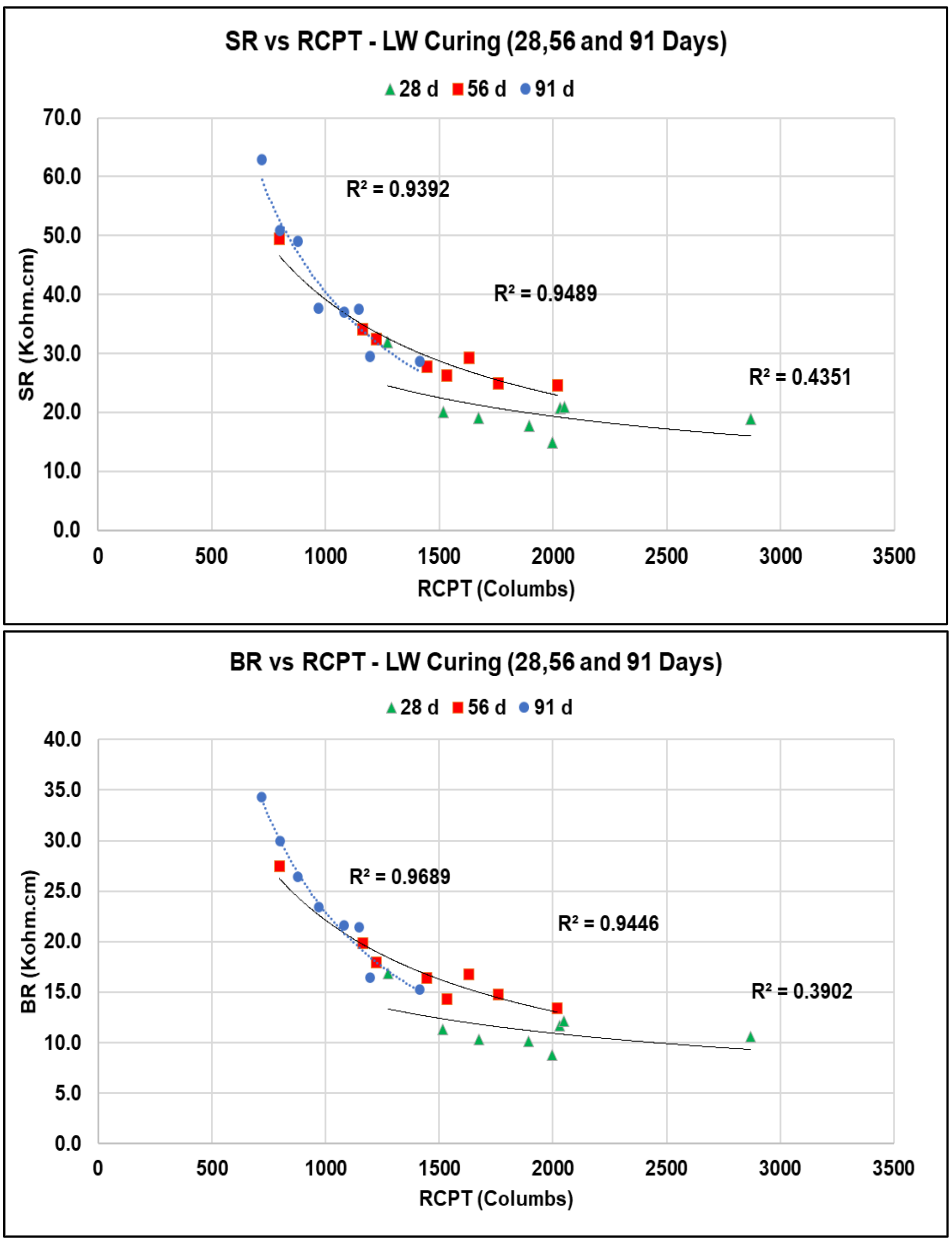

Figure 4-22: Correlation of SR and BR with RCPT Measurements of HPC Mixtures.

Based on results from Figure 4-22, both BR and SR resistivity of HPC mixtures appear to correlate well with RCPT measurements at 56 and 91 days. Between the two resistivity tests, the BR of HPC mixtures demonstrated a marginally stronger relationship with the RCPT than SR at

all ages. A lower COV in BR measurements at 56 and 91 days compared to SR possibly explains the stronger BR–RCP relationships at 91 days. Additionally, for both SR and BR, the resistivity–RCP relationship improved from 28 to 91 days. A significant increase in BR and SR noted for binary and ternary Class F HPC mixtures from 28 to 91 days possibly explains the improved resistivity–RCP relationships.

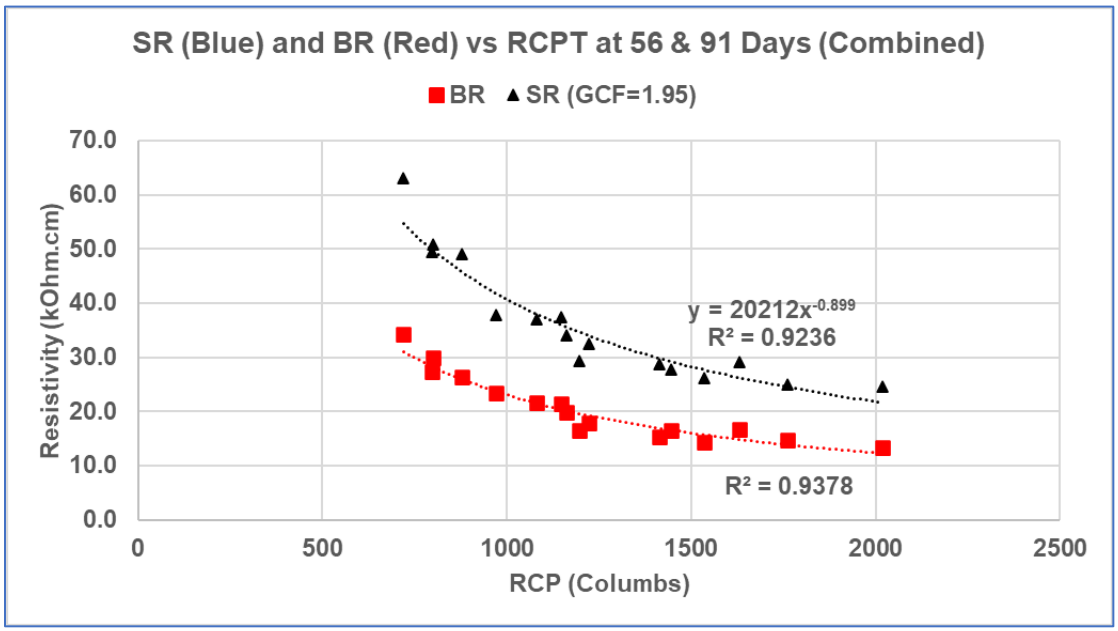

Figure 4-23: Combined 56- and 91-Day Resistivity vs. RCPT Relationship

Currently, TxDOT specifications require RCPT measurements for HPC mixtures at 56 days to qualify mix performance. Therefore, the 56- and 91-day SR–RCP relationships were combined (Figure 4-23) to develop a predictive function (Equation 4-8), and threshold performance limits for SR of HPC mixtures were determined based on the SR–RCP relationship. In addition, the threshold performance limits for BR were determined based on the BR–SR relationship of HPC mixtures in LW curing (7 to 180 days).

Equation 4-8 $$SR\ (kOhm \cdot cm) = 20212 \cdot (RCP)^{-0.899}$$

Table 4-26 shows the SR- and BR-based chloride ion permeability classification (threshold performance limits) for HPC mixtures.

Table 4-26: Performance Limits for SR and BR of HPC Mixtures (56 and 91 Days, LW Curing)

PERMEABILITY CLASSIFICATION	RCPT, COLUMBUS	SR LIMITS 4 × 8-INCH CYLINDER (KOHM-CM) *A= 38 MM; GCF=1.95*	BR LIMITS 4 × 8-INCH CYLINDER (KOHM-CM)
High	>4000	<12	<6
Moderate	4000–2000	12–22	6–11
Low	2000–1000	22–41	11–21
Very Low	1000–100	41–320	21–165
Negligible	<100	>320	>165

4.4.6.5.5.1 Performance Classification Based on Resistivity Measurements for LW Curing

The 56 and 91-day RCPT and BR and SR test measurements of HPC mixtures were classified for chloride ion penetrability using the threshold performance limits identified in Table 4-27, and the results are shown in Table 4-28.

Table 4-27: Performance Classification of HPC Mixtures for LW Curing

MIX #ID	RCPT		BR		SR	
	56 days	91 days	56 days	91 days	56 days	91 days
CEM	Moderate	Low	Low	Low	Low	Low
6SF	Low	Low	Low	Low	Low	Low
25F	Low	Very Low	Low	Very Low	Low	Very Low
20F5SF	Very Low	Very Low	Very Low	Very Low	Very Low	Very Low
35F	Low	Very Low	Low	Very Low	Low	Very Low
35C	Low	Low	Low	Very Low	Low	Very Low
29C6SF	Low	Low	Low	Very Low	Low	Very Low
35C10SF	Low	Very Low	Low	Very Low	Low	Very Low

Almost all HPC mixtures (except two) demonstrate the same chloride ion performance classification in RCPTs and resistivity tests at 56 and 91 days. A consistent performance classification between the two test methods validates the applicability of new performance limits established for resistivity tests. For example, although Mix 35C and 29C6SF demonstrated a low-performance classification based on 91-day RCPTs, the RCPT values of these two mixtures remain very close to the boundary line of 1000 (35C-1148 and 29C6SF-1081 coulombs) and can be practically classified as a very low performance category. Interestingly, these two mixtures are classified as very low based on BR and SR-based classification systems at 91 days, further validating the consistency of new performance limits established for the resistivity test methods.

As shown in Figure 4-24, higher variability in 28-day resistivity measurements causes ineffective performance classification of the mixtures. In contrast, a resistivity measurement at 91 days demonstrates lower variability and consistent performance classification. It seems SCM's

pozzolanic reactions, change of PSC due to alkali leaching, and microstructure improvement reached a stable stage by 91 days' time, which resulted in a consistent performance classification. However, extending the curing duration from 91 to 180 days does not change performance classification for HPC mixtures. Therefore, the 91-day resistivity (both BR and SR) measurements of HPC mixtures appear to be best suited for the performance classification of HPC mixtures for the LW normal curing regimen.

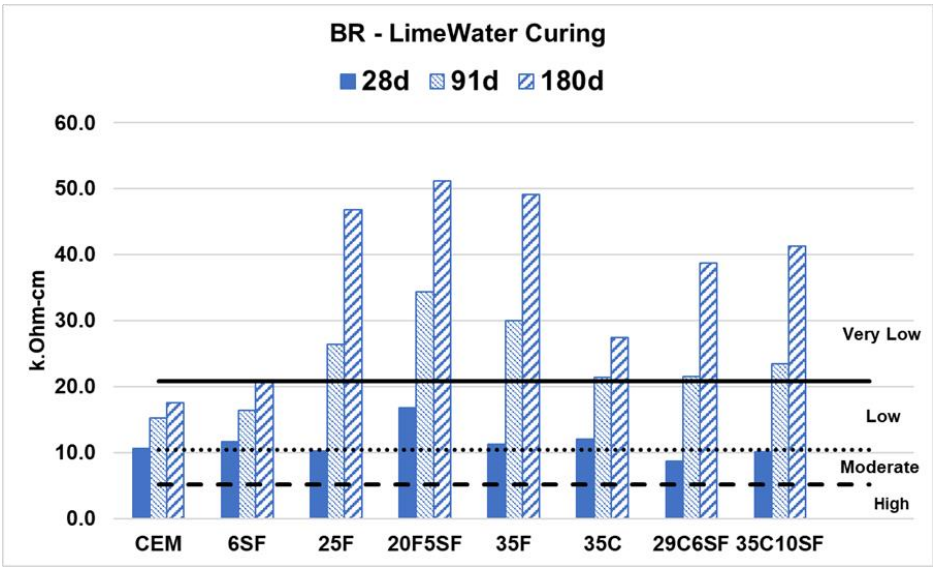

Figure 4-24: BR Performance Classification of HPC Mixtures 28–180 Days in LW Curing

4.4.6.5.6 SPS Curing and MPS Curing Regimen

Five replicate test samples of each HPC mix design were tested for BR and SR measurements at 7, 28, 56, 91, and 180 days of the SPS and MPS curing regimen. Permeability classification limits for apparent resistivity (i.e., resistivity measurements under submerged curing regimens such as SPS/MPS) were derived using AASHTO PEM'S performance limits for saturated resistivity. Table 4-28 shows threshold performance classification limits for chloride ion penetrability determined for apparent resistivity (SR and BR) at the DOS (= 72 percent) and saturation correction factor (n = 2.0), and the rationale for selecting is explained in Section 7 (discussion for saturation correction factors). HPC mixtures' performance classification for BR and SR measurements in MPS and SPS curing regimen are shown in Table 4-29.

Table 4-28: Performance Classification Limits for Apparent Resistivity for HPC Mixtures

CHLORIDE ION PERMEABILITY CLASSIFICATION	SATURATED RESISTIVITY (ρ_{sat}) [AASHTO PEM] 4X8 INCH CYLINDER (KOHM-CM)	APPARENT RESISTIVITY (ρ_{app}) $\frac{\rho_{sat}}{\rho_{app}} = (DOS)^n$ *4X8 INCH CYLINDER (KOHM-CM)*
High	<5.2	<10
Moderate	5.2–10.4	10–20
Low	10.4–20.8	20–40
Very Low	20.8–207	40–400
Negligible	>207	>400

Table 4-29: Performance Classification for BR in SPS vs. BR in MPS Curing

MIX #ID	BR- SPS CURING REGIMEN			BR–MPS CURING REGIMEN		
	28 days	91 days	180 days	28 days	91 days	180 days
CEM	Moderate	Moderate	Moderate	High	Moderate	Moderate
6SF	Moderate	Low	Low	Low	Low	Low
25F	Moderate	Low	Low	Moderate	Low	Low
20F5SF	Low	Low	Very Low	Low	Very Low	Very Low
35F	Moderate	Low	Very Low	Moderate	Low	Very Low
35C	Moderate	Low	Low	Moderate	Moderate	Low
29C6SF	Low	Very Low	Very Low	Low	Low	Low
35C10SF	Low	Very Low	Very Low	Low	Low	Low

The composition of the curing solution directly affects its resistivity performance. Between the SPS and MPS curing regimen, the following observations were noted:

- The conductivity of the curing solution for Class C FA mixtures in the MPS curing regimen is 1.5 times higher than in SPS curing (114 S/m in MPS vs. 78.74 S/m in SPS), which resulted in lower resistivity measurements for Class C FA mixtures at all ages in MPS curing compared to SPS curing.
- Similarly, a lower conductivity of curing solution for Class F FA mixtures in MPS curing than in SPS curing (72.34 S/m in MPS vs. 78.74 S/m in SPS) resulted in higher resistivity measurements for binary and ternary Class F FA mixtures in MPS curing.

Differences in curing solution composition and conductivity directly influence the resistivity measurements for HPC mixtures. Thus, resistivity measurements for the same HPC mixtures cannot be compared between different curing regimens. Results from Table 4-29 also demonstrate that the 28-day curing period is inadequate to classify HPC mixtures based on resistivity measurements for both SPS and MPS normal curing regimens. Performance classification for all HPC mixtures changes from 28 to 91 days of the curing regimen. In addition, resistivity measurements (both BR and SR) for the 91-day PS normal curing regimen demonstrate lower COV than 28-day measurements. However, results from Table 4-29 also

demonstrate that extending the curing regimen up to 180 days from 91 days appears to be more beneficial for classifying HPC mixtures containing fly ashes. For both SPS and MPS curing regimens, the performance classification for HPC mixtures containing slower reacting SCMs, such as Class F FA, appears to change from 91 to 180 days. Also, the average COV at 180 days (~3.4 percent) for resistivity measurements is significantly lower for both BR and SR tests than at 91 days (~ 4.5 percent) and 28 days (~5.6 percent). Therefore, the 180-day resistivity measurements of HPC mixtures appear to be best suited for the performance classification of HPC mixtures for SPS and MPS normal curing regimens.

Between SPS and MPS curing regimens, BR measurements for HPC mixtures at 28, 91, and 180 days of the MPS curing regimen showed a relatively lower COV (3.9 percent, 3.2 percent and 3.4 percent) than did the SPS curing regimen (4.6 percent, 4.3 percent, and 4.1 percent). Although SPS curing minimizes alkali leaching, PS conductivity measurements (discussed in the next section) demonstrate higher COV for SPS curing (7.3 percent) than MPS curing (4.8 percent). Therefore, between the SPS and MPS curing regimens, the MPS curing regimen is better suited to evaluate resistivity (and thus, FF) performance based on lower COV, higher reliability, and repeatability in both concrete resistivity and PSC measurements.

4.4.6.6 Conclusions

Concrete resistivity measurements are a function of three primary parameters: (1) PS composition—ionic conductivity, (2) pore structure characteristics—pore volume and pore connectivity, and (3) saturation state—moisture connectivity. Therefore, the curing regimen for concrete samples influences resistivity measurements primarily through moisture connectivity, in other words, the DOS (sealed < submerged curing) and leaching of ionic species (typically Na and K) from concrete (LW > SPS > MPS).

Supplementary cementing materials, such as FA and SF, improve pore structure and reduce hardened concrete's permeability. However, SCM incorporation also significantly affects the PS chemistry of hardened concrete. For the same mix composition, compositional variability in cementitious materials significantly affects the PS chemistry of hardened concrete. A strong inverse relationship was noted between concrete resistivity test measurements and PSC for HPC mixtures with SCMs. Thus, using concrete resistivity measurements to assess permeability reduction directly could result in an incorrect assessment of SCM's influence on permeability reduction and durability performance for HPC mixtures.

4.4.6.6.1 Submerged Curing Regimen

4.4.6.6.1.1 LW Curing Regimen

A strong correlation was noted between the RCPT and SR/BR measurements at 56 and 91 days of LW curing. However, LW curing influences resistivity measurements due to alkali leaching from the concrete PS. The influence of alkali leaching contributes to the observed highest COV in resistivity measurements (4.7 percent–5.9 percent) when compared to all other submerged curing regimens. A 28-day LW normal curing is inadequate for the performance classification of

HPC mixtures; however, extending the curing duration from 91 to 180 days does not change the performance classification for HPC mixtures. For LW normal curing, the 91-day resistivity measurements of HPC mixtures appear to be best suited for the performance classification of HPC mixtures.

4.4.6.6.1.2 SPS and MPS Curing Regimen

Differences in curing solution composition and conductivity directly influence the resistivity measurements for HPC mixtures. Hence, resistivity performance classification for HPC mixtures cannot be compared between curing regimens. COV for resistivity measurements in MPS (~3.2 percent–3.9 percent) is less than SPS (~ 4.1– 4.8 percent) curing regimens for all ages. Although SPS curing minimizes alkali leaching, PS measurements demonstrate higher variability in conductivity measurements for SPS curing than MPS curing. The 28-day and 91-day curing periods are inadequate to classify HPC mixtures containing slower reacting pozzolans based on their resistivity measurements because the performance classifications change up to 180 days of curing. For SPS and MPS normal curing, the 180-day resistivity measurements of HPC mixtures appear to be best suited for the performance classification of HPC mixtures.

4.4.7 Resistivity Tests: Factors of Influence

4.4.7.1 Background and Objective

An earlier section described how electrical measurements in concrete are primarily a function of three primary parameters: (a) PS *composition*—ionic conductivity, (b) *pore structure characteristics*—pore volume and pore connectivity, and (c) *saturation state*—moisture connectivity (*47*). Therefore, interpretations of concrete's microstructure development based on resistivity measurements require proper accountability of PS chemistry/conductivity other than the effects of pore structure characteristics and moisture connectivity.

In the current section, secondary parameters such as specimen geometry, temperature, curing regimen, leaching, sample inhomogeneity, drying (moisture loss), etc., that additionally influence resistivity test measurements are investigated. A general equation was proposed (*49*) to account for factors of influence that affect concrete resistivity measurements in the laboratory, as depicted in Equation 4-9:

$$\textbf{Equation 4-9}\quad \boldsymbol{\rho_{Tref} = \left(\frac{\rho_{ps}}{\phi * \beta}\right) * f(S) * f(Leach) * f(T_{test}) * f(Geometry) * f(microstructure)}$$

$where, \rho_{Tref}$ represents concrete resistivity at ref temperature and equivalent age (maturity), ρ_{ps} represents Pore solution resistivity of concrete, $f(S)$-Saturation correction function, $f(Leaching) -$ represents correction function for alkali leaching from pore solution, $f(T_{test})$ denotes influence of Test Temperature, $f(Geometry)$represents correction function for test geometry or Geometric Correction Factor (GCF) and $f(microstructure)$ represents Influence of curing temperature on microstructure and hydration.

Resistivity tests were performed using 4 × 8-inch (4 ± 0.08 inch diameter and 8 ± 0.16 inch height) concrete cylinders for each HPC mix design. The GCF (Equation 4-9) generally varies as a function of test samples' geometry and dimensions and the probe spacing of the test device, all of which are constant in experimental work. Furthermore, laboratory resistivity measurements were performed at 23 +/−2°C (i.e., 21 to 25°C [70 to 77°F]) in accordance with the AASHTO PEM recommendations (AASHTO PP 84-18). At the time of testing, test specimens' temperatures were recorded to be between 23 and 25 °C. In previous research, an Arrhenius form of a correction function following the activation energy of conduction (*61*) was applied to assign temperature corrections (i.e., 0.98–1.01) for resistivity measurements. The same correction factors (0.98–1.01) were used in this study without conducting any further investigation. ASTM C 1876 stipulates that concrete samples be tested for BR measurements within 2 minutes of their removal from the curing solution, also referred to as the allowable time outside the curing solution. In contrast, AASHTO T 358 does not have a maximum or allowable time stipulation for SR measurements. However, depending upon ambient lab conditions (temperature and RH), a greater time interval (more than optimum) between the sample's removal from the curing tank before testing can result in moisture loss from the surface of samples and contribute to additional variability in resistivity measurements(*47*). Therefore, an optimum time interval needs to be fixed for the SR measurements.

The current research investigated two primary factors pertinent to sample curing procedures that influence concrete resistivity measurements in the laboratory: (1) DOS, and (2) ionic leaching from PS. In addition, experimental work was also performed to investigate the effect of surface drying or moisture loss from test specimens on SR measurements and establish an *optimum allowable time* interval for SR tests for each test specimen.

4.4.7.2 Test Methods

The test matrix to evaluate shrinkage performance of HPC mixtures is shown in Table 4-30 and discussed in the following sections.

Table 4-30: Test Matrix for Evaluating Factors That Influence Resistivity Performance

PARAMETER	AGE OF TESTING	CURING REGIMEN
DOS	28, 91, and 180 days	SE, Sat LW Curing, SPS & MPS
Ionic Leaching of PS Alkalis	91 days	All except SE
Drying (Moisture Loss)	28, 56, and 91 days	All except SC (SE)
SR/BR Ratio (Sample Homogeneity)	7 to 180 days	All (SE, LW, SPS, and MPS)

4.4.7.2.1 Concrete Porosity and DOS

Porosity (the volume of permeable voids) and the DOS of concrete specimens was determined by using ASTM C 642, except that vacuum pressure was used to saturate the specimens instead of

the boiling method recommended in the specification (*62*). At each test age, concrete samples (4 × 8-inch concrete cylinders) from different curing regimens were cut using a wet saw to obtain 2-inch (50 mm)-thick specimens from its midsection. The 2-inch concrete specimens were first oven-dried at 105 ± 2°C (212 ± 3.6°F) to a constant mass (36~48 hours), then placed in a desiccator connected to a vacuum pump, and the vacuum pressure was maintained for 3 hours. Subsequently, DI water was then drawn into the chamber, and vacuum pressure was maintained for an additional 1 hour. After the vacuum session, the pressure was released, and the specimens were left submerged in the solution for the next 21 hours. Specimens' masses were recorded before and after oven drying and after vacuum saturation in SSD condition and after being suspended in water. As per ASTM C 642, these mass measurements were used to calculate specimens' porosity and DOS.

4.4.7.2.2 Saturated Conditioning of Concrete Specimens

After resistivity testing at 28, 91, and 180 days, test samples (4 × 8-inch concrete cylinders) from LW, SPS, and MPS curing regimens were cut using a wet saw to obtain 2-inch (50 mm)-thick specimens from its midsection. First, the 4 × 2-inch specimens were towel-dried to SSD conditions and measured for BR. Next, the specimens were oven-dried at 105 ± 2°C (212 ± 3.6°F) to a constant mass (36~48 hours), then placed in a desiccator connected to a vacuum pump, and the vacuum pressure was maintained for 3 hours. Subsequently, an appropriate solution matching the curing regimen (LW, SPS, MPS) was drawn into the chamber, and the vacuum pressure was maintained for an additional 1 hour. After the vacuum session, specimens were left submerged in the solution for the next 21 hours, following which, samples were removed, towel-dried to SSD condition, and measured for saturated BR.

4.4.7.3 Results and Discussion

4.4.7.3.1 DOS

In an air-entrained concrete, the total permeable pore space (porosity) in concrete comprises matrix porosity (gel, capillary, and chemical shrinkage pores), entrapped and entrained air voids, and aggregate porosity. In SC, PS from hydration occupies gel and capillary pore space in the hydrated paste matrix, and this level of saturation is called sealed saturation (DOS_{SE}). However, in submerged curing, when concrete samples are immersed in buckets containing LW or PS, the curing solution saturates chemical shrinkage pores of the matrix and PS occupying the gel and capillary pores of the matrix. Based on sorptivity studies, this level of saturation associated with the complete filling of matrix pores is defined as *nick point* saturation (DOS_{NP}).

HPC specimens subjected to sealed, LW, and PS curing regimens were measured for the DOS per ASTM C 642 at 28, 91, and 180 days of curing. Results in Table 4-31 show the DOS_{SE} for HPC specimens subjected to a SC regimen and the DOS_{NP} for two submerged curing regimens (LW and PS curing). In addition, HPC specimens subjected to SPS and MPS curing regimen demonstrated similar DOS measurements at the same testing age. Thus, the average DOS_{NP} measurements are reported in Table 4-31 for each HPC mix at each testing age.

Table 4-31: DOS for HPC Specimens at 28, 91, and 180 Days of SE, LW, and PS Curing

MIX #ID	DOS (ASTM C 642)								
	DOS_{SE}			DOS_{NP} with LW			DOS_{NP} with SPS and MPS (avg)		
	28d	91d	180d	28d	91d	180d	28d	91d	180d
CEM	57%	55%	53%	68%	69%	71%	66%	67%	70%
6SF	57%	55%	53%	67%	68%	70%	68%	69%	72%
25F	66%	63%	59%	73%	74%	75%	71%	73%	74%
20F5SF	64%	62%	58%	76%	76%	78%	71%	73%	73%
35F	70%	66%	63%	74%	75%	77%	73%	74%	74%
35C	69%	66%	63%	72%	73%	74%	74%	75%	75%
29C6SF	66%	64%	60%	73%	74%	75%	74%	75%	75%
35C10SF	70%	67%	63%	73%	74%	76%	71%	72%	72%

The DOS in sealed conditions decreased from 28 to 180 days for all HPC mixtures, possibly due to water consumption by hydration reactions. However, the DOS_{NP} measured under LW and PS curing increased with the test age for all HPC mixtures. Based on sorptivity experiments, Todak et al. (*63*) hypothesized that complete matrix saturation (gel + capillary + chemical shrinkage pores) could be achieved within 56–91 days of submerged curing regimen. Therefore, the minor increase noted between 28–91 days could result from the curing fluid's gradual filing of air voids of HPC mixtures. However, DOS_{NP} measurements at 180 days demonstrated nil to < 1 percent increase in saturation levels (compared to 91 days), highlighting that a prolonged submerged curing regimen does not ensure a *fully saturated* condition in concrete mixtures with entrained air voids.

4.4.7.3.2 Saturation Correction Function (Saturation Function Parameter "n")

From previous discussions, it is clear that a long-term submerged curing regimen does not guarantee saturated conditioning of samples, especially for air-entrained concrete. Entrained/entrapped air voids in concrete are typically 10–1000 μm and can only be saturated under vacuum pressure(*62*). However, the FF determination requires resistivity measurements on saturated concrete specimens. Thus, experimental work was performed to measure the resistivity of concrete specimens under saturated conditions (ρ_{sat}). Next, resistivity measurements on saturated concrete (ρ_{sat}) were correlated with resistivity measurements in submerged conditions ($\rho_{LW,SPS,MPS}$) through a power-law function (Equation 4-10), and the saturation correction factor (n) was determined for HPC mixtures under different curing regimens. The saturation correction function facilitates a direct and rapid determination of ρ_{sat} based on $\rho_{LW\ or\ SPS\ or\ MPS}$ measurements in the laboratory.

Equation 4-10

$$\frac{\rho_{sat}}{\rho_{LW,SPS,MPS}} = (\boldsymbol{DOS})^{\boldsymbol{n}}$$

Figure 4-25 show the saturation correction factor (n) for HPC specimens determined for the SE, LW, SPS, and MPS curing regimen, respectively. Between the three submerged curing regimens, MPS and SPS resistivity measurements show a consistent and definite power-law relationship with the DOS to estimate ρ_{sat}. For SPS curing, the factor n, was determined to be 2.81, with a

COV of ±8.5 percent for all HPC mixtures. However, for MPS curing, the saturation correction factor, n, was determined to be 2.24, with a COV of ±12.3 percent for all HPC mixtures. The higher COV in MPS curing could be attributed to the fact that MPS curing comprises three different sets of curing solutions resulting in higher variability in the determination of saturation parameters. However, no definite and consistent relationship could be established for the LW curing regimen. The saturation correction factor, n, was noted to range from 1.7 to 4.6, with an average COV ±20.5 percent. This high COV can be attributed to an overall high COV for BR measurements in LW curing due to different degrees of alkali leaching in HPC test specimens.

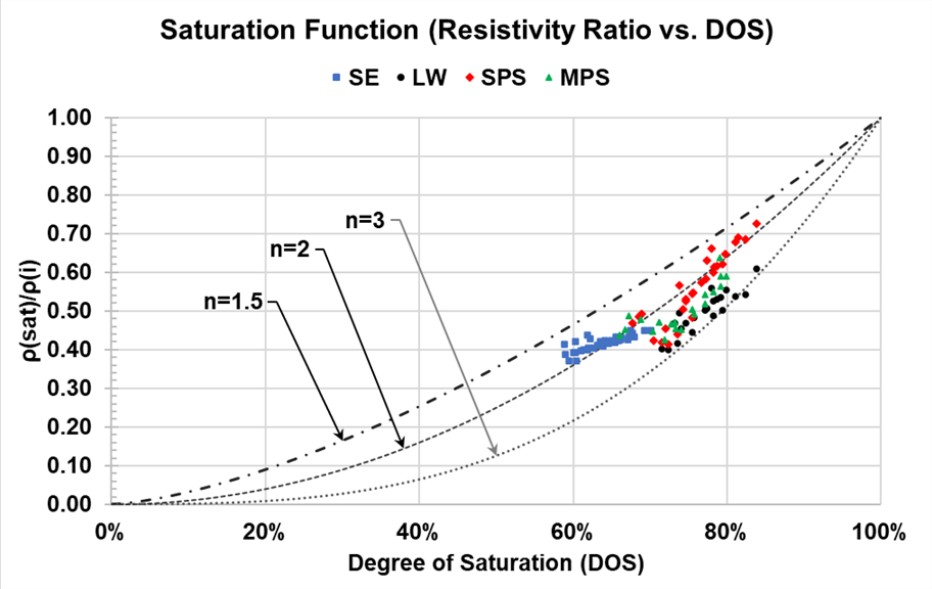

Figure 4-25: Relationship between ρ_{sat} and ρ_i as Function of DOS

4.4.7.3.3 Ionic Leaching of PS Alkalis in Different Submerged Curing Regimens

Differences in concentration between the PS of concrete and the curing solution (surrounding the sample) lead to diffusion of ionic species (Na, K) between bulk concrete and the curing solution(*64*). Therefore, an ionic leaching phenomenon is prevalent if the curing solution is devoid of Na and K alkalis (e.g., LW curing) or contains a sufficiently lower alkali concentration than concrete PS.

In the current research, an attempt was made to quantify the leaching of PS alkalis by measuring the concentrations of Na and K ions in the surrounding LW curing solution. First, three representative solution samples were taken from LW curing tanks at 91 days. Next, an XRF device was used to measure the alkali (Na and K) concentration in the solution and compare it with the alkali concentration in reference solutions to determine the extent of alkali leaching. Figure 4-26 shows that a substantial amount of alkalis were measured in samples taken from LW curing tanks at 91 days.

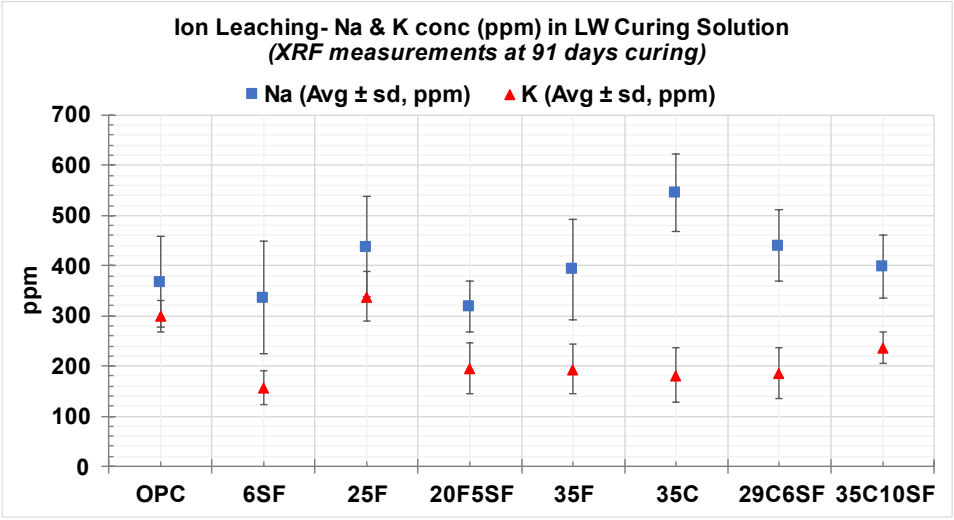

Figure 4-26: XRF Measurements of Na and K (with COV percent) in LW Curing Solutions

Approximately 400 ppm and 250 ppm of leached alkali Na and K were measured in LW curing solutions across all HPC mixtures. However, no clear correlation was observed between the measured alkali leaching and HPC mix type or alkali content in ingredients. In addition, the overbearing presence of calcium and hydroxide ions in LW curing samples resulted in high variability in Na and K determination. Based on three trials, the average COV in alkali measurements ranged between 13 percent and 58 percent for each HPC mix.

The FF of concrete is calculated as the ratio of the specimen's resistivity to the resistivity of its PS. However, a common practice for FF determination in different curing regimens is to consider the conductivity of the curing solution as the conductivity of concrete PS. In Figure 4-27, the conductivities of curing solutions from the LW, SPS, and MPS curing regimen were measured at 91 days and compared with the average PSC determined for Class C and F FA mixtures based on GEMS modeling.

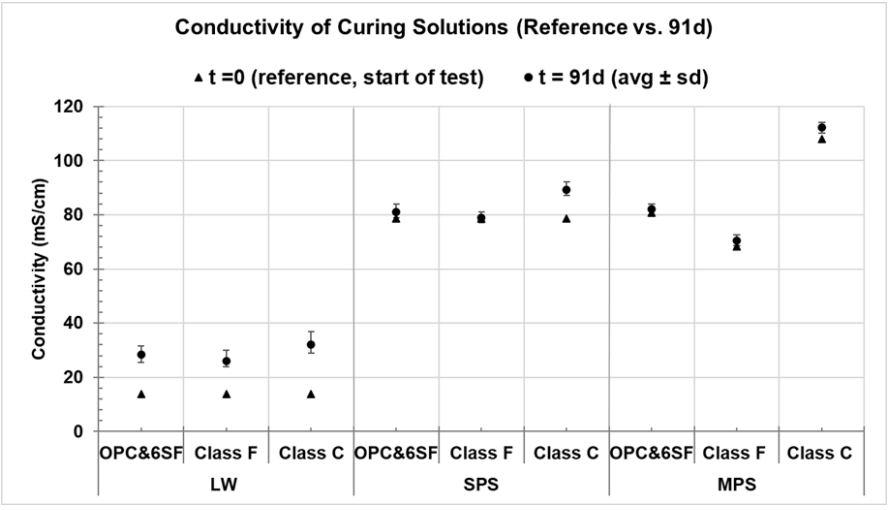

Figure 4-27: 91-Day Conductivity Measurements of LW, SPS, and MPS Curing Solutions vs. PSC

Results in Figure 4-27 demonstrate that MPS curing is the closest representation of the above assumptions, wherein the MPS solution conductivity is within one standard deviation of PSC of individual concrete mixtures. In contrast, conductivity measurements for the standard SPS curing solution demonstrated a 10–15 percent COV, possibly due to common ion effects from different ions present in the curing solution. Moreover, the average conductivity of the SPS curing solution is seen to be 20–30 percent lower than the true PSC of Class C FA mixtures. Thus, an incorrect consideration (30 percent lower) of concrete PSC based on curing solution conductivity measurements, especially for Class C FA mixtures, can result in an error of similar proportions for FF determination.

More importantly, Figure 4-27 indicates that LW curing solutions containing alkali leached from concrete samples do not represent equilibrium with concrete's PS. The LW curing solution conductivity is 8 to 10 times lower than the PSC of concrete mixtures. A lower PSC consideration in combination with a high measurement variability can result in significant error in FF determination and assessing concrete mixtures for FF performance based on LW curing.

4.4.7.3.4 Effect of Sample Drying on SR Measurements

Typically after removing a sample from the curing solution, operators at the TTI laboratory first performed BR tests followed by SR tests, wherein eight measurements were taken around the circumference, which sometimes resulted in a total test time of up to 10 minutes/sample. However, results from the two resistivity tests for HPC mixtures demonstrated that the drying rate (moisture loss from the test specimen's surface), had a more dominant effect on its SR than BR. An uneven drying of the sample's surface generally contributes to a higher variability and a lower precision of SR measurements. Furthermore, across all submerged curing regimens—LW, SPS, and MPS—the COV in SR measurements was higher than BR for all samples and all ages.

Thus, experiments were performed to establish an *optimum allowable time*, wherein surface drying would cause a statistical difference between the readings. At 28, 56, 91, and 180 days of curing ages, test samples were tested for SR at every 5-minute interval from 0 to 30 minutes after their removal from the curing tank. A single-tail t-test at a 95 percent confidence interval was employed to evaluate statistical significance in SR measurements at each time increment. Because moisture loss from the sample's surface will only increase the SR measurements, a single-tail t-test was selected to be more suitable for this evaluation.

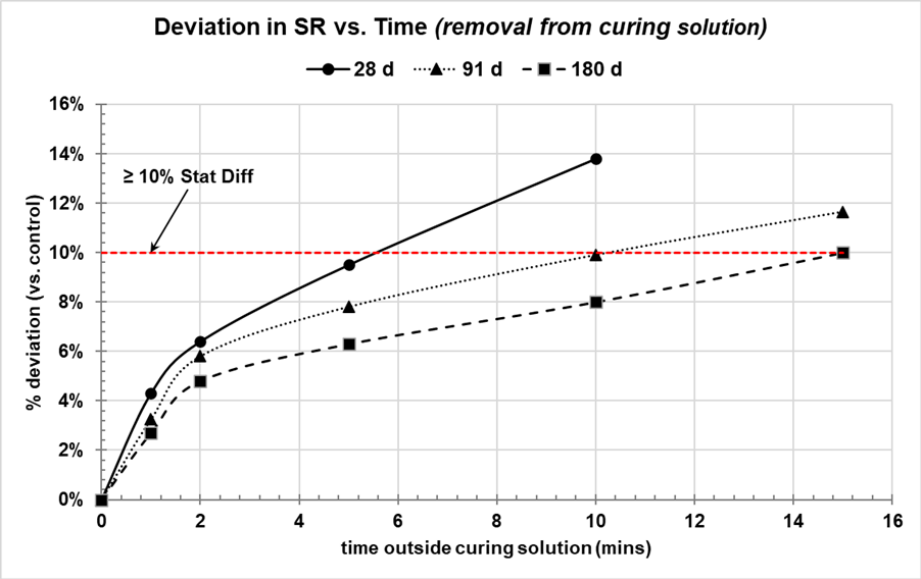

Figure 4-28: Statistical Variation in SR Measurements vs. Time Outside the C Solution

Results from Figure 4-28 show that SR measurements vary by more than 10 percent compared to control (<30 sec) if the allowable time exceeds 5 minutes at 28 days, 10 minutes at 56 days, and around 15 minutes at 91 days. Moreover, the observations of allowable time for SR measurements remained consistent between LW, SPS, and MPS curing with no significant differences between the three submerged curing regimens. Also, the allowable time outside a curing solution correlates well with the microstructure refinement due to SCMs' pozzolanic reaction; a longer curing age allows a more extended test time before getting a statistically different SR measurement.

Thus, the optimum allowable time for the SR test is within 5 minutes of sample removal from the curing solution. Results demonstrate that SR measurements could increase beyond one standard deviation for test times exceeding 5–10 minutes after sample removal from the curing solution.

4.4.7.3.5 Effect of Curing Regimen on Variation in SR vs. BR Measurements

Resistivity is an intrinsic parameter, and therefore, both BR and surface concrete resistivity tests after applicable geometry and test configuration corrections should yield a similar value. However, secondary factors such as alkali leaching from concrete PS, moisture loss from the surface during resistivity measurements, improper consolidation, etc., could cause a heterogeneity between the bulk interior versus outer surface and thus result in different BR and SR measurements. Furthermore, Spragg et al. (*65*) demonstrated that the SR/BR ratio is a good indicator for assessing the sample's homogeneity and degree/extent alkali leaching in test specimens. In the current study, the average SR/BR ratio of different HPC mixtures was evaluated as a function of different curing conditions from 7–180 days of the curing period, and the results are shown in Figure 4-29.

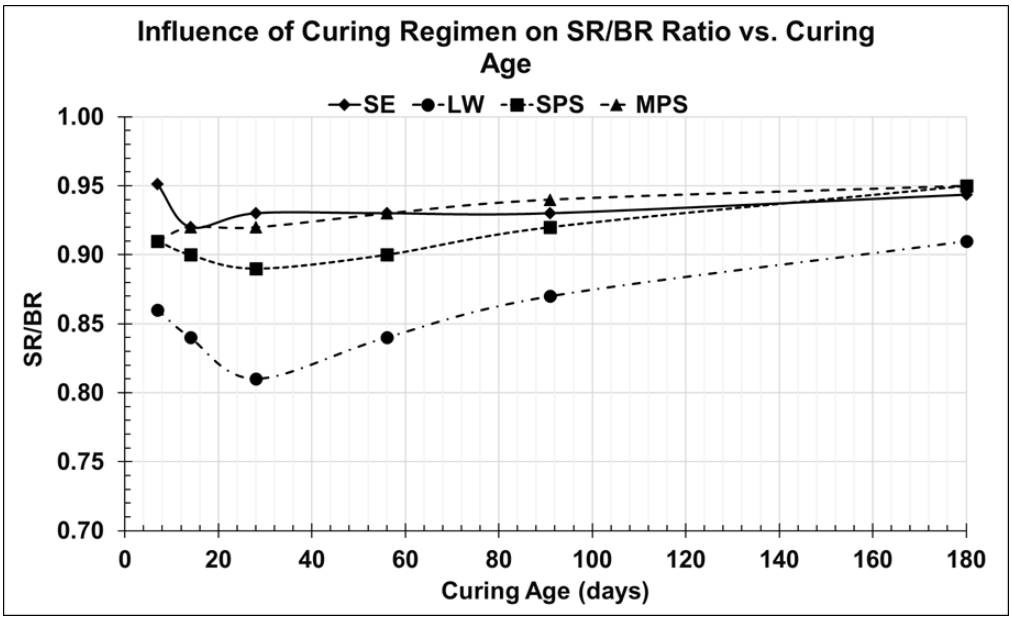

Figure 4-29: Influence of Curing Regimen on SR to BR Ratio

The SR/BR variation for SC ranged from 0.90–0.95, possibly from a lower DOS and drying/moisture loss influencing resistivity measurements. Among different submerged curing regimens, the MPS curing resulted in the most consistent BR and SR measurements and the lowest variation (0.91–0.99) in SR/BR at all ages, followed by SPS curing (SR/BR ~ 0.86–0.92). In contrast, LW curing samples demonstrated the highest SR/BR ratio variability, with values ranging from 0.79 at early ages to 0.90 at later curing ages. A low SR/BR ratio at the early stages of hydration (7–28 days) can be attributed to localized leaching of concrete PS alkalis into the surrounding LW solution, leading to a concentration gradient between the outer surface and the bulk interior. The gradual increase in SR/BR ratio from 28–180 days could be due to (1) possible reduction in alkali leaching from microstructure densification by SCMs' pozzolanic reactions, or (2) a homogeneity in bulk and surface PS concentration attained after sufficient leaching.

4.4.7.4 Conclusions

The curing regimen for concrete samples influences resistivity measurements primarily through moisture connectivity (DOS) and leaching of ionic species (typically Na and K) from concrete mixtures. Results from this section highlight various aspects in the following paragraphs.

Sealed Curing: SC does not suffer from error due to leaching since leaching does not exist with SC, which results in a minimal variation between BR and SR measurements, thus rendering an SR/BR ratio close to unity. However, a significantly lower DOS in SC samples can affect its microstructure development and thereby influence the resistivity measurements.

LW Curing: HPC test samples under LW curing demonstrated significantly high leaching of PS alkalis into LW. However, no clear correlation was observed between the quantity of alkali leaching and HPC mix type or alkali content in ingredients due to a high COV in measurements.

Therefore, the current study could not establish a consistent and definitive leaching correction function to determine FF based on LW curing resistivity measurements for HPC mixtures. In addition, a low SR/BR ratio further indicates that a high alkali leaching has created some kind of inhomogeneity (difference between surface and core) in the specimens that caused variability in measurements. Thus, a higher variation can be noted between the measurements from BR and SR tests.

SPS and MPS: ASTM C 1876 SPS solution contains Na and K and Ca alkalis, commonly found in concrete PS, and thus has significantly minimized alkali leaching compared to LW curing. However, an SPS may not represent all mixtures; as in current work, the conductivity of the SPS curing solution was 20–30 percent lower than the average PSC of Class C FA mixtures. In contrast, the MPS curing regimen minimized the variability between the concrete PSC and curing solution. The benefits of an MPS curing regimen over an SPS curing regimen, especially toward FF implementation, are seen in three ways:

- Lower COV in MPS, BR, and SR measurements for all HPC mixtures compared to SPS.
- Lower COV in conductivity measurements of the MPS curing solution compared to the SPS.
- Facilitation by MPS instigates avoiding the creation of difference between periphery and core, which results in a higher SR/BR ratio. This step ensures more consistent and similar BR and SR measurements for MPS curing than SPS.

4.4.8 Resistivity Tests: Part II—Accelerated Temperature Conditioning

4.4.8.1 Background and Objective

The curing temperature directly affects concrete microstructure development. While the porosity decreases as concrete hydrates, the resistivity generally increases. However, when concrete samples are cured at a higher temperature, it accelerates the hydration and microstructure development, thus increasing resistivity faster than samples cured at a lower temperature (*59*). For example, Bu et al. (*66*) showed that samples at 36°C develop resistivity at approximately twice the rate of samples at 23°C.

A specimen's age is typically associated with curing duration under standard laboratory temperature 23 +/− 1°C. Currently, AASHTO PEM recommends that the resistivity measurement at 91 days of standard room temperature (23 +/− 1°C) curing with LW/moist room is most representative for assessing transport properties of concrete, especially when evaluating different SCMs. However, resistivity results for HPC mixtures under NC (discussed in previous sections) demonstrated that extending the curing times from 91 days up to 120–180 days was required for effective performance evaluation of the HPC mixtures containing slower reacting pozzolans. Furthermore, HPC mixtures with SPS and MPS - NC changed performance classification when the curing age increased from 91 to 180 days. Thus, 180 days of standard normal temperature curing was recommended to evaluate performance-binary HPC mixtures

with FA based on resistivity measurements. These observations are supported by previous research studies (*56*, *67*) that also recommend extending the curing period up to 120–180 days for resistivity-based performance evaluation of concrete mixtures containing slowly reacting pozzolans.

The primary objective of the current work was to evaluate and establish an acceptable accelerated curing (AC) procedure such that concrete properties' maturity at 180 days under standard room temperature curing (i.e., normal curing at 23 +/− 1°C) can be attained at 28 days of AC. Two AC procedures (AC1 and AC2) were evaluated in this study to achieve the above objective as well as to evaluate and compare the resistivity development of HPC mixtures at 28 days. In addition, the resistivity-based performance classification of tested HPC mixtures at 28 days of AC regimen was compared with 91- and 180-day classification under normal temperature curing to establish an acceptable AC procedure for practice.

4.4.8.2 Rationale of AC1 versus AC2 Curing Regimen

AC1 was in accordance with ASTM C 1202, meaning 7 days of normal temperature (23 +/− 2°C) curing followed by 21 days of curing in LW maintained at 38 +/− 2°C. The AC2 curing regimen involves curing for 3 days under standard room temperature curing (i.e., normal curing at 23 +/− 1°C), followed by curing at elevated temperatures of 50 ± 2 °C for 25 days. The proposed AC2 curing regimen has recently been incorporated under draft specifications for AC regimens of concrete mixtures under PS curing in AASHTO TP 119.

Previous studies proposed an Arrhenius form of a correction factor using activation energy of hydration (Equation 4-11) to account for the effect of high-temperature curing (AC1 or AC2) on microstructure development and thus resistivity measurements of concrete mixtures. The proposed correction function determines the resistivity equivalent to the 91–180 days of normal curing temperatures based on the age and the resistivity measurements at elevated curing temp (*59*).

Equation 4-11

$$\boldsymbol{\rho_{Age,ref} = \rho_{Age,T} * \left[-\frac{E_{a,Hyd}}{R}\left(\frac{1}{T_{curing}+273} - \frac{1}{T_{ref}+273}\right)\right]}$$

$\rho_{Age,ref}$ represents resistivity of Concrete measured at "x" days at reference temp (typ.23C), $\rho_{Age,T}$ represents resistivity of Concrete at curing/measured temperature, $E_{a,hyd}$ is the activation energy of hydration (typically 41.5 kJ/mol) and R − universal gas constant,(8.314 J/(mol K).

Typically for HPC materials and mixtures, the compound activation energy for hydration (cement and cement with SCMs) varies between 30 to 52 kJ/mol, with a typical value of 41.5 kJ/mol (*56*). However, research by Weiss et al.,(*56*) demonstrated that for the range of activation energies used in typical HPC mix development, AC1's regimen could potentially achieve a 91-day equivalent age between 50–62 days of AC. To achieve a 91-day equivalent age at an earlier age (~ 28 days), the AC2 was applied as an alternative curing regimen.

4.4.8.3 Test Matrix

The test matrix to evaluate resistivity performance of HPC mixtures under AC is shown in Table 4-32 and discussed in the following sections.

Table 4-32: Test Matrix for Evaluating Resistivity Performance of HPC Mixtures (AC)

PARAMETER	CURING REGIMEN	CURING SPECIFICATION AND *PROTOCOL*	AGE OF TESTING	CURING TYPE EVALUATED
BR & SR	AC: Procedure 1 (AC1)	ASTM C 1202 *Curing Protocol:* 23 ± 2 °C for 7 days followed by 38 ± 2 °C for 21 days *(extended until 56 days)*	7, 14, 28, and 56 days	1. LW Curing 2. SPS Curing (ASTM C 1876)
	AC: Procedure 2 (AC2)	AASHTO TP 119 *Curing Protocol:* 23 ± 2 °C for 3 days followed by 50 ± 2 °C for 25 days	7, 14, and 28 days	1. SPS Curing (ASTM C 1876)

4.4.8.4 Test Methods

4.4.8.4.1 LW Curing with AC1 (LW-AC1)

AC1 in LW was performed using ASTM C 1202 guidelines. After demolding, test samples (4 × 8-inch concrete cylinders) were immersed in saturated LW baths maintained at 23 ± 2 °C for 7 days, followed by immersion in lime-saturated water at 38 ± 2 °C for 21 days, until a total sample age of 28 days. After the 28th-day resistivity measurements, test samples were re-immersed in saturated LW baths at 38 ± 2 °C for an additional 28 days of curing, followed by a resistivity measurement at 56 days. LW baths were prepared and monitored via ASTM C 511 recommendations, and a storage solution to sample volume ratio of 2:1 was maintained throughout the testing period.

4.4.8.4.2 SPS Curing with both AC1 and AC2

The SPS for curing was conducted per ASTM C 1876 specifications. In a 5-gallon (18.9 L) bucket, 102.6 g of dry NaOH, 143.9 g of dry KOH, and 27 g of dry Ca(OH)2 were added, which was followed by adding water to prepare a 3.6 gal (13.5 L) SPS with a conductivity of 78.74 mS/cm. The storage solution to sample volume of 8:1 was maintained in each SPS bucket. At each testing age, samples were removed from the buckets, gently washed with tap water to remove simulated PS from the surface, and blotted off to SSD condition with a clean damp cloth prior to resistivity measurements.

4.4.8.4.3 SPS with AC1 (SPS-AC1)

After demolding, test samples (4 × 8-inch concrete cylinders) were immersed in sealed buckets containing SPS maintained at 23 ± 2 °C for 7 days, followed by immersion in SPS buckets maintained at 38 ± 2 °C for 21 days. After the 28th-day resistivity measurements, test samples were re-immersed in SPS buckets at 38 ± 2 °C for an additional 28 days of curing, which was

followed by a resistivity measurement at 56 days. Before 28- and 56-day resistivity measurements, the sealed SPS buckets were moved to a controlled environmental chamber maintained at 23 ± 2 °C, where the solution and the immersed samples were allowed to cool to room temperatures for 12–18 hours before resistivity measurements.

4.4.8.4.4 SPS with AC2 (SPS-AC2)

After demolding, test samples (4 × 8-inch concrete cylinders) were immersed in sealed buckets containing SPS maintained at 23 ± 2 °C for 3 days, followed by immersion in SPS buckets maintained at 50 ± 2 °C for 25 days, for a total sample age of 28 days. On the 28th day, the sealed SPS buckets were moved to a controlled environmental chamber maintained at 23 ± 2 °C, where the solution and the immersed samples were allowed to cool to room temperatures for 12–18 hours before resistivity measurements.

4.4.8.5 Results

BR and SR measurements were performed on the test samples of eight HPC mixtures at 28 and 56 days of LW-AC1 and SPS-AC1, as well as at 28 days of the SPS-AC2 curing regimen. For brevity, only the results from BR tests for HPC mixtures and their chloride permeability classification for 28 days (and 56 days for AC1) pertinent to appropriate performance classification limits are discussed in the following sections. However, SR test measurements after necessary correction factors also demonstrated the same performance classification as BR and were verified for all curing regimens.

4.4.8.5.1 LW-AC1

Both BR and SR measurements were performed on the test samples of eight HPC mixtures at 28 and 56 days of LW-AC1 curing. Accordingly, resistivity measurements were classified for chloride ion permeability following the performance limits of the LW normal curing regimen, as shown in Table 4-33. Results from 28- and 56-day LW-AC1 resistivity tests and performance classification for HPC mixtures are shown in Figure 4-30.

Table 4-33: Performance Limits for SR and BR of HPC Mixtures in LW Curing

PERMEABILITY CLASSIFICATION	RCPT, COLUMBUS	SR LIMITS 4 × 8-INCH CYLINDER (KOHM.CM) A = 38 MM; GCF = 1.95	BR LIMITS 4 × 8-INCH CYLINDER (KOHM.CM)
High	>4000	<10.2	<5.2
Moderate	4000–2000	10.2–20.4	5.2–10.4
Low	2000–1000	20.4–40.6	10.4–20.8
Very Low	1000–100	40.6–403	20.8–208
Negligible	<100	>403	>208

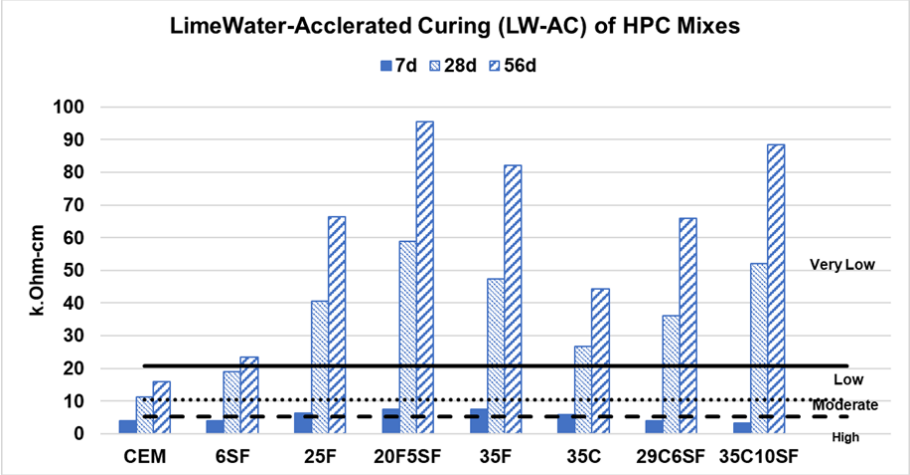

Figure 4-30: LW AC of HPC Mixtures at 7, 28, and 56 Days

The 91 and 180-day resistivity-based performance classification of HPC mixtures under LW-normal temperature curing regimen is compared with the 28 and 56-day performance classification under LW-AC1, and the results are presented in Table 4-34.

Table 4-34: Performance Classification for Normal Curing (91 and 180 days) vs. AC1 (28 and 56 Days)

MIX #ID	LW NORMAL TEMPERATURE CURING (LW)		LW-AC1	
	91 days	180 days	28 days	56 days
CEM	Low	Low	Low	Low
6SF	Low	Low	Low	*Low–Very Low**
25F	Very Low	Very Low	Very Low	Very Low
20F5SF	Very Low	Very Low	Very Low	Very Low
35F	Very Low	Very Low	Very Low	Very Low
35C	*Low–Very Low**	Very Low	Very Low	Very Low
29C6SF	*Low–Very Low**	Very Low	Very Low	Very Low
35C10SF	Very Low	Very Low	Very Low	Very Low

* Performance classification changes considering lower and upper bounds (average± std. dev) for the resistivity measurements.

4.4.8.5.2 ASTM C 1876 SPS Curing with AC1 (SPS-AC1)

Resistivity measurements were classified for chloride ion permeability following the performance limits of the SPS for the normal curing temperature regimen, as shown in Table 4-35. Results from 28 and 56-day SPS-AC1 resistivity tests and performance classification for HPC mixtures are shown in Figure 4-31.

4.4.8.5.3 ASTM C 1876 SPS Curing with AC2 (SPS-AC2)

Results from 28-day SPS-AC2 resistivity tests and performance classification for HPC mixtures are shown in Figure 4-32. Resistivity measurements were classified for chloride ion permeability following the performance limits shown in Table 4-35.

Table 4-35: Performance Limits for Resistivity of HPC Mixtures in PS Curing

PERMEABILITY CLASSIFICATION	RCPT, COLUMBUS	APPARENT RESISTIVITY CLASSIFICATION 4X8 CYLINDER (KOHM.CM) *[DOS = 72 PERCENT, N = 2.0]*
High	>4000	<10
Moderate	4000–2000	10–20
Low	2000–1000	20–40
Very Low	1000–100	40–400
Negligible	<100	>400

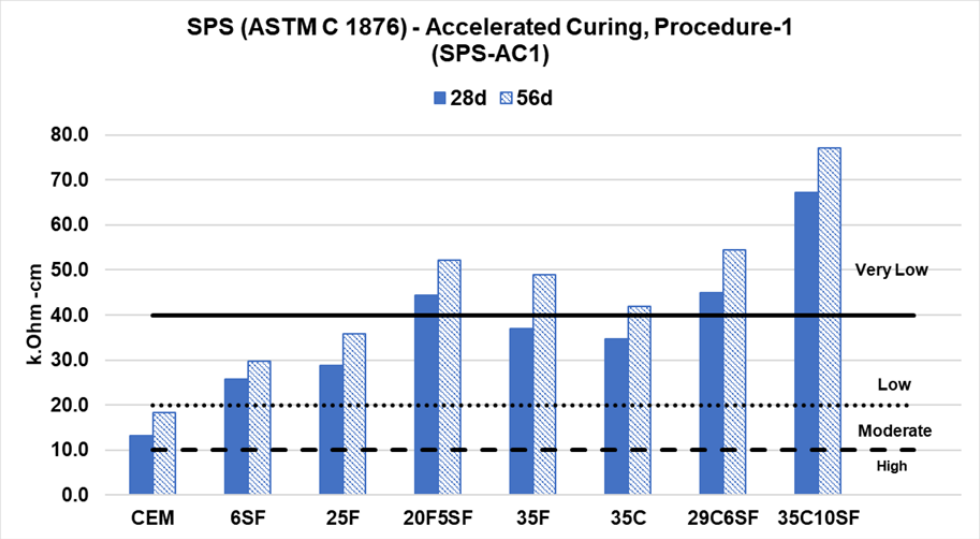

Figure 4-31: Performance Classification of HPC Mixtures in SPS-AC1 Curing Regimen

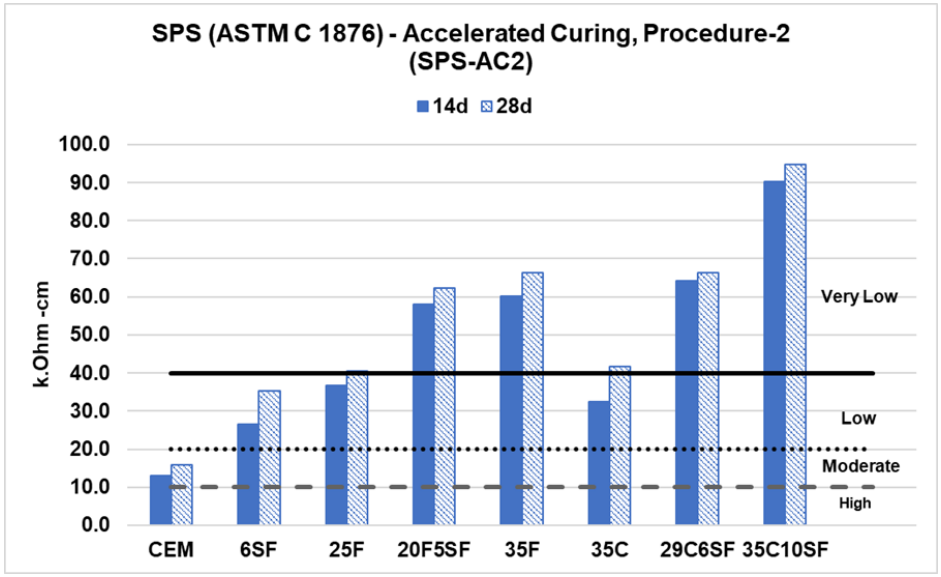

Figure 4-32: Performance Classification of HPC Mixtures in SPS-AC2 Curing Regimen

Resistivity-based performance classification of HPC mixtures were compared for three different SPS curing regimens: (1) 91 and 180 days for SPS with normal temperature curing, (2) 28 and 56 days for SPS-AC1, and (3) 28 days for SPS-AC2. Results from the comparative assessment are presented in Table 4-36.

Table 4-36: Performance Classification SPS Normal Curing vs. SPS-AC1 and SPS-AC2

MIX #ID	SPS NORMAL CURING		SPS-AC1		SPS-AC2
	91 days	**180 days**	**28 days**	**56 days**	**14 days**
CEM	Moderate	Moderate	Moderate	Moderate	Moderate
6SF	Low	Low	Low	Low	Low
25F	Low	Low	Low	Low	Low
20F5SF	*Low—Very Low**	Very Low	Very Low	Very Low	Very Low
35F	Low	Very Low	Low	Very Low	Very Low
35C	Low	Low	Low	*Low—Very Low**	Low
29C6SF	*Low—Very Low**	Very Low	Very Low	Very Low	Very Low
35C10SF	Very Low	Very Low	Very Low	Very Low	Very Low

* Performance classification changes considering lower and upper bounds (average± std. dev) for the resistivity measurements.

4.4.8.6 Discussion and Conclusions

The conclusions from the AC of HPC mixtures are presented in Table 4-37.

Table 4-37: Conclusions from AC of HPC Mixtures

CURING TYPE	COMMENTS ON CURING REGIMEN AND APPLICABLE AGE FOR RESISTIVITY-BASED PERFORMANCE CLASSIFICATION		
	Normal Curing Regimen NC 23 ± 2 °C for 180 days	AC: Procedure 1 (ASTM C 1202) AC1 23 ± 2 °C for 7 days followed by 38 ± 2 °C for 21 days (extended until 56 days)	AC: Procedure 2 (AASHTO TP 119) AC2 23 ± 2 °C for 3 days followed by 50 ± 2 °C for 25 days
Saturated LW Curing (ASTM C 511)	91-day BR and SR best suited for the performance classification	28-day LW-AC1 curing ≈ 91-day LW-NC (BR and SR)	N/A
SPS Curing (ASTM C 1876) (Similar observations for MPS curing regimen)	91-day BR/SR May not be adequate for HPC mixtures with slow reacting pozzolans (e.g., Class F FA mixtures) 180-day BR and SR best suited for the performance classification	28-day SPS-AC1 curing May not be adequate for HPC mixtures with slow reacting pozzolans (e.g., Class F FA mixtures) 56-day SPS-AC1 curing ≈ 180-day SPS-NC (BR and SR)	28-day SPS-AC2 curing ≈ 180-day SPS-NC (BR and SR)

Note: N/A = Not Applicable; n/a = not available.

4.4.9 Formation Factor

4.4.9.1 Background and Approach

The FF is an empirical parameter and a fundamental material property that describes microstructure characteristics—the permeable pore volume (ϕ) and pore connectivity (β) of a saturated porous material (*49*). Numerally, FF is calculated as the ratio of concrete resistivity (ρ_{conc}) to the resistivity of its PS (ρ_{ps}), as shown in Equation 4-12:

Equation 4-12

$$FF = \frac{\rho^{o}_{conc}}{\rho^{o}_{ps}} = \frac{1}{\phi \cdot \beta}$$

Where the superscript *o* denotes parameter determined/measured under fully saturated conditions. Because the FF normalizes the effect of PSR (function of PS chemistry) on concrete resistivity measurements, it is a better descriptor of concrete microstructure performance, that is, the pore network properties (transport properties). Previous research studies have demonstrated the FF can be related to concrete transport properties, such as chloride ion diffusion, water

sorptivity, and permeability, that control deterioration mechanisms influencing the durability of concrete mixtures (*56*, *68*, *69*). Because the concrete pore network characteristics control the transport mechanisms for chloride ion migration and rate of fluid absorption, developing specifications and service life models based on FF can serve as a tool to control, monitor, and accurately predict the performance of field concrete. Thus, a primary benefit of implementing FF into specifications is that a simple resistivity measurement of concrete mix in a field or laboratory can be used to assess durability and service life performance based on FF–transport properties' relationships.

In an air-entrained concrete, the total permeable pore space (porosity) in concrete comprises matrix porosity (gel, capillary, and chemical shrinkage pores), entrapped and entrained air voids, and aggregate porosity. Different curing regimens and conditioning procedures lead to different moisture levels and varying saturation states in concrete samples. Consequently, varying moisture levels impact fluid volume in pores, PSR, and the moisture continuity in pores, and thus the resistivity measurements. Therefore, the definition and interpretation of the FF is contingent upon the DOS (s_w) of the concrete samples during resistivity measurements.

In SC, PS from hydration occupies gel and capillary pore space in the hydrated paste matrix, and this level of saturation is called *sealed saturation*. However, in submerged curing, when concrete samples are immersed in buckets containing LW or PS, the curing solution saturates chemical shrinkage pores of the matrix in addition to PS occupying the gel and capillary pores of the matrix. Based on sorptivity studies, this level of saturation associated with the complete filling of matrix pores is defined as *nick point saturation*. When oven-dried concrete samples are saturated with a conducting fluid under vacuum pressure, theoretically, the entire void space of concrete (including air voids) is completely saturated with the conducting fluid (PS equilibrated by conducting fluid). Concrete samples after the saturated conditioning are commonly denoted to be in *fully saturated* condition. Therefore, for different curing regimen, the FF is calculated as shown in Equation 4-13:

Equation 4-13

$$\boldsymbol{FF_{sw} = \frac{\rho_{conc}^{sw}}{\rho_{ps}^{sw}} = \frac{1}{(\phi * s_w)(\beta * \eta_w)}}$$

Where ρ_{conc}^{sw} represents the concrete resistivity measurements for curing regimen (SC or submerged curing—SPS, LW, and MPS), and ρ_{ps}^{sw} is the PSC of concrete mixtures and corrected for the applicable saturation state during the concrete resistivity measurements. Consequently, contingent on the level of saturation, three formal definitions of FF—(a) *sealed FF* (FF_{SE}), (b) *nick point FF* (FF_{NP}), and (c) *Saturated FF* (FF_{SAT} *or* FF)—can be found in the literature (*54*, *59*, *70*). Additionally, in some research studies (*49*), the nick point FF (FF_{NP}) is also referred to as the apparent FF (AFF).

4.4.9.2 Evaluation Matrix

The test matrix to evaluate FF performance of HPC mixtures is shown in Table 4-38 and discussed in the following sections.

Table 4-38: Test Matrix for Evaluating FF Performance of HPC Mixtures

PARAMETER	TEST METHOD	AGE OF TESTING	CURING REGIMEN
FF	AASHTO PEM	7–180 days *Curing Regimen:* *Normal Curing (23 ± 2 °C)*	1. SC (SE) 2. Sat LW Curing 3. SPS 4. MPS

4.4.9.3 Results and Discussion

4.4.9.3.1 Sealed FF

The sealed FF (FF_{SE}) describes the microstructure quality of the matrix phase of concrete. It can be used separately from the air void system to evaluate the influence of binder composition and SCMs on the durability of matrix phase. For eight HPC mixtures evaluated in this study, the FF_{SE} was calculated using Equation 4-14, and the results are plotted in Figure 4-33.

Equation 4-14

$$FF_{SE} = \frac{\rho_{conc}^{SE}}{\rho_{ps}^{SE}}$$

For sealed FF determination, (ρ_{conc}^{SE}) represents the BR measurements of HPC mixtures subjected to a SC regimen from 28–180 days with normal temperature curing. PSR in sealed conditions (ρ_{ps}^{SE}) was determined based on TTI Model-2.

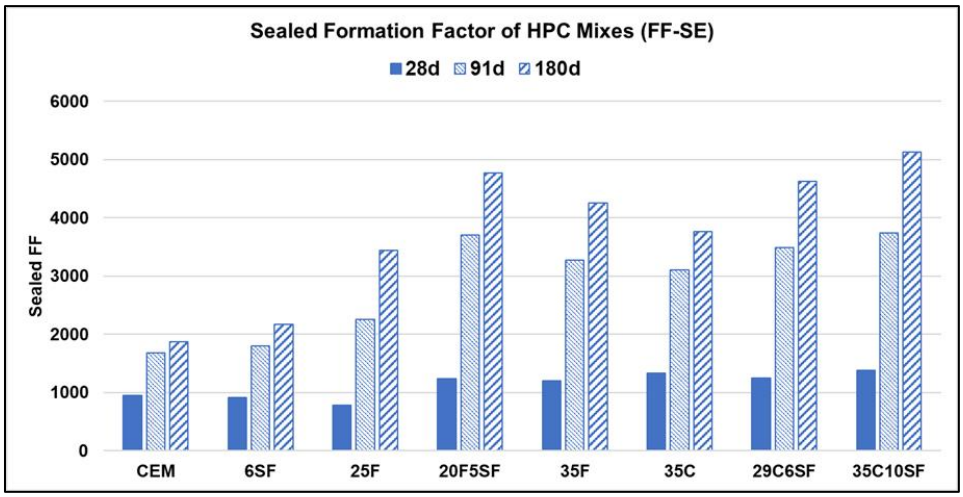

Figure 4-33: Sealed FF of HPC Mixtures from 28–180 Days

For a relative assessment of FF performance in the microstructure performance of HPC mixtures, a sealed FF index, FF(sealed), is the FF value of a mix expressed as a percentage of the 100 percent OPC mix at the same curing age. Results from the FF(sealed) index for HPC mixtures is shown in Figure 4-34.

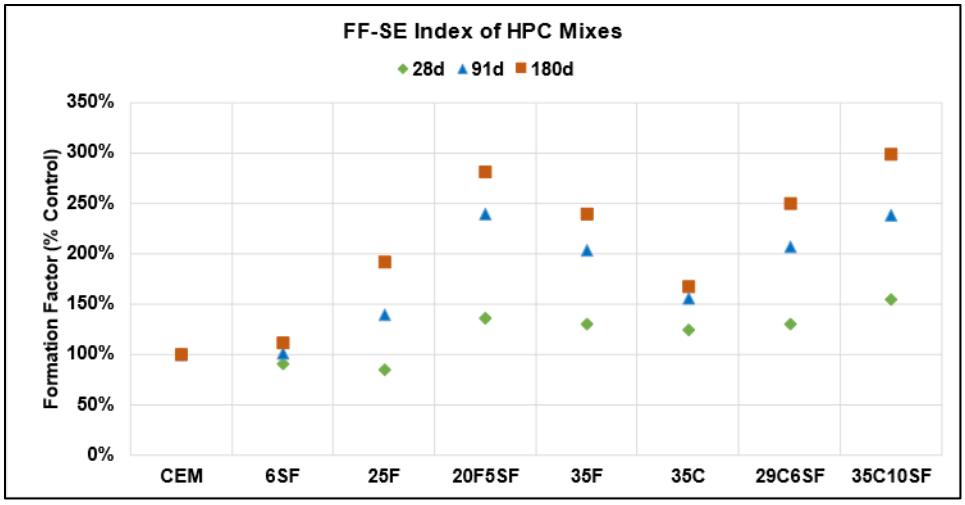

Figure 4-34: FF(Sealed) Index for HPC Mixtures at 28, 91, and 180 Days

Cement replacement with 6 percent SF only marginally improves the microstructure quality in comparison to the OPC mix. Furthermore, cement replacement with Class F FA significantly improves the microstructure quality of HPC mixtures, especially at later ages of 90–180 days. Compared to the binary Class F FA mixtures, the ternary 20F5SF mix with 5 percent SF demonstrated better microstructure quality at 28 days and an overall highest FF_{SE} at both 91 and 180 days. Similarly, for Class C FA mixtures, the ternary combination of Class C FA with SF has the most significant influence on the quality of microstructure in HPC mixtures, especially at early ages and when compared with binary 35C HPC mix.

4.4.9.3.2 The Apparent FF (AFF)—SPS and MPS Curing Regimen

The AFF was calculated for eight HPC mixtures subjected to a submerged curing regimen—SPS and MPS curing represented in Equation 4-15. BR measurements of HPC mixtures from 28–180 days subjected to SPS curing regimens (ρ_{sps}^{conc}) and MPS curing regimens (ρ_{mps}^{conc}) under normal temperature curing were used to calculate respective AFFs. For PSR, a value of ρ_{sps}^{ps} = 0.127 Ohm.m was used for an SPS curing regimen based on composition/conductivity of curing solution prepared as per ASTM C 1876. For the MPS curing regimen, concrete resistivity measurements were normalized—with a ρ_{mps}^{ps} value of 0.11 Ohm.m for CEM and 6SF mixtures, 0.13 Ohm.m for Class F FA HPC mixtures (25F, 20F5SF and 35F), and 0.09 Ohm.m for Class C FA HPC mixtures (35C, 29C6SF and 35C10SF)—based on composition and conductivities of respective curing solutions.

Equation 4-15

$$AFF_{SPS} = \frac{\rho_{sps}^{conc}}{\rho_{sps}^{ps}} \quad \text{and} \quad AFF_{MPS} = \frac{\rho_{mps}^{conc}}{\rho_{mps}^{ps}}$$

The average AFF values for SPS and MPS curing regimens at 28, 91, and 180 days are summarized in Table 4-39.

Table 4-39: AFF of HPC Mixtures—SPS and MPS Curing (28–180 Days)

MIX #ID	AFF—SPS CURING REGIMEN			AFF—MPS CURING REGIMEN		
	28 days	91 days	180 days	28 days	91 days	180 days
CEM	937	1244	1417	657	978	1066
6SF	1559	2102	2189	1533	2044	2336
25F	1063	2047	2669	971	2059	2774
20F5SF	1950	3094	3638	2270	3117	3650
35F	1386	2520	3472	1272	2759	3285
35C	1205	2205	2528	1372	1955	2570
29C6SF	2417	3386	3543	2646	3186	3456
35C10SF	2913	3937	4173	2894	3640	3780

4.4.9.3.3 Performance Classification Based on AFF of the HPC Mixtures under SPS and MPS Curing Regimens

Chloride Ion Permeability classification limits for the AFF were derived based on AASHTO PEM classification limits for the FF, as shown in Table 4-40. Performance limits for AFF were determined at DOS = 72 percent and a saturation correction factor of n = 2.2 based on discussions from previous sections.

Table 4-40: Performance Classification Limits for AFF

CHLORIDE ION PERMEABILITY CLASSIFICATION	FF [AASHTO PEM] ASSUMING (ρ_{ps}^{o}=0.127 OHM.M)	AFF $\frac{FF}{AFF} = (DOS)^{n}$
High	<407	<810
Moderate	407–815	810–1620
Low	815–1630	1620–3250
Very Low	1630–16299	3250–32500
Negligible	>6299	>32500

HPC mixtures' performance classification for AFF in the MPS and SPS curing regimens are shown in Table 4-41 and plotted in Figure 4-35 and Figure 4-36.

All HPC mixtures demonstrate a similar AFF performance classification in the SPS and MPS curing regimens at 90–180 days. When comparing AFF performance of different HPC mixtures at different ages, the SCM type and replacement level were found to be influential primary parameters that affect microstructure quality.

Table 4-41: AFF Performance Classification of HPC Mixtures—SPS vs. MPS Curing

MIX ID	AFF-SPS CURING			AFF-MPS CURING		
	28 days	**91 days**	**180 days**	**28 days**	**91 days**	**180 days**
CEM	Moderate	Moderate	Moderate	High	Moderate	Moderate
6SF	Moderate	Low	Low	Moderate	Low	Low
25F	Moderate	Low	Low	Moderate	Low	Low
20F5SF	Low	Low	Very Low	Low	Low	Very Low
35F	Moderate	Low	Very Low	Moderate	Low	Very Low
35C	Moderate	Low	Low	Moderate	Low	Low
29C6SF	Low	Very Low	Very Low	Low	Very Low	Very Low
35C10SF	Low	Very Low	Very Low	Low	Very Low	Very Low

Compared to the OPC mix (CEM), all HPC mixtures containing SCMs demonstrated better performance classification. Mix 6SF cement replacement with 6 percent SF improved the microstructure quality and the AFF performance classification compared to the OPC mix. For Class F FA mixtures, the ternary 20F5SF mix with 5 percent SF demonstrated improved microstructure performance as early as within 28 days (i.e., achieving low-performance classification by 28 days) and achieving a *very low* classification within 180 days. However, binary mixtures (i.e., 25F and 35 F took a significantly longer time (e.g., 91 days) to achieve the same *low* performance classification due to slower reacting Class F ash. By 180 days, 35F mix achieved *a very low* category status but no change in classification was noticed for the 25F mix. Therefore, it seems increasing FA dosage up to 35 percent (35F) is needed to achieve optimum improvement in microstructure development; this step resulted in *very low* performance classification by 180 days. Therefore, 180 days is required to effectively differentiate the F ash mixtures based on AFF-based performance classification.

Compared with the binary Class C mix (35C), the ternary mixtures with SF (e.g., 29C6SF, 35C10SF) demonstrated a significant improvement in microstructure development and permeability reduction through SF pozzolanic reactions, especially at early ages. In addition, the ternary mixtures achieve a *very low* chloride ion permeability classification between 28–91 days.

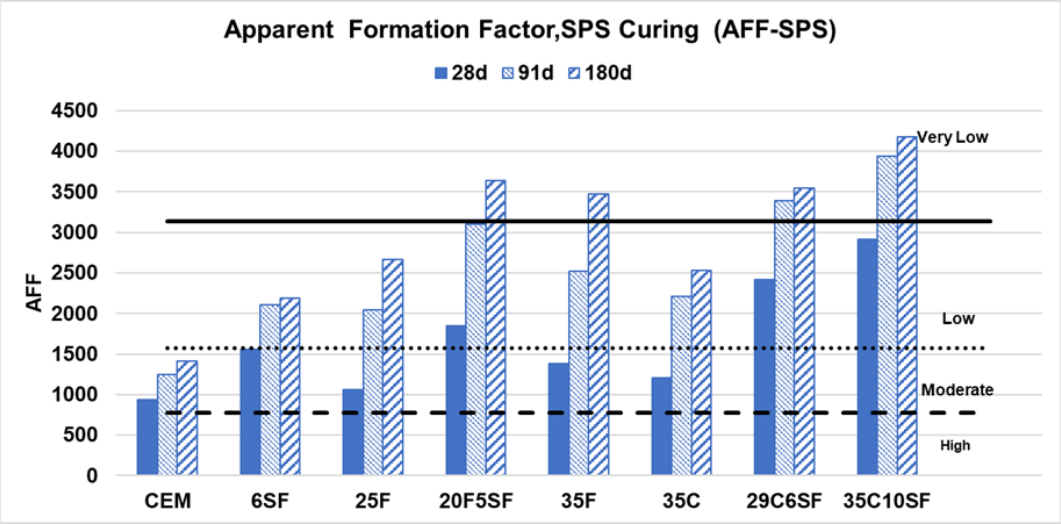

Figure 4-35: AFF Performance Classification of HPC Mixtures—SPS Curing

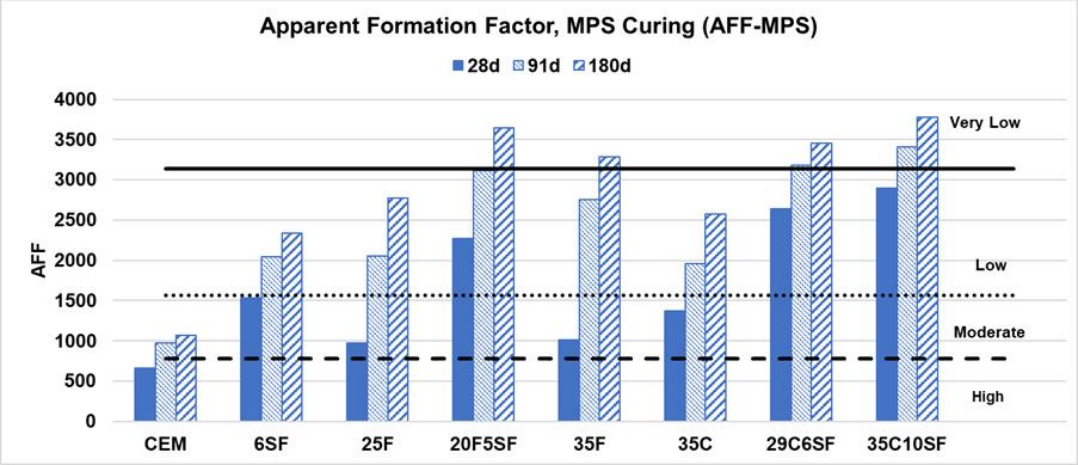

Figure 4-36: AFF Performance Classification of HPC Mixtures—MPS Curing

4.4.9.3.4 Effect of Curing Solution Conductivity on Resistivity versus AFF performance

In previous sections, the conductivity of the curing solution was revealed to influence the BR measurements on HPC mixtures directly. As such, performance classification of HPC mixtures following BR measurements in MPS and SPS curing were different at the same curing ages. However, AFF determination has been seen to normalize the influence of curing and PSC on resistivity measurements, and the comparative results are shown in Table 4-42.

Notably, for Class C FA mixtures, the conductivity of curing solution in MPS (111.5 S/m) was 1.5 times the SPS curing solution conductivity (78.75 S/m). This factor resulted in BR-SPS measurements being approximately 1.5 higher than BR-MPS measurements. In contrast, normalizing with curing solution conductivity resulted in a ratio of AFF-SPS to AFF-MPS that was close to 1.0 for these mixtures. Results from Table 4-42 also demonstrate the normalizing effect of PSC on AFF since the ratio of AFF-SPS to AFF-MPS is close to 1.0 for all HPC mixtures and test ages. As a result, AFF-based performance classification with both SPS and

MPS remain similar for all the HPC mixtures. However, FF (saturated)-based classification is expected to show some differences and highlight the benefits of MPS.

Table 4-42: Influence of Curing Solution Conductivity on BR and AFF Measurements—SPS vs. MPS

MIX #ID	SPS VS. MPS CURING REGIMEN					
	Ratio of Resistivity			Ratio of AFF		
	28d	91d	180d	28d	91d	180d
CEM	1.3	1.2	1.2	1.2	1.3	1.3
6SF	0.9	1.0	0.9	1.0	1.0	0.9
25F	1.0	0.9	0.9	1.1	1.0	1.0
20F5SF	0.8	0.9	0.9	0.9	1.0	1.0
35F	1.3	0.8	1.0	1.1	0.9	1.1
35C	1.2	1.5	1.3	0.9	1.1	1.0
29C6SF	1.3	1.5	1.4	0.9	1.1	1.0
35C10SF	1.4	1.6	1.5	1.0	1.1	1.1

4.4.9.3.5 AFF–LW Curing Regimen

An attempt was made to calculate the AFF for HPC mixtures using 91-day BR measurements from the LW curing regimen and considering two different case scenarios. In the first case, concrete resistivity measurements were normalized with PSC of HPC mixtures determined at 91 days under sealed conditions (TTI-Model 2) under assumptions of considering no alkali leaching from concrete PS into the LW curing solution. In the second case, alkali concentration (Na and K) measured in LW curing solution at 91 days was removed from their constituent composition in the PS to account for effects of alkali leaching from concrete PS. The results from the two approaches are plotted in Figure 4-37. In addition, the AFF determined for HPC mixtures at 91 days for SPS and MPS curing is additionally shown for comparative evaluation.

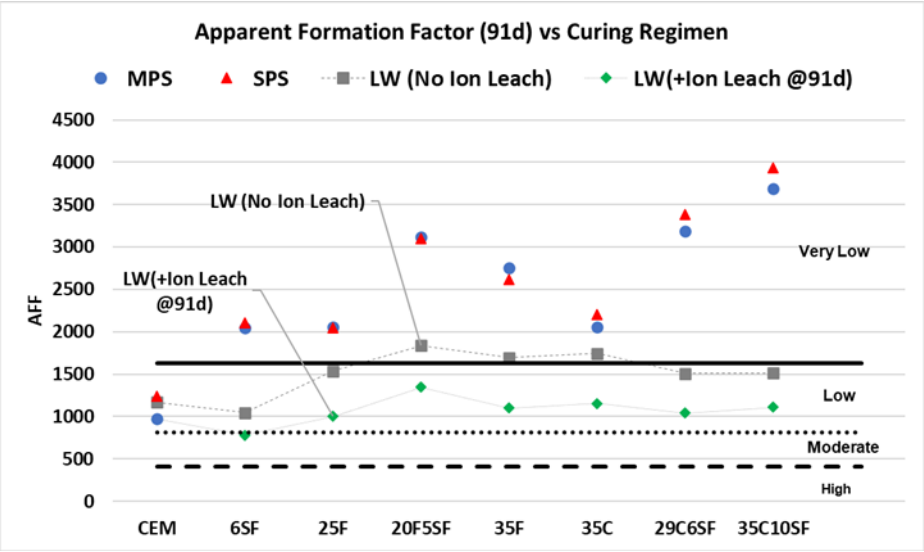

Figure 4-37: AFF—LW Curing (2 Cases) vs. AFF—SPS and MPS Curing at 91 Days

As discussed in the previous section, the conductivity of the LW curing solution is approximately 8–10 times lower than the true PS conductivity of HPC mixtures. Thus, it cannot be used to normalize the resistivity measurements for AFF-LW determination. Furthermore, AFF determined for LW curing under assumptions of no ionic leaching appears to significantly vary from AFF determined from SPS and MPS curing regimen. Thus, consideration of PSC in sealed conditions does not appear to be realistic for AFF determination and performance evaluation of HPC mixtures based on LW curing. Similarly, for the second case, consideration of alkali leaching from PS decreases its concentration and lowers the PSC of HPC mixtures. Therefore, based on this approach, consideration of lower PSC (or increased resistivity) further lowers AFF determination of HPC mixtures in LW curing.

Overall, resistivity measurements in LW curing generally demonstrated a high COV due to influence from ionic leaching in comparison to SPS and MPS curing regimens. The low SR/BR values for LW curing also pointed to a lack of homogeneity in PS between the outer surface and bulk core, possibly due to active leaching. High variability in resistivity measurements compounded by challenges in *true* AFF determination of HPC mixtures makes the LW curing regimen not suitable for both performance classification and performance evaluation based on AFF of HPC mixtures.

4.4.9.3.6 Saturated FF

Following the BR measurements on saturated, conditioned HPC specimens initially subjected to submerged SPS and MPS curing, the FF (Equation 4-16) was calculated for HPC mixtures at 28, 91, and 180 days.

Equation 4-16

$$FF_{SPS} = \frac{\rho_{sps}^{conc-SAT}}{\rho_{sps}^{ps}} \quad \text{and} \quad FF_{MPS} = \frac{\rho_{mps}^{conc-SAT}}{\rho_{mps}^{ps}}$$

Where $\rho_{sps}^{conc-SAT}$ and $\rho_{mps}^{conc-SAT}$ represent the BR measurements on saturated, conditioned HPC specimens for SPS and MPS curing, respectively. As HPC specimens were saturated with the appropriate curing regimen (SPS or MPS) solution, ρ_{sps}^{ps} = 0.127 Ohm.m was used to calculate FF_{MPS}. Similarly, the value of ρ_{mps}^{ps} was taken to be 0.11 Ohm.m for CEM and 6SF mixtures, 0.13 Ohm.m for Class F FA HPC mixtures, and 0.09 Ohm.m for Class C FA HPC based on conductivities of respective curing solutions and saturating solution. The average AFF values for SPS and MPS curing regimens at 28, 91, and 180 days are summarized in Table 4-43.

Table 4-43: FF of HPC Mixtures—SPS and MPS Curing (28–180 Days)

MIX #ID	FF—SPS CURING			FF—MPS CURING		
	28d	91d	180d	28d	91d	180d
CEM	326	412	459	282	407	438
6SF	540	689	701	637	824	930
25F	471	826	1174	505	1026	1369
20F5SF	941	1469	1849	1304	1728	2005
35F	660	1102	1692	556	1442	1702
35C	563	939	1049	687	936	1215
29C6SF	1277	1592	1773	1370	1585	1698
35C10SF	1405	1795	1862	1527	1732	1891

4.4.9.3.7 Performance Classification for FF of HPC Mixtures

HPC mixtures were classified chloride ion permeability based on 28, 91, and 180-day SFF, following AASHTO PEM performance limits, as shown in Table 4-44.

Table 4-44: Performance Classification Limits for FF

CHLORIDE ION PERMEABILITY CLASSIFICATION	FF [AASHTO PEM] ASSUMING (ρ^{o}_{ps}=0.127 OHM.M)
High	<407
Moderate	407–815
Low	815–1630
Very Low	1630–16299
Negligible	>16299

HPC mixtures performance classification for AFF in MPS and SPS curing regimens are shown in Table 4-45 and plotted in Figure 4-38 and Figure 4-39.

Table 4-45: FF Performance Classification of HPC Mixtures—SPS vs. MPS Curing Regimen

MIX ID	FF—SPS CURING REGIMEN			FF—MPS CURING REGIMEN		
	28d	91d	180d	28d	91d	180d
CEM	High	Moderate	Moderate	High	High	Moderate
6SF	Moderate	Low	Low	Moderate	Low	Low
25F	Moderate	Low	Low	Moderate	Low	Low
20F5SF	Low	Low	Very Low	Low	Very Low	Very Low
35F	Moderate	Low	Very Low	Moderate	Low	Very Low
35C	Moderate	Low	Low	Moderate	Low	Low
29C6SF	Low	Low	Very Low	Low	Low	Very Low
35C10SF	Low	Very Low	Very Low	Low	Very Low	Very Low

All HPC mixtures demonstrated a similar FF performance classification in SPS and MPS curing regimens at 28, 91, and 180 days. In addition, all ternary HPC mixtures demonstrated a significant beneficial influence from pozzolanic reactions on improving microstructure quality at early ages (~ 28 days) when compared to their binary counterparts. As seen from Figure 4-38 and Figure 4-39, all ternary HPC mixtures—20F5SF, 29C6SF, and 35F10SF—show a *Very Low* FF performance classification at around 91 days. However, the pozzolanic effect of slower reacting Class F FA takes significantly longer to provide a beneficial effect to improve pore structure. The binary 35F mix shows *very low* FF performance classification close to 180 days. Other HPC mixtures—25F, 35C and 6SF—demonstrate a similar *low* FF performance classification at both 90 and 180 days.

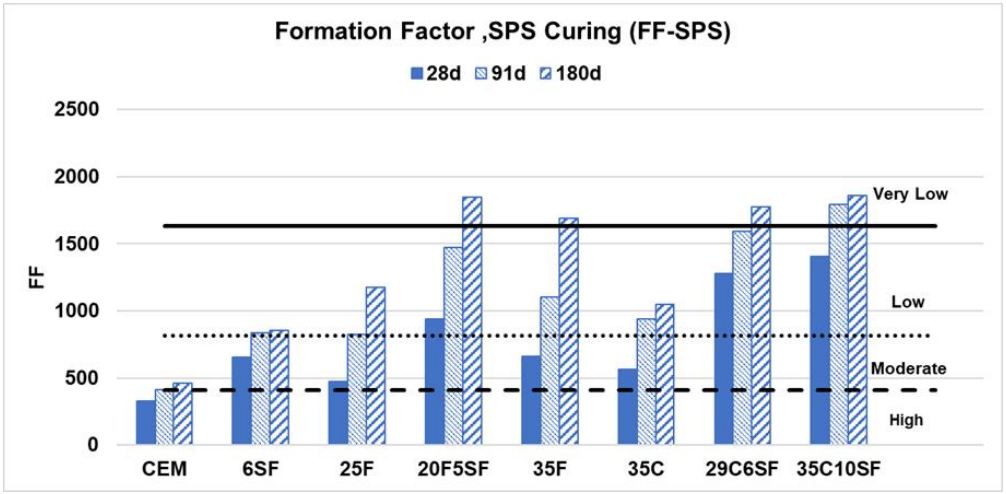

Figure 4-38: FF Performance Classification of HPC Mixtures—SPS Curing

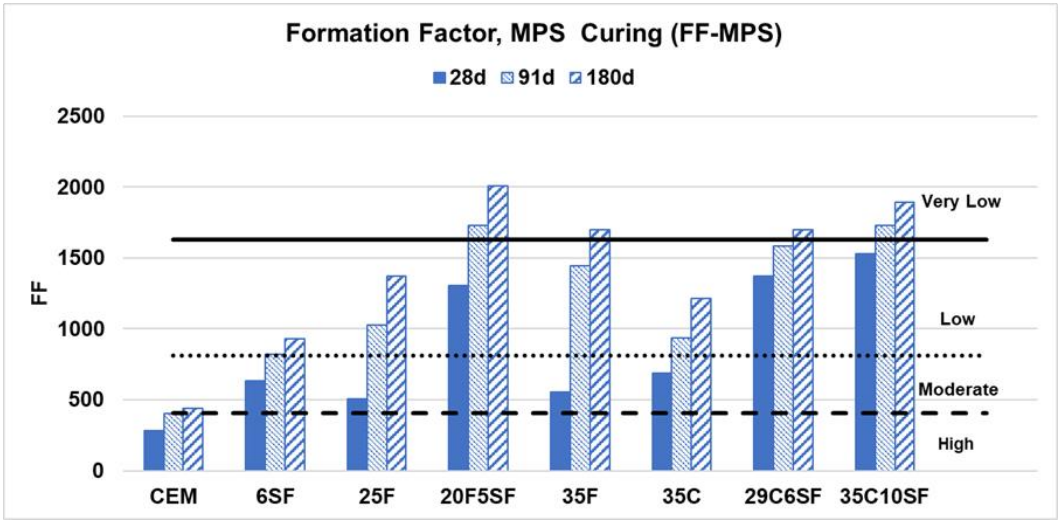

Figure 4-39: FF Performance Classification of HPC Mixtures—MPS Curing

4.4.9.4 Conclusion

The conclusions for FF evaluation of HPC mixtures, along with applicable comments for each curing regimen (i.e., a summary of above sections), are presented in Table 4-46.

Table 4-46: Conclusions for FF Evaluation of HPC Mixtures

CURING TYPE	BR & SR				PRIMARY FACTORS INFLUENCING RESISTIVITY MEASUREMENTS		COMMENTS ON FF DETERMINATION
	% COV	SR/BR (7–180d)	Drying (Moisture Loss)	Performance Limits (Normal and Acc Curing)	Saturation	Leaching	
SC	BR—3.0% SR—4.1%	0.91 – 0.94	✓ SR > BR	N/A	Lowest 55–60%	Nil	× Two levels of saturation correction required ✓ PSC = TTI Model 2 ✓ No leaching, low variability ✓ Good for quality control
Saturated LW Curing (ASTM C 511) LW	BR—4.8% SR—6.2%	0.77 - 0.89	✓ SR > BR	✓ 91-day NC ≈ 28-day AC1	~Nick Point 68–72%	✓ Definite, High and Variable	✓ Single saturation correction function × Leaching is variable; no definite leaching correction × conductivity of PS ≠ LW curing solution conductivity × High variability in FF determination
SPS Curing (ASTM C 1876) SPS	BR—4.3% SR—5.0%	0.86 – 0.92	✓ SR > BR	✓ 180-day NC ≈ 28–56-day AC1 ≈ 28-day AC2	~Nick Point 68–72%	Minimal	✓ Min. leaching; no correction required ✓ Single saturation correction function ✓ Conductivity of PS ≈ Curing solution conductivity × High variability in curing solution conductivity measurements
MPS Curing MPS	BR—3.8% SR—4.4%	0.91 – 0.95	✓ SR > BR	✓ 180-day NC ≈ 28–56-day AC1 ≈ 28-day AC2	~Nick Point 68–72%	Minimal	✓ Min. leaching; no correction required ✓ Single saturation correction function ✓ Conductivity of PS ≈ Curing solution conductivity ✓ Low variability in resistivity, curing solution conductivity measurements and FF determination

Note: N/A = Not Applicable; n/a = not available.

4.4.10 Chloride Diffusion

4.4.10.1 Test Matrix

The test matrix to evaluate chloride diffusion performance of HPC mixtures is shown in Table 4-47 and discussed in the following sections.

Table 4-47: Test Matrix for Evaluating Chloride Diffusion Performance of HPC Mixtures

PARAMETER	TEST METHOD/ APPROACH	AGE OF TESTING/ EVALUATION	CURING REGIMEN
Apparent Chloride Diffusion	ASTM C 1556	91 days	56-day moist curing followed by 35-day chloride exposure
Chloride Binding	Paste Samples and Isotherms	91 days	Saturated LW curing (6 levels of chloride exposure)
Effective Diffusion Coefficient *(Calculated)*	Finite Difference Modeling	91 days	N/A
Effective Diffusion Coefficient *(Predicted)*	Based on FF	91 days	N/A
Service Life Assessment	ConcreteWorks Based on FF (TxDOT Tool)	Time to corrosion initiation for different levels of (1) surface chloride exposure conditions and (2) rebar protection	N/A

Note: N/A = Not Applicable; n/a = not available.

4.4.10.2 Test Methods

4.4.10.2.1 Bulk (Apparent) Chloride Diffusion

Apparent chloride diffusion for each HPC mix was determined based on the ASTM C 1556 chloride ponding test, except that test specimens were subjected to a 56-day chloride exposure instead of the 35-day exposure period recommended in the specification.

For diffusion tests, three replicate samples of 4 × 8-inch (4 ± 0.08 inch diameter and 8 ± 0.16 inch height) concrete cylinders were cast for each HPC mix design. Cylinders were demolded at the age of 24 ± 2 hours and moist cured for 56 days in a controlled environmental chamber maintained at 23 ± 2 °C and 98 ± 2 percent RH, as per ASTM C 511 recommendations. At 56 days, 4 × 8-inch samples were cut using a wet saw to obtain two 3-inch (50 mm) thick specimens from its midsection. After the concrete surfaces were dry, a Sikadur 32 Hi-Mod epoxy was used to seal the specimens' sides and bottom to force a unidirectional ingress of chloride ions into the specimen from the top surface. Based on recommendations of a previous study (*71*), the epoxied specimens were immersed in a saturated LW soak solution for 36–48 hours to reduce the effect of absorption (capillary suction) on chloride ingress. After this soaking period, test

specimens were rinsed with tap water and immersed in baths containing 2.8M NaCl (16.2 percent NaCl by wt percent) for 56 days and placed in an environmental chamber maintained at 23 ± 2 °C and 98 ± 2 percent RH. At the end of the exposure period, specimens were removed, washed with tap water to rinse salt deposits, and then dried for 1 day in a drying room maintained at 23 ± 2 °C and 50 ± 3 percent RH. Test specimens were cut, sliced into eight 0.5-inch layers at specific depths, and pulverized to a powder (< 850 microns) for chloride analyses. The powdered samples obtained depth-wise from each test specimen were used to determine acid-soluble chloride content, as in ASTM C 1152.

4.4.10.2.2 Chloride Binding Isotherms

To evaluate the chloride binding capacity of HPC mixtures and to separate the influence of chloride binding from bulk (apparent) diffusion measurements, chloride binding isotherms were developed for HPC mixtures based on general procedures outlined by Tang and Nilsson (*72*). Three replicates of paste specimens were prepared based on ASTM C 1738 guidelines for each HPC mix design, and the specimens were demolded at 24 ± 2 hours. Subsequently, the paste samples were immersed in sealed containers containing saturated LW and placed in an environmental chamber maintained at 23 ± 2 °C and 98 ± 2 percent RH for 91 days. At 91 days, paste samples were crushed and dried in a sealed desiccator maintained at 11 percent RH for 72 hours. A laboratory-grade lithium chloride (LiCl) was used to control the RH inside the desiccator, which was equipped with a commercially available sensor for continuous monitoring of humidity levels. After conditioning, 25-gram powdered samples of each HPC mix were immersed in sealed containers containing 100 ml of lime-saturated NaCl solution of five different chloride concentrations—0.1, 0.4, 0.8, 1.0, and 2.0—and 3.0 mol/L for 56 days. At the end of the ponding period, the solution's residual chloride concentration was measured based on silver nitrate titration using a commercially available auto-titrator manufactured by ThermoFisher Scientific. The bound chloride and free chloride (equilibrium) contents for a sample from each container were plotted, and the resulting curves were fitted using a Freundlich binding isotherm to determine binding coefficients.

4.4.10.3 Methodology of Evaluation

4.4.10.3.1 Apparent Chloride Diffusion

The depth-wise acid-soluble chloride content determined from ASTM C 1556 test specimens was used to calculate the apparent chloride diffusion coefficient (D_a) of the mixtures based on assumptions of constant diffusion coefficient with time, as per Fick's 2nd Law of Diffusion, as shown in Equation 4-17:

Equation 4-17

$$C_{x,t} = C_s - (C_s - C_i)\, erf\left(\frac{x}{\sqrt{4D_a t}}\right)$$

Where $C_{x,t}$ is the acid-soluble chloride concentration (mass percent) measured at depth x and exposure time t; C_s is the surface chloride content (mass percent); C_i is the initial chloride content (mass percent), x is the depth below the exposed surface (mm), t is the exposure time (s), D_a is the apparent chloride diffusion (m^2/s), and the *erf* is the error function.

4.4.10.3.2 Chloride Binding

The change in chloride concentration of the exposure solution before and after 56-day ponding with powdered samples was used to calculate the bound chloride content, based on Equation 4-18:

Equation 4-18 $$C_b = 35.45\, V \frac{C_1 - C_o}{W * 1000}$$

Where C_b is the bound chloride of each mixture (mg/g of paste), V is the volume of solution (ml), W is the dry weight of the paste used in the test (g), and C_o and C_1 are the chloride concentration (M) in the exposure solution before and after the test. For the bound chloride (C_b) and free chloride content (C_f) at equilibrium, different concentrations were plotted for each HPC mix, and the resulting curves were fitted using a Freundlich binding isotherm to determine binding coefficients, as shown in Equation 4-19:

Equation 4-19 $$C_b = \alpha\, C_f^{\beta}$$

Where α and β are Freundlich isotherm parameters. Previous studies (*69*, *73*) have shown Freundlich isotherms to be a better descriptor of the binding phenomenon for free chloride concentrations of 0.05 M or higher in PS.

4.4.10.3.3 Effective Chloride Diffusion

In the current research, the effective chloride diffusion coefficient (D_e) for HPC mixtures was determined by analyzing the acid-soluble chloride profile with the inclusion of the chloride binding effect on Fick's 2nd Law based on steps shown in Equation 4-20. A finite-difference modeling approach with a time and depth step was used to calculate chloride profiles compared against the total (the acid-soluble) chloride content for the same exposure period. Finally, the Microsoft Excel solver function was used to minimize the error function and determine the effective diffusion coefficient.

Equation 4-20 $$D_a = \frac{D_e}{1 + \left(\frac{1}{\phi}\right)\left(\frac{dC_b}{dC_f}\right)} = \frac{D_e}{\left(1 + \frac{1}{\phi}\alpha\beta C_f^{\beta-1}\right)}$$

Where D_e represents the effective diffusion coefficient of free chlorides in the PS, D_a is the apparent chloride diffusion (m^2/s) (C 1556, Equation 4-17), α and β are Freundlich chloride binding isotherm coefficients (kg/m3), the chloride binding capacity parameter ($\frac{dC_b}{dC_f}$) is determined based on a Freundlich isotherm (Equation 4-19), ϕ is the volume of permeable pore space in concrete (ASTM C 642), and C_f denotes the concentration of free chloride in concrete PS.

4.4.10.3.4 FF-Based Diffusion Coefficient Prediction

In saturated concrete, the primary transport mechanism of chloride ions in PS (i.e., effective diffusion) is driven by the chloride concentration gradient. Consequently, based on the Nernst Einstein relationship, the self-diffusion coefficient of chloride ions in water ($D_o = 2.03 \cdot$

$10^{-9}\frac{m^2}{s} at\ 25°C$) can be related to its diffusion coefficient (D_{eff}) in PS through FF, as shown in Equation 4-21:

Equation 4-21 $$\boldsymbol{D_{eff} = \frac{D_o}{FF}}$$

Based on the $FF\ and\ D_{eff}$ relationship, the effective diffusion coefficient ($\overline{D}_e^{FF}$) can be determined based on consideration of chloride binding, as shown in Equation 4-22:

Equation 4-22 $$\boldsymbol{\overline{D}_e^{FF} = \frac{D_{eff}}{\phi\cdot\left(1+\frac{dC_b}{dC_f}\right)} = \frac{\frac{D_o}{\phi\cdot FF}}{\left(1+\frac{1}{\phi}\alpha_F\beta_F C_f^{\beta-1}\right)}}$$

ASTM C 1556 determines the diffusion coefficient based on total acid soluble chloride content, so as such the Equation 4-22 can be rewritten by setting the term $\frac{dC_b}{dC_f} = 0$, as shown in Equation 4-23:

Equation 4-23 $$\boldsymbol{\overline{D}_a^{FF} = D_a(C\ 1556) = \frac{D_o}{\phi\cdot FF}}$$

4.4.10.3.5 FF-Based Service Life Prediction (Time to Corrosion Initiation in Structures)

The time to corrosion initiation was determined based on Crack's solution to Fick's Second Law, as shown in Equation 4-24:

Equation 4-24 $$\boldsymbol{C_t = C_s - (C_s - C_i)\,erf\left(\frac{x}{\sqrt{4\left(\frac{\frac{D_o}{\phi\cdot FF}}{\left(1+\frac{1}{\phi}\alpha_F\beta_F C_f^{\beta-1}\right)}\right)\cdot t_{corr}}}\right)}$$

Where C_t is the threshold chloride concentration required to initiate corrosion as a function of rebar type and corrosion inhibitor dosage in the mix; C_s is the maximum surface chloride content for various exposure levels (based on fib 2010 durability code) C_i—the background chloride content and $C_i = 0.02\ percent$ (a constant value)—was used for calculations.

4.4.10.3.6 Results and Discussion

4.4.10.3.6.1 Apparent Chloride Diffusion (Dapp)

Table 4-48 shows the measured acid-soluble chloride content, expressed as percent by mass of concrete, for ASTM C 1556 HPC test specimens. Chloride contents are reported depth-wise and are the average of three test specimens. The apparent chloride diffusion coefficient (D_a) was calculated based on Crank's solution to Fick's 2nd Law of diffusion by removing the initial/background chloride concentration of Co = 0.02 percent; a chloride exposure time = 0.25 years (90 days) and chloride content for the top 2 layers were omitted from the analysis.

Table 4-48: ASTM C 1556 Depth wise Acid Soluble Chloride Profile (%concentration) for HPC Mixtures

DEPTH (MM)	CONTROL	6SF	25F	20F5SF	35F	35C	29C6SF	35C10SF
1	0.862	0.651	0.589	0.437	0.464	0.628	0.491	0.419
2	0.888	0.669	0.603	0.450	0.484	0.634	0.502	0.431
4	0.793	0.561	0.491	0.339	0.382	0.506	0.386	0.319
6	0.770	0.529	0.397	0.235	0.373	0.503	0.268	0.308
8	0.550	0.334	0.401	0.283	0.332	0.320	0.232	0.145
12	0.444	0.248	0.141	0.061	0.069	0.177	0.114	0.059
16	0.210	0.099	0.133	0.037	0.084	0.058	0.049	0.035
22	0.050	0.035	0.030	0.014	0.079	0.027	0.020	0.025
27	0.063	0.075	0.017	0.029	0.091	0.025	0.009	0.020
32	0.031	0.021	0.021	0.067	0.016	0.013	0.065	0.022
37	0.065	0.016	0.020	0.018	0.079	0.018	0.082	0.050
42	0.001	0.061	0.075	0.019	0.076	0.023	0.016	0.038
47	0.079	0.029	0.038	0.028	0.038	0.091	0.014	0.023

The apparent chloride diffusion coefficient (D_a) (average and COV) and surface chloride concentration (Cs) for HPC specimens obtained using the regression analysis of ASTM C 1556 data are shown in Table 4-49

Table 4-49: Parameters—Da and Cs Determined Using Regression Analysis

PARAM	CONTROL	6SF	25F	20F5SF	35F	35C	29C6SF	35C10SF
Da (m2/sec)	9.9E-12	5.4E-12	4.4E-12	2.9E-12	3.6E-12	4.0E-12	3.2E-12	2.7E-12
COV	13.3%	12.2%	18.2%	15.4%	13.4%	10.8%	17.6%	18.8%
Cs (%)	1.186%	0.984%	0.925%	0.776%	0.796%	0.973%	0.832%	0.759%

The chloride contents for all concrete specimens decrease with depth. Generally, HPC mixtures with SCMs demonstrate lower diffusion coefficients than OPC, which is primarily attributed to microstructure refinement (i.e., decreased pore connectivity) through pozzolanic reactions. The presence of SF is seen to have the greatest influence on reducing chloride contents compared to other SCMs. Cement replacement with 6 percent SF reduces the diffusion coefficient by 45 percent in comparison to the OPC mix. For Class F FA mixtures, the ternary 20F5SF mix demonstrates the largest reduction in diffusion coefficient (followed by 35F and 25F) when compared to the control. Similarly, ternary Class C FA mixtures with 10 percent SF (35C10SF) and 6 percent SF (29C6SF) demonstrate a 73 percent and 68 percent reduction in diffusion coefficients when compared to control.

4.4.10.3.6.2 Chloride Binding Capacity

Results from chloride binding experiments performed on HPC paste specimens are shown in Table 4-50 and plotted in Figure 4-40 to Figure 4-42.

Table 4-50: Results from Chloride Binding Experiments on Paste Specimens

MIX #ID	BOUND CHLORIDE (MG/G OF PASTE)						FREUNDLICH ISOTHERM COEFFICIENTS		
	0.1 M	0.4 M	0.8 M	1 M	2 M	3 M	α (mg/g)	β	R2
CEM	4	7.2	9.7	10.3	14	16.7	10.5	0.39	0.99
6SF	4.3	7.4	8.9	9.5	13.2	14	9.82	0.35	0.98
25F	4.8	8.2	10.9	11.6	15.2	17.7	11.67	0.38	0.98
20F5SF	5.1	8	10	10.4	13.8	15.8	10.83	0.32	0.97
35F	5.2	9	11.3	12	15.7	18.2	12.21	0.38	0.99
35C	5.4	8.1	10	11.1	13.3	15.1	10.82	0.30	0.97
29C6SF	4.9	7.5	9.5	10.2	12.9	14.5	10.21	0.32	0.98
35C10SF	4.6	7.4	9.3	10.1	12.5	13.9	9.92	0.35	0.97

Chloride binding comprises two aspects: (1) chemical binding—chemical reaction of free chloride ions in PS with unhydrated cementitious phases (e.g., C3A, C4AF) or hydrated phases (e.g., monosulfoaluminate Afm phases), and (2) physical binding—adsorption of free chloride ions on the surface of CSH gel. Accordingly, the chloride binding capacity of HPC mixtures primarily depends upon the binder composition: the SCM type, the replacement level, and the composition of cementitious materials. Therefore, results from chloride binding experiments shown in Figure 4-40 to Figure 4-42 can be evaluated based on four major compositional parameters:

- C3A and sulfate content in cement.
- Alumina content in SCMs.
- Quantity of primary hydration product—CSH.
- C/S ratio of CSH because lower C/S reduces the chloride binding capacity (physical adsorption capacity) of CSH gel.

For plain cement pastes, the chloride binding ability can be attributed to the chemical reaction of free chlorides with an alumina-ferric oxide-monosubstituted (Afm) phase and unhydrated C3A and C4AF phases and from physical adsorption of free chlorides by the CSH gel. However, cement replacement with 6 percent SF reduces the chloride binding capacity (Figure 4-40). This reduction can be attributed to two factors: (1) a slight dilution in C3A content of binder due to cement replacement, and (2) reduction in the C/S ratio of the CSH (SF pozzolanic reaction) reduces the physical binding capacity of the CSH gel to adsorb chloride ions.

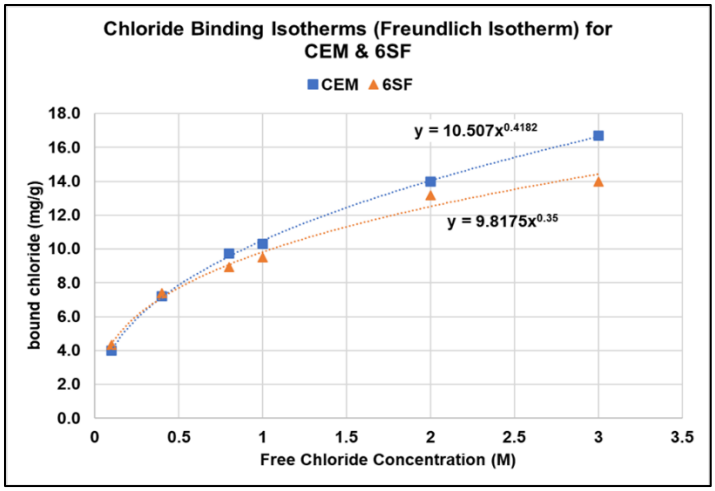

Figure 4-40: Chloride Binding Isotherms for OPC and 6SF Mix

In contrast with SF, cement replacement with alumina-rich Class F FA improves the binder's ability to react chemically, with more free chlorides in the PS to form Friedel salts. This factor explains the results from Table 4-50 and Figure 4-41, wherein binary Class F FA mixtures 25F and 35F (35F slightly higher than 25F) demonstrate a higher chloride binding capacity than OPC. The chloride binding in 20F5SF is lower than both 25F and 35F but still higher than the CEM. This lowering in chloride binding in 20F5SF is possibly due to dilution in the alumina content from fly ashes and reduction in physical adsorption by CSH due to a reduction in its C/S ratio.

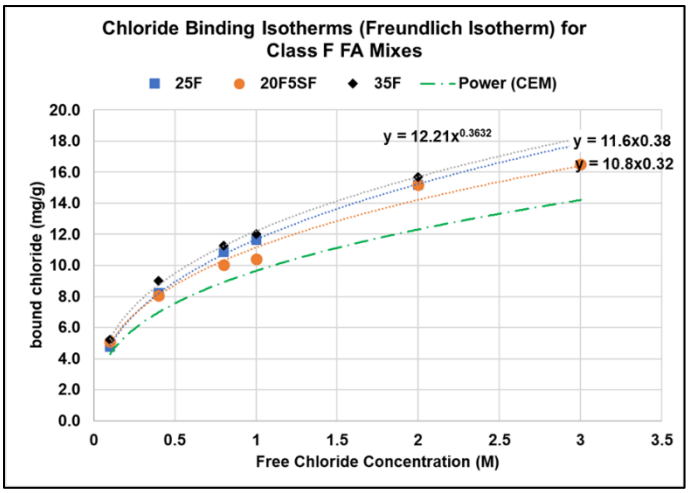

Figure 4-41: Chloride Binding Isotherms for Class F FA Mixtures (OPC as reference)

The Class C FA used in current research contained comparable levels of Al_2O_3 as Class F FA. Consequently, the incorporation of Class C FA improves the chloride binding capacity of the 35C mix in comparison to the control mix, as seen from Figure 4-42. However, QXRD measurements demonstrate that a higher fraction of bulk alumina is present in Class C FA than in Class F FA as a nonreactive crystalline phase (mullite and gehlenite), which explains a lower

binding capacity of 35C mix compared to the 35F mix. Furthermore, partial substitution of Class C FA with 6 percent SF decreases the chloride binding capacity of ternary 29C6SF mix in comparison to 35C. For ternary mix 35C10SF, 45 percent cement replacement and presence of 10 percent SF significantly reduced its chloride binding capacity to levels below the plain OPC and 6SF mix due to the formation of more CSH with low Ca/Si.

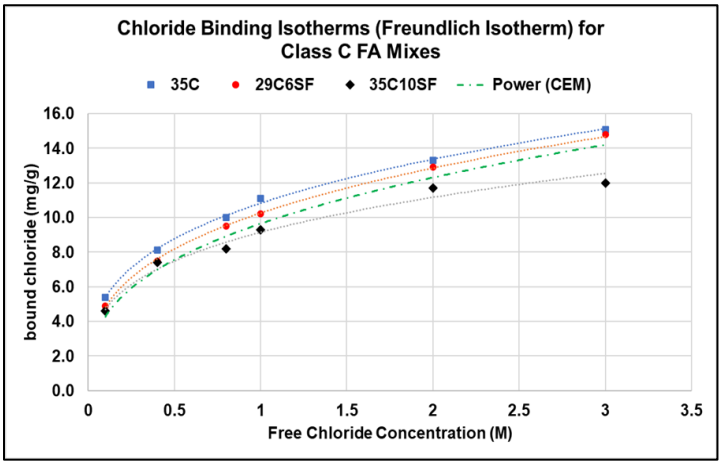

Figure 4-42: Chloride Binding Isotherms for Class C FA Mixtures (OPC shown for reference)

4.4.10.3.6.3 Effective Chloride Diffusion

The effective chloride diffusion (D_e) was determined based on two different approaches: (1) it was measured using a finite difference approach based on the acid-soluble chloride profiles measured on HPC specimens with the inclusion of chloride binding (Figure 4-43), and (2) it was predicted based on the 91-day FF and AFF of HPC mixtures (Equation 4-21 to Equation 4-23). Comparative assessments of results from the two approaches are shown in Table 4-51.

Table 4-51: Effective Chloride Diffusion of HPC Mixtures—Calculated vs. Predicted

MIX	FINITE DIFFERENCE APPROACH (CALCULATED)	BASED ON 91-DAY FF (PREDICTED)			BASED ON 91-DAY AFF (PREDICTED)		
	$D_e\ (m^2/s)$	FF (91 days)	$D_{eff}\ (m^2/s)$	$\overline{D}_e^{FF}(m^2/s)$	AFF (91 days)	$D_{eff}\ (m^2/s)$	$\overline{D}_e^{FF}(m^2/s)$
CEM	4.3E-12	407	4.7E-12	1.8E-11	978	2.1E-12	7.6E-12
6SF	2.5E-12	824	2.3E-12	9.5E-12	2044	9.9E-13	3.8E-12
25F	1.5E-12	1026	1.9E-12	8.8E-12	2059	9.9E-13	4.4E-12
20F5SF	1.0E-12	1728	1.1E-12	6.0E-12	3117	6.5E-13	3.3E-12
35F	1.2E-12	1442	1.3E-12	6.2E-12	2759	7.4E-13	3.2E-12
35C	1.8E-12	936	2.0E-12	1.1E-11	1955	1.0E-12	5.3E-12
29C6SF	1.3E-12	1585	1.2E-12	6.5E-12	3186	6.4E-13	3.2E-12
35C10SF	1.0E-12	1732	1.1E-12	4.7E-12	3413	5.9E-13	2.4E-12

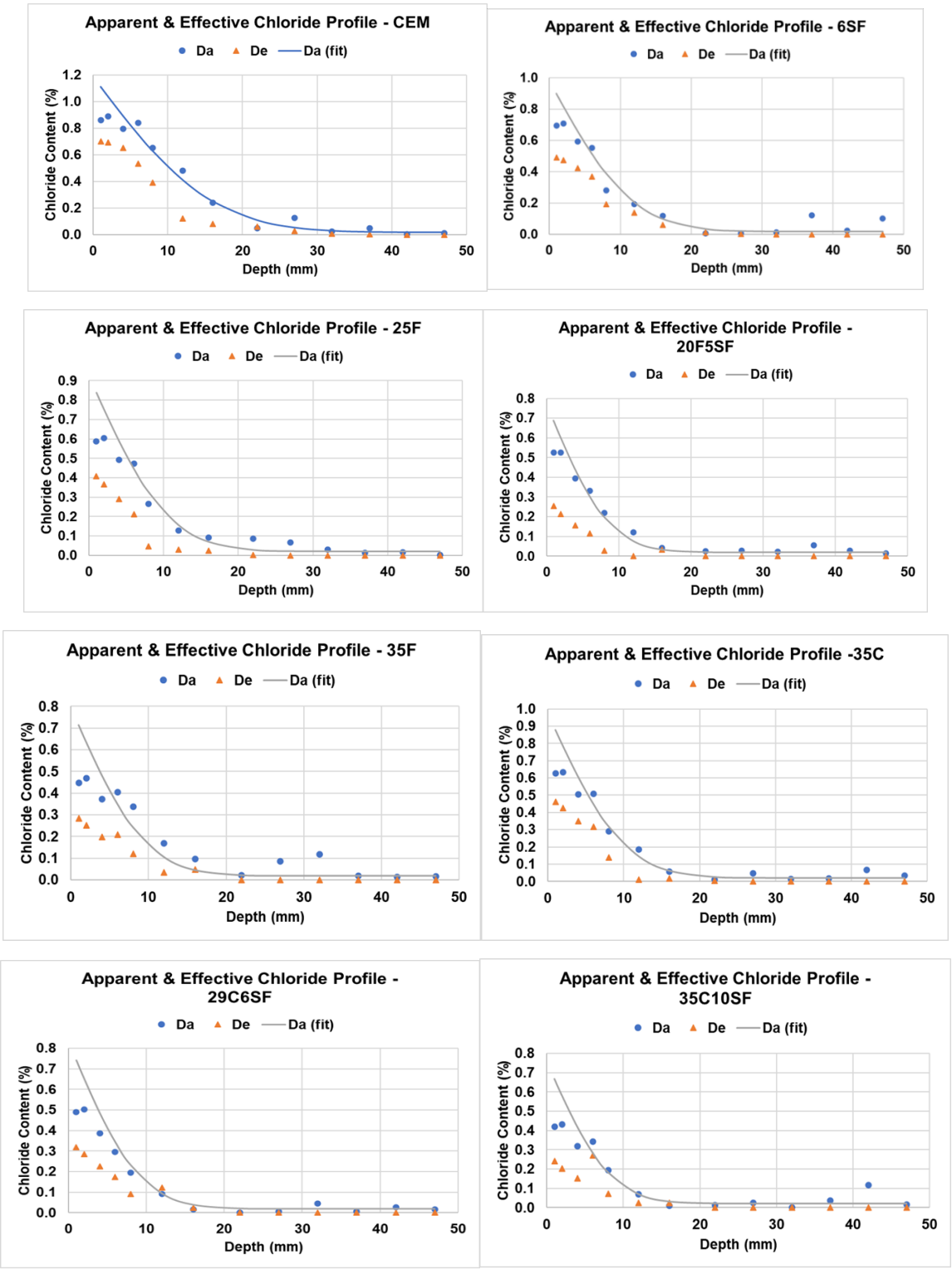

Figure 4-43: Apparent Chloride (ASTM C 1556) and Effective Chloride Content (% Concentration) Profile for HPC Mixtures

The diffusion coefficients—the measured apparent (D_a) and effective (D_e) diffusion coefficients for HPC mixtures—were compared with the diffusion coefficients predicted based on the FF and AFF, and the results are plotted in Figure 4-44 and Figure 4-45.

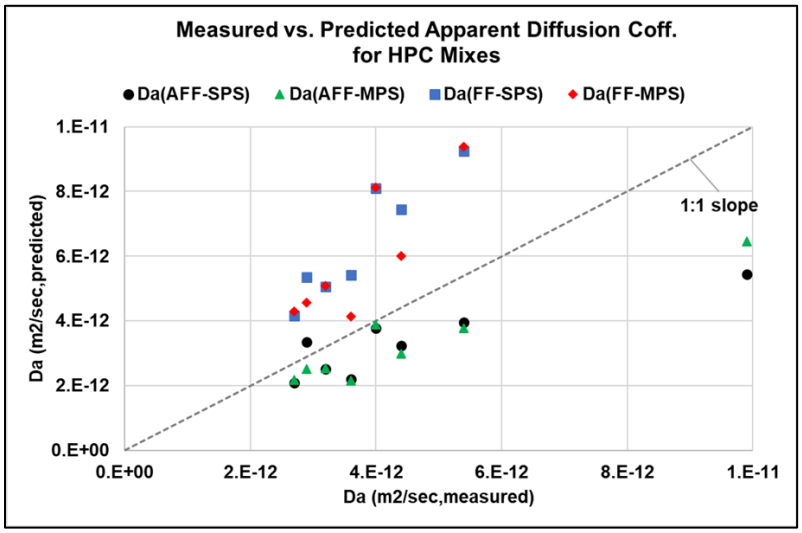

Figure 4-44: Correlation between Da (Measured) and vs. Da (Predicted from FF)

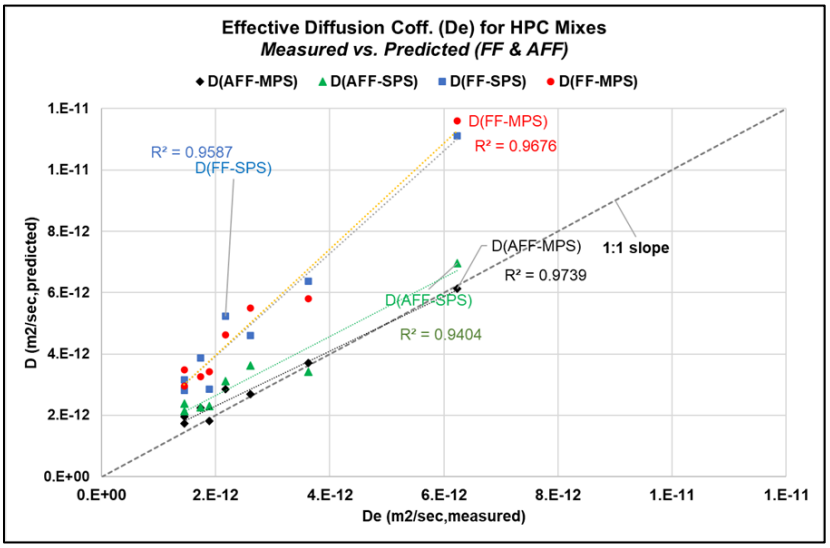

Figure 4-45: Correlation between De (Measured) and vs. De (Predicted from AFF)

Based on Figure 4-44, FF-based diffusion coefficients (D_{eff}) demonstrate a strong linear relationship (1:1 slope) with the measured effective diffusion coefficients from the acid-soluble chloride profiles for all the studied HPC mixtures. In contrast, the apparent diffusion coefficients are higher than predicted based on FF. However, based on results in Figure 4-45, the AFF-based diffusion coefficients (De) demonstrate a strong linear relationship (1:1 slope) with the measured effective diffusion coefficients for all the studied HPC mixtures. Therefore, observations from this section demonstrate three critical conclusions:

- The ASTM C 1556 apparent diffusion coefficient determined based on the acid-soluble chloride content is a composite of free chlorides transported in concrete PS and chemically bound and physically adsorbed chlorides.
- As opposed to total chlorides, the transport of free chloride ions in the concrete PS is responsible for corrosion initiation in structures. The effective diffusion coefficient describes the transport of free chloride ions through concrete.
- FF, which describes the microstructure properties (i.e., pore connectivity and pore volume) of concrete mixtures, is a robust and reliable predictor of the effective chloride diffusion coefficient (D_{eff}) in concrete mixtures. However, the computation of D_{eff} does not take into account the chloride exposure level or the chloride binding effects.

The AFF-based effective chloride diffusion coefficient (D_e) on the other hand considers both chloride exposure and chloride binding and presents an equally closer match with the measured effective diffusion coefficients. Thus, AFF-based prediction of diffusion presents an equally robust and reliable approach to determine effective chloride diffusion coefficient (D_{eff}) of HPC mixtures.

4.4.11 F/T Performance

4.4.11.1 Test Method

HPC mixtures were evaluated for F/T performance according to ASTM C 666 using Procedure A to freeze and thaw the test specimens in water. For the F/T test, two replicate beam specimens of size 3 × 4 × 16 inches (width × depth × height) were prepared for each HPC mix design. Test specimens (prisms) were demolded at the age of 24 ± 2 hours and moist cured in a controlled environmental chamber maintained at 23 ± 2 °C and 98 ± 2 percent RH for 56 days. As opposed to the 14-day moist curing recommended by ASTM C 666, extending the moist curing enables the HPC mixtures with slower-reacting SCMs to achieve a greater level of hydration and therefore potential durability properties. In addition, the 56-day extended curing regimen for mixtures containing SCMs is consistent with the curing practices recommended by ASTM C 1202 and previous research studies (*74–76*). Prior to the F/T test, HPC test specimens were air-dried in a drying chamber maintained at 23 ± 2 °C and 50 percent RH for 7 days to simulate the F1 exposure class, per ASTM C 318. Then, the F/T test was conducted on test specimens for a total of 324 cycles. The relative dynamic MOE (RDM) was determined every 36 cycles, and the durability factor (DF) was calculated at the test termination based on the approach outlined in the specification.

4.4.11.2 Results

The RDM of HPC mixtures (average of two specimens) is plotted as a function of F/T cycles in Figure 4-46 to Figure 4-48. In addition, the DF of the HPC test specimens is shown in Table 4-52.

Table 4-52: DF of HPC Test Specimens

PARAM	CEM	6SF	25F	20F5SF	35F	35C	29C6SF	35C10SF
DF	80	80	85	84	89	87	83	73
COV	*4.8%*	*5.5%*	*7.8%*	*9.1%*	*8.8%*	*8.7%*	*9.0%*	*11%*

Typically, concrete mixtures with RDM > 80 percent at 300 cycles are considered to demonstrate excellent F/T performance. Based on the results, almost all HPC mixtures indicated excellent F/T performance except for the 35C10SF mix. Five out of eight HPC mixtures achieved an RDM greater than 80 percent at the end of 324 cycles, while two mixtures—CEM and SF—demonstrated an avg RDM of 80 percent. HPC Mix 35C10SF showed a reduced performance, with an average RDM of 73 percent and COV of 10.3 percent; however, the first test specimen of this mix achieved an RDM > 80 percent at the end of 324 cycles. Although there are no limits to classifying F/T performance based on mass loss of test specimens, the average mass loss of all mixtures varied between 4.8 to 8.7 percent at the end of 324 cycles.

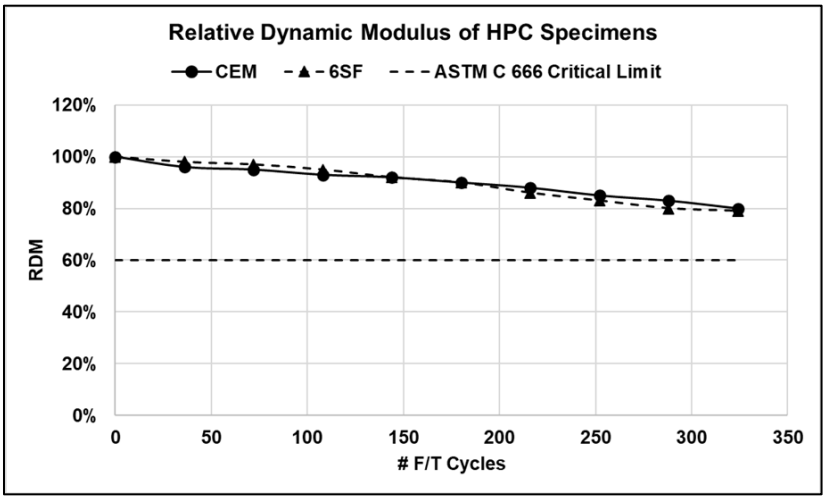

Figure 4-46: RDM vs. F/T Cycles—CEM and SF

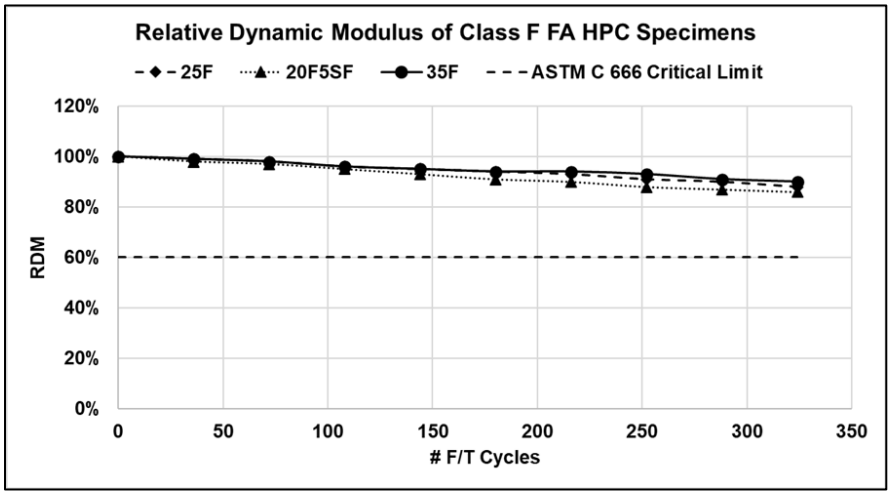

Figure 4-47: RDM vs. F/T Cycles—Class F FA Mixtures

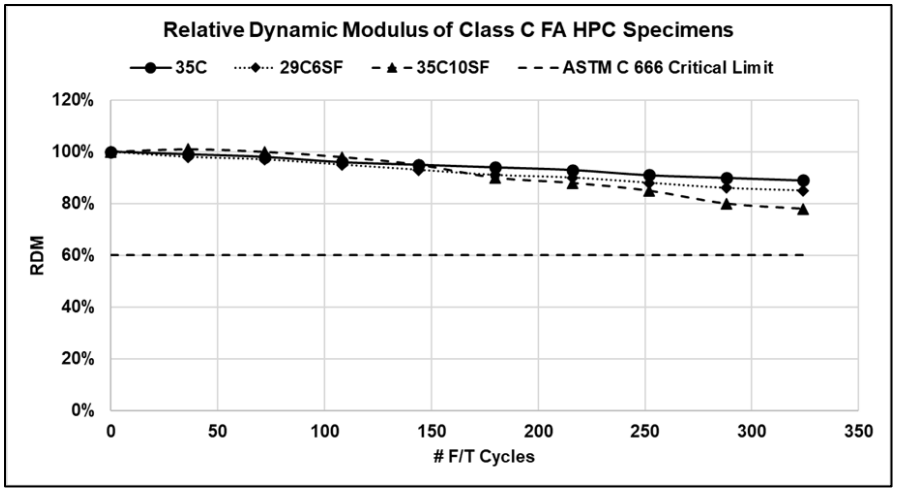

Figure 4-48: RDM vs. F/T Cycles—Class C FA Mixtures

4.4.12 Rate of Water Absorption (Sorptivity)

4.4.12.1 Test Methods

4.4.12.1.1 Rate of Water Absorption (Sorptivity)

Sorptivity, or water absorption rate, for different HPC mixtures was determined using ASTM C 1585. For sorptivity tests, a replicate of nine 4 × 8-inch (4 ± 0.08 inch diameter and 8 ± 0.16 inch height) concrete cylinders were cast for each HPC mix design. Concrete cylinders were demolded at the age of 24 ±2 hours and placed in a controlled environmental chamber maintained at 23 ± 2 °C and 98 ± 2 percent RH, as per ASTM C 511 recommendations on moist curing regimens. Sorptivity tests were performed at 28, 91, and 180 days of moist curing and for three replicate specimens of each HPC mix design.

At specified testing ages, three replicate 4 × 8-inch samples of each HPC mix design were removed from the moist room and cut using a wet saw to obtain 2-inch (50 mm) thick specimens from its midsection. Next, a Sikadur 32 Hi-Mod epoxy was used to seal the sides, and the specimens were left to dry for 5 hours. After drying, the 2-inch test specimens were placed in a sealed desiccator containing sodium bromide solution and placed inside an oven maintained at 50 ± 2 °C for 3 days. A laboratory-grade sodium bromide was used in this work to control the RH levels of 80 ±3 percent inside the desiccator, which was equipped with a commercially available sensor for continuous monitoring of humidity levels. After 3 days, the desiccators were placed at room temperature (23 ± 2 °C) for the next 15 days for a homogenous redistribution of moisture inside the specimens.

Specimens for sorptivity tests were sealed on the top and sides with plastic sheets and duct tape to force unidirectional water absorption through the exposed surface. Before the test, the mass of the specimens was recorded before and after the application of the plastic sheet. Then, specimens were immersed in water containers, with the exposed surface facing down and 1–3 mm beneath the water level. Mass measurements were obtained at specific time intervals for 14 days, as per

ASTM C 1585. At the end of the test period, the specimens were used to determine the DOS, as outlined in ASTM C 642, after removing the seal/duct tape.

4.4.12.2 Results and Discussion

Three replicate test specimens of each HPC mix design were tested for water absorption measurements via ASTM C 1585 guidelines at 56 and 180 days of curing. ASTM C1585 identifies absorption (I) as the increase in a test specimen's mass normalized by the product of the test specimen's exposed area to water and density of water; the results are shown in Figure 4-49.

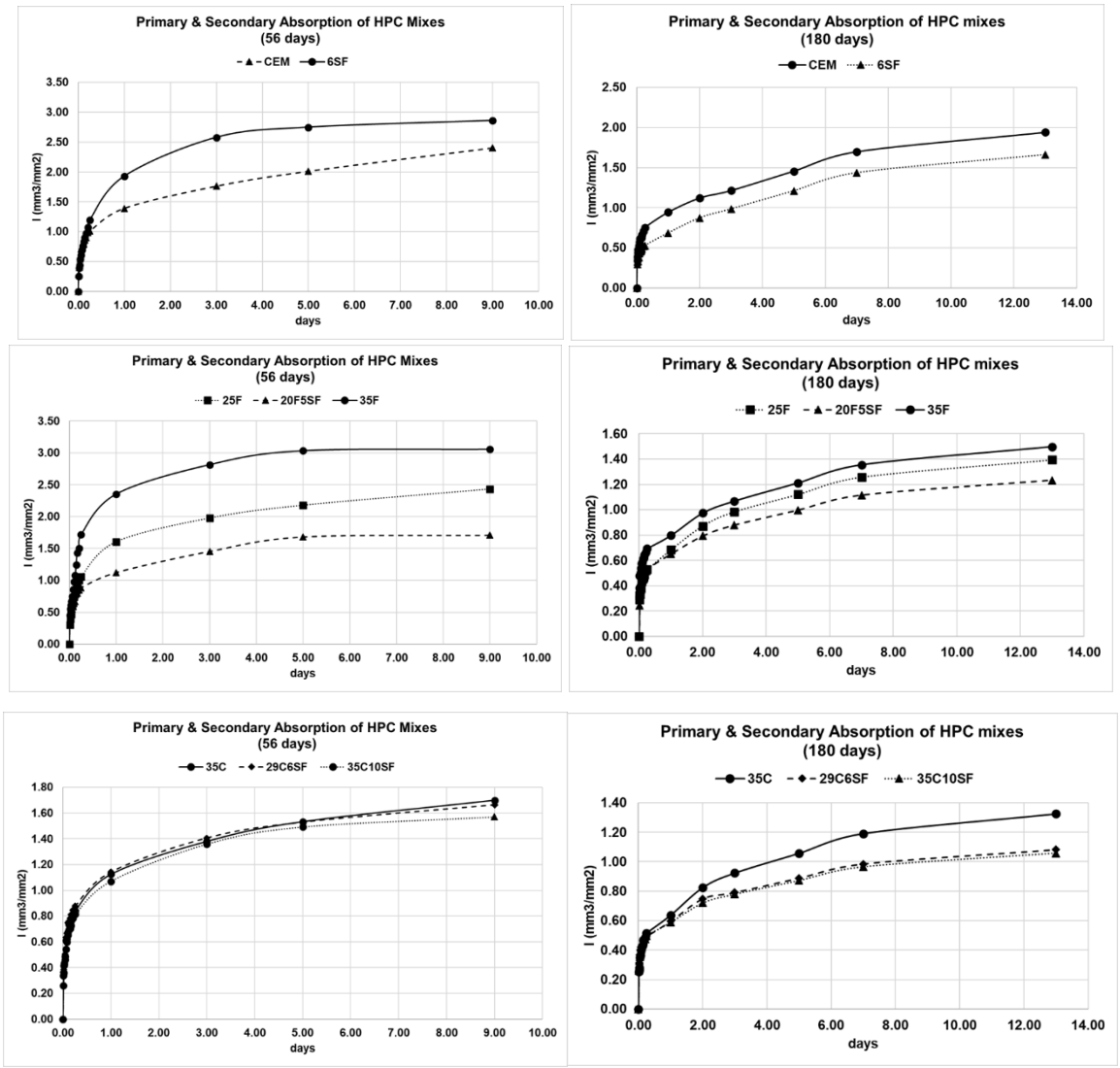

Figure 4-49: Primary and Secondary Absorption Plots at 56 Days and 180 Days

However, two distinct slopes (or parameters) are identified for air-entrained concrete when absorption is plotted as a function of time. Initial absorption corresponds to water absorption for the first 6 hours of the test, and the secondary absorption corresponds to mass increase between 1–7 days of the test. Accordingly, slope parameters were determined based on Equation 4-25 and Equation 4-26, as shown in Table 4-53.

Equation 4-25 $$i\left(t_{5\ min}^{6\ hrs}\right) = S_1\sqrt{t} \quad \textbf{and} \quad i\left(t_{1d}^{7\ d}\right) = S_2\sqrt{t} + A$$

Equation 4-26 $$\Delta m\left(t_{5\ min}^{6\ hrs}\right) = s_1\sqrt{t} \quad \textbf{and} \quad \Delta m\left(t_{1d}^{7\ d}\right) = s_2\sqrt{t} + B$$

Where $S_1 and\ S_2$ (Equation 4-25) are determined as the slope of the absorption-versus-√t curves during the first 6 hours and 1 to 7 days, respectively; $s_1 and\ s_2$ (Equation 4-26) are determined as the slope of the mass gain versus-√t curves during the first 6 hours and 1 to 7 days, respectively; and A, B are regression constants.

Table 4-53: Sorptivity Parameters Determined Based on Initial and Secondary Abs Curves at 56 and 180 Days

MIX #ID	ABSORPTION VS. TIME (I VS. √T, SEC)				MASS GAIN VS. TIME (ΔM VS. √T, SEC)			
	56 days		180 days		56 days		180 days	
	S_1	S_2	S_1	S_2	s_1	s_2	s_1	s_2
CEM	6.7	1.5	4.3	1.4	54.7	12.3	35.2	11.0
6SF	7.9	1.6	3.0	0.9	63.7	12.6	23.9	10.6
25F	7.0	1.2	3.0	0.9	57.1	10.1	23.9	7.5
20F5SF	5.5	1.0	3.2	0.8	44.3	8.3	26.3	6.2
35F	11.0	1.2	3.7	0.9	88.9	9.8	29.8	7.4
35C	5.6	1.0	3.0	0.9	45.0	7.9	24.6	7.2
29C6SF	5.7	0.9	2.9	0.6	46.2	7.2	23.7	5.0
35C10SF	5.0	0.8	2.8	0.6	40.3	6.9	22.9	4.9

During the sorptivity test, the initial absorption parameters primarily relate to filling the smallest pores first (gel, capillary pores, and chemical shrinkage). In contrast, the secondary absorption corresponds to the filling of larger voids, such as entrained or entrapped air. The rate of secondary absorption is related to the quality of the paste (w/c and SCM use) and the quality of the air void system. Therefore, the secondary slope parameters (S_2) identifies the influence of the concrete pore structure on the gradual filling of concrete air voids to reach threshold-critical DOS and initiate a F/T failure. The change in S_2 parameter for HPC mixtures at 28 and 180 dayts in plotted in Figure 4-50.

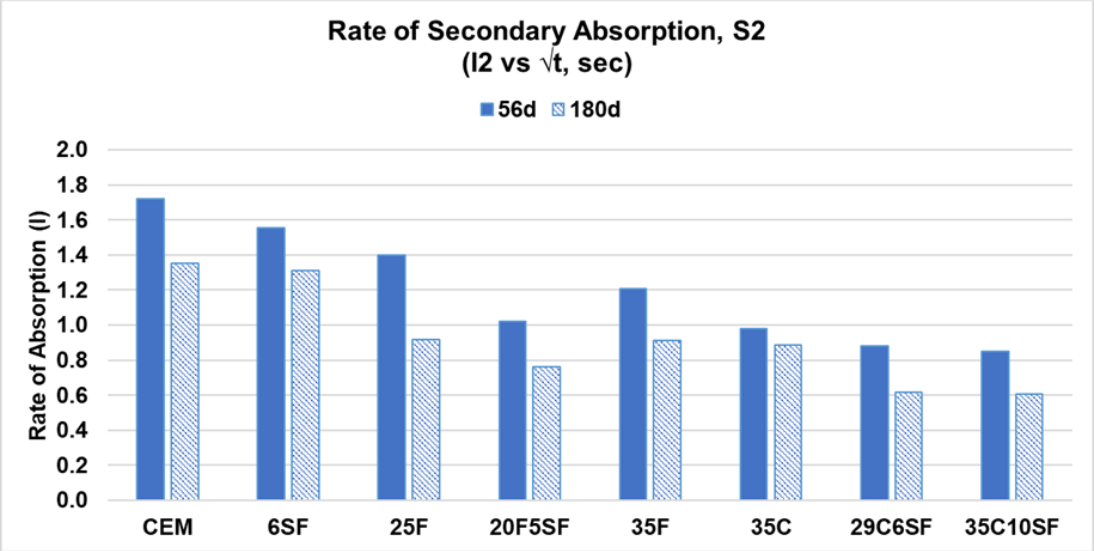

Figure 4-50: Rate of Secondary Absorption at 28 and 180 Days for HPC Mixtures

Results plotted above demonstrate an evident influence of cement replacement with SCMs in decreasing the sorptivity of HPC mixtures. The effect of SF incorporation on sorptivity reduction appears to be dominant for ternary FA-SF mixtures. Incorporating very fine pozzolanic materials such as SF increases the reaction rate in cementitious systems. In addition, due to its relatively high pozzolanic activity, the pore structure of paste containing SF becomes depercolated at significantly early ages. Therefore, the ternary HPC mixtures containing FA and SF greatly benefited from combined pozzolanic (and hydraulic for Class C FA) reactions of SCMs to refine their pore structure, especially at early ages. A finer pore structure with a discontinuous capillary porosity explains a significant reduction in absorption for 20F5SF, 29C6SF, and 35C10SF mixtures at both 56 and 180 days. Notably, the ternary 20F5SF mix demonstrated a 40 percent lower sorptivity (versus control) at 56 days due to an enhanced microstructure refinement at early ages from SF incorporation. In contrast to ternary SF mixtures, the cement replacement with 6 percent SF increased the sorptivity of the 6SF mix at 56 days compared to control. A potential agglomeration of SF particles possibly explains the increase in sorptivity. While SF incorporation densifies paste matrix through a substantial pore structure refinement, Weiss et al.(*77*) noted that ternary SF mixtures are likely to contain a higher fraction of pores that become depercolated with time. A substantial pore structure refinement could result in a less efficient air-void system to relieve pressure during F/T expansions. Slow-reacting SCMs such as Class F fly ashes take significantly longer to benefit capillary depercolation and pore-size refinement compared to Class C fly ashes. Thus, compared to CEM, binary FA mixtures (25F and 35F) demonstrated a substantial sorptivity reduction at longer ages of 180 days (40–50 percent) as opposed to 56 days (20–30 percent). In contrast, the binary 35C mix showed a 40–50 percent reduction in sorptivity at both 56 and 180 days when compared to the control mix.

4.4.12.2.1 Time to Critical Saturation (TTRCS) Model

The damage caused by freezing and thawing cycles is a major concrete durability problem in cold environments. However, current durability specifications (ACI 318–14) require a minimum target air volume and a maximum w/c ratio in concrete mixtures based on environmental exposure conditions. In contrast, concrete durability in F/T environments can be evaluated using a performance-based approach that uses Fagerlund's TTRCS model (*78*), which was extended in subsequent studies (*79–81*). The TTRCS model, as shown in Equation 4-27, relies on a two-stage absorption model based on ASTM C 1585. Concrete's resistance to F/T deterioration is determined based on three key parameters: critical DOS (DOS_{CR}), nick point (or matrix) saturation (DOS_{MAT}) and secondary absorption rate (S_2'), measured as per ASTM C 1585 guidelines:

Equation 4-27 $$\boldsymbol{DOS_{CR} = DOS_{MAT} + S_2'\sqrt{t}}$$

In addition, recent work (*82*) has shown that the rate of secondary sorption (S_2') is linearly related to the reciprocal of the square root of the AFF. A comprehensive analysis of TTRCS of HPC mixtures based on ASTM C 1585 test results as well as investigation of AFF-S2's relationship for HPC mixtures is currently in progress. Through this investigation, the current research aims to establish a linear relationship to predict S2 based on AFF, thereby saving substantial time in sample preparation and testing as per ASTM C 1585.

4.4.12.3 Conclusions

Because the concrete pore network characteristics control the transport mechanisms for rate of fluid absorption, developing specifications and service life models based on FF serve as a tool to control, monitor, and accurately predict the performance of field concrete. Thus, a primary benefit of implementing FF into specifications is that a simple resistivity measurement of concrete mix in a field or laboratory can be used to assess durability and service life performance based on FF–transport properties' relationships. In addition, the fluid absorption properties are vital when evaluating the service life of concrete structures subjected to freezing-and-thawing cycles.

CHAPTER 5: TXDOT TOOL OVERVIEW AND GUIDELINES FOR COMPREHENSIVE PERFORMANCE-BASED EVALUATION OF HPC MIXTURES USING TXDOT TOOL

This chapter presents an overview of the TxDOT Tool, its features, and guidelines for performing a comprehensive durability-based performance evaluation of HPC mixtures using the TxDOT Tool. TTI has developed a simplified, user-friendly Excel spreadsheet (known as *TxDOT Tool*) to enable DOT practitioners and contractors to perform rapid durability-based performance evaluation of CIP–HPC bridge deck mixes covering four major aspects: (1) ASR mitigation, (2) shrinkage, (3) durability to resist chloride ion ingress, and (4) F/T durability.

TxDOT Tool incorporates two key functionalities—(1) rapid prediction of durability properties/performance of HPC bridge deck mixtures (i.e., optimum SCM dosage for ASR mitigation, AS and DS strains, DS-based CP, FF [microstructure], apparent and effective diffusion coefficients, and sorptivity) in place of conducting long-term laborious ASTM/AASHTO tests; and (2) facilitates rapid estimation of in-field service life of HPC mixtures, covering resistance to chloride ion ingress (time to corrosion initiation and probability of cracking) and F/T exposure cycles (TTRCS) by leveraging established and scientific relationships between deterioration mechanisms and transport properties.

5.1 Features of TxDOT Tool

The overview of different aspects of TxDOT Tool are shown in Figure 5-1 and discussed in subsequent sections.

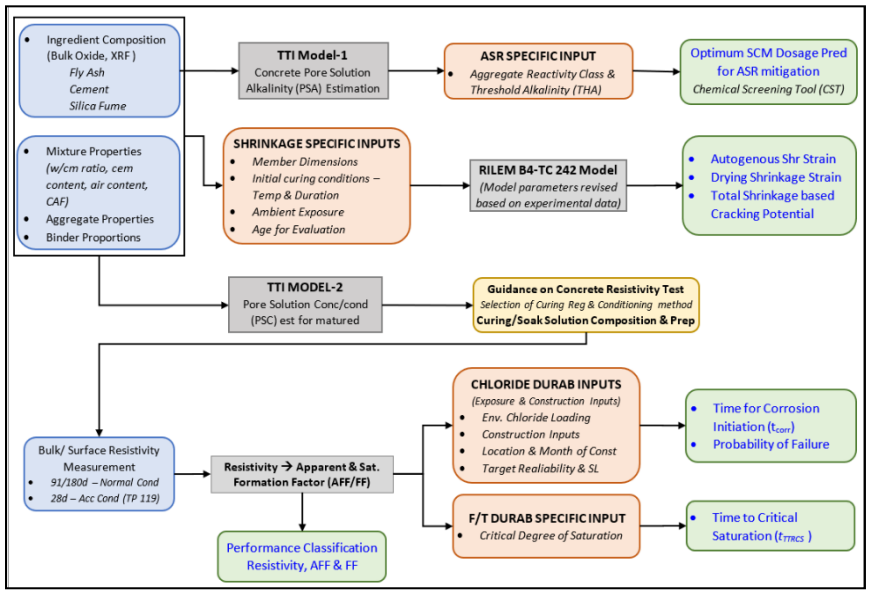

Figure 5-1: TxDOT Tool: Overview of Inputs, Associated Models, and Outputs

5.1.1 Concrete PS Chemistry Prediction

TxDOT Tool incorporates two proprietary models to predict the PS chemistry of concrete mixtures at early and later ages of hydration.

5.1.1.1 TTI Model-1

TTI Model-1 predicts the early-age concrete mixtures' PSA based on the combined effect of soluble alkali contribution from cement and WSA from fly ashes into concrete PS (*1*, *2*). TTI Model-1 uses empirical equations proposed by Snyder et al. (*3*) but modified to account for WSA contribution from cement and fly ashes to estimate ion concentrations in PS as a function of SCM replacement levels—as shown in Equation 5-1 and Equation 5-2.

Equation 5-1
$$Na^{+}\left(\frac{mol}{L}\right) = \frac{\sum_i^n\left(2m_{f,i}^{(Na_2O)}\cdot\frac{M_i}{M_{cm}}\cdot f_i\right)}{(2\cdot 22.99+15.99)}\cdot\frac{1000}{\frac{w}{cm}-(\sum_i^n k_i\alpha_i)}$$

Equation 5-2
$$K^{+}\left(\frac{mol}{L}\right) = \frac{\sum_i^n\left(2m_{f,i}^{(K_2O)}\cdot\frac{M_i}{M_{cm}}\cdot f_i\right)}{(2\cdot 39.098+15.99)}\cdot\frac{1000}{\frac{w}{cm}-(\sum_i^n k_i\alpha_i)}$$

Where mass fraction Na_2O and K_2O in cement and SCMs (m_i^{Na2O} and m_i^{K2O}) and their proportions in total cementitious materials (M_i/M_{cm}) determine alkali content. The alkali factor f_i, the ratio of WSA/TA, indicates early-stage (7–28 days) soluble alkali contribution (before considering SCMs' pozzolanic effects) (*4*). PS volume accounts for the initial w/cm ratio minus bound water and chemical shrinkage from cement ($k_i = 0.23$ g/g) and SCM ($k_i = 0.18$ g/g) reactions (*5*). The degree of hydration (α_i) of 75 percent for cement, 10 percent for Class F FA and natural pozzolans, and 15 percent for Class C FA are used to minimize alkali binding's impact on PSA (*3*, *5*). Finally, PSA is calculated in Equation 5-3:

Equation 5-3
$$PSA\ (N) = Na^{+} + 0.59K^{+}$$

5.1.1.2 TTI Model-2

TTI Model-2 estimates the PS concentration of binary and ternary concrete mixtures containing Class C and Class F FA and SF at long-term hydration ages based on a balanced consideration of ingredients' soluble alkali contribution into PS and the effects of alkali binding of pozzolanic hydration products. As per the conceptual framework of NIST+ASTM C 311 proposed by Mukhopadhyay et. al. (*6*), the alkali dissolution from concrete ingredients is determined by combining the total soluble alkali contribution from cement and SF (= 75 percent of bulk alkali, NIST Model) and available alkali (ASTM C 311) from fly ashes. The effect of alkali binding is incorporated using distribution ratios developed by Hong and Glassier (*7*) based on the stoichiometric predictions of CSH for cement (*8*, *9*), fly ashes (*10–12*), and SF (*13*, *14*) hydration reactions and GEMS modeling (*15*). Over 150 experimental data points of PS extraction measurements (7–365 days) were compiled based on laboratory measurements and published research studies to calibrate model parameters and refine TTI Model-2 predictions of PSC for binary and ternary concrete mixtures.

TTI Model-2 uses empirical equations proposed by Snyder (*3*) and Chen and Brouwers (*16*) that were extended to incorporate alkali dissolution from concrete ingredients based on soluble alkali contribution from cement, fly ashes, and SF and to incorporate alkali binding by the hydration products. As a result, the sodium (Na) and potassium (K) ion concentrations in PS as a function of time are determined as an equilibrium between alkali released from ingredients and alkali bound to CSH (hydration product), as shown in Equation 5-4 and Equation 5-2:

Equation 5-4

$$\boldsymbol{Na^{+}}\left(\frac{\boldsymbol{mol}}{\boldsymbol{L}}\right)=\frac{\sum_{i}^{n}\left(2m_{f,i}^{(Na_2O)}\cdot\frac{M_i}{M_{cm}}\cdot f_i\right)}{mm_{Na_2O}}}{\left[\left(\frac{w}{cm}-\sum_{i}^{n}k_i\alpha_i\right)+\left(\sum R_d\cdot m_{CSH}\right)\right]}$$

Equation 5-5

$$\boldsymbol{K^{+}}\left(\frac{\boldsymbol{mol}}{\boldsymbol{L}}\right)=\frac{\sum_{i}^{n}\left(2m_{f,i}^{(K_2O)}\cdot\frac{M_i}{M_{cm}}\cdot f_i\right)}{mm_{K_2O}}}{\left[\left(\frac{w}{cm}-\sum_{i}^{n}k_i\alpha_i\right)+\left(\sum R_d\cdot m_{CSH}\right)\right]}$$

The numerator in Equation 5-4 and Equation 5-5 uses an empirical approach to estimate the moles of alkali ions (Na and K) released into PS as a function of total soluble alkali contribution from cementitious materials. The parameters m_i^{Na2O} *and* m_i^{K2O}represent a mass fraction of Na_2O and K_2O in cement, FA and SF; the ratio $\frac{M_i}{M_{cm}}$ represents the mass fraction of a cementitious material to the total mass of cementitious materials in the system. The parameter $\boldsymbol{f_i}$ denotes the alkali factor (i.e., the fraction of soluble to bulk alkali) released from the cementitious material into PS. Consistent with the assumptions of the NIST model, the alkali factor of 75 percent was used for cement (f_{cem}) and SF (f_{SF})(*4*). Following the conceptual framework of NIST+ASTM C 311 (*6*), the alkali factor for FA (f_{FA}) was taken to represent the ratio of available alkali (AA) from fly ashes to bulk (total) alkali (TA) [either measured (ASTM C 311) or machine learning prediction model outputs]. The coefficient (k_i) represents the sum of bound water and chemical shrinkage accompanying cement hydration ($k_{cem} = 0.23$) and pozzolanic reactions of FA ($k_{FA} = 0.18$) and SF ($k_{SF} = 0.21$) (*5*, *12*, *17*). Parameters mm_{Na_2O} and mm_{K_2O} represent the molar mass of sodium and potassium oxides.

However, the denominator in Equation 5-4 and Equation 5-5 incorporates a kinetic approach to determine the volume of PS and proportion of alkali binding as a function of the ingredients' degree of reaction. The volume of the PS is calculated as a function of the initial w/cm ratio (w/cm) in the system and degree of reaction (α_i). Empirical factors for cement hydration with time were determined based on Parrot and Killoh's (8) model for clinker dissolution and follow the approach outlined by Lothenbach et al. (*18*). Correspondingly, cement hydration (α_{cem}) is modeled as a function of time increasing from 75 percent at 28 days to 90 percent at 180 days. The degree of reaction SF (α_{SF}) was estimated based on literature data (*13*, *19*, *20*) for 5–15 percent replacement levels in concrete and is modeled as a function of time increasing from 50 percent at 28 days to 85 percent at 180 days. The degree of FA reaction was estimated based on extensive investigation of literature data quantifying the rate of FA reaction in concrete (*10*, *13*, *21–25*) and encompassing Class C and F fly ashes and 20–40 percent replacement levels.

Although the FA degree of reaction decreases with increasing replacement levels, a previous study (*26*) noted that fly ashes demonstrate comparable reactivity at similar replacement levels. Correspondingly, depending upon the type and replacement levels of FA, different degrees of FA reaction (α_{FA}) (10–20 percent at 28 days to 35–50 percent at 180 days) are assumed for modeling.

As shown in Equation 5-4 and Equation 5-5, the effect of alkali binding is incorporated using distribution ratios ($\boldsymbol{R_d}$) proposed by Hong and Glassier (*7*) based on the stoichiometric predictions of mass of CSH ($\boldsymbol{m_{CSH}}$) for cement hydration (*8*, *9*), Class C and Class F fly ashes hydration (*10–12*), and SF hydration (*13*, *14*) reactions and is refined based on GEMS thermodynamic modeling (*15*) predictions of CSH. The effect of alkali binding is modeled based on a linear binding model (*16*, *27*) that assumes a linear relationship between the molar concentration of alkalis in CSH and the alkali concentration in the solution. The linear binding model enables using fixed distribution ratios ($\boldsymbol{R_d}$) for CSH based on its stoichiometric C/S ratio.

Finally, based on the net ion concentration of Na and K in the PS, the PS concentration is calculated using Equation 5-6:

Equation 5-6 $$\boldsymbol{PSA\ (N) = Na^{+} + K^{+}}$$

5.1.2 ASR Mitigation

Recently, researchers at TTI developed a CST (*28*) to determine the optimum dosage of SCMs for ASR mitigation within 1–2 days (*2*), and the methodology is illustrated in Figure 5-2. The CST uses two fundamental chemical parameters of concrete mixtures—concrete PSA and aggregate THA—and estimates the optimum dosage for ASR prevention based on their relationship (i.e., concrete PSA ≤ aggregate THA) (*6*, *29*). CST incorporates an innovative inbuilt model (TTI Model-1) to determine concrete PSA based on combined effects of soluble alkali contribution from cement and WSA from SCMs into PS. The CST can predict SCM dosages for concrete mixtures comprising varying aggregate reactivity levels, from highly reactive (R3) to nonreactive (R1) types, as defined by AASHTO R 80. The THA for an aggregate with known reactivity can be predicted using a reactivity–THA relationship developed in a previous study done by these researchers (*29*). However, for aggregates with unknown reactivity or high source variability, a rapid test such as AASHTO T 364 or AASHTO TP142 is recommended to determine the reactivity with acceptable reliability. CST predictions for optimum dosage for conventional (Class C and F), blended, reclaimed, and more recently, for natural pozzolans have been favorably validated by the highly reliable ACCT (AASHTO TP 142) as well as Accelerated Mortar Bar Test (AMBT; ASTM C 1567) (*28*, *30*). Additionally, CST demonstrated the capability to identify the limitations on use of AMBT for optimum SCM dosage determination of certain SCMs, especially SCMs with high levels of soluble alkali contribution into PS.

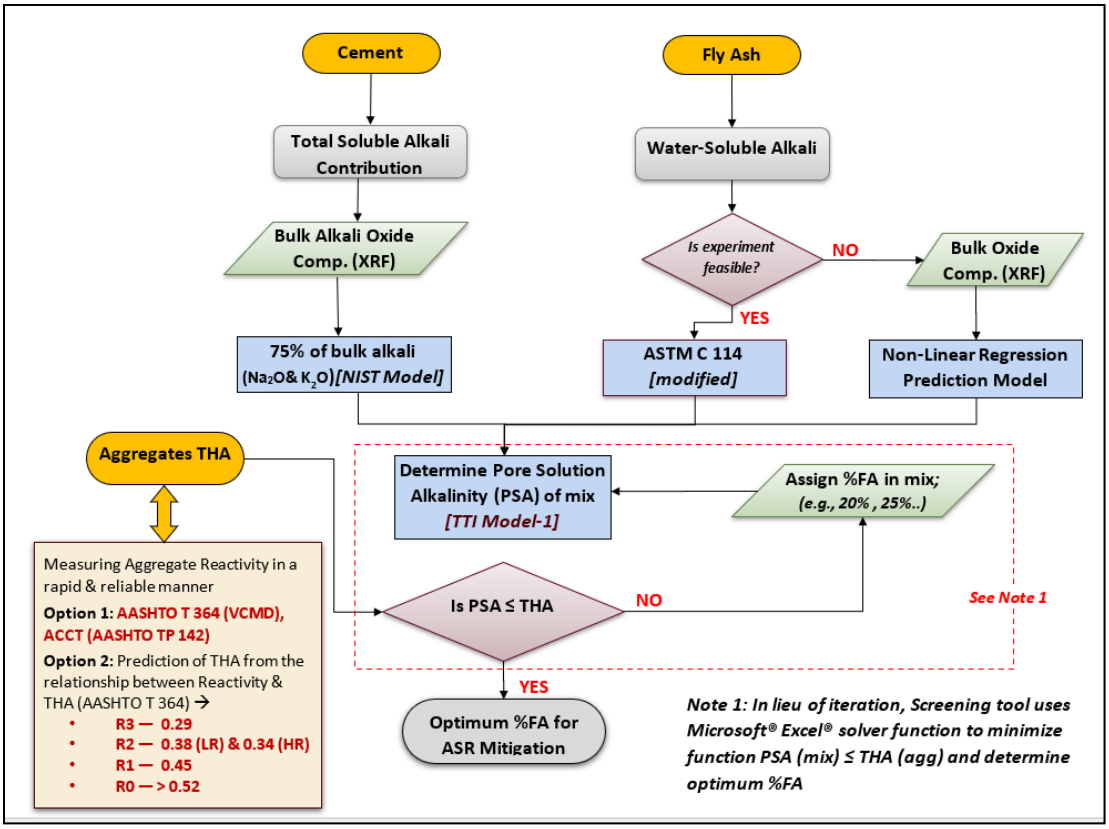

Figure 5-2: Flowchart of CST Methodology

(Note: Aggregate reactivity notation: R3—very highly reactive, R2—highly reactive, R1—moderately reactive, R0—nonreactive, and LR and HR—lower and higher range, respectively)

TTI has developed a performance-based approach using a CST–ACCT combination with the judicious use of ASTM C1567 (presented below), which has been successfully implemented for TxDOT.

1. Use the CST to estimate SCM dosages for the selected SCMs as a function of aggregate reactivity (R1–R3) satisfying concrete PSA ≤ aggregate THA criterion.
2. Conduct ASTM C 1567 (AMBT) to determine optimum dosages for the selected SCMs.
3. Perform comparative assessment between the dosages estimated by the CST and AMBT to decide whether validation using a more reliable concrete testing [e.g., AASHTO TP 142 (ACCT): 75–90 days or ASTM C 1293 (CPT): 2 years] is required or not:
    a. ACCT validation is mandatory if the difference in dosage between CST and AMBT is > 5 percent (~ 8–10 percent).
    b. ACCT validation can be considered optional if the difference is < 5 percent.
    c. ACCT validation testing is also mandatory if CST predicts unrealistically high dosages.

The guidelines (listed below) provided in the recently published NCHRP 10-103 report can be incorporated into this study's performance-based approach (depending on TxDOT needs) to ensure an additional level of control for the judicious use of C1567 for SCM evaluation:

- If aggregate reactivity is known with high reliability (i.e., the same reactivity prediction by multiple tests, such as ASTM C1260, AASHTO T 380 and ACCT methods) ASTM C1567 can be used to determine SCM dosage based on 0.10 percent at the 28-days' criteria.
- The 2-year CPT using an expansion limit of 0.04 percent is not recommended at this time to evaluate preventive measures to mitigate ASR. It was found to underestimate the amount of SCMs needed to mitigate ASR expansion in high alkali loading exposure blocks.

5.1.3 Shrinkage

The TxDOT Tool incorporates a modified RILEM B4 model (RILEM TC 242) to estimate AS (0–28 days), DS (7–180 days) strains, and creep, thereby predicting the DS-based CP of HPC mixtures. The tool predictions for HPC mixtures' CP were validated following the restrained single-ring test (ASTM C 1581) and field studies.

5.1.4 Curing Regimen Selection for Concrete Resistivity Tests

Current specifications for concrete resistivity testing, such as ASTM C 1876 and AASHTO TP 119, advocate for a SPS curing method to enhance measurement accuracy by reducing the impact of alkali leaching and negating the need to determine mixtures' PSC for FF determination. However, the effectiveness of this curing regimen relies on the assumption that a single SPS with a fixed conductivity value of 78.74 mS/cm adequately represents PSCs of varying concrete mixtures with different types of SCMs. However, a recent study by Saraswatula et al. (*31*) noted that this incorrect assumption for certain concrete mixtures containing Class C FA led to a 20–22 percent error in their FF determination because their average PSC was 20–40 percent higher than SPS. Furthermore, a recent FDOT study (32) developed a mix-specific simulated curing regimen prepared based on extracting PS from 38 concrete mixture types. Although the study reduced alkali leaching and enhancing accuracy, the researchers acknowledged the method's complexity, and labor demands make it impractical for field use. To improve FF determination, researchers at TTI devised a novel MPS curing approach, wherein different mixtures were grouped based on the influence of SCMs (type/replacement levels) on their long-term PSC; the mixtures were thereby cured in a simulated solution that matches the average PSC of each group. The MPS approach demonstrated lower resistivity measurement variability, improved FF determination, and FF-based transport property prediction reliability and presents a simplified approach for implementation by industry practitioners (*31*).

5.1.5 Resistivity to FF

TxDOT Tool uses concrete surface/BR measurements to determine the AFF and SFF of HPC mixtures. The Tool facilitates a direct resistivity to FF determination covering three different curing regimens: sealed (AASHTO TP 119), simulated PS (AASHTO TP 119), and the recently developed MPS curing (*31*). Through inbuilt correction factors for specimen geometry, test

configuration, temperature, and saturation were developed through an extensive laboratory investigation. In addition, the integrated TTI Model-2 PSC predictions are used to assist the selection of appropriate curing regimen resistivity tests (SPS vs. MPS) and design an optimal MPS curing solution for accurate FF determination and reliable FF-transport property predictions for HPC mixtures (*31*).

5.1.6 Transport Property Predictions

The TxDOT Tool predicts HPC mixtures' transport properties, such as apparent diffusion and sorptivity coefficients, based on AFF or FF-based transport properties relationships developed based on extensive laboratory investigation, thereby eliminating the need to perform laborious long-term C 1556 and C1585 performance tests.

- ***Diffusion Coefficients:*** The TxDOT Tool uses BR/SR measurements to calculate FF/AFF and thereby predict the apparent diffusion coefficients of HPC mixtures. Furthermore, the Tool incorporates a novel chloride binding model proposed by Azeez et al. (*33*) to determine the effective diffusion coefficients for HPC mixtures, which is a better descriptor of free chloride ion transport in concrete mixtures and also responsible for rebar corrosion initiation in RC structures.
- ***Sorptivity Coefficient:*** The TxDOT Tool uses bulk/SR measurements to determine AFF and thereby predict sorptivity coefficients of HPC mixtures.

5.1.7 Service Life (SL) Performance Evaluation

The TxDOT Tool facilitates rapid service life evaluation and performance assessment of HPC mixtures under field conditions to ambient chloride exposure (*time to rebar corrosion initiation* and *probability of failure)* and F/T exposure cycles (TTRCS) by linking their deterioration mechanisms to transport properties based on established and scientific approaches.

- ***Chloride Durability*—**TxDOT Tool AFF-based effective diffusion coefficient predictions are combined with user inputs for ambient surface and threshold chloride concentration, construction inputs (rebar type, cover, and use of corrosion inhibitor), and information pertinent to ambient environmental conditions (temperature and humidity) to estimate the anticipated time to rebar corrosion initiation and probability of failure [Strategic Highway Research Program (SHRP2)-AASHTO probabilistic deterioration modeling].
- **F/T Durability—**TxDOT Tool AFF-based sorptivity coefficient predictions combined with user inputs for the critical DOS to evaluate F/T service life based on the estimation of TTRCS.

5.2 Guidelines for Comprehensive Performance-Based Evaluation of HPC Mixtures

TxDOT Tool can be used at two stages of the project cycle—during the mix design stage and during the trial batch stage, as shown in Figure 5-3. The TxDOT tool currently can perform mixture classification and performance evaluation based on resistivity measurements of HPC

mixtures/specimens subjected to standard normal temperature conditioning only. Efforts are underway to expand its capabilities to include mix classification and performance assessment after 28-day accelerated conditioning, as per AASHTO TP 119. Additionally, researchers are developing an advanced spreadsheet to simplify inputting raw resistivity data (both BR and SR) from two major manufacturers. This update is intended to enhance the tool's accuracy and versatility in material property assessment.

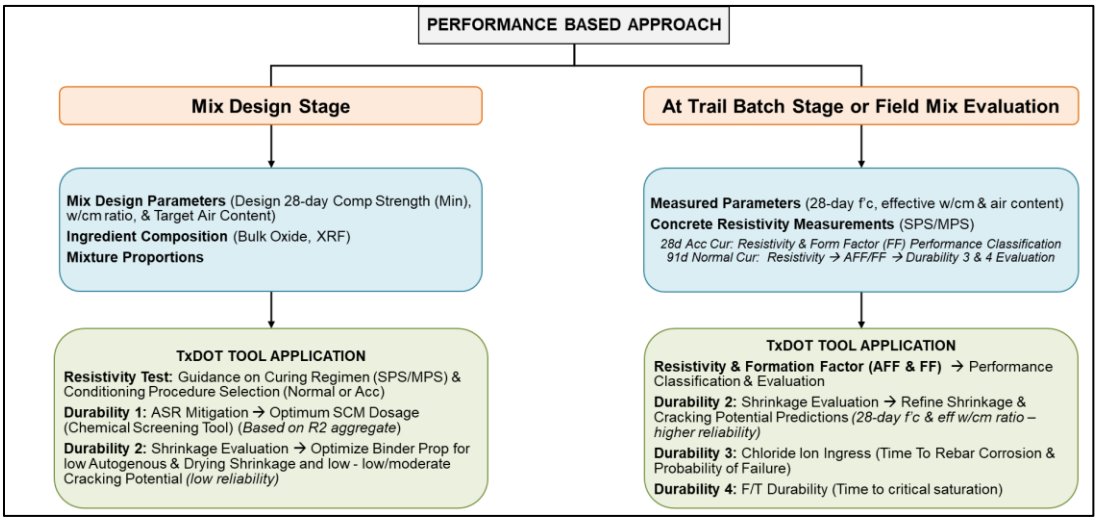

Figure 5-3: Performance-Based Approach for TxDOT Tool Usage

The following steps are recommended as guidelines for performing comprehensive durability-based performance evaluation of HPC mixtures.

1. Review the durability-related exposure categories—D, S, and F as outlined in Table 5-1 and assign class designations (XD1-XD3, XS1-XS3, and/or XF1-XF3) based on anticipated environmental (exposure) conditions for them and their relative intensity.
2. Use Table 5-2 to review the anticipated durability performance of different HPC mixtures based on comprehensive laboratory evaluation and follow Table 5-3 recommendations for preliminary selection of HPC mixtures for construction
3. Use the TxDOT Tool to determine the optimum FA dosage (the optimum SCM replacement level required for ASR mitigation). Inputs required: FA (or natural pozzolans) composition and aggregate THA values. Refer to Table 5-4 for selecting an appropriate THA aggregate based on its reactivity parameters. For comprehensive guidelines and recommendations on evaluating ASR performance, see *Guidelines for ASR Evaluation of HPC Mixtures.*
4. Use TxDOT Tool's integrated RILEM B4 model (RILEM TC-242-MDC [2015]) to estimate the AS potential, DS potential, and DS-based CP of HPC mixtures for different SCM combinations (binary and ternary) and replacement levels during the mix design development.
    a. Reproduce the selective HPC mixtures (finalized from above) and measure AS from 0–28 days (sealed concrete prisms, modified ASTM C 1698) and DS from 7–28 days

(ASTM C 157) and determine 28-day DS-based CP of the mix. Use guidelines based on Table 5-5 and Table 5-6 for shrinkage evaluation of HPC mixtures.

5. Use the TxDOT Tool to enter the material composition of other ingredients (cement, SF, etc.) and the mix design parameters (binder composition, w/cm ratio, aggregate properties) so that the PS concentration of HPC mixtures can be determined by following TTI Model 2.
6. Use PSC determined from Step 5 (above) and follow the guidelines from Figure 5-4 to select an appropriate curing regimen and conditioning procedures for resistivity tests/evaluation of HPC mixtures.
7. Reproduce the above-selected HPC mixtures in the lab, follow the applicable curing/conditioning regimens based on TxDOT Tool guidelines and measure BR (ASTM C 1876/AASHTO TP 119) and/or SR (AASHTO T 358) at regular intervals for up to 91 days for the normal conditioning regimen (23°C ± 2°C) or 28 days for AASHTO TP 119 accelerated conditioning. The precision statements for the BR and SR test measurements are outlined in Table 5-7. Additionally, it is recommended to prepare three additional test cylinders and follow a 91-day normal curing regimen (23°C ± 2°C) for developing saturation correction factors.
8. Performance Classification for Quality assurance/quality control (QA/QC) procedures
    a. Use the TxDOT Tool to enter 91-day BR or SR values along with a selection of appropriate curing regimens and normal conditioning procedures and determine resistivity (BR/SR), AFF, and SFF-based performance classification of HPC mixtures, also shown in Table 5-8, Table 5-9, and Table 5-10.
9. Durability-Based Performance Evaluation:
    a. Use the TxDOT Tool to determine (1) the anticipated time to rebar corrosion initiation and (2) probability of failure *(SHRP2 model)* based on different chloride exposure parameters, such as (a) the intensity of surface chloride exposure (surface concentration levels), (b) rebar type and protection level estimated for construction, (c) geographic location, and (d) anticipated month of construction.
    b. Use the TxDOT Tool to determine the TTRCS (i.e., anticipated F/T performance) based on inputs for the critical DOS, which can be (a) measured following ASTM C 666, or (b) assumed to be a constant value of 86 percent.
10. Use Table 5-11 for guidance on the final selection of HPC mixtures for construction.

Table 5-1: Chloride Exposure Classes for Concrete with Reinforcement (Fib, 2010)

EXPOSURE CATEGORY	CLASS DESIGNATION	ENVIRONMENTAL CONDITIONS	EXAMPLES
No Risk of Corrosion Attack	X0	Exposure to very dry environment	Components with no risk of corrosion or attack
Exposure Category D Corrosion induced by chlorides other than from seawater (e. g. chlorides from deicing agents)	XD1	Exposure to moderate humid environment and chlorides from sources other than from seawater	Surfaces exposed to airborne chlorides
	XD2	Exposure to wet or rarely dry environment and chlorides from sources other than from seawater	
	XD3	Exposure to cyclic wet and dry environment and chlorides from sources other than from seawater	Components exposed to spray containing chlorides
Exposure Category S Corrosion induced by chlorides from seawater	XS1	Exposure to airborne salt but not in direct contact with seawater	Surfaces near to or on the coast
	XS2	Exposure to permanent saturation in seawater	Components of marine structures permanently submerged in seawater.
	XS3	Exposure to seawater in tidal, splash, and spray zones	Components of marine structures
Exposure Category S Freeze and Thaw Attack	XF1	Exposure to F/T cycles and moderate water saturation without deicing agent,	Vertical surfaces exposed to rain and freezing
	XF2	Exposure to F/T cycles moderate water saturation in combination with deicing agent	Vertical surfaces of road structures exposed to freezing and airborne deicing agents
	XF3	Exposure to F/T cycles and high-water saturation without a deicing agent.	Horizontal surfaces exposed to rain and freezing
	XF4	Exposure to F/T cycles and high-water saturation in combination with deicing agent	Road and bridge decks exposed to deicing agents; surfaces exposed to direct spray containing deicing agents and freezing; splash zone of marine structures exposed to freezing

Table 5-2: Summary of Laboratory Performance Evaluation of HPC Mixtures

# MIX ID	SHRINKAGE (MICROSTRAIN)				FF *(MPS AND NORMAL CURING)*			APPARENT AND EFFECTIVE CL DIFF COEFFICIENT (X 10^{-12} M^2/SEC)		SORPTIVITY S_2 (SECONDARY) (I VS. √T, SEC)		F/T *DF*
	AS		DS	Strain Ratio								
	AS-7d	AS-28d	DS-28d	AS/DS-28d	28d	91d	180d	Da	De	56d	180d	
CEM	89	150	400	38%	282	407	459	9.9	4.3	1.5	1.4	81
6SF	102	165	436	38%	637	824	854	5.4	2.5	1.6	0.9	80
25F	55	50	250	20%	505	900	1174	4.4	1.5	1.2	0.9	85
20F5SF	70	90	280	32%	1304	1728	1849	2.9	1.0	1	0.8	84
35F	50	45	230	20%	556	1442	1692	3.6	1.2	1.2	0.9	89
35C	65	80	300	27%	687	936	1215	4.0	1.8	1	0.9	87
29C6SF	69	122	350	35%	1370	1585	1773	3.2	1.3	0.9	0.6	83
35C10SF	80	154	382	40%	1527	1732	1862	2.7	1.0	0.8	0.6	78

Table 5-3: Recommendations on HPC Mix Design Usage for Different Exposure Conditions

#GRP	CLASS DESIGNATION FROM FIB 2010	RELATIVE INTENSITY OF CHLORIDE EXPOSURE FOR REINFORCEMENT CORROSION		RECOMMENDED CLASS S HPC MIX DESIGN [ITEM 421, TXDOT (2104)]	POTENTIAL CONCERNS WITH MIX DESIGN USAGE
		Approx. Surface chloride concentration	Example Geographic Regions		
1	X0 XD1	None to Low (Cs ~ 0–0.3%)	Austin Laredo	Option 1 [25F] Option XB [35C]	Slower Microstructure Development for Binary FA Mixtures
2	XD2 XF1	Moderate (Cs ~ 0.4–0.5%)	Dallas, Atalanta, El Paso, Houston	Option 1 [25F and 35F] Option XB [35C]	
3	XD3* XS1, XS2 XF2	Moderate–High (Cs ~ 0.5–0.6%)	Galveston Corpus Christi (~0.5 – 1 mile away from the coast) Dallas & Atalanta	Option 1 [Only 35F] Option 3 [20F5SF] Option 5 [29C6SF and 35C10SF]	Slower Microstructure Development for 35% F FA mix High AS for ternary HPC
4	XS3 XF3 and XF4	High (Cs ~ 0.6%–0.8% Cl concentration)	Galveston Corpus Christi Amarillo & Lubbock	Option 3 [20F5SF] and Option 5 [29C6SF and 35C10SF]	High ambient temperatures may increase AS and potential for early-age crack formation

*Cyclic wet and dry conditions increase chloride absorption.

Table 5-4: Selection of Aggregate THA Based on Aggregate Reactivity

AGGREGATE REACTIVITY CLASS	AGGREGATE REACTIVITY	AASHTO T364, KJ/MOL	THRESHOLD ALKALI LOADING (TAL), LB/CY	THA, N(A)	ASTM C 1260 EXPANSION (%)	ASTM C 1293 EXPANSION (%)	AASHTO TP 142 (ACCT) EXPANSION (%)
R0	Nonreactive	≥60	4.0 to 4.5	>0.52	≤0.1	≤0.04	≤0.04
R1	Moderately reactive	45–60	3.5 to 4.0	0.45	0.1–0.3	0.04–0.12	0.04–0.12
R2	Highly reactive	30–45	3.0 to 3.5	0.38 (mild range) and 0.34	0.3–0.45	0.12–0.24	0.12–0.24
R3	Very highly reactive	≤30	≤3.0	<0.34	>0.45	>0.24	>0.24

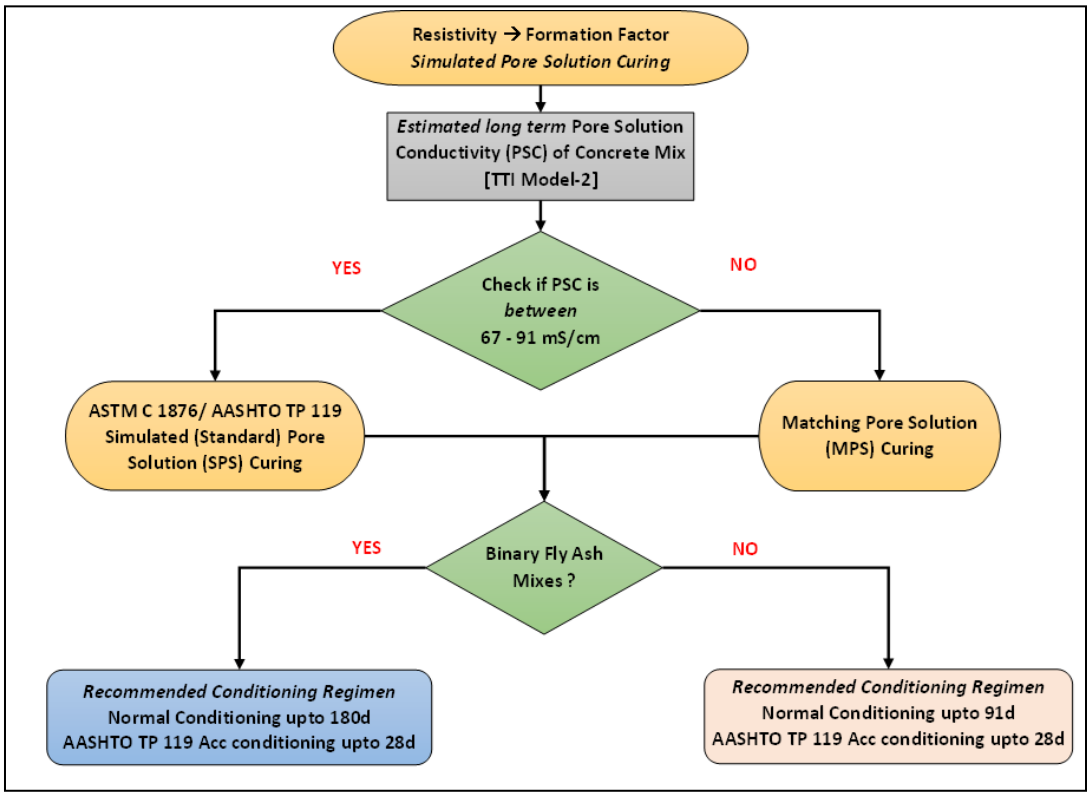

Figure 5-4: Selection of Curing and Accelerated Conditioning for 28-Day Resistivity Measurements

Table 5-5: Performance Evaluation for Shrinkage

Shrinkage	Parameter	*Recommended Threshold Performance Limit*	Notes
AS	28-day AS/DS	*≤ 30%*	• If 28-day AS/DS ≥ 30%, internal curing is recommended
DS	28-day DS	*≤ 400 microstrains*	• If 28-d DS ≥ 400 μS, shrinkage reducing admixtures are recommended
CP	CP based on 28-day DS	*Low (Table 5-6)*	• For moderate and high CP, appropriate mitigation strategy from above is recommended

Table 5-6: CP Classification Based On 28-Day CPI and CP

CPI	CP	*POTENTIAL FOR CRACKING*
CPI ≥ 4.0	**CP > 1.5**	*High*
3.0 ≤ CPI < 4.0	**1 < CP ≤ 1.5**	*Moderate–High*
2.5 ≤ CPI < 3.0		*Moderate–Low*
CPI < 2.5	**CP ≤ 1**	Low

Table 5-7: Precision Statements for BR and SR Tests

TEST METHOD (SPECIFICATION)	SINGLE-OPERATOR PRECISION		MULTI-OPERATOR VARIABILITY	
	Single Test	Two Tests	Single Test	Two Tests
BR (ASTM C 1876)	4.3%	12.0%	13.2%	37.4%
SR (AASHTO T 358)	6.3%	21.0%	12.5%	35.2%

Table 5-8: Performance Limits for (Saturated) BR and SR of HPC Mixtures

PERMEABILITY CLASSIFICATION	RCPT, COLUMBUS	BR LIMITS 4X8 CYLINDER (KOHM.CM)	SR LIMITS 4X8 CYLINDER (KOHM.CM) A= 38 MM; GCF=1.95
High	>4000	<5.2	<10.2
Moderate	4000–2000	5.2–10.4	10.2–20.4
Low	2000–1000	10.4–20.8	20.4–40.6
Very Low	1000–100	20.8–208	40.6–403
Negligible	<100	>208	>403

Table 5-9: Performance Limits for (Apparent) BR and SR

PERMEABILITY CLASSIFICATION	RCPT, COLUMBUS	BR LIMITS 4 × 8 CYLINDER (KOHM.CM)	SR LIMITS 4 × 8 CYLINDER (KOHM.CM) A = 38 MM; GCF = 1.92
High	>4000	<10	<19.2
Moderate	4000–2000	10–20	19.2–38.4
Low	2000–1000	20–40	38.4–76.8
Very Low	1000–100	40–400	76.8–768
Negligible	<100	>400	>68

Table 5-10: Performance Limits for SFF and AFF

PERMEABILITY CLASSIFICATION	RCPT, COLUMBUS	SFF (ρ_{ps}^{o} = 0.127 OHM.M)	AFF (*DOS = 72%, N = 2.0*)
High	>4000	<407	<810
Moderate	4000–2000	407–815	810–1620
Low	2000–1000	815–1630	1620–3250
Very Low	1000–100	1630–16299	3250–32500
Negligible	<100	>16299	>32500

Table 5-11: Final Selection of HPC Mixtures for Construction

PERFORMANCE/ PARAMETERS	INPUT PARAMETERS	CRITERIA FOR SELECTION OR EVALUATION
Preliminary Selection	Table 5-2: Intensity of Chloride Exposure Conditions and Levels Table 5-2: Anticipated Properties of HPC Mixtures	Table 5-3
ASR Mitigation	Use TxDOT Tool, Input Parameters, Table 5-4: Selection of Aggregate THA Based on Aggregate Reactivity	TxDOT Tool Outputs
Shrinkage	Use TxDOT Tool, Input Parameters Material Composition Mix Design Parameters Test Conditions	Table 5-5 Table 5-6
	Selective Experimental Validation Testing AS: Experiment 0–28 days, ASTM C 1698 DS: Experiment 7–28 days, ASTM C 157 CP: Based on ASTM C 157 shrinkage	
Resistivity and FF	Use TxDOT Tool, Input Parameters Concrete Mixture's Resistivity Measurements Check for precision statements in Table 5-7	TxDOT Tool Outputs Very Low Performance Desired Based on Table 5-8 Table 5-9 Table 5-10
Chloride Exposure Evaluation	Use TxDOT Tool, Input Parameters Surface Chloride Exposure Rebar Type and Protection Level Location and Month of Construction	TxDOT Tool Output Time to Rebar Corrosion Initiation Probability of Failure Based on Target Reliability Levels
F/T Service Life	Use TxDOT Tool, Input Parameters Critical DOS	TxDOT Tool Output TTRCS

CHAPTER 6: FIELD EVALUATION PROGRAM

This chapter covers the field evaluation of selective HPC mixtures to advance the project's TRL from 6 to 8. An overview of the evaluation approach and tasks performed are outlined in Table 6-1. To achieve TRL 7, the program selected three field projects in Euless and Dumas, Texas (Table 6-1). During the evaluation of these field projects, cylinder, and beam specimens were cast using job concrete mix in the field (field-cast specimens) at the time of concrete pouring, and additional specimens were cast in the laboratory (lab-cast specimens) using ingredients collected from the ready-mix plants associated with the bridge deck construction. These specimens were then evaluated at the TTI laboratory for resistivity under normal and AC conditions and shrinkage (i.e., AS and DS).

Table 6-1: Research Overview of Different Activities Performed

DISTRICT BRIDGE ID / CSJ	HPC MIX DESIGN	FIELD VISIT DATE	SPANS COVERED DURING EVALUATION	TASKS PERFORMED
EULESS, TX IH 820 SBGP SH 121 and TRE Overpass CSJ 0008-13-221	25% Class F FA (Option 1)	February 21, 2023	Span 9 and 10	• Collection of field-cast specimens. • Ingredients' collection from the ready-mix plant.
		August 8, 2023 *(Follow Up)*	All (Spans 1–10)	• Performing (nondestructive) SR tests. • Visual assessment/ documentation of any potential shrinkage-related cracks on HPC deck concrete (for Spans 1–10) ranging in age from 1 to 6 months.
DUMAS, TX FM 119 Bridge (Sherman County) CSJ: 0702-02-023	29% Class C FA + 6% SF (Option 5)	May 16–17, 2023	All	• Monitoring deck pour. • Casting specimens in the field during the deck pour. • Ingredients' collection from the ready-mix plant.
DUMAS, TX RM 2277 (Hutchinson County) CSJ: 2127-01-010	29% Class C FA + 6% SF (Option 5)	May 16–2023	Spans 3 and 4	• Performing (nondestructive) SR tests. • Visual assessment/documentation of any potential shrinkage-related cracks.

Field- and lab-cast beam specimens were measured for AS from 0 to 28 days and DS from 7 to 180 days. Subsequently, the TxDOT Tool was used to predict 28-day CP, which was validated using the measured values in the lab. Additionally, it sought to confirm the 28-day 400 microstrain limit established for DS tests in ASTM C 157. After demolding, field- and lab-cast cylinder specimens were subjected to the appropriate curing regimen determined using the TxDOT Tool. Specimen conditioning procedures included 180 days of normal conditioning and 28 days of accelerated conditioning, as per AASHTO TP 119. Resistivity measurements were evaluated for performance classification based on the applicable chloride permeability performance limits, and FFs were determined using the TxDOT tool to predict the durability performance in terms of corrosion and F/T potential.

Advancing to TRL 8 involved utilizing the same projects to conduct regular site visits at 28, 56, 90, and 180 days to measure SR on bridge decks and monitor shrinkage-related crack development. The TxDOT Tool was employed to monitor field property development for quality assurance and control and to update and verify durability performance predictions using field SR data. These predictions were compared with those predictions made for achieving TRL 7 using both laboratory and field mix specimens.

6.1 Materials and Mix Design

Table 6-2 summarizes the bulk oxide composition (XRF) of cementitious materials, and Table 6-3 summarizes the properties of coarse and fine aggregates obtained directly from ready-mix plants used for respective cast-in-place bridge deck construction in Dumas and Euless, TX.

Table 6-2: Bulk (XRF) Composition of Cementitious Materials

XRF	**29% CLASS C FA + 6% SF (DUMAS, TEXAS)**			**25% CLASS F FA (EULESS, TEXAS)**	
Phase	Cement (Type IL)	Class C FA	SF	Cement (Type IL)	Class F FA
CaO	61.86	23.63	-	62.3	12.78
SiO2	18.91	35.56	97.9	20.82	53.31
Al2O3	4.40	20.69	0.18	5.35	21.32
Fe2O3	3.15	6.66	0.07	3.11	5.26
SO3	2.81	1.43	0.17	3.22	0.60
MgO	3.01	4.98	0.21	0.96	2.72
Na2O	0.3	1.59	0.12	0.114	0.36
K2O	0.56	0.55	0.59	0.732	0.91
Na2Oeq (Bulk)	0.67	1.96	0.51	0.59	0.96
C3S	66.06	N/A	N/A	27.30	
C2S	4.37			39.09	
C3A	6.33			8.93	
C4AF	9.58			9.48	

Table 6-3: Coarse and Fine Aggregate Properties

PARAM	29C6SF MIX (DUMAS, TX)		25F (EULESS, TX)		
	Coarse Agg Big Creek Sand and Gravel	Fine Agg Big Creek Sand and Gravel	Coarse Agg Hanson	Fine Agg (1) Arcosa	Fine Agg (2) Hanson
Specific Gravity SSD Tex-403-A	2.64	2.6	2.66	2.71	2.64
Dry rodded Unit Wt Tex-404-A (lb/ft3)	98.90	N/A	104.40		
Fineness Modulus Tex-402-A	N/A	2.64		2.67	3.04
Absorption (%) Tex-403-A	0.5	0.5	0.9	1.9	1.2
Unit Weight (SSD)	99.4		105.3		

Mix design information (Table 6-4) was obtained from respective project engineers (mix design sheets, truck tickets, etc.). The mix designs were later reproduced at the TTI laboratory to prepare the corresponding lab-cast specimens.

Table 6-4: Mix Proportions for HPC Mixtures from Dumas and Euless, TX

Mix Designation	29C6SF (Dumas, TX)	25F (Euless, TX)
Total Cementitious Content (lb/cy)	565	494
Cement (lb/cy)	367	371
FA, (lb/cy)	164 (Class C)	124 (Class F)
SF, (lb/cy)	34	-
Coarse Aggregate (lb/cy)	1884	1820
Fine Aggregate (lb/cy) (Natural Sand)	1156	884
Fine Aggregate (lb/cy) (Manufactured)		535
Mixing Water (lb/cy)	240 *(w/cm – 0.42)*	215 *(w/cm ~ 0.43)*
AEA, (fl. oz/ cy)	5.64	9.88
Type A-Water Reducer, (fl. oz/ cy) Chryso/Envriomix 144	45.12	-
Type A-Water Reducer, (fl. oz/ cy) Chryso/Envriomix 300	33.84	-
Type D-Water Reducer, (fl. oz/ cy) GCP/Recover	-	9.88
Type F-Water Reducer, (fl. oz/ cy) Mira 110	-	49.4
Fibers (lb/cy)	0.5	-
Temperature, °F (ASTM C 1064)	70	71
SL, in (ASTM C 143)	4	4.5
Air Content (ASTM C 231)	5.0%	4.5%

6.2 HPC Mix Evaluation—Dumas, Texas (29% Class C FA + 6% SF)

6.2.1 Field Visit

6.2.1.1 FM 119 Bridge Deck: May 16–17, 2023 (Pictures 1, 2, and 3; Figure 6-1)

On May 16, the deck concrete pour started at 6:30 am TxDOT and the consultant lab carried out the SL and air content tests for each truck, with SL values around 5 to 5.5 inches and air content around 4–5 percent. Next, TTI cast a total of eight 4 × 8-inch cylinders, four 4 × 4 × 12-inch shrinkage beams, and one 3 × 6-inch cylinder (MSA ~1 inch, ACCT test). Field activities were documented, and truck tickets were collected from the project manager. A follow-up site visit on May 17 revealed that the deck was covered entirely with wet mats/burlaps as curing continued. Therefore, visual assessment for early-age shrinkage-related crack development and SR measurements could not be performed. Subsequently, raw ingredients (cement, FA, SF, aggregates, and admixtures) were collected from the Vulcan Plant in Dumas, TX, and the field-cast cylinders and beams were transported to the TTI laboratory for evaluation.

Field work at FM 119

Curing ongoing at FM 119

Curing of field-cast samples—FM 119

FM 2277 Bridge deck at the time of visit

SR tests on deck—FM 2277

Isolated cracks on deck—FM 2277

Figure 6-1: Field Work at Dumas, TX

6.2.1.2 Highway RM 2277: May 16, 2023 (Pictures 4, 5 and 6, Figure 6-1)

A field visit was performed to the FM 2277 Bridge Deck 14 days after the deck concrete pour. Curing was still ongoing, with the deck covered by burlaps and wet mats (Picture 4, Figure 6-1). Upon obtaining permission from the TxDOT project manager, we moved mats at two span locations to perform 40–50 SR measurements along the 450-ft bridge length. Preliminary visual inspection at these sections revealed cracks about 3–5 ft from the deck railing. Though they did not appear to be shrinkage-caused, no other crack types were noted. All field observations and

measurements were carefully documented, and the curing mats were returned to their original position upon completion of the work.

6.2.1.2.1 Nondestructive SR Testing on RM 2277 Bridge Deck

SR measurements were conducted on a bridge deck covering Spans 1–5. For each span, readings were taken at three horizontal locations: 1 ft from the left edge, at the center, and 1 ft from the right edge. Within each span, one or multiple readings were captured at intervals of approximately 3–5 ft spacing; these measurements were determined by accessibility (i.e., not covered by curing mats). This systematic approach ensured comprehensive coverage of the entire bridge deck during the field study and the results are summarized below:

- Variation within each span:
  - Span 1: The readings fluctuated, with a highest percent variation of around 34 percent between the lowest (5.5 at the center) and the highest value (9.6 at the center). This span sees the center readings sometimes surpassing both left and right, especially with a 30 percent increase from 7.4 to 9.6.
  - Span 2: The center reading of 10.6 showed a 67 percent increase compared to the left reading of 5.8. Overall, the highest percent variation within this span is about 82 percent (from 5.8 on the right to 10.6 in the center).
  - Span 3: The highest variation in this span is on the right side, with a percent variation of 29 percent between its lowest (7.9) and highest (10.2) readings. Generally, the readings on the right edge are higher than those on the left.
  - Span 4: The range is narrow, with only a 6 percent variation between the highest (10 at center) and the lowest value (9.1 on the right).
  - Span 5: The readings begin with a percent variation of 11 percent from left to right, but this variation narrows down to near uniformity toward the end of the span.
- Overall variability across Span 1-5:
  - The SR measurements show a general increasing trend from left to right with a few exceptions, such as the spike in Span 2. For instance, in Span 3, the rightmost readings are consistently higher, with an average increase of approximately 7 percent over the left readings. However, this trend is not uniform across all spans. Moving from the initial reading of Span 1 (8.1 on the left) to the final reading of Span 5 (10.5 on the left), a gradual 30 percent increase occurs in SR.
  - Overall, the bridge deck SR readings exhibit considerable variability within and between spans. The SR measurements, taken 14 days post-deck pour, ranged from 5.5 to 11.8 kOhm.cm, averaging 8.2 kOhm.cm and displaying a COV of 20.33 percent. In contrast, SR values for specimens tested in the lab (field- and lab-cast) were noted to be between 4–6 kOhm.cm at 14 days. This indicates that field SR measurements might not align with lab-tested specimen results. Furthermore, despite the entire deck (Spans 1–5) being poured in 1 day and undergoing consistent curing processes thereafter, varied factors (structural, material, or environmental) or non-homogenous

conditions across the bridge could influence field SR measurements, which need further examination.

6.2.2 Laboratory Evaluation

6.2.2.1 Resistivity and FF

6.2.2.1.1 Curing Regimen Selection

The ingredient bulk oxide composition and mix proportions were used to estimate the concrete mixture's PSC, which was determined to be 119.18 mS/cm using the TTI Model-2 in the TxDOT Tool. Accordingly, MPS was adopted for specimen curing regimen following TxDOT Tool recommendations, comprising of 15.4 g/L NaOH, 12.8 g/L KOH, and 2 g/L Ca(OH)2. Table 6-5 shows resistivity measurements for field and lab cast specimens subjected to SPS curing and NC conditioning procedures from 7 to 180d. Table 6-6 provides a comparison of resistivity and FF performance classification of field and lab cast specimens subjected to SPS curing and NC conditioning procedures.

Table 6-5: Resistivity Measurements Using MPS Curing and NC

DAYS	FIELD-CAST SPECIMENS					LAB-CAST SPECIMENS				
	BR (kOhm.cm)		SR (kOhm.cm)		SR/BR	BR (kOhm.cm)		SR (kOhm.cm)		SR/BR
	Avg	COV	Avg	COV		Avg	COV	Avg	COV	
7d	2.2	5.5%	1.93	7.3%	0.88	3.8	2.5%	3.5	4.7%	0.92
14d	4.6	5.3%	4.13	6.7%	0.90	6.1	5.4%	5.8	4.4%	0.95
28d	8.9	4.8%	7.98	5.7%	0.90	8.6	5.3%	7.7	4.2%	0.90
56d	14.2	3.5%	13.49	5.2%	0.95	13.9	2.6%	13.1	4.0%	0.94
91d	21.1	3.8%	19.51	5.3%	0.92	22.8	3.5%	21.9	3.8%	0.95
180d	30.4	3.9%	28.7	6.7%	0.94	32.1	3.5%	31.0	3.5%	0.96

Table 6-6: Resistivity and FF (Performance Classification)—MPS Curing, NC, and Age 91 Days

FIELD-CAST			LAB-CAST		
Permeability Classification (Value and Class)			Permeability Classification (Value and Class)		
Resistivity (Measured) kOhm-cm	30.4	Low	Resistivity (Measured) kOhm-cm	32.1	Low
Resistivity (Sat), kOhm-cm	18	Low	Resistivity (Sat), kOhm-cm	19	Low
AFF	3611	Low	AFF	3813	Low
FF	2146	Low	SFF	2266	Low

Table 6-7 shows resistivity measurements for field and lab cast specimens subjected to MPS curing and NC conditioning procedures from 3 and 28d. Table 6-8 provides a comparison of resistivity and FF performance classification of field and lab cast specimens subjected to MPS curing and AC conditioning procedures.

Table 6-7: Resistivity Measurements Using MPS Curing and AASHTO TP 119 AC

DAYS	FIELD-CAST SPECIMENS					LAB-CAST SPECIMENS				
	BR (kOhm.cm)		SR (kOhm.cm)		SR/BR	BR (kOhm.cm)		SR (kOhm.cm)		SR/BR
	Avg	COV	Avg	COV		Avg	COV	Avg	COV	
3d	1.6	3.5%	1.5	7.3%	0.90	2.6	2.5%	2.0	4.7%	0.78
28d	32.8	4.7%	32	5.3%	0.99	35.8	5.3%	34.0	4.2%	0.93

Table 6-8: Resistivity and FF (Performance Classification)—MPS Curing, AC and Age 28 Days

FIELD-CAST			LAB-CAST		
Permeability Classification (Value and Class)			Permeability Classification (Value and Class)		
Resistivity (Measured) kOhm-cm	35.8	Low	Resistivity (Measured), kOhm-cm	32.8	Low
Resistivity (Sat), kOhm-cm	24	Very Low	Resistivity (Sat), kOhm-cm	22	Very Low
AFF	4247	Low	AFF	3891	Low
FF	2876	Very Low	SFF	2635	Very Low

6.2.2.1.2 Observations and Conclusions

Based on the resistivity tests, the field-cast specimens demonstrated performance metrics similar to those of the lab-cast specimens under both NC and AC. These observations suggest that, for QA/QC purposes, contractors may utilize field-cast specimens to measure BR or SR per the TxDOT Tool-recommended curing guidelines and achieve similar performance (values and performance classification) as lab-cast specimens with a reasonable level of confidence. However, further evaluation in several field projects through an implementation project is highly warranted to establish a strong validation, which will lead to the inclusion of the Tool in TxDOT's specification.

However, it is also important to note that a comparison of the resistivity measurements and permeability classification of a mix between NC and AC is not advisable. For example, at 180 days, both field and lab-cast specimens in NC indicated a low permeability classification using the limits based on both measured and saturated resistivity measurements as well as FFs (both AFF and SFF). However, under the AC regimen at 28 days, both lab-cast and field-cast specimens are classified as *low with resistivity* (measured) in an AFF-based classification, but both are classified as *very low with resistivity* (saturated) in an SFF-based classification. So, based on resistivity (measured) and AFF-based classification, the mix is identified as low at both 91 days (NC) and 28 days (AC), which indicates that 28-day resistivity measurements with AC provide the same classification that matches with 91 days NC. However, a significant amount of further evaluation using several field projects through an implementation project is highly warranted to validate if 28 days of resistivity measurements in conjunction with resistivity

(measured) and AFF-based classification systems is acceptable and can reliably be used to do performance-based mix classification.

6.2.2.2 Shrinkage Evaluation

Over the recorded period, field-cast samples generally exhibited lower AS values (e.g., 145 microstrains at 28 days) than lab-cast specimens (e.g., 165 microstrains at 28 days), possibly due to specimens' variability of w/cm ratio in field conditions. Table 6-9 and Table 6-10 summarize the results from AS and DS measurements, respectively, for lab cast specimens for the mixture.

Table 6-9: AS Measurements for Field and Lab Cast Specimens

DAYS	FIELD-CAST SPECIMENS			LAB-CAST SPECIMENS		
	Microstrain (-10-6 strain)	Mass (g)	%mass change	Microstrain (-10-6 strain)	Mass (g)	%mass change
1	0	6746.7	-	0	7021.7	-
3	18	6746.1	0.01%	27	7021.7	0.00%
7	40	6745.1	0.02%	65	7020.8	0.01%
14	68	6741.7	0.07%	88	7019.9	0.03%
21	123	6739.1	0.11%	113	7018.6	0.04%
28	140	6738.1	0.13%	125	7014	0.11%
COV (at 28 d)	6.2%	0.1%		4.4%	4.9%	

Table 6-10: DS Measurements for Field and Lab Cast Specimens

DAYS	FIELD-CAST SPECIMENS			LAB-CAST SPECIMENS		
	Microstrain (*-10^{-6} strain)*	**Mass *(g)***	**%mass change**	**Microstrain (*-10^{-6} strain)***	**Mass *(g)***	**%mass change**
7	0	6627.4	-	0	7041.9	0.00%
14	195	6606.5	0.32%	165	6971.5	1.00%
21	214	6597.8	0.45%	190	6957.4	1.20%
28	250	6591.3	0.54%	235	6943.3	1.40%
56	300	6579.5	0.72%	280	6939.8	1.45%
91	329	6587.7	0.60%	300	6937.7	1.48%
180	*Terminated at 91d*			329	6897.0	1.50%
COV (at 180 d)	*7.3%*	*0.1%*		*15.3%*	*3.9%*	

During the ASTM C 157 DS tests, a malfunction occurred in the 23°C and 50 percent RH curing chamber, leading to uncontrolled temperature and humidity levels in the chamber after that. Consequently, the specimens were exposed to temperatures nearing 40°C and inconsistent RH levels. This anomaly significantly skewed the DS measurements around the 91st day for field-cast specimens and thus were terminated thereafter. Table 6-11 compares the shrinkage parameters prediction from TxDOT Tool with measurements from field and lab cast specimens.

Table 6-11: Shrinkage Strains—TxDOT Tool-Based Predictions versus Measured

VALUES AT 28 DAYS	FIELD-CAST		LAB-CAST		TXDOT TOOL PREDICTIONS	
AS (μS)	140E-6	High	125.6E-6	High	121.7E-6	High
DS (μS)	250E-6		235E-6		227.9E -6	
Total shrinkage (μS)	390E-6	Moderate	385E-6	Moderate	348.6E-6	Moderate
Strain ratio (AS/TS-28 day)	32%		32%		35%	
DS-based CP	1.1	Moderate	1.06	Moderate	0.93	Low

Based on the above 28-day data, the TxDOT Tool's shrinkage predictions are slightly lower than the field-cast specimen measurements, possibly due to the significant variability in mix design parameters like the w/cm ratio, as seen in truck tickets. It is important to note that field samples were cast across different pours, introducing variability. In contrast, the TxDOT Tool operates under the assumption of normalized conditions for these parameters. While the tool's prediction for AS and DS strains displayed 16–22 percent deviation from the field-cast specimens, the tool's prediction for the strain ratio was relatively closer, with only a 7 percent difference. In terms of classification, both the TxDOT Tool and field-cast specimens exhibited consistent categorization, which was especially evident in their close estimates for CPs. This result underscores that despite quantitative deviations in some metrics, the tool predictions provide similar assessments for field and/or lab-cast specimens.

6.3 HPC Mix Evaluation—Euless, Texas (25 percent Class F FA)

6.3.1 Field Visit

6.3.1.1 IH 820 Bridge Deck (Spans 9 and 10): February 21, 2023 (Pictures 1, 2 in Figure 6-2)

The deck concrete for Spans 9 and 10 was poured on February 20, 2023. Due to a scheduling conflict, the project team could not visit the field on the day of the pour; however, the project consultant, LJA Engineering, cast five 4 × 8-inch cylinders for evaluation. The project team visited the project site the next day and observed the ongoing curing process. The deck surface was completely covered with wet mat burlaps, preventing visual inspections and SR measurements. Subsequently, raw ingredients (cement, FA, aggregates, and chemical admixtures) were collected from the ready-mix plant used for deck construction. Field samples (~ 24 hours' age) were transported to the TTI laboratory for evaluation.

6.3.1.1.1 IH 820 Bridge Deck (Spans 1–10): August 8, 2023 (Pictures 3, 4, 5, and 6 in Figure 6-2)

A follow-up field visit was conducted at the IH 820 bridge site (IH 820 SBGP SH 121 and TRE Overpass) in Euless, TX, on August 8, 2023. Work comprised performing SR tests (nondestructive) and visual assessment/documentation of any potential shrinkage-related cracks on the studied HPC deck concrete (for different spans) ranging in age from 1 to 6 months. (Date of concrete pour: Spans 9 and 10 on February 20, 2023; Spans 1 and 2 on May 21, 2023; Spans 3

and 4 on June 30, 2023; and Spans 5, 6, 7, and 8 on July 19, 2023). Cracks were noted on Spans 9 and 10; however, their occurrence was isolated and did not appear to be shrinkage related.

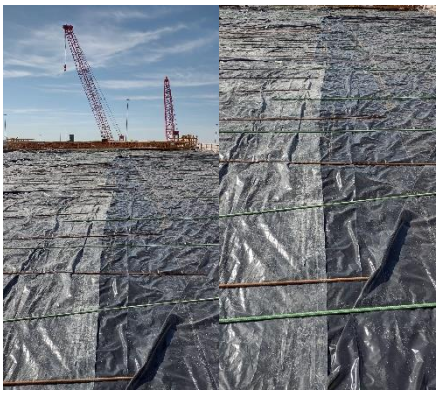

Curing ongoing at field visit, Spans 9 and 10 (February 2023)

SR tests on deck, Span 8 (August 2023)

SR tests on deck, Span 3 (August 2023)

Transverse cracks on deck, Span 5 (August 2023)

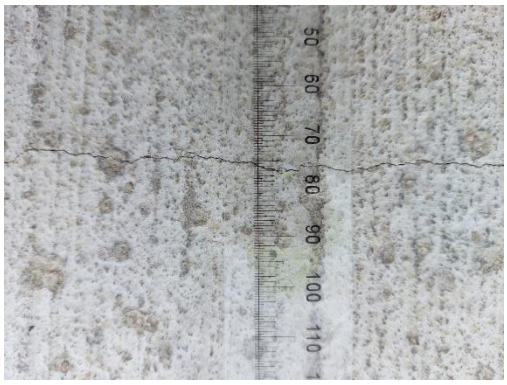

Cracking observed on Span 9 (August 2023)

Cracking observed on Span 10 (August 2023)

Figure 6-2: Field Visit to Euless, TX

6.3.1.2 Field SR Measurements

SR measurements were conducted on the bridge deck covering Spans 1–10. For each span, readings were taken at three horizontal locations: 1 ft from the left edge, at the center, and 1 ft from the right edge. Within each span, multiple readings were captured at intervals of approximately 3–5 ft spacing, as determined by accessibility (i.e., not covered by curing mats).

This systematic approach ensured comprehensive coverage of the entire bridge deck during the field study. Based on a detailed analysis of the data, the main points are summarized below:

Table 6-12: Variation of SR within Spans for Bridge Deck IH-820

SPAN NUMBER	POUR DATE	AGE IN DAYS AT EVALUATION	AVG. SR IN KOHM-CM	SD	COMMENTS/OBSERVATIONS
1	05/21/23	79	207.4	97.3	High variability (i.e., 73% between the maximum and minimum center values)
2			162.1	32.9	Relatively lower variability (26%)
3	06/30/23	39	61.1	21.9	Lower average, 68% variability
4			93.4	20.7	Steady average, 35% variability
5	07/19/23	20	36.3	8.9	Relatively stable, 50% variability
6			38.4	9.5	Minor fluctuations with a 44% difference in the center readings
7			35.1	13.8	67% variation from left to right
8			45.0	19.4	66% variation between the minimum and maximum center readings
9	2/20/23	169	123.3	58.3	High variability (i.e., 88% difference between the leftmost and rightmost readings)
10			109.2	15.2	Uniformity in readings, 22% data variability at the center.

6.3.1.2.1 Age-Related Variation

The spans poured in May and February showcase relatively higher readings compared to those poured in June and July. Higher resistivity measurements indicate denser microstructure of these spans with age. SR readings were also noted to stabilize (i.e., low variability) as the concrete matures, but further research is needed to validate these observations.

6.3.1.2.2 Variation from Left to Right

For most spans, a definite fluctuation is observed when progressing from the left edge to the center and then to the right. The pattern is not universally consistent across all spans, suggesting local factors influencing each span's readings.

6.3.1.2.3 Conclusion

Analysis of SR provides insights into the systematic variations both within individual spans and across the 10 spans. The age of the concrete significantly influences the readings. Overall, the bridge deck SR readings exhibit considerable variability within and between spans. When compared with SR values for lab-cast specimens, SR measurements on the bridge deck show significant deviation at similar ages. Furthermore, the spans that are typically poured at the same time also exhibit considerable SR measurement variability. The high variability could be

attributed to varied factors (structural, material, or environmental) or non-homogenous conditions across the bridge that could influence field SR measurements; these factors need further examination.

6.3.2 Laboratory Evaluation

6.3.2.1 Resistivity and FF

The ingredient bulk oxide composition and mix proportions were used to estimate the concrete mixture's PSC, which was determined to be 77.06 mS/cm using the TTI Model-2 in TxDOT Tool. Accordingly, the ASTM C 1876 recommended SPS was adopted for the specimen curing regimen following TxDOT Tool recommendations, comprising of 7.6 g/L NaOH, 10,6 g/L KOH, and 2 g/L Ca(OH)2. Table 6-13 shows resistivity measurements for field and lab cast specimens subjected to SPS curing and NC conditioning procedures from 7 to 180d. Table 6-14 provides a comparison of resistivity and FF performance classification of field and lab cast specimens subjected to SPS curing and NC conditioning procedures.

Table 6-13: Resistivity Measurements with SPS Curing and NC

DAYS	FIELD-CAST SPECIMENS					LAB-CAST SPECIMENS				
	BR (kOhm-cm)		SR (kOhm-cm)		SR/BR	BR (kOhm-cm)		SR (kOhm-cm)		SR/BR
	Avg	COV	Avg	COV		Avg	COV	Avg	COV	
7d	2.7	5.5%	2.4	7.3%	0.88	3.0	2.5%	2.8	4.7%	0.94
14d	3.5	5.3%	3.1	6.7%	0.90	3.9	5.4%	3.5	4.4%	0.91
28d	4.8	4.8%	4.5	5.7%	0.90	5.3	5.3%	5.2	4.2%	0.98
56d	8.3	3.5%	7.9	5.2%	0.95	9.1	2.6%	8.9	4.0%	0.97
91d	9.0	3.8%	8.5	5.3%	0.92	9.9	3.5%	9.6	3.8%	0.97
180d	16.7	3.3%	16.0	3.4%	0.98	18.5	3.3%	17.8	4.3%	0.96

Table 6-14: Resistivity and FF (Performance Classification)—SPS Curing, NC, and Age 180 Days

FIELD-CAST			LAB-CAST		
Permeability Classification (Value and Class)			Permeability Classification (Value and Class)		
Resistivity (Measured) kOhm-cm	16.7	Moderate	Resistivity (Measured) kOhm-cm	18.5	Moderate
Resistivity (Sat), kOhm-cm	14	Low	Resistivity (Sat), kOhm-cm	15	Low
AFF	1315	Moderate	AFF	1457	Moderate
SFF	1090	Low	SFF	1208	Low

Table 6-15 shows resistivity measurements for field and lab cast specimens subjected to SPS curing and AC conditioning procedures from 3 and 28 days. Table 6-16 provides a comparison of resistivity, AFF and FF performance classification of these specimens subjected to SPS curing and AC conditioning procedure.

Table 6-15: Resistivity Measurements Using SPS Curing and AASHTO TP 119 AC

DAYS	FIELD-CAST					LAB-CAST				
	BR (kOhm-cm)		SR (kOhm-cm)		SR/BR	BR (kOhm-cm)		SR (kOhm-cm)		SR/BR
	Avg	COV	Avg	COV		Avg	COV	Avg	COV	
3d	1.4	3.5%	1.5	7.3%	0.90	2.6	2.5%	2.5	4.7%	0.78
28d	18.8	4.7%	17	5.3%	0.90	19.2	5.3%	18.7	4.2%	0.97

Table 6-16: Resistivity and FF (Performance Classification)—SPS Curing, AC, and Age 28 Days

FIELD-CAST			LAB-CAST		
Permeability Classification (Value and Class)			Permeability Classification (Value and Class)		
Resistivity (Measured) kOhm-cm	18.8	Moderate	Resistivity (Measured) kOhm-cm	19.2	Moderate
Resistivity (Sat), kOhm-cm	16	Low	Resistivity (Sat), kOhm-cm	16	Low
AFF	1480	Moderate	AFF	1512	Moderate
SFF	1243	Low	SFF	1270	Low

Based on the resistivity tests, the field-cast specimens demonstrated performance metrics similar to those of the lab-cast specimens under normal conditioning and AC. These observations suggest that, for QA/QC purposes, contractors may use field-cast specimens to measure BR or SR per the TxDOT Tool-recommended curing guidelines and achieve similar performance (values and performance classification) as lab-cast specimens with a reasonable level of confidence. However, further evaluation in several field projects through an implementation project is highly warranted to establish a strong validation, which will lead to the inclusion of the Tool in TxDOT's specification. It is also important to note that while resistivity measurements from NC and AC cannot be directly compared, both resistivity and FF for NC at 180 days and AC at 28 days demonstrate similar performance classifications. Because 28-day resistivity measurements with AC have provided the same classification that matches with 180 days NC, performance classification based on 28-day resistivity measurements with AC was found to be acceptable (time-saving) in this case. However, a significant amount of further evaluation using several field projects through an implementation project is highly warranted to validate if performance-based mix classification based on 28 days of resistivity measurements is reliably acceptable.

6.3.2.2 Shrinkage Evaluation

Table 6-17 and Table 6-18 summarize the results from AS and DS measurements, respectively, for lab cast specimens for the mixture. Table 6-19 presents a comparison of TxDOT Tool predictions for shrinkage parameters of the mixture with laboratory measured values.

Table 6-17: AS Measurements for Lab Cast Specimens

Days	LAB-CAST		
	Microstrain (*-10^{-6} strain)*	**Mass *(g)***	**%mass change**
1	0	6813.1	-
3	9	6813	0.00%
7	4	6812.7	0.01%
14	18	6812.2	0.01%
21	33	6811.5	0.02%
28	41	6808.6	0.07%
COV (at 28 d)	*3.4%*	*3.2%*	

Table 6-18: DS Measurements for Lab Cast Specimens

Days	LAB-CAST		
	Microstrain (*-10^{-6} strain)*	**Mass *(g)***	**%mass change**
7	0	6888.3	0.00%
14	90	6841.5	0.68%
21	145	6819.4	1.00%
28	175	6801.5	1.26%
56	260	6796.7	1.33%
91	330	6791.9	1.40%
180	350	6785.0	1.50%
COV (at 56 d)	*17.3%*	*5.9%*	

Table 6-19: Shrinkage Strains—TxDOT Tool-Based Predictions versus Measured

VALUES AT 28 DAYS	**LAB-CAST**		**TXDOT TOOL PREDICTIONS**	
AS (μS)	41E-6	*low*	32.4E-6	*Low*
DS (μS)	175.6E-6		209E -6	
Total Shrinkage (μS)	216.6E-6	*Low*	241.6E-6	*Low*
Strain Ratio (AS/TS-28 day)	18%		13%	
CP	0.64	*Low*	0.68	*Low*

Based on the above 28-day data, the TxDOT Tool's AS predictions were ~ 20 percent lower than the lab-cast specimen measurements, possibly due to the marginal differences in mix design parameters used for TxDOT Tool analysis and variability in mix proportions for lab-cast specimens. In terms of classification, both the TxDOT Tool and lab-cast mixtures exhibited consistent categorization, which was especially evident in their close estimates for CPs. This result underscores that despite quantitative deviations in some metrics, the tool predictions provide similar qualitative assessments as lab-cast specimens.

CHAPTER 7: INTERLAB REPEATABILITY AND COMPARISON OF THE RESISTIVITY METHOD

This chapter presents an in-depth analysis of the repeatability and variability of electrical resistivity test methods based on resistivity measurements using a single concrete mixture in two different laboratories in order to ascertain within-laboratory variability and interlaboratory repeatability.

7.1 Synopsis

Researchers at TTI prepared 24 4 × 8-inch concrete cylinders and divided them into four sets with 6 specimens for each set. Concrete specimens containing 25 percent Class F FA (i.e., replication of the Class S HPC mix design (Option 1) used in the IH 820 project in Euless, TX—details are in Chapter 6) were prepared. Concrete mix's PSC, estimated using ingredients composition and mix design parameters following TTI Model-2 (TxDOT Tool), was determined to be 75.43 mS/cm. Accordingly, ASTM C 1876 SPS was selected for specimen curing as mixture's PSC was within ± 1-5% of SPS conductivity (=78.74 mS/cm). Concrete specimens from each set were subjected to two different conditioning procedures, with half undergoing normal conditioning at 23°C for up to 180 days and the other half subjected to accelerated conditioning (i.e., 3 days at 23°C and 25 days at 50°C) as per AASHTO TP 119 guidelines. BR and SR tests were conducted at 3, 7, 14, 28, and 56 days with normal conditioning and at 3 and 28 days with accelerated conditioning by two different laboratories (TTI and TxDOT), with Sets 1–3 evaluated by three different operators at the TxDOT laboratory and Set 4 assessed at the TTI laboratory by a single operator. The resistivity measurement was to obtain 91 and 180 days of data with normal conditioning. These data were used to evaluate within-laboratory variability and multi-laboratory variability of the resistivity test method.

7.2 Background

Service life evaluation of concrete structures necessitates the determination of concrete transport properties that control ion and fluid ingress into structures. However, the current performance tests to measure concrete transport properties, such as ASTM C 1556 (chloride diffusion), ASTM C 1585 (water absorption), etc., are labor-intensive, time consuming, and demonstrate high variability/poor reproducibility of the measured properties and thus are not suited for rapid performance assessment and quality control purposes (*56*, *68*). Therefore, instead of direct measurements by the above methods, resistivity measurement is recommended as an indirect way to assess concrete transport properties (*83*). Recently, concrete resistivity tests such as bulk/uniaxial resistivity (ASTM C 1876/AASHTO TP 119) and SR (AASHTO T 358) are gaining interest as a rapid approach to characterize the pore network of concrete mixtures (*49*).

Because concrete resistivity tests are easy to perform and have better precision than ASTM C1202, state DOTs and highway agencies have more recently been moving toward using/implementing the resistivity tests in practice for mixture qualification, QA/QC, and

durability evaluation of concrete pavements mixtures (AASHTO PP84) (*83*). However, the current multitude of ASTM/AASHTO test standards for concrete resistivity tests, encompassing two distinct test approaches and five different specimen curing regimens, creates a complex range of options for selecting the most appropriate approach for practice.

7.3 Influence of Test/Measurement Procedure

Although resistivity is a material property, commercially available devices measure concrete resistance, which is corrected for specimen geometry to obtain resistivity, as shown in Equation 7-1:

Equation 7-1 $$\boldsymbol{\rho = k.R_{cylinder}}$$

where R is the resistance of concrete, and k is a geometrical factor that depends on the size and shape of the specimen and the distance between the probes on the testing device.

7.3.1 SR Tests

In both TTI and TxDOT labs, SR measurements for concrete specimens are performed using a commercially available 4-point Wenner probe SR meter (example: Resipod manufactured by Proceeq) shown in Figure 7-1.

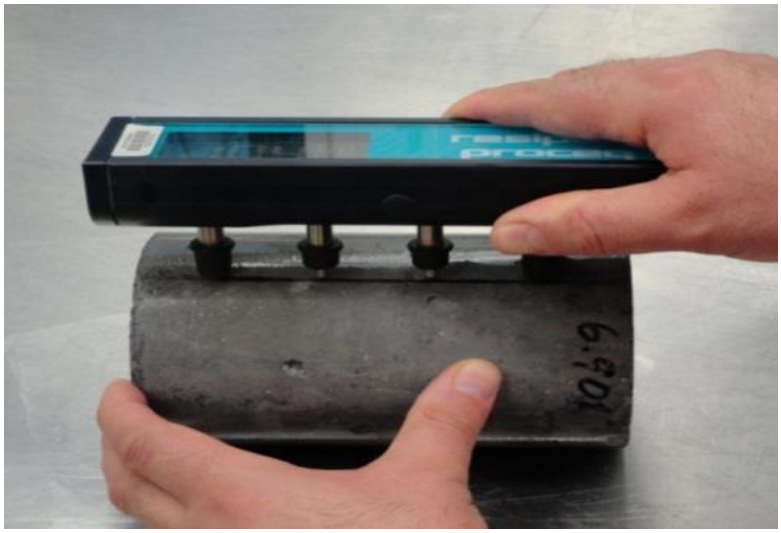

Figure 7-1: SR Tests Using Resipod by Proceeq

The SR test device utilizes four equally spaced surface contacts to measure the resultant potential difference (i.e., voltage [V]) between the two inner electrodes when a small alternating current (I) is passed through the concrete between the outer pair of contact probes, as shown in Equation 7-2:

Equation 7-2 $$\boldsymbol{\rho = \frac{V}{I} * k}$$

Where the geometric factor (k) is given by Equation 7-3:

Equation 7-3 $$k = \frac{k_1}{k_2}$$

Where the factor k_1, defined as the probe spacing correction, represents the assumption of an infinite half-space, meaning the spacing of the electrodes (a) is much smaller than the depth (d) of the material being measured (e.g., slab evaluation in the field), as shown in Equation 7-4:

Equation 7-4 $$k_1 = 2 * \pi * a$$

However, the assumption of infinite-half space is not applicable for SR testing in the laboratory when using cylindrical concrete specimens because probe spacing remains higher than the evaluation depth (smaller specimen size) to prevent interferences with coarse aggregates (*52*). Accordingly, a second correction factor—geometric factor k_2—is employed to account for constricted current flow through the lab cylindrical concrete specimen, and Equation 7-5 shows a second-order approximation based on a previous research study (*47*) .

Equation 7-5 $$k_2 = 1.10 - \left(\frac{0.73}{\frac{d}{a}}\right) + \left(\frac{7.34}{\left(\frac{d}{a}\right)^2}\right)$$

Where a represents the spacing of the electrodes, and d is the diameter of the test cylinder. It should be noted that this correction is only valid when $d/a \leq 6.0$ and $L/a \geq 6.0$, where L is the length of the cylinder. For testing on a standard 100 mm x 200 mm test cylinder, the k_2 value ranges from 1.8 to 1.9. The three primary factors that affect SR measurements are (1) concrete homogeneity, (2) surface contact, and (3) size and geometry of the specimen. Accordingly, the apparent SR is determined to account for geometrical correction, as seen in Equation 7-6:

Equation 7-6 $$\rho_{app} = \frac{\rho_{measured}}{K}$$

Where K is the GCF. Table 7-1 shows geometric factors obtained from different studies.

Table 7-1: Geometric Corrections Determined from the Literature

RESEARCH	K VALUE FOR 4 × 8 CYLINDER WITH SPACING A = 1.5 INCHES (38 MM)
Morris et al (*52*)	1.96
Spragg et al (*47*)	1.86
Kessler et al (*84*)	1.8
Ghosh et al. (*67*)	1.95
Saraswatula et al.,(*85*) [HPC Project]	1.92

7.3.2 BR Tests

Uniaxial resistivity, or a BR test, measures electrical resistivity from a uniform current distribution through the bulk of the concrete specimen using an alternate current at 1kHz AC frequency. Commercial BR test devices measure resistance to current flow through concrete bulk material as a function of the ratio of applied voltage (V) to resulting current (I), multiplied by

geometric/cell constant *k*, where electric charge is carried through ions dissolved in the PS, as shown in Equation 7-7:

Equation 7-7 $$\rho = \frac{V}{I} * k$$

One of the critical requirements of this test is to establish a good electrical connection between the test specimen and the electrodes, which is typically accomplished through the use of a conductive medium (e.g., a sponge immersed in artificial PS or LW or conducting fluid gel). Although the use of the above conductive medium greatly minimizes resistance to the current flow, some resistance will still be there; Equation 7-8 has been proposed to account for this kind of influence (*47*):

Equation 7-8 $$R_{cylinder} = R_{mea} - R_{top\ sponge} - R_{bottom\ sponge}$$

7.3.2.1 BR Measurements using RCON

In the TTI laboratory, BR measurements were performed using a commercially available resistivity meter RCON, manufactured by Giatech Scientific, at a frequency of ~1 kHz at 23 ± 2°C as shown in Figure 7-2.

Figure 7-2: BR Measurement Using RCON by Giatech Scientific

RCON devices measure concrete resistance, which is corrected for specimen geometry to obtain resistivity, as shown in Equation 7-9:

Equation 7-9 $$\rho = k.R_{cylinder}$$

Where R is the resistance of concrete, and k (Equation 7-10) is a geometrical factor that depends on the size and shape of the tested specimen and the distance between the probes on the testing device. A is the cross-sectional area of the specimen, and L is the length of the specimen.

Equation 7-10 $$\boldsymbol{k = \frac{A}{l}}$$

An RCON device uses conducting fluid gel to prewet the sponges prior to resistivity measurements and, accordingly, is noted to have a negligible impact on overall concrete resistivity measurements.

7.3.2.2 BR Measurements using SR Resipod Device

In the TxDOT lab, BR measurements were performed using the same Resipod device that was used to measure SR as shown in Figure 7-3.

Figure 7-3: BR Measurement Using Resipod by Proceeq

However, unlike RCON, Resipod devices measure concrete resistance (R), which is corrected for probe spacing correction (K_c) and specimen geometry (k_g) to obtain resistivity, as shown in Equation 7-11:

Equation 7-11 $$\boldsymbol{\rho = \frac{k_g}{k_c} * R_{cylinder}}$$

Where k_c = Probe spacing correction = 2πa and $k_g = cell\ const\ corxn\ (geometry) = \pi \frac{d^2}{4} \frac{1}{L}$.

One of the critical assumptions of this measurement approach is that there is a good electrical connection between the test specimen and the electrodes, typically accomplished through a conductive medium. Accordingly, the influence of contact resistance is determined with Equation 7-12 (*47*).

Equation 7-12 $$\boldsymbol{R_{cylinder} = R_{mea} - R_{top\ sponge} - R_{bottom\ sponge}}$$

7.4 Materials and Mix Designs

Concrete ingredients obtained directly from the IH 820 Bridge Project (Euless, TX) and used for the preparation of concrete specimens, as with the 25F mix design. Cementitious materials' composition, aggregates properties and mix design/proportions are presented/discussed previously in Chapter 5 and thus are not presented here.

7.5 Evaluation Methodology

Resistivity tests were performed in TxDOT and TTI laboratories. Operators 1 to 3 evaluated Sets 1-3 at TxDOT, while Operator 4 assessed Set 4 at TTI as shown in Figure 7-4.

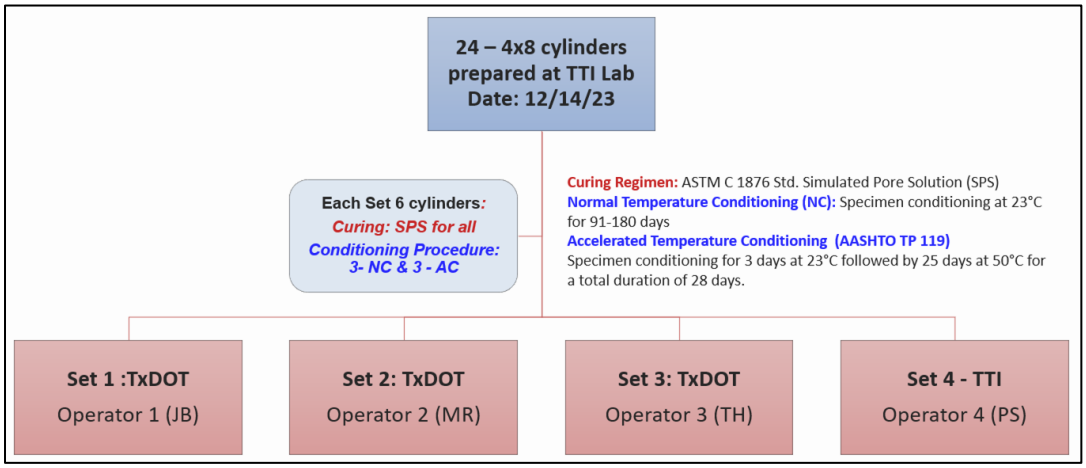

Figure 7-4: Approach for Interlab Resistivity Evaluation

7.5.1 Curing Regimen Selection

The bulk oxide composition and mix proportions were used to estimate the concrete mixture's PSC, which was determined to be 77.06 mS/cm using the TTI Model-2 in the TxDOT Tool. Since the difference between the TxDOT Tool-based PSC prediction (i.e., 77.06 mS/cm) and ASTM C 1876 recommended PSC (i.e., 78.74 mS/cm) for simulated PS is negligible, the SPS curing was selected. Following ASTM C 1876, SPS was prepared by dissolving 102.6 g of dry NaOH, 143.9 g of dry KOH, and 27 g of dry Ca(OH)2, in a 3.6 gal (13.5 L) of water. Test samples were cured in sealed SPS buckets with a solution-to-sample ratio of 4:1(by volume) and placed in a controlled environmental chamber (23 ± 2 °C, RH 98 ± 2%) for the duration of testing.

7.5.2 Specimen Conditioning

Concrete specimens from each set were subjected to two different conditioning procedures, with half undergoing normal conditioning at 23°C for up to 180 days and the other half subjected to accelerated conditioning as per AASHTO TP 119 guidelines.

7.5.3 Experimental Work

Replicate 4 × 8-inch concrete cylinders (4±0.08 inch diameter and 8±0.16 inch height) were cast, demolded at the age of 24±2 hours, and subjected to curing regimens, as described below. Concrete specimens at each test age were removed from the sealed buckets, gently washed with tap water to remove any adhered soak solution from the surface, and blotted off to SSD condition with a clean damp cloth before resistivity tests. All resistivity test measurements were conducted at room temperature (23±2°C) in compliance with standard specifications.

BR measurements were performed according to ASTM C 1876 /AASHTO TP 119 specifications. BR measurements at TTI were performed using a commercially available resistivity meter, RCON, manufactured by Giatech Scientific, at an operating frequency of ~1kHz at 23 ± 2°C. Before the BR test, the device's end sponges were saturated with conductive gel to ensure sound electrical contact with the cylinder ends. Based on the test cylinders' dimensions (4 × 8 inches), a GCF of 1.57 inches (3.98 cm) was used for BR determination (*47*). However, BR measurements at TxDOT were performed using Resipod, a commercially available 4-point Wenner probe meter manufactured by Proceq.

SR measurements at both labs followed AASHTO T 358 specifications using a commercially available 4-point Wenner probe meter manufactured by Proceq. Based on the test cylinders' dimensions (4 × 8 inches) and 1.5 inches (38 mm) probe spacing for the test device, the GCF of 1.92 was used in the SR determination (*49*).

BR and SR tests were run at testing ages of 3, 7, 14, 28, and 56 days under normal conditioning (testing at 91 and 180 days yet to be performed) and for 3 and 28 days under accelerated conditioning.

7.6 Results and Discussion

7.6.1 Part 1: Evaluation of Within the Lab Repeatability of Resistivity Measurements

Table 7-2 presents the average resistivity and COV for concrete specimens tested under normal conditioning by four different operators from the two institutions (i.e., TxDOT and TTI).

Table 7-2: Average and COV in the Resistivity Measurements (Normal Conditioning, kOhm-cm)

TEST		TXDOT - OPERATOR 1		TXDOT - OPERATOR 2		TXDOT - OPERATOR 3		TTI – OPERATOR 1	
Age	Param	SR	BR	SR	BR	SR	BR	SR	BR
3	avg	2.3	1.5	2.3	1.9	2.3	1.2	2.3	2.5
	cov	3.9%	2.2%	4.6%	0.9%	3.7%	7.9%	4.5%	5.4%
7	avg	2.5	2.1	2.6	2.2	2.5	2.1	2.4	2.6
	cov	3.9%	18.7%	4.7%	6.4%	2.9%	9.3%	4.0%	5.1%
14	avg	3.5	3.1	3.4	3.1	3.4	3.2	3.1	3.5
	cov	4.8%	10.2%	4.3%	3.9%	4.1%	3.1%	4.1%	4.4%
28	avg	5.8	5.6	5.8	5.6	5.7	5.5	5.6	5.3
	cov	3.8%	2.0%	4.5%	3.6%	4.2%	1.3%	3.1%	3.1%
56	avg	10.1	10.3	10.3	10.3	10.4	9.6	9.4	9.5
	cov	5.4%	1.9%	5.1%	1.3%	4.2%	2.5%	5.7%	1.7%

For both SR and BR, the averages tend to increase with the age of the concrete, indicating that resistivity improves (increases) over time. At early ages (3 days), the averages for SR and BR are low, ranging from 2.3 to 2.5 kOhm-cm and 1.2 to 2.5 kOhm-cm, respectively. By 56 days, the averages have generally increased to ≥ 9.4–10.6 kOhm-cm for SR and BR. The COV (measuring the variability relative to the average) shows some differences between operators and test ages. Notable high COV values are seen at 7 days for TxDOT Operator 1 in BR (18.7 percent) and at 14 days for the same operator in BR (10.2 percent). TxDOT Operator 3 also had elevated COV values at early ages (7.9 percent at 3 days and 9.3 percent at 7 days for BR). By 56 days, the COV values are all relatively low, typically below 5.7 percent for both SR and BR tests, suggesting consistency in the measurements at this mature age of the concrete. Under accelerated conditioning, results shown in Table 7-3 exhibit a marked increase in both SR and BR from 3 to 28 days across all operators, suggesting enhanced concrete resistivity over time. Initially, at 3 days, the average resistivity values are low (2.3–2.6 kOhm-cm for SR, 0.9–2.6 kOhm-cm for BR), but by 28 days, these values rise substantially (31.0–34.8 kOhm-cm for SR, 28.9–35.0 kOhm-cm for BR).

Table 7-3: Average and COV in Resistivity Measurements (Accelerated Conditioning, kOhm-cm)

TEST		TXDOT - OPERATOR 1		TXDOT - OPERATOR 2		TXDOT - OPERATOR 3		TTI – OPERATOR 1	
Age	Param	SR	BR	SR	BR	SR	BR	SR	BR
3	avg	2.3	1.4	2.3	1.5	2.4	0.9	2.4	2.6
	cov	6.5%	4.3%	4.2%	3.3%	6.1%	4.3%	7.3%	3.8%
28	avg	31.4	28.9	31.0	29.6	32.5	29.0	34.8	35.0
	cov	6.7%	4.4%	7.5%	4.5%	6.4%	3.7%	3.5%	1.6%

7.6.2 Part 2: Evaluation of Intralab (i.e., Within Lab) Repeatability of Resistivity Measurements

Table 7-4 summarizes the average resistivity and COV for concrete specimens cured normally and tested by TxDOT and TTI over a range of ages from 3 to 56 days for NC and 3 to 28 days for AC. For TxDOT, the average SR and BR generally increase with age, from 2.3 kOhm-cm and 1.6 kOhm-cm at 3 days to 10.3 kOhm-cm and 10.1 kOhm-cm at 56 days, respectively. The COV decreases from initially high values (19.8 percent for BR at 3 days) to much lower values (2.5 percent for SR and 3.8 percent for BR at 56 days), indicating more consistent results as the concrete matures. TTI's results show a similar trend, with average resistivities increasing from 2.3 kOhm-cm and 2.5 kOhm-cm at 3 days to 9.4 kOhm-cm and 9.5 kOhm-cm at 56 days for SR and BR, respectively. The COV values are lower compared to TxDOT, with an initial 4.6 percent for SR and 6.2 percent for BR at 3 days, decreasing to 4.1 percent and 2.7 percent at 56 days, thus reflecting a very consistent testing outcome at that age.

Table 7-4: Average and COV in Resistivity Measurements Comparison (Within Lab)

CONDITIONING	**TEST**		**TXDOT – WITHIN LAB & 3 OPERATORS**		**TTI – WITHIN LAB & 1 OPERATOR**	
Type	Age(day)	Param	SR	BR	SR	BR
Normal Conditioning	3	avg	2.29	1.6	2.3	2.5
		cov	2.4%	19.8%	4.5%	5.4%
	7	avg	2.55	2.1	2.4	2.6
		cov	1.8%	8.4%	4.0%	5.1%
	14	avg	3.45	3.1	3.1	3.5
		cov	2.5%	2.7%	4.1%	4.4%
	28	avg	5.77	5.6	5.6	5.3
		cov	2.5%	2.6%	3.1%	3.1%
	56	avg	10.28	10.1	9.4	9.5
		cov	2.5%	3.8%	5.7%	1.7%
Accelerated Conditioning	3	avg	2.3	1.3	2.4	2.6
		cov	4.9%	22.3%	7.3%	3.8%
	28	avg	31.6	29.2	34.8	35.0
		cov	5.9%	3.7%	3.5%	1.6%

For AC conditioned specimens, the average SR and BR are low at 3 days (2.3 and 1.3 kOhm-cm, respectively), with high COV, especially for BR (22.3 percent) for TxDOT. By 28 days, average resistivity increases substantially (31.6 for SR, 29.2 for BR), and COV decreases (5.9 percent for SR, 3.7 percent for BR), indicating improved consistency. TTI results start with a slightly higher average SR and BR at 3 days (2.4 and 2.6 kOhm-cm, respectively) and lower COV (7.7 percent for SR, 4.3 percent for BR). At 28 days, the average increases to 34.8 for SR and 35.0 for BR, with a significant reduction in COV to 2.3 percent for SR and 1.7 percent for BR, thus showing a more consistent measurement at this stage. In summary, both TxDOT and TTI observed

increased average resistivity and decreased COV over time, with TTI showing higher average resistivity and lower COV at both testing ages.

7.6.3 Part 3: Interlaboratory Comparison

Table 7-5 shows the interlaboratory comparison between TxDOT and TTI for concrete resistivity testing under NC and AC conditions and reveals the following. For normal curing, the average SR and BR increase with the concrete's age, starting at 2.3 and 1.8 kOhm-cm at 3 days and reaching 10.1 and 9.9 kOhm-cm at 56 days, respectively. The COV for both SR and BR decreases significantly from the initial testing stage to the later stages, starting from a high of 27.7 percent for BR at 3 days and stabilizing at below 5 percent at 56 days, indicating more consistent results as concrete cures over time. Under AC, there is also a notable increase in average resistivity values from 3 to 28 days (2.3 to 32.4 kOhm-cm for SR, and 1.6 to 30.7 kOhm-cm for BR). However, the COV is substantially higher, particularly at 3 days, with BR showing a COV of 40 percent. By 28 days, the COV for both SR and BR decreases to 6.7 percent and 9.1 percent, respectively, though it remains higher compared to normal curing.

Table 7-5: Interlaboratory Resistivity Evaluation (NC and AC)

CONDITIONING	**TEST**		**TXDOT & TTI INTERLAB & ALL OPERATORS**	
Type	Age(day)	Param	SR	BR
Normal Conditioning	3	avg	2.3	1.8
		cov	2.9%	27.7%
	7	avg	2.5	2.2
		cov	3.5%	11.7%
	14	avg	3.4	3.2
		cov	4.9%	5.8%
	28	avg	5.7	5.5
		cov	2.9%	3.2%
	56	avg	10.1	9.9
		cov	4.6%	4.4%
Accelerated Conditioning	3	avg	2.3	1.6
		cov	5.3%	40.0%
	28	avg	32.4	30.7
		cov	6.7%	9.1%

7.7 Conclusions

This study concludes that resistivity testing, as a rapid and nondestructive method, offers an efficient approach for quality control of concrete mixtures. The test minimizes time spent on sample conditioning and allows for multiple age measurements from a small number of samples. Unlike other tests that destroy samples, resistivity tests can be conducted on cylinders also used

for compressive or tensile strength tests, thus enhancing mixture evaluation efficiency. However, the accuracy of resistivity measurements can be affected by specimen geometry and testing equipment, which necessitates geometry correction factors and careful preparation to ensure minimal resistance from sponges used to establish electrode contact.

Precision statements for BR tests are specified under ASTM C 1876, with a noted single-operator COV of 4.3 percent and a multilaboratory COV of 13.2 percent. No equivalent precision statements exist for SR tests under AASHTO T 358.

Data from the above interlaboratory study involving two laboratories and tests of 3 replicate specimens by each operator for each test (SR or BR) have quantified the operator and multilaboratory precision for both BR and SR tests. This quantification was based on the average COV and provided insights into the variability inherent to these resistivity test methods.

The within-laboratory and multilaboratory COV for SR and BR tests indicates a trend of variability dependent on the age of the concrete and the curing method applied. Both within-laboratory and interlab COV tends to decrease with the age of the concrete, suggesting that as concrete cures, the repeatability of resistivity measurements improves. For multilaboratory comparisons, the COV is generally higher than within laboratory, reflecting the variability introduced by different operators and equipment between laboratories. Overall, the multilaboratory COV also decreases over time—to 4.6 percent (SR) and 4.4 percent (BR) at 56 days with NC, and 6.7 percent (SR) and 9.1 percent (BR) at 56 days with AC (in compliance with the multilaboratory COV of 13.2 percent), thereby implying that discrepancies between laboratories lessen as the concrete ages.

CHAPTER 8: CONCLUSIONS, FUTURE WORK, IMPLEMENTATION RECOMMENDATIONS

This section summarizes the main findings of this study and offers recommendations for future work and implementation.

The literature review highlights the industry's transition toward performance-based specifications for HPC implementation that emphasize durability, quality, and constructability. Standard guide specifications have identified several performance characteristics and established threshold limits for various durability requirements. Moreover, various highway and state agencies' adoption of performance-based approaches, including proprietary mix designs and ERSs, underscores a commitment to meeting field durability requirements through innovative and flexible specification strategies.

The study evaluated critical durability indicators for HPC mixtures through performance evaluations of selected in-service bridge decks through visual inspections, NDT methods, and laboratory testing of field cores, including service life evaluation with ConcreteWorks. It aimed to assess if existing mix designs satisfied mechanical and durability criteria and whether current specifications addressed durability effectively. The research further formulated a broad spectrum of HPC mixtures covering Mix Options 1–5 (TxDOT specifications) and conducted detailed durability property investigations. The investigation resulted in the following major findings:

- *ASR Mitigation:* The traditional method for optimizing SCM dosage for ASR mitigation involves long-term performance testing across multiple replacement levels. This research developed a Chemical Screening Tool (CST) for rapid estimation of optimal SCM dosage within 1-2 days by leveraging the established concrete pore solution and aggregate reactivity relationship. CST's scientific approach for dosage predictions diminishes reliance on prolonged laborious ASR tests and offers substantial time and cost savings for both industry and DOT stakeholders.
- *Shrinkage:* Analysis revealed that TxDOT's HPC mix design practice (500–600 lb/cy cem content and 0.42 w/cm ratio) is optimized for DS. The research established 400 microstrains at the 28-day threshold limit for DS performance of HPC mixtures, though further validation is needed. However, mixture practice of low w/cm ratio (0.40–0.42) and aided by chemical admixtures (HRWR) to meet slump targets resulted in high AS, especially with SF in binary/ternary mixes. Additionally, high AS coupled with large thermal strains (i.e., thermal gradient from early morning placements), possibly contributed to early-age cracking noted at certain bridge decks in Amarillo, TX (Mix 29 percent C+6 percent SF).
- *Concrete Pore Solution Chemistry (PSC), Resistivity and FF*: The use of SCMs such as FA and SF in HPC mixtures improves durability by reducing permeability but also significantly alters the mixture's PSC through their soluble alkali contribution and alkali binding. PSC impacts widely used concrete resistivity tests used for mixture qualification

and QA/QC, while in contrast, the FF offers an accurate microstructural description essential for predicting transport properties and enabling rapid durability assessments. This research developed Resistivity, AFF and FF performance classification thresholds for HPC mixtures.

  - Resistivity measurements are reliant on PSC and microstructure, of which are altered differently by SCMs like FA and SF in HPC mixtures, thereby complicating direct resistivity-based comparisons for HPC mixtures.
  - FF study reveals binary FA HPC mixtures display low early-age FF due to slow microstructure development, potentially limiting their performance in harsh ambient conditions like seawater exposure. Conversely, ternary HPC mixtures with SF show enhanced early and later-age FF, indicating better early microstructure development and improved resistance to transport properties, making them more effective in demanding environments

- *Resistivity and Curing Regimen*:. Curing methods further affect resistivity through changes in saturation, leaching, and microstructure development, challenging uniformity in measurements.
  - AASHTO TP 119's SC methods can lead to self-desiccation in low w/cm mixtures, affecting hydration and increasing resistivity variability.
  - Recent specifications for concrete resistivity tests (ASTM C 1876/AASHTO TP 119) advocate a single/std simulated pore solution (SPS) curing to simplify the FF determination by eliminating the need for pore solution resistivity determination. However, this study found that SPS does not uniformly represent the PSC across various HPC mixtures. SPS curing regimen proved ineffective for certain Class C HPC mixtures with higher average PSC [~ 20–40 percent higher than SPS], which resulted in significant resistivity measurement variability and 22 percent error in FF determination.
  - The research prompted the development of an innovative Matching Pore Solution (MPS) curing regimen. Under MPS, HPC mixtures were grouped based on SCM's impact on PSC (e.g., Group 1: no FA mixtures with an average PSC of 85.1 mS/cm; Group 2: Class F FA mixtures with an average PSC of 73.5 mS/cm; Group 3: Class C FA mixtures with an average PSC of 114.5 mS/cm, etc.) and thereby, cured using a simulated solution that aligns with the group's average PSC. MPS curing aligns curing solutions closer to the mixture's actual PSC, reduces variability in/between BR and SR measurements, and notably improves FF determination accuracy and FF-based transport property predictions, evidenced by enhanced predictive correlations in HPC mixtures.

- *Chloride Diffusion*: The current performance test, ASTM C 1556, to measure chloride transport requires laborious sample conditioning, is time-consuming, is slow in implementation, and provides limited information on the measured properties. Moreover,

the transport of free chloride ions through concrete's PS rather than total chlorides (ASTM C 1556) triggers the initiation of corrosion in structures. The research findings show that the effective diffusion coefficient, crucial for assessing corrosion risk in concrete, is primarily influenced by concrete microstructure, pore structure, and connectivity. The AFF-based approach for estimating effective diffusion coefficients was found to be effective in providing results with reasonable accuracy. This study developed a predictive model for AFF-based effective chloride diffusion prediction for HPC mixes, incorporating chloride binding, offering a reliable method for determining corrosion potential.

A simplified, user-friendly Excel tool known as the TxDOT Tool was developed to facilitate the practical application and implementation of research findings into practice. TxDOT tool aids DOT practitioners and contractors in conducting rapid, durability-based performance evaluations of Class S CIP HPC bridge deck mixes, covering four critical aspects: ASR mitigation, shrinkage, resistance to chloride ion ingress, and freeze-thaw durability.

With the goal of elevating the project's Technology Readiness Level (TRL) from 6 to 8, the research conducted a field evaluation program followed by an inter-lab comparison of the resistivity method. Three field projects in the Euless and Dumas regions of Texas were selected to evaluate the performance of project-specific HPC mixtures by comparing laboratory evaluations of field-cast and lab-cast specimens with predictions from the TxDOT Tool for durability performance. Results showed that HPC mixture performance classification using 28-day accelerated conditioning (AC) resistivity measurements could serve as a viable alternative to normal 91d or 180d conditioning periods, but it needs additional validation across various SCM types. Initial field evaluations indicate that field-cast specimens align well with laboratory-cast specimens in terms of performance classification and evaluation, suggesting that contractors might rely on field-cast specimens for comparable QA/QC outcomes following the guidelines provided by the TxDOT Tool. However, to confirm these findings, more extensive field testing is recommended.

The Interlab program investigated concrete BR and SR measurements on a single concrete mixture, subjected to different conditioning procedures in two labs to determine/establish the test method's within-laboratory variability and inter-laboratory repeatability. Interlab evaluation with a single HPC mix (subjected to different conditioning procedures across two labs) showed that resistivity test methods met the lab's repeatability standards within and between labs.

8.1 Future Work

The current research indicated that the use of SF in conjunction with Class C ash (e.g., 29 percent Class C ash + 6 percent SF, HPC mix with ternary blends) provided the required transport properties for the Amarillo bridges. Similarly, 20 percent Class F + 5 percent SF mix instead of the current 25 percent Class F mix can provide the required transport properties to qualify as HPC for the Galveston bridge under the splash zone. However, the use of SF increases

AS in general (especially under high ambient temperature), with AS of 29 percent Class C + 6 percent SF > AS of 20 percent Class F + 5 percent SF. The higher the AS, the higher the early-age CP. To qualify a mix as an HPC mix in certain geographic locations with high-severity exposure conditions, the use of a ternary blend instead of binary is recommended. Since ternary blend with SF is being used in Texas, the use of the TxDOT Tool to evaluate the effectiveness of commonly used mitigation measures (e.g., internal curing using lightweight aggregates) in reducing AS potential should be considered in future research. This step will lead to the inclusion of internal curing in performance-based specifications for HPC. If the use of other suitable SCMs (e.g., metakaolin, colloidal silica, etc.) to make a ternary blend is justified based on supply and demand criteria in Texas, durability evaluation using the TxDOT Tool will be very useful.

The use of SF may be discontinued in the Amarillo and Lubbock areas, and the use of mixes with Class C ash alone may not be adequate to fully mitigate ASR and satisfy the transport properties requirements (may reduce the resistance to chloride ingress and F/T cycles). The evaluation of one Class C ash mix (35 percent Class C ash) in the current research has indicated that this mix did not provide the required transport properties. Therefore, adding another suitable SCM component (other than SF) to make an effective ternary blend could be a viable option that can be evaluated by our TxDOT Tool-based approach. If making a ternary blend using another SCM is not a practically viable option, the selection of appropriate steel to counteract the mix design deficiencies needs to be considered as an important area of further research.

Change in materials' availability and/or mix designs leads to changes in concrete transport properties, which has a direct connection with the selection of the most appropriate reinforcing option. The TxDOT Tool can be used to verify if a mix is adequate to provide high performance under a particular exposure condition (geographic location) and provide recommendations on mix design modifications whenever the current mix design practice is inadequate to meet the major durability requirements. However, this tool can be extended to establish a link between mix design controls (a performance indicator representing transport properties), selection of reinforcements, and exposure conditions to develop this kind of performance requirement. This kind of performance requirement will allow districts to optimize between the use of mix design controls (needed to meet certain criteria) and the selection of the most appropriate reinforcing option and decide where and when to use epoxy-coated steel. On one hand, this will ensure cost optimization (cost savings), and on the other hand will ensure long-lasting durable concrete that meets the exposure conditions.

As the need for alternative SCMs to make durable concrete increases, the research to modify and update the TxDOT Tool to accommodate alternative SCMs (e.g., natural pozzolans) becomes another important area of future research. The TTI Model-2 developed in the current research presents a simplified approach to predict PSC of binary and ternary concrete mixes containing SF, Class C, and Class F fly ashes to select curing regimens for the resistivity measurements and to estimate FF effectively. TTI Model-1 is effective in estimating PSA and determining SCM dosage rapidly for ASR mitigation using TTI's CST method for conventional SCMs. Both

models are built in the TxDOT Tool. However, the applicability of both TTI Model-1 and TTI Model-2 for all potential alternative SCMs needs to be verified. Integrating thermodynamic modeling with the current service life prediction models is the recent national trend. Therefore, integrating GEMS modeling in the TxDOT Tool should be another area of future research to increase the reliability of PSA, PSC, and PSR estimation and improve resistivity/FF determinations for all the alternative SCMs.

Two slag grinding facilities are coming to Texas this year, and TxDOT expects slag to become more common in Texas. These grinding facilities are going to get their slag granules from different sources and will be able to blend to design slag with variable chemistry and particle sizes to meet the project needs. Detailed research to evaluate the effectiveness of available slag in Texas in making durable concrete through the necessary modification of the TxDOT Tool to accommodate slag should be considered an important area of future research.

In the current research, the creep behavior of HPC mixes was estimated based on the existing B4 models to estimate CP. Future work is needed to investigate the creep behavior of HPC mixes experimentally.

A recently published NCHRP report recommends using ASTM C1567 to determine SCM dosage based on 0.10 percent at 28 days criteria if the aggregate reactivity is known with higher reliability. In our performance-based approach, we compared CST-based dosages with the dosages estimated by the C1567 (0.1 percent at 14 days) method and sorted out the ashes that needed further validation by the ACCT method. Using C1567 with a 0.1 percent expansion limit at 28 days may improve the comparison between CST and C1567, and the need for the ACCT method (75–90 days) to validate the sorted-out SCMs can be greatly minimized, which can save time and money. This approach needs to be evaluated.

8.2 Implementation Recommendations

The main item for implementation will be to apply the TxDOT TOOL to evaluate the current mix design practices for several field projects and examine if the current mix designs qualify as HPC matching with the durability requirements in the field projects.

Based on limited field validation studies, the resistivity-based performance classification using 28-day resistivity measurements with accelerated conditioning was found to be acceptable. However, a significant amount of further evaluation using several field projects through an implementation project is highly warranted to validate if performance-based mix classification based on 28 days of resistivity measurements with AC is reliably acceptable.

- During field validation, the research team went to the field during the day of concrete pouring. The mix design selection and verification through trial batch operations were already conducted by the contractors. In the proposed implementation plan, the research team will work with the contractors of the selected field projects from the beginning (i.e., mix design and trail batch stages) and identify the deficiencies (if any) of the selected

mix designs and provide recommendations on improving the mixes through modifications (mostly minor). If the deficiencies are identified and the recommended mix design changes cannot be implemented because of some limitations (e.g., an additional ingredient cannot be accommodated in a batch plant or recommended materials may not be available locally), the importance of better steel selection (an important area of future work explained above) will greatly increase to overcome the mix design deficiencies.

- A connection between classification category and performance evaluation will be established that is expected to be useful in selecting a particular class category (e.g., low or very low) for a particular location meeting the requirement of severity of exposures. In the future, TxDOT can use resistivity or FF-based performance classification (within 28 days) to verify if the selected mix is qualified as HPC for a project and avoid doing performance evaluation through conducting long-term testing.

Based on evaluating one mix, the resistivity test methods have satisfied the within-the-lab and between-the-lab repeatability requirements. However, various representative mix designs need to be evaluated to establish acceptable within-the-lab and between-the-lab repeatability requirements.

Resipod by Proceeq is a commonly used device for measuring SR, whereas Resipod by Proceeq with a changed configuration and RCON by Giatech Scientific both are commonly used for measuring BR. The raw data from different devices cannot be compared, and this feature needs to be corrected (geometry corrections, minimal resistance from sponges, etc.) before using them for performance classification and estimating different durability performance indicators. To accommodate resistivity measurement by different devices, the research team has developed an Excel sheet (preliminary level) to estimate corrected resistivity values from the raw measured resistivity values. Further work is needed to improve the sheet and fill the gaps. The next step will be to integrate this sheet into the main TxDOT Tool, which needs significant effort. This integration will allow the users to input the raw resistivity values directly into the Tool (user-friendly approach), and the Tool will calculate the corrected resistivity values, then follow with taking the corrected resistivity values as input for estimating the other durability-based performance indicators.

REFERENCES

1. TxDOT. Item 421 – Hydraulic Cement Concrete. *Standard Specifications for Construction and Maintenance of Highways, Streets, and Bridges*.
2. Douglas Hooton, R. Future Directions for Design, Specification, Testing, and Construction of Durable Concrete Structures. *Cement and Concrete Research*, Vol. 124, No. August, 2019, p. 105827. https://doi.org/10.1016/j.cemconres.2019.105827.
3. Russell, H. G. *NCHRP Synthesis 441: High Performance Concrete Specifications and Practices for Bridges.* Transportation Research Board of the National Academies, Washington, D.C., 2013.
4. Mukhopadhyay, A. K., and K. Liu. Innovative Approach for Formulating ASR-Resistant Mixtures. *Concrete International*, 2018, pp. 39–45.
5. Caldarone, M. A., P. C. Taylor, R. J. Detwiler, and S. B. Bhide. *Guide Specification for High Performance Concrete for Bridges*. 2005.
6. Russell, H. G. NCHRP Synthesis of Highway Practice 333: Concrete Bridge Deck Performance. *Transportation Research Board of the National Academies, Washington, DC*, 2004, p. 188.
7. Lindquist, W. D. *Development and Construction of Low-Cracking High-Performance Concrete (LC-HPC) Bridge Decks: Free Shrinkage, Mixture Optimization, and Concrete Production*. University of Kansas, 2008.
8. AASHTO - R 101 Standard Practice for Developing Performance Engineered Concrete Pavement Mixtures. *AASHTO*.
9. Krauss, P. D., and E. A. Rogalla. *Transverse Cracking in Newly Constructed Bridge Decks (NCHRP Report 380)*. 1996.
10. Malakooti, A. Investigation of Concrete Electrical Resistivity As a Performance Based Test. No. March, 2017, pp. 1–106. https://doi.org/10.13140/RG.2.2.28525.69603.
11. NCDC. National Climatic Data Center. Quality Controlled Local Climatological Data (QCLCD), Https://Www.Ncdc.Noaa.Gov/Qclcd/QCLCD. 13.
12. Krauss, P., T. Nelson, and E. Nadelman. *Investigation of Bridge Decks MONTANA DEPARTMENT OF TRANSPORTATION (MDT)*. 2017.
13. RUSSELL, H. G. *Control of Concrete Cracking in Bridges (NCHRP SYNTHESIS 500)*. 2017.
14. Mindess, S., and J. F. Young. Concrete : 2nd Ed. *Hoboken: Prentice Hall. 2nd ed.*, 2002, p. 644.
15. Qiao, P., D. I. McLean, and J. Zhuang. *Mitigation Strategies for Early-Age Shrinkage Cracking in Bridge Decks*. Washington (State). Dept. of Transportation, 2010.

16. Brooks, J., … J. C.-A. S. of, and undefined 1999. 11 Factors Affecting the Autogenous Shrinkage OF Silica Fume High-Strength Concrete. *books.google.com*.

17. Alaskar, A. *Early Volume Change of High Performance Concrete*. University of Toronto, 2017.

18. Wang, K., S. M. Schlorholtz, S. Sritharan, H. Seneviratne, X. Wang, and Q. Hou. Investigation into Shrinkage of High-Performance Concrete Used for Iowa Bridge Decks and Overlays. 2013.

19. Sakata, K., T. S.-J. of A. C. Technology, and undefined 2004. Recent Progress in Research on and Code Evaluation of Concrete Creep and Shrinkage in Japan. *jstage.jst.go.jp*, Vol. 2, No. 2, 2004, pp. 133–140.

20. Fu, T., T. Deboodt, and J. H. Ideker. Development of Shrinkage Limit Specification for High Performance Concrete Used in Bridge Decks. *Cement and Concrete Composites*, Vol. 72, 2016, pp. 17–26.

21. Fu, T., T. Deboodt, and J. H. Ideker. Development of Shrinkage Limit Specification for High Performance Concrete Used in Bridge Decks. *Cement and Concrete Composites*, Vol. 72, 2016, pp. 17–26.

22. Bazant, Z., S. B.-A. S. Publications, and undefined 2000. Creep and Shrinkage Prediction Model for Analysis and Design of Concrete Structures: Model B3. *cee.northwestern.edu*, 2000, pp. 1–83.

23. Saraswatula, P., A. Mukhopadhyay, and K.-W. Liu. Development of a Screening Tool for Rapid Fly Ash Evaluation for Mitigating Alkali Silica Reaction in Concrete. *Transportation Research Record: Journal of the Transportation Research Board*, 2022, p. 036119812210942. https://doi.org/10.1177/03611981221094291.

24. Mukhopadhyay, A. K., P. Saraswatula, and K. W. Liu. Rapid Estimation of Natural Pozzolan Dosages for Mitigating ASR Using the Innovative Chemical Screening Tool (CST). *Construction and Building Materials*, Vol. 408, 2023, p. 133609. https://doi.org/10.1016/J.CONBUILDMAT.2023.133609.

25. Mather, B. Concrete Durability. *Cement and Concrete Composites*, Vol. 26, No. 1, 2004, pp. 3–4. https://doi.org/10.1016/S0958-9465(02)00122-1.

26. Lindgård, J., Ö. Andiç-Çakir, I. Fernandes, T. F. Rønning, and M. D. A. Thomas. Alkali – Silica Reactions (ASR): Literature Review on Parameters Influencing Laboratory Performance Testing. *Cement and Concrete Research*, Vol. 42, No. 2, 2011.

27. Detwiler, R. *The Role of Fly Ash Composition in Reducing Alkali-Silica Reaction*. Publication PCA R & D Serial No. 2092. 1997.

28. Diamond, S. Alkali Silica Reactions - Some Paradoxes. *Cement and Concrete Composites*, Vol. 19, No. 5–6, 1997, pp. 391–401.

29. Lindgård, J., Ö. Andiç-Çakir, I. Fernandes, T. F. Rønning, and M. D. A. Thomas. Alkali-Silica Reactions (ASR): Literature Review on Parameters Influencing Laboratory Performance Testing. *Cement and Concrete Research*, Vol. 42, No. 2, 2012, pp. 223–243.

30. Haha, M. Ben, K. De Weerdt, and B. Lothenbach. Quantification of the Degree of Reaction of Fly Ash. *Cement and Concrete Research*, Vol. 40, No. 11, 2010, pp. 1620–1629.

31. Schäfer, E., and B. Meng. Influence of Cement and Additions on the Quantity of Alkalis Available for an Alkali-Silica Reaction. *Beton*, Vol. 51, No. 10, 2004, pp. 145–156.

32. Shehata, M. H., and M. D. A. Thomas. Alkali Release Characteristics of Blended Cements. *Cement and Concrete Research*, Vol. 36, No. 6, 2006, pp. 1166–1175. https://doi.org/10.1016/j.cemconres.2006.02.015.

33. Shehata, M. H., M. D. A. Thomas, and R. F. Bleszynski. The Effects of Fly Ash Composition on the Chemistry of Pore Solution in Hydrated Cement Pastes. *Cement and Concrete Research*, Vol. 29, No. 12, 1999, pp. 1915–1920. https://doi.org/10.1016/S0008-8846(99)00190-8.

34. Deschner, F., B. Lothenbach, F. Winnefeld, and J. Neubauer. Effect of Temperature on the Hydration of Portland Cement Blended with Siliceous Fly Ash. *Cement and Concrete Research*, Vol. 52, 2013, pp. 169–181. https://doi.org/10.1016/j.cemconres.2013.07.006.

35. Lothenbach, B., K. Scrivener, and R. D. Hooton. Supplementary Cementitious Materials. *Cement and Concrete Research*, Vol. 41, No. 12, 2011, pp. 1244–1256. https://doi.org/10.1016/j.cemconres.2010.12.001.

36. Hummel, W., U. Berner, E. Curti, F. J. Pearson, and T. Thoenen. Nagra/PSI Chemical Thermodynamic Data Base 01/01. *Radiochimica Acta*, Vol. 90, No. 9–11, 2002, pp. 805–813. https://doi.org/10.1524/RACT.2002.90.9-11_2002.805.

37. T Wagner, D. K. F. H. S. D. GEM-Selektor Geochemical Modeling Package: TSolMod Library and Data Interface for Multicomponent Phase Models. *Can Miner*, Vol. 50, No. 5, 2012, pp. 1173–1195. https://doi.org/10.3749/canmin.50.5.1173.

38. Lothenbach, B., D. A. Kulik, T. Matschei, M. Balonis, L. Baquerizo, B. Dilnesa, G. D. Miron, and R. J. Myers. Cemdata18: A Chemical Thermodynamic Database for Hydrated Portland Cements and Alkali-Activated Materials. *Cement and Concrete Research*, Vol. 115, 2019, pp. 472–506.

39. Hong, S. Y., and F. P. Glasser. Alkali Binding in Cement Pastes : Part I. The C-S-H Phase. *Cement and Concrete Research*, Vol. 29, No. 12, 1999, pp. 1893–1903. https://doi.org/10.1016/S0008-8846(99)00187-8.

40. Kulik, D. Improving the Structural Consistency of C–S–H Solid Solution Thermodynamic Models. *Cem Concr Res*, Vol. 41, No. 5, 2011, pp. 477–495. https://doi.org/10.1016/j.cemconres.2011.01.012.

41. Snyder, K. A., X. Feng, B. D. Keen, and T. O. Mason. Estimating the Electrical Conductivity of Cement Paste Pore Solutions from OH-, K+ and Na+ Concentrations. *Cement and Concrete Research*, Vol. 33, No. 6, 2003, pp. 793–798. https://doi.org/10.1016/S0008-8846(02)01068-2.

42. Lothenbach, B., D. Rentsch, and E. Wieland. Hydration of a Silica Fume Blended Low-Alkali Shotcrete Cement. *Physics and Chemistry of the Earth*, Vol. 70–71, 2014, pp. 3–16. https://doi.org/10.1016/j.pce.2013.09.007.

43. De Weerdt, K., M. Ben Haha, G. Le Saout, K. O. Kjellsen, H. Justnes, and B. Lothenbach. Hydration Mechanisms of Ternary Portland Cements Containing Limestone Powder and Fly Ash. *Cement and Concrete Research*, Vol. 41, No. 3, 2011, pp. 279–291. https://doi.org/10.1016/j.cemconres.2010.11.014.

44. Glosser, D. *Equilibrium and Non-Equilibrium Thermodynamic Modeling of Cement Pastes Containing Supplementary Cementitious Material*. Oregon State University, 2020.

45. Shi, C. Another Look at the Rapid Chloride Permeability Test (ASTM C1202 or AASHTO T277). *FHWA Resource Center, Baltimore*, 2003.

46. Shi, C., Z. Shi, X. Hu, R. Zhao, and L. Chong. A Review on Alkali-Aggregate Reactions in Alkali-Activated Mortars/Concretes Made with Alkali-Reactive Aggregates. *Materials and Structures/Materiaux et Constructions*, Vol. 48, No. 3, 2015, pp. 621–628. https://doi.org/10.1617/S11527-014-0505-2.

47. Spragg, R. P., Y. Bu, K. A. Snyder, D. P. Bentz, and J. Weiss. Electrical Testing of Cement-Based Materials: Role of Testing Techniques, Sample Conditioning, and Accelerated Curing. 2013, p. 23. https://doi.org/10.5703/1288284315230.

48. Tanesi, J., L. Montanari, and A. Ardani. *Formation Factor Demystified and Its Relationship to Durability*. Publication No. FHWA-HRT-19-030. United States. Federal Highway Administration, 2019.

49. Spragg, R., C. Villani, K. Snyder, D. Bentz, J. W. Bullard, and J. Weiss. Factors That Influence Electrical Resistivity Measurements in Cementitious Systems. *Transportation Research Record*, No. 2342, 2013, pp. 90–98. https://doi.org/10.3141/2342-11.

50. Bu, Y., and J. Weiss. Saturation of Air Entrained Voids and Its Implication on the Transport of Ionic Species in Concrete. 2014.

51. Nokken, M. R., and R. D. Hooton. Using Pore Parameters to Estimate Permeability or Conductivity of Concrete. *Materials and Structures/Materiaux et Constructions*, Vol. 41, No. 1, 2008, pp. 1–16. https://doi.org/10.1617/s11527-006-9212-y.

52. Morris, W., E. I. Moreno, and A. A. %J C. Sagüés. Practical Evaluation of Resistivity of Concrete in Test Cylinders Using a Wenner Array Probe. *Cement Concrete Research*, Vol. 26, No. 12, 1996, pp. 1779–1787.

53. Presuel-Moreno, F. J. *Chloride Diffusivity and Resistivity of Cured and Mature Binary / Ternary Concrete*. Publication BDV27-977–09. 2019.

54. Barrett, T. J. *Improving Service Life of Concrete Structures through the Use of Internal Curing: Impact on Practice*. Purdue University, 2015.

55. Weiss, J., K. Snyder, J. Bullard, and D. Bentz. Using a Saturation Function to Interpret the Electrical Properties of Partially Saturated Concrete. *Journal of Materials in Civil Engineering*, Vol. 25, No. 8, 2013, pp. 1097–1106. https://doi.org/10.1061/(Asce)Mt.1943-5533.0000549.

56. Weiss, W. J., C. Qiao, B. Isgor, and J. Olek. Implementing Rapid Durability Measure for Concrete Using Resistivity and Formation Factor. *Joint Transportation Research Program*, 2020, p. 24. https://doi.org/10.5703/1288284317120.

57. Riding, K. A., C. Ferraro, M. Almarshoud, H. Mosavi, R. Alrashidi, and M. H. Alyami. *Durability Evaluation Of Ternary Mix Designs For Extremely Aggressive Exposures Phase I & II*. Publication BDV-31-977-100. Florida, 2020.

58. Obla, K., P. E. C. L. Lobo, P. E. R. Hong, and S. Sherman. Improving the Reliability of Resistivity Tests of Concrete. 2020.

59. Spragg, R. P. *Development of Performance Related Specifications That Include Formation Factor*. Purdue University, 2017.

60. Tanesi, J. J., L. Montanari, A. Ardani, L. Montanari, A. Ardani, and L. Montanari. *Formation Factor Demystified and Its Relationship to Durability*. Publication No. FHWA-HRT-19-030. United States. Federal Highway Administration, 2019.

61. Coyle, A. T., R. P. Spragg, P. Suraneni, A. N. Amirkhanian, M. Tsui-Chang, and W. J. Weiss. Activation Energy of Conduction for Use in Temperature Corrections on Electrical Measurements of Concrete. *Advances in Civil Engineering Materials*, Vol. 8, No. 1, 2019, pp. 158–170. https://doi.org/10.1520/Acem20180045.

62. Bu, Y., and J. Weiss. Saturation of Air Entrained Voids and Its Implication on the Transport of Ionic Species in Concrete. 2014.

63. Todak, H. Durability Assessments of Concrete Using Electrical Properties and Acoustic Emissions. 2015, p. 158.

64. Rajabipour, F., and J. Weiss. Electrical Conductivity of Drying Cement Paste. *Materials and Structures*, Vol. 40, No. 10, 2007, pp. 1143–1160. https://doi.org/10.1617/s11527-006-9211-z.

65. Spragg, R., S. Jones, Y. Bu, Y. Lu, D. Bentz, K. Snyder, and J. Weiss. Leaching of Conductive Species: Implications to Measurements of Electrical Resistivity. *Cement & Concrete Composites*, Vol. 79, 2017, pp. 94–105. https://doi.org/10.1016/j.cemconcomp.2017.02.003.

66. Bu, Y., R. Spragg, C. Villani, and J. Weiss. The Influence of Accelerated Curing on the Properties Used in the Prediction of Chloride Ingress in Concrete Using a Nernst-Planck Approach. *Construction and Building Materials*, Vol. 66, 2014, pp. 752–759. https://doi.org/10.1016/j.conbuildmat.2014.04.138.

67. Ghosh, P., Q. %J I. J. of C. S. Tran, and Materials. Correlation between Bulk and Surface Resistivity of Concrete. Vol. 9, No. 1, 2015, pp. 119–132.

68. Khanzadeh Moradllo, M., C. Qiao, R. M. Ghantous, M. Zaw, H. Hall, M. T. Ley, and W. J. Weiss. Quantifying the Freeze-Thaw Performance of Air-Entrained Concrete Using the Time to Reach Critical Saturation Modelling Approach. *Cement and Concrete Composites*, Vol. 106, No. November 2019, 2020, p. 103479. https://doi.org/10.1016/j.cemconcomp.2019.103479.

69. Jafari Azad, V., A. R. Erbektas, C. Qiao, O. B. Isgor, and W. J. Weiss. Relating the Formation Factor and Chloride Binding Parameters to the Apparent Chloride Diffusion Coefficient of Concrete. *Journal of Materials in Civil Engineering*, Vol. 31, No. 2, 2019, p. 04018392. https://doi.org/10.1061/(asce)mt.1943-5533.0002615.

70. Qiao, C. Y., M. K. Moradllo, H. Hall, M. T. Ley, and W. J. Weiss. Electrical Resistivity and Formation Factor of Air-Entrained Concrete. *ACI Materials Journal*, Vol. 116, No. 3, 2019, pp. 85–93. https://doi.org/10.14359/51714506.

71. Riding, K. A., and M. Almarshoud Hossein Mosavi Raid Alrashidi Mohammed Hussain Alyami. Durability Evaluation of Ternary Mix Designs for Extremely Aggressive Exposures. No. May, 2018.

72. Nilsson, L.-O. Prediction Models for Chloride Ingress and Corrosion Initiation in Concrete Structures. *Nordic Mini Seminar & fib TG 5.5 meeting, Göteborg*, 2001.

73. Wang, Y., Z. Shui, X. Gao, R. Yu, Y. Huang, and S. Cheng. Understanding the Chloride Binding and Diffusion Behaviors of Marine Concrete Based on Portland Limestone Cement-Alumina Enriched Pozzolans. *Construction and Building Materials*, Vol. 198, 2019, pp. 207–217. https://doi.org/10.1016/j.conbuildmat.2018.11.270.

74. Russell, H. G., and H. C. Ozyildirim. Revising High-Performance Concrete Classifications. *Concrete International*, Vol. 28, No. 8, 2006, pp. 43–49.

75. Obla, K., C. Lobo, and L. Lemay. Specifying Concrete for Durability-Performance Based Criteria Offer Best Solutions. *Concrete InFocus*, Vol. 4, No. 4, 2006, pp. 42–50.

76. Ozyildirim, C. Evaluation of High-Performance Concrete Pavement in Newport News, Virginia. *Transportation Research Record*, No. 1775, 2001, pp. 118–124. https://doi.org/10.3141/1775-14.

77. Castro, J., R. Spragg, and J. Weiss. Water Absorption and Electrical Conductivity for Internally Cured Mortars with a W/C between 0.30 and 0.45. *Journal of Materials in Civil*

Engineering, Vol. 24, No. 2, 2012, pp. 223–231. https://doi.org/10.1061/(Asce)Mt.1943-5533.0000377.

78. G Fagerlund. Modeling the Service Life of Concrete Exposed to Frost. *International conference on ion and mass transport*, 2001.

79. Todak, H., M. Tsui, T. Ley, and J. Weiss. Freeze-Thaw Resistance of Concrete: The Influence of Air Entrainment, Water to Cement Ratio, and Saturation. *Brittle Matrix Composites 11*, 2015, pp. 101–109.

80. Bentz, D., and M. Ehlen. Sorptivity-Based Service Life Predictions for Concrete Pavements. *Citeseer*, Vol. 1, No. 7, 2001, pp. 181–193.

81. Moradllo, M. K., C. Qiao, M. Keys, H. Hall, M. Tyler Ley, S. Reese, and W. Jason Weiss. Quantifying Fluid Absorption in Air-Entrained Concrete Using Neutron Radiography. *ACI Materials Journal*, Vol. 116, No. 6, 2019, pp. 213–226. https://doi.org/10.14359/51716980.

82. Moradllo, M. K., C. Qiao, B. Isgor, S. Reese, and W. J. Weiss. Relating Formation Factor of Concrete to Water Absorption. *ACI Materials Journal*, Vol. 115, No. 6, 2018, pp. 887–898. https://doi.org/10.14359/51706844.

83. Weiss, W. J., O. Burkan Isgor, M. T. Ley, W. J. Weiss, R. P. Spragg, and T. Van Dam. Toward Performance Specifications for Concrete: Linking Resistivity, RCPT and Diffusion Predictions Using the Formation Factor for Use in Specifications. *Springer*, 2017.

84. Kessler, R. J., R. G. Powers, and M. A. Paredes. Resistivity Measurements of Water Saturated Concrete as an Indicator of Permeability. No. 05295, 2005, pp. 1–27.

85. Saraswatula, P., and A. Mukhopadhyay. Increasing the Reliability of Formation Factor-Based Transport Property Prediction for High Performance Concrete Mixtures Through Innovative Matching Pore Solution Curing. *https://doi.org/10.1177/03611981231164078*, 2023, p. 036119812311640. https://doi.org/10.1177/03611981231164078.